

**Millimetre-Wave Optically Injection-Locked Oscillators
for Radio-Over-Fibre Systems**

A thesis submitted to The University of Kent at Canterbury for The Degree
of Doctor of Philosophy in Electronic Engineering

Xu Wang

Feb 2004

Abstract

Theoretical analysis and experimental results for millimetre-wave optically injection-locked oscillators are presented in this thesis. Such oscillators can be employed to replace conventional photodiode plus amplifier receivers for local oscillator signal reception in millimetre-wave radio-over-fibre systems.

The theories for electrical injection-locked oscillators are reviewed in detail. Three differences between Adler's and Kurokawa's equations for locking bandwidth are highlighted for the first time. These differences are the absence of $1/\cos\theta$ factor in Adler's equation, larger bandwidth predicted by Kurokawa's equation, and a difference in definition of Q factors. Locking bandwidth equations for optically injection-locked oscillators are developed based on the theories of electrical injection-locked oscillators and are then used to design optically injection-locked oscillators.

A novel millimetre-wave indirect optically injection-locked oscillator is presented. An edge-coupled photodiode is used to detect the optical signal. Negative resistance and computer simulation techniques were used for predicting the free running oscillation frequency. The maximum output power of the oscillator is 5.3 dBm, and the maximum locking bandwidth is measured to be 2.6 MHz with an output power of -12 dBm. Results from a comparison with conventional optical receivers show that the gain of the optically injection-locked oscillator is more than 10 dB higher than that of a photodiode plus amplifier receiver, that the oscillator output power remains constant with input signal power variations whereas the output power of the photodiode plus amplifier receiver changes (linearly) with the input signal power, and that, at high-offset frequencies, the phase noise of the optically injection-locked oscillator is much lower than that of the photodiode plus amplifier receiver. These advantages make the optically injection-locked oscillator an ideal replacement for the photodiode plus amplifier receiver in radio-over-fibre systems. An improved wide-band design for millimetre-wave optically injection-locked oscillators is presented for future work.

Acknowledgements

I would like to express my fullest thanks to Dr Nathan Gomes for his dedicated supervision, advice, and encouragement during my PhD study at the University of Kent at Canterbury (UKC). I would also like to thank Dr David Wake of British Telecom Laboratories for supplying the photodiodes required by this work.

During the years I have spent in UKC, I have made many friends and received a lot of support, especially those I have worked very closely with. I would like to express my gratitude to Dr. Luis Gomez-Rojas, Dr David George, Prof Philip Davies, Pengbo Shen, Robert Davis, Clive Birch and all those who have give me support during the study. Without their advice, support, and pressure (some time), this work would never be finished.

I would also like to thank UKC, my former employer, who provided the financial support for my PhD study.

Finally, I would show my deepest thanks to my parents, sister, and brother-in-law for all their support during my four and half years study in the UK. I would like to thank my wife, Xin Li, for her continuous support during the writing of this thesis.

Xu Wang

To my family

Publications List

- [1] L.A. Johansson, X. Wang, N.J. Gomes, and A.J. Seeds, "Optical delivery of millimetre-wave carriers using double injection locking", *IEEE 2001 International Topical Meeting on Microwave Photonics, MWP'01*, Long Beach, CA, USA, Digest pp. 89-92, January 7 - 9, 2002
- [2] X.Wang, N.J.Gomes, L.Gomez-Rojas, P.A.Davies and D.Wake, "Indirect optically injection locked oscillator for millimetre-wave communication system," *IEEE Trans. Microwave Theory Tech.*, Vol. 48, No. 12, pp. 2596-2603, Dec 2000.
- [3] X.Wang, N.J.Gomes, L.Gomez-Rojas, P.A.Davies and D.Wake, "30 GHz microstrip HEMT oscillator using indirect optical injection locking," *2000 IEEE MTT-S International Microwave Symposium Digest*, Vol. 3, pp1753-1756, June 2000.
- [4] L. Gomez-Rojas, N.J.Gomes, X.Wang, and P.A.Davies, "Simple technique for tuning of impedance matching circuits for the millimetre-wave region", *IEE Colloquium on Interconnects and packaging at microwave and millimetre-wave frequencies, London*, Vol. 83, pp 7/1-12, Jun 2000.
- [5] L. Gomez-Rojas, X.Wang, N.J.Gomes, P.A.Davies, and D.Wake, "High performance optical receiver using a PIN photodiode and amplifier for operation in the millimetre-wave Region", *30th European Microwave Conference Digest*, Vol.3, pp392-394, EUMW2000, Oct 2000.
- [6] L. Gomez-Rojas, X.Wang, N.J.Gomes, and P.A.Davies, "Efficient photoreceivers for millimetre-wave cellular system base stations", *MWP2000 Digest*, pp 194-197, Sep 2000.

[7] X.Wang, N.J.Gomes, "Locking bandwidth equations for electrically and optically injection-locked oscillators", submitted to IEE proceedings-Optoelectronics.

Content

1. INTRODUCTION.....	1
1.1. Introduction.....	1
1.2. Optically injection-locked oscillators	3
1.3. Achievements of the work presented in this thesis.....	3
1.4. Thesis outline.....	4
References.....	7
2. OPTICALLY INJECTION-LOCKED OSCILLATORS.....	9
2.1. Introduction.....	9
2.2. Photosensitive devices.....	10
2.2.1. Energy band gaps and photon absorption.....	10
2.2.2. Photodetectors.....	11
2.3. Introduction of electrical injection-locked oscillators.....	18
2.4. Optically injection-locked oscillators.....	20
2.4.1. Definition and classification of optically injection-locked oscillators....	20
2.4.2. Advantages and disadvantages of optically injection-locked oscillators	
.....	22
2.5. The state of current research into optically injection-locked oscillators.....	23
2.5.1. Theoretical work on electrical injection-locked oscillators.....	23
2.5.2. Experimental work on electrical injection-locked oscillators.....	24
2.5.3. Theoretical work on optically injection-locked oscillators.....	25
2.5.4. Experimental work on optically injection-locked oscillators.....	26
2.6. Applications of optically injection-locked oscillators.....	27
2.7. Microwave/millimetre-wave fibre radio systems.....	27
2.8. Radio-over-fibre system architectures employing optically injection-locked	
oscillators.....	29
2.9. A 30 GHz radio-over-fibre system.....	33
2.10. Other applications of optically injection-locked oscillators.....	37
2.11. Summary.....	38
References.....	40
3. DESIGN OF MICROWAVE OSCILLATORS AT HIGH FREQUENCIES.....	46
3.1. Introduction.....	47
3.2. Oscillator design methods.....	47
3.2.1. Close loop gain design method.....	47
3.2.2. Negative resistance design method.....	48
3.3. GAAS HEMT model.....	51
3.3.1. HEMT structure	51
3.3.2. Other types of high frequency transistors.....	52

3.3.3.	Small signal model.....	53
3.3.4.	Large signal model.....	54
3.4.	Design of high frequency oscillator using computer simulation	58
3.4.1.	Choice of device and device modelling.....	58
3.4.2.	Choice of bias topology.....	60
3.4.3.	Choice of oscillator configuration.....	62
3.4.4.	RF choke design.....	63
3.4.5.	Small signal simulation.....	66
3.4.6.	Large signal simulation.....	67
3.4.7.	Design example.....	68
3.5.	Summary.....	69
	References.....	71
4.	THEORETICAL ANALYSIS OF OPTICALLY INJECTION-LOCKED OSCILLATOR.....	73
4.1.	Introduction.....	73
4.2.	Reflection type injection locking.....	74
4.2.1.	Small-signal injection locking theory.....	74
4.2.2.	Kurokawa locking bandwidth equations.....	78
4.2.3.	Adler's locking bandwidth equation.....	83
4.2.4.	Differences between Adler's and Kurokawa's locking bandwidth equation.....	89
4.2.5.	Noise of an injection-locked oscillator.....	93
4.2.6.	The locking transient.....	96
4.3.	Transmission type injection-locked oscillator.....	96
4.4.	Optically Injection-locked Oscillators.....	99
4.4.1.	Introduction.....	99
4.4.2.	Locking bandwidth of optically injection locked oscillators.....	99
4.4.3.	Noise of an indirect optically injection-locked oscillator.....	101
4.5.	Summary.....	102
	References.....	104
5.	MILLIMETRE-WAVE INDIRECT OPTICALLY INJECTION-LOCKED OSCILLATOR DESIGN AND MEASUREMENT RESULTS.....	106
5.1.	Introduction.....	106
5.2.	Design targets and procedures.....	107
5.2.1.	Design targets.....	107
5.2.2.	Design procedures.....	107
5.3.	Implementation Techniques.....	110
5.3.1.	Substrate.....	110
5.3.2.	Active device.....	110
5.3.3.	Photodiode.....	115
5.3.4.	Bondwire.....	117
5.3.5.	Circuit fabrication.....	120
5.4.	Design of the millimetre-wave indirect injection-locked oscillators.....	122
5.4.1.	Design of the oscillation part.....	123

5.4.2.	Design of the resonator part.....	124
5.4.3.	Design of the photodiode insertion circuit.....	127
5.4.4.	Completed optically injection-locked oscillator.....	129
5.5.	Experimental results.....	130
5.5.1.	Set-up.....	130
5.5.2.	Measurements of 30 GHz optically injection-locked oscillators.....	132
5.6.	Noise performance comparison with a photodiode plus amplifier module.....	136
5.7.	Performance comparison with commercial packaged PD+AMP receiver.....	138
5.7.1.	Experimental setup.....	138
5.7.2.	Experiment results.....	139
5.7.3.	Analysis.....	142
5.7.4.	Summary.....	143
5.8.	Summary.....	143
	References.....	145
6.	IMPROVEMENT OF THE LOCKING BANDWIDTH OF THE MILLIMETRE-WAVE OPTICALLY INJECTION-LOCKED OSCILLATOR.....	148
6.1.	Introduction.....	148
6.2.	Resonator design.....	149
6.2.1.	Photodiode matching.....	150
6.2.2.	Photodiode insertion point.....	152
6.2.3.	Summary.....	153
6.3.	Design of new optically injection-locked oscillator.....	154
6.4.	Measurement results and problems.....	155
6.5.	Summary.....	156
	References.....	157
7.	CONCLUSIONS AND FUTURE WORK.....	158
7.1.	Summary of the thesis.....	158
7.1.1.	Summary of theoretical work.....	158
7.1.2.	Summary of design and measurement work.....	160
7.2.	Achievements of the work.....	160
7.2.1.	Difference between Adler's and Kurokawa's locking bandwidth equation.....	161
7.2.2.	Locking bandwidth equation for optically injection-locked oscillators..	161
7.2.3.	First millimetre-wave indirect optically injection-locked oscillator working with long wavelength signals.....	162
7.2.4.	Experimental demonstration of advantages of optically injection-locked oscillator.....	162
7.3.	Suggestions for future work.....	163
7.3.1.	Extensions to theoretical work.....	163
7.3.2.	Future experimental work.....	164
	References.....	167
	Appendix I Other applications of optically injection-locked oscillators.....	168

Appendix II Design of oscillator at 15 GHz.....	178
Appendix III LPD200-P70 Specifications.....	193
Appendix IV EC2612 Specifications.....	198

Chapter 1

Introduction

1.1 Introduction

Electrical injection-locked oscillators have been intensively researched since the 1920s [1]-[11]. Optical injection-locked oscillators, designed based on electrical injection-locked oscillators, became a hot research topic in more recent years because of their possible application in radio-over-fibre systems [6], [12].

The concept of microwave/millimetre-wave radio-over-fibre systems has been introduced in order to meet the increasing demand for transmitting data over wireless networks with a high bit rate. Compared with conventional radio systems, optical fibres are used to transmit data and local oscillator signals between the central station and base stations with low insertion loss. Conventionally, photodiode plus amplifier receivers are employed at the base stations for optical-electrical conversion. The use of optically injection-locked oscillators in these systems may give advantages such as high gain and low-cost. Microwave optically injection-locked oscillators working with long wavelength signals (1550nm) have been demonstrated [5]. At millimetre-wave frequency, the first

indirect optically injection-locked oscillator working with long wavelength signals was demonstrated in this work [6].

The main aim of this work is to develop a millimetre-wave indirect optically injection-locked oscillator working with long wavelength signals. To achieve this main aim, the work has been broken down into several small aims as follows:

1. To review the application of and the progress of research into optically injection-locked oscillators. By achieving this aim, the importance and novelty of developing the millimetre-wave optically injection-locked oscillators will be identified.
2. To review and identify design methods for designing high frequency oscillators. The design method of millimetre-wave optically injection-locked oscillators is based on that of electrical injection-locked oscillators. The design method for high frequency oscillators must be well understood for a good optically injection-locked oscillator design.
3. To review and compare the theories for electrical and optical injection-locked oscillators. A good optically injection-locked design comes from a good understanding of optically injection-locked oscillator theory. The theory of optically injection-locked oscillators is developed from that of the electrical injection-locked oscillators. Therefore, both electrical and optically injection-locked oscillator theory must be reviewed.
4. To design and build the first millimetre-wave optically injection-locked oscillator working with long wavelength signals. By combining the knowledge gained from the previous three aims, the millimetre-wave optically injection-locked oscillator working with long wavelength can be developed.
5. To compare the performance of millimetre-wave optically injection-locked oscillators with conventional optical receivers, and demonstrate the advantages/disadvantages of the use of such oscillators.

1.2 Optically injection-locked oscillators

With appropriate conditions, the application of an external RF signal to the input of a free-running oscillator will cause the oscillator frequency to shift or lock to the frequency of the applied frequency; a well-known phenomenon called injection locking. Electrical injection-locked oscillators can be classified as reflection-type or transmission-type injection-locked oscillators according to the point at which the injection signal is applied.

Optically injection-locked oscillators were developed from electrical injection-locked oscillators. A photosensitive device is required for an optically injection-locked oscillator. An electrical injection signal is first modulated onto an optical carrier. The photosensitive device is illuminated by the electrically modulated optical carrier. The injection signal is converted from the optical domain to the electrical domain by the photosensitive device and injected into the oscillator electrically. Optically injection-locked oscillators can be also classified as reflection-type or transmission-type injection-locked oscillators according to the point at which the injection signal is applied.

A detailed introduction to electrical and optically injection-locked oscillators will be presented in Chapter 2.

1.3 Achievements of the work presented in this thesis

The main achievement of this work has to been to design and build the first millimetre-wave indirect optically injection-locked oscillator working at long wavelengths (1550nm). Other achievements presented in this thesis are:

- a. For the first time, the differences between Adler's and Kurokawa's injection-locking bandwidth equations are identified.
- b. Locking bandwidth equations for optically injection-locked oscillators are set out.

- c. The performance of the millimetre-wave optically injection-locked oscillator is compared experimentally with conventional photodiode plus amplifier receivers.
- d. The phase noise of the millimetre-wave optically injection-locked oscillator is measured and compared with that of conventional photoreceivers.
- e. A new oscillator structure for higher locking bandwidth is designed for future work.

1.4 Thesis outline

The thesis reports on the theory, analysis and design of millimetre-wave optically injection-locked oscillators. It is structured as follows:

Different types of photosensitive devices that can be used in optically injection locked oscillator are introduced first in Chapter 2. The detailed classification of electrical and optically injection-locked oscillator is introduced. Discussion of the advantages and disadvantages of different types of optically injection-locked oscillator follows. The current stage of research of optically injection-locked oscillators is reviewed to emphasise the importance of this work. The target application of optically injection-locked oscillators in radio-over-fibre systems is discussed in detail. In particular, radio-over-fibre system structures using photodiode plus amplifier photoreceivers and optically injection-locked oscillators are described. The advantages of using optically injection-locked oscillators are highlighted. A radio-over-fibre base station module that is being developed at the University of Kent is given as an example of the use of optically injection-locked oscillators in radio-over-fibre system.

The aim of Chapter 3 is to provide a detailed description of high frequency oscillator design using computer simulation. Oscillator design topologies both at high and low frequencies are introduced at the beginning of this chapter. The negative impedance design topology for the design of high frequency oscillators is discussed in detail, and this

method is chosen for designing the millimetre-wave optically injection-locked oscillators in this work. Small-signal and large signal models for High Electron Mobility Transistors (HEMTs) that are used to design oscillators at high frequencies are introduced. The steps involved in the design of high frequency oscillators using HP Microwave Design System (MDS) are discussed. Chapter 3 provides a detailed description of high frequency oscillator design using computer simulation in such a way that the design procedure will not need to be described in detail again in later chapters.

Chapter 4 presents the theoretical background for optically injection-locked oscillators. The theory of electrical injection-locked oscillators is treated first as it is this that the theory of optically injection-locked oscillators is based on. Theories of reflection type injection-locked oscillators introduced by Adler and Kurokawa are discussed in detail. The difference between the equations derived by Adler and Kurokawa is analysed and discussed. Then, the theory of transmission type injection locking introduced by Tajima is described, and the locking equation derived by Tajima is presented. At the end of the chapter, the concept of optical injection locking and optical injection locking techniques are introduced. Locking bandwidth equations for both transmission type and reflection type optically injection-locked oscillators are derived by the author. The theories and equations for the injection-locked oscillator described in Chapter 4 provide the theoretical directions for the design of the millimetre-wave optically injection locked oscillator to be discussed in later chapters.

Chapter 5 describes the design of a transmission type millimetre-wave optically injection-locked oscillator based on the theories described in Chapter 4. The design issues and challenges particularly related to the millimetre-wave injection-locked oscillator are discussed. The fabricated optically injection-locked oscillator has been tested and measurements demonstrating its suitability for use in the radio-over-fibre system are presented in later sections. This is the first millimetre-wave oscillator using a hybrid integration approach that has been optically injection-locked to a millimetre-wave modulated long-wavelength optical signal. Finally, the performance of optically

injection-locked oscillators is compared to that of conventional photodiode plus amplifier receivers.

Chapter 6 discusses a new resonator configuration to improve the oscillator locking bandwidth. Two improvements are expected from the new resonator configuration. The oscillator quality factor is lower and the injection signal coupling is higher. The matching circuit of the photodiode for maximum injection of RF signal power and low Q has first been investigated. The insertion point of the photodiode within the resonator is then investigated. A short-circuited resonator is chosen as the resonator for simplicity and low Q. The photodiode is inserted at the end of the resonator (near the transistor). The use of this oscillator configuration for the future research of wideband optically injection-locked oscillators is discussed.

Chapter 7 presents the conclusion of this thesis. Summaries for the previous chapters are presented first. The conclusion for the whole thesis follows. Suggestions for future work are given at the end of the chapter.

References

- [1] V. D. Pol, "Forced Oscillation in a Circuit with Nonlinear Resistance," *Phil. Mag.*, Vol. 3, pp. 65-68, Jan 1927.
- [2] R. Adler, "A study of locking phenomena in oscillators," *Proceedings of the I.R.E. and Waves and Electronics*, pp. 351-357, Aug 1946.
- [3] K. Kurokawa, "Injection locking of microwave solid-state oscillators," *Proceedings of the IEEE*, vol.61, No.10, pp. 1386-1410, Oct 1973.
- [4] Y. Tajima and K. Mishima, "Transmission-Type Injection Locking of GaAs Schottky-Barrier FET Oscillators," *IEEE Trans. on Microwave Theory and Tech.*, Vol. MTT-27, No.5, pp. 386-391, May 1979.
- [5] D. Sommer and N. J. Gomes, "Wide-locking bandwidth optically injection-locked oscillators: S-parameter design and modulation effects," *IEEE Transactions on Microwave Theory and Tech.*, Vol. 43, pp. 1424-1434, Jul 1995.
- [6] X. Wang, N. J. Gomes, L. Gomez-Rojas, P. A. Davies, D. Wake, "Indirect optically injection-locked oscillator for millimeter-wave communication system," *IEEE Trans. Microwave Theory Tech.*, Vol 48, No. 12, pp. 2596-2603, 2000.
- [7] S. Kudzusz, W.H. Haydl, M. Neumann, A. Bangert, A. Hülsmann, "Subharmonically Injection Locked 94 GHz MMIC HEMT Oscillator Using Coplanar Technology," *IEEE MTT-S Int. Microwave Symp. Dig.*, pp. 1585-1588, Jun 1998.
- [8] J. Y. Lee, U. S. Hong, "Push-push Subharmonically Injection-locked Oscillator," *Electronic Letters*, Vol. 32, No. 19, pp. 1792-1793, Sep 1996.
- [9] K. Kamogawa, T. Tokumitsu, and I. Toyota, "A 20-GHz-Band Subharmonically Injection-locked Oscillator MMIC with Wide Locking Range," *IEEE Microwave and Guided Wave Letters*, Vol. 7, No.8, pp. 233-235, Aug 1997.
- [10] H. P. Moyer and A. S. Daryoush, "A Unified Analytical Model and Experimental Validations of Injection-locking Processes," *IEEE Trans. on Microwave Theory and Tech.*, Vol.48, No.4, pp. 493-499, Apr 2000.

[11] A. J. Seeds and J. R. Forrest, "Initial Observations of Optical Injection Locking of a X-band IMPATT Oscillator," *Electron. Lett.*, Vol. 14, pp. 829-830, 1978.

[12] D. Wake, L.D. Westbrook, N. G. Walker and I. C. Smith, "Microwave and millimetre-wave radio fibre," *BT Technol. J.*, Vol. 11, No. 2, pp. 76-78, Apr 1993.

Chapter 2

Optically Injection-locked Oscillators

2.1 Introduction

In Chapter 1, the definition and classification of electrical and optical injection-locked oscillators have been reviewed briefly. This chapter will give a detailed review of optically injection-locked oscillators.

In this chapter, different types of photosensitive devices and microwave components and circuits that are used to build optically injection-locked oscillators are discussed first. Reviews of the classification of electrical and optically injection-locked oscillators follow. The current stage of research for optically injection-locked oscillators is also reviewed. The applications of optically injection-locked oscillators are then discussed to show the value and importance of research on optically injection-locked oscillators.

2.2 Photosensitive devices

For an optically injection-locked oscillator, the electrical injection signal is first modulated on an optical carrier, and then the electrically modulated optical signal is transmitted and injected into the optically injection-locked oscillator. Inside the optically injection-locked oscillator, the photosensitive device will convert the injection signal from the optical domain to the electrical domain and electrically injection-lock the oscillator. The photosensitive device can be a PIN photodiode, an avalanche photodiode (APD), a phototransistor, or the oscillator active device itself. For photosensitive devices used by optically injection-locked oscillators, the most important parameters are the working optical wavelength, responsivity, and microwave operation frequency. The following subsections review different photosensitive devices used in optically injection-locked oscillators with respect to these three parameters.

2.2.1 Energy band gaps and photon absorption

Light which enters a semiconductor may give rise to the creation of an electron-hole pair in a quantum interaction in which a single photon is absorbed [1]. If there is an electric field present, the electron and hole separate and a change in current may be detected in the external circuit of which the semiconductor is an element. In order to be absorbed by the semiconductor material, the photon energy must be greater than the band gap energy of the semiconductor material. The relation of incident optical signal power and current generated in the semiconductor device is described by its responsivity,

$$R = \frac{I_p}{P_{optical}} \quad (\text{A/W}) \quad (2.1)$$

where I_p is the output photocurrent in amperes and $P_{optical}$ is the incident optical power in watts.

2.2.2 Photodetectors

The following sections will discuss the optical detectors that can be used by optically injection-locked oscillators.

1. GaAs transistors

GaAs transistors are not normally designed for optical detection. However, as GaAs transistors are widely used in direct optically injection-locked oscillators as photodetectors, here they are discussed as photodetectors [2]-[7]. As GaAs transistors are designed to be used in conventional microwave/millimetre-wave applications (amplifiers, oscillators, etc.) the frequency response of such devices can be very high. However, the optical performance of such devices is not optimised, thus they suffer from low responsivity. Also, they are limited by the GaAs material bandgap, and can only operate with short wavelength optical signals (up to around 850 nm).

2. PIN photodiodes

PIN photodiodes are widely used in optical communication systems. Fig 2.1 shows the presence of a depletion region in a reverse biased PIN photodiode [1]. In order to allow maximum optical power to be absorbed in the depletion layer, an intrinsic layer is added between the p type and n type materials to increase the width of the depletion layer. The depletion region is formed by immobile positively charged donor atoms in the i type semiconductor material and immobile negatively charged acceptor atoms in the p type material. Free electron-hole pairs are generated in the photodiode as a result of photon absorption. In the depletion region the electron-hole pairs separate and drift under the influence of the electric field. Outside the depletion region, the electrons and holes must diffuse towards the depletion region in order to be collected, and this region is called the diffusion region.

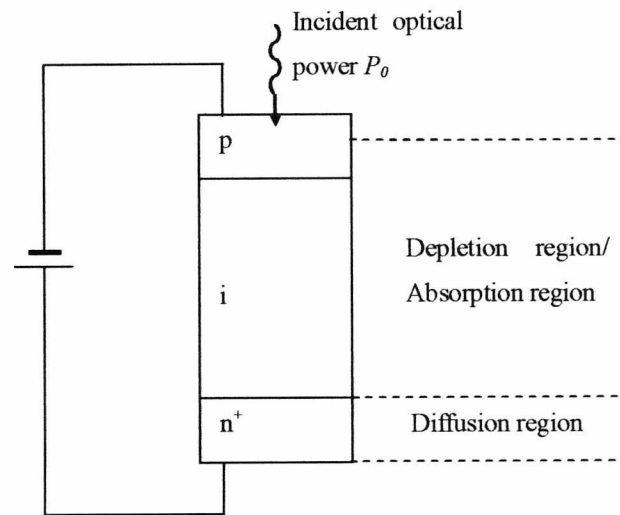


Fig 2.1 PIN photodiode showing combined absorption and depletion region [1]

The vertical illuminated photodiode (VPD) where the optical signal is illuminated on the top of the photodiode is the most commonly used PIN photodiode [1]-[8]. This type of photodiode is widely used in lower frequency applications. There are frequency response and responsivity trade-offs for VPDs in high frequency applications.

The frequency response of a PIN photodiode is strongly dependent on the thickness of the depletion region. Assuming the photocurrent is dominated by the drift of carriers, the speed of response for a photodiode is fundamentally limited by the time it takes photogenerated carriers to drift across the depletion region (transit time). The depletion region thickness needs to be minimised in order to increase the transit-time limited cut-off frequency of a PIN photodiode. However, a thin depletion region leads to low responsivity. Diffusion time also limits the frequency response of a PIN photodiode, as the diffusion process is very slow compared to drift, and a thin depletion region can result in more diffusion current

The photodiode capacitance also limits the frequency response. The photodiode cut-off frequency is inversely related to the photodiode capacitance. The capacitance of the photodiode is that of the junction capacitance together with the capacitance of the bonding pad and packaging. Therefore, high frequency VPDs have to be very small to minimise the photodiode capacitance. However, small diode size has problems such as static sensitivity, and poor power handling.

A low responsivity VPD (<0.4 A/W) with a bandwidth over 100 GHz has been demonstrated [9]. The low responsivity is a result of the frequency response and responsivity trade-off.

Several technologies have been developed to increase the PIN photodiode bandwidth while maintaining high responsivity. Classified according to the technology employed, there are two major types of high frequency PIN photodiodes: waveguide edge-coupled PIN photodiodes (WGPD), and travelling-wave PIN photodiodes (TWPD).

The WGPD was introduced to overcome the bandwidth and responsivity trade-off for VPD [9]-[11]. The WGPD, as its name implies, has an optical waveguide structure within it. The WGPD structure permits the bandwidth and responsivity to be specified almost independently because the responsivity is determined not by the absorption layer thickness but by the waveguide length. High responsivity (>0.5 A/W) WGPDs with a bandwidth over 100 GHz have been used in high-speed measurement systems [10]. This type of PIN photodiode is the most widely used at millimetre-wave frequencies. WGPDs were used to build optically injection-locked oscillators in this work [11].

The TWPD was introduced to increase the bandwidth of the WGPD further [12]. Diode capacitance limits the bandwidth of the VPD and the WGPD. The diode capacitance is minimised by reducing the diode size for VPD and WGPD. However, small diode size has problems such as poor power handling and static sensitivity. The TWPD has a similar structure to the WGPD, but it has an electrically distributed electrode structure to increase the bandwidth further [12]. The diode's metal electrodes are designed to allow the

generated RF signal to travel in phase synchronism with the light. If this velocity matching is achieved, the maximum bandwidth of the TWPD is only limited by the carriers' transit time. In theory, the bandwidth of this type of photodiode is independent of the waveguide length. However, very large size TWPDs are still very difficult to fabricate practically as the matching is more difficult. In general however, high frequency and large size TWPDs can be made with good power handling capability. A TWPD with a bandwidth of 172 GHz has been reported [12]. This type of photodiode is generally still in the research stage, and is not available commercially.

3. APD photodiodes

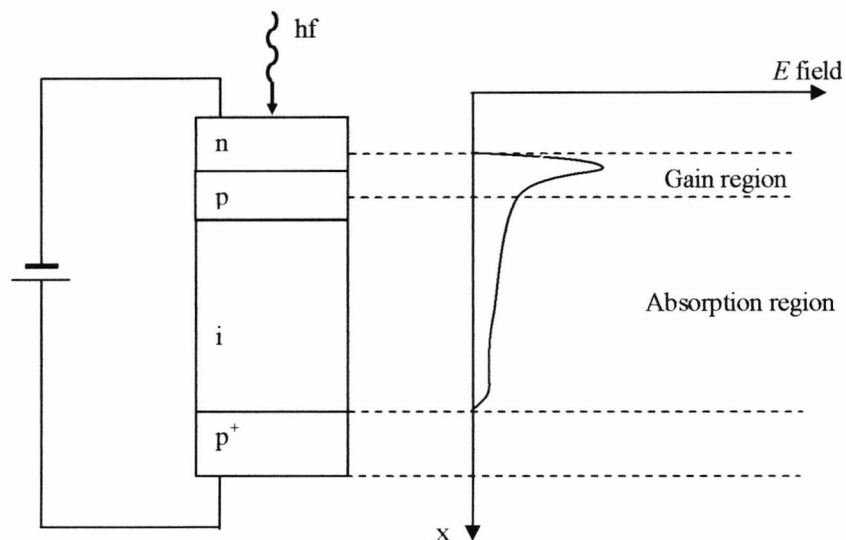


Fig 2.2 Structure of avalanche photodiode [1].

The second major type of optical communication photodetector is the avalanche photodiode (APD) [1]. The APD has a more sophisticated structure than that of the PIN photodiode, one which creates an extremely high electric field region (Fig 2.2). As well as the depletion region where most of the photons are absorbed and the primary carrier pairs generated, holes and electrons in the high field region can acquire sufficient energy to excite new electron-hole pairs. This process is known as impact ionization (avalanche multiplication process) and is the phenomenon that leads to avalanche breakdown in many ordinary reverse biased diodes. APDs often require high reverse bias voltage to

achieve the avalanche multiplication process. As the carriers will persist longer in the APD because of the secondary generation of electron-hole pairs, the response time of APDs is longer than that of PINs. Therefore, the bandwidth of APDs is lower than that of PINs.

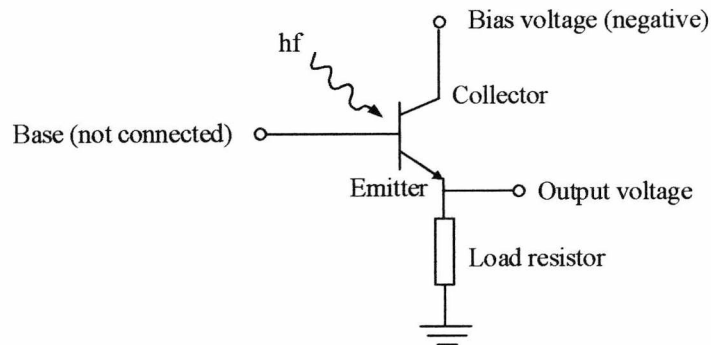
APDs have a distinct advantage over PIN photodiodes for the detection of very low levels of optical signal often encountered in optically injection-locked oscillators. They generally provide an increase in sensitivity of between 5 and 15 dB over PIN photodiodes. APDs also have drawbacks compared with PIN photodiodes:

1. Fabrication difficulties due to their more complex structure and hence increased cost.
2. The random nature of the gain mechanism that gives an additional noise contribution.
3. The high bias voltages required (typically 30 to 400V).
4. The variation of the gain (multiplication factor) with temperature; thus temperature compensation is necessary to stabilize the operation of the device.
5. The bandwidth of APD is limited to microwave frequencies.

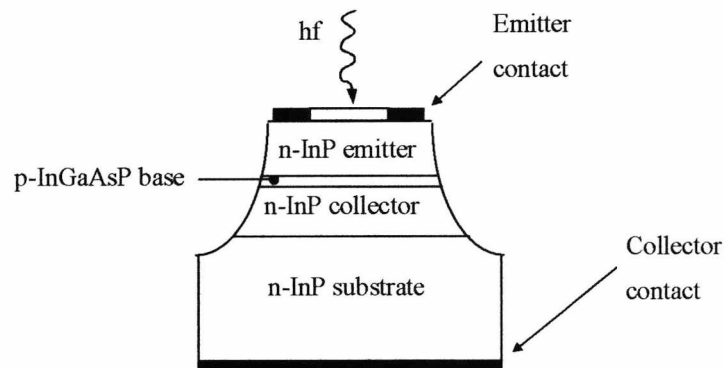
One of the advantages of optically injection-locked oscillators over the PD+Amp photoreceiver is less additive noise. However, additional noise generated by the APD will lead to a deterioration of the noise performance of the optically injection-locked oscillator. The high bias voltage required by the APD would make the bias circuit of an optically injection-locked oscillator significantly more complicated. Thus, the APD is not a good choice for microwave/millimetre-wave optically injection locked oscillators.

4. Phototransistors

Low speed phototransistors have been used in lower speed optical applications. Here we concentrate on high-speed work, so only heterojunction photo transistors (HPTs) are discussed. In common with the APD, the phototransistor (HPT) provides internal gain of the photocurrent.



(a) Symbolic representation of the n-p-n phototransistor showing the external connections.

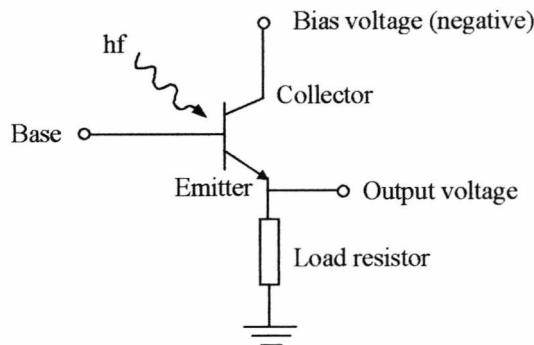


(b) Cross section of an n-p-n InGaAsP/InP heterojunction phototransistor

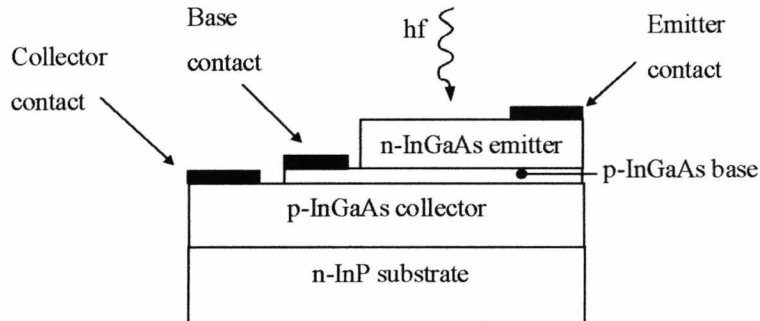
Fig 2.3 Phototransistor without base contact [13]

HPTs can be classified as HPTs with and without base contact. Fig 2.3 shows a *n-p-n* HPT with no base contact [13]. Radiation incident on the device passes unattenuated through the wide bandgap emitter and is absorbed in the base, base-collector depletion region and the collector. The base-collector junction is photosensitive to the operating optical wavelength. The current amplification characteristics of HPTs are similar to NPN transistors. The absorbed light affects the base current giving a multiplication of β to the primary photocurrent (collector current) through the device.

HPTs with base contacts have been developed in recent years [14]-[15]. Fig 2.4 shows a HPT with base contact [15]. A metal contact is fabricated on the transistor base. Comparing with the phototransistor without base contact, this device can amplify the electrical signal fed into the base as well as the photocurrent [14]-[15]. These HPTs can be used for designing high bandwidth direct optically injection-locked oscillators. This type of HPTs is very difficult to fabricate and still under the development stage.



(a) Schematic of a phototransistor with base contact



(b) Simplified cross section of a phototransistor with base contact. The detailed structure can be found in [15]

Fig 2.4 Phototransistor with base contact.

Wide locking bandwidth indirect optically injection-locked oscillators using phototransistors without base contact have been demonstrated at low frequencies [14]-[15]. Millimetre-wave long wavelength phototransistors were demonstrated only recently [14], and no such component was available during this work.

5. Summary

GaAs transistors are used by direct optically injection-locked oscillators. These transistors only work with short wavelength optical signals and have a low responsivity. PIN photodiodes are good photodetectors suitable for microwave/millimetre-wave indirect optically injection-locked oscillators. However, the optically injection-locked oscillator using PIN photodiodes suffers problems of low injection power. APD gives higher output power than that of the PIN photodiode. It is not suitable however to be used as the photodetector of the optically injection-locked oscillator because of high noise, and high bias voltage. Because of high internal electrical gain and low noise, the phototransistor is the most suitable photodetector for building both the indirect and direct optically injection-locked oscillator. The locking bandwidth of millimetre-wave optically injection-locked oscillators may be significantly improved by using such components [14].

2.3 Introduction to electrical injection-locked oscillators

Electrical injection-locking of an oscillator was first theorised by Van de Pol [19] in the 1920s. Extensive research work has been carried out since then (e.g. [20]-[35]). Electrical injection-locked oscillators can be built using various active devices. The discussion in this chapter is mainly based on the widely used transistor injection-locked oscillator.

A simplified circuit diagram to aid the understanding of the electrical injection-locking of an oscillator is shown in Fig 2.5a. The injection signal at port_1 is applied to an oscillator's output by a circulator. At the oscillator output (port_2), the injected signal is mixed with the oscillator output signal, and injection locking occurs. The injection-locked signal presented at port_3 may be observed by an electrical spectrum analyser (ESA). As the injection signal is applied at the oscillator output, we define this type of injection locking as reflection type injection-locking.

The injection signal can also be applied at the resonator of a free-running oscillator as shown Fig 2.5b. Again, a transistor is employed as the active device of the oscillator, and the resonator is connected with the transistor base. The injection signal is applied at the transistor base. No circulator is required for this type of oscillator. The injection-locked output can be observed at the oscillator output by an ESA. For this type of injection-locking, the injection signal is applied at the input port and amplified by the transistor. We define this type of injection-locking as transmission type injection-locking.

A free-running oscillator can also be locked harmonically (injection signal frequency is at a harmonic frequency of the free-running frequency) and subharmonically (injection signal frequency is at a subharmonic frequency of the free-running frequency) [29]-[31].

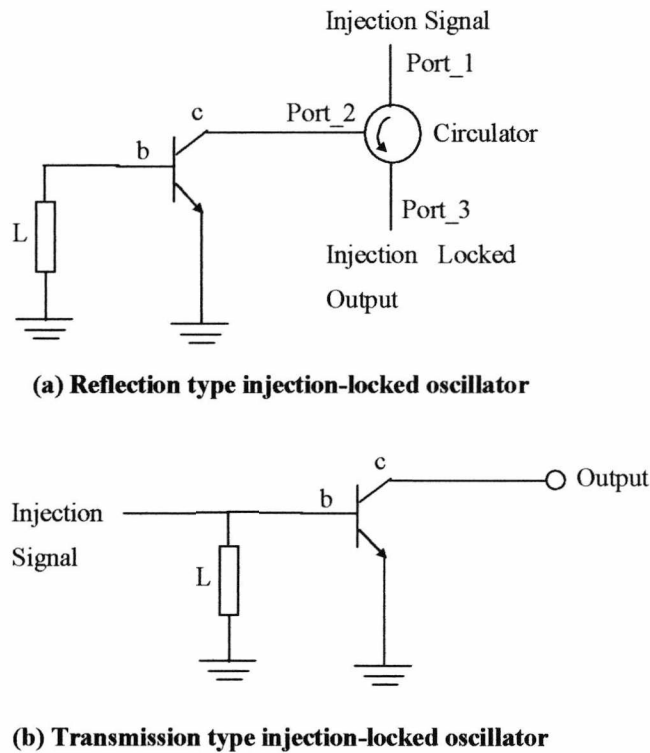


Fig 2.5 Configuration of injection-locked and optical injection-locked oscillator

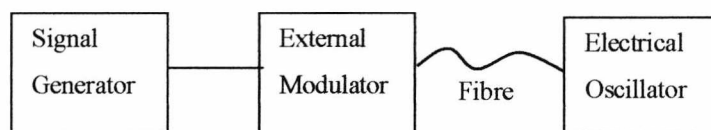
2.4 Optically injection-locked oscillator

2.4.1 Definition and classification of optically injection-locked oscillators

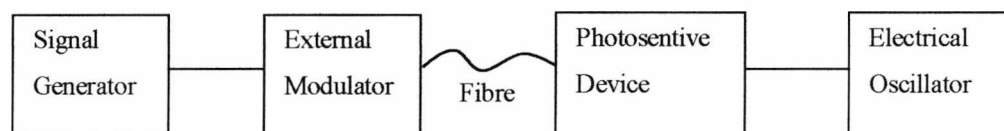
Optically injection-locked oscillators can be classified as direct optically injection-locked oscillators and indirect optically injection-locked oscillators according to the way the injection signal is converted from the optical domain into the electrical domain.

In order to optically injection-lock an oscillator directly, the electrical injection signal is first modulated onto an optical carrier (light), and this optical signal is used to illuminate the active area of the transistor (active device) of an electrical oscillator (Fig 2.6a).

For an indirect optically injection-locked oscillator, a photosensitive device inside the oscillator will convert the injection signal from the optical domain to the electrical domain and the electrical injection signal is then applied to the electrical oscillator (Fig 2.6b). Indirect optically injection-locked oscillators can also be classified as reflection type indirect optically injection-locked oscillators and transmission-type indirect optically injection-locked oscillators.



(a) Direct injection-locked oscillator

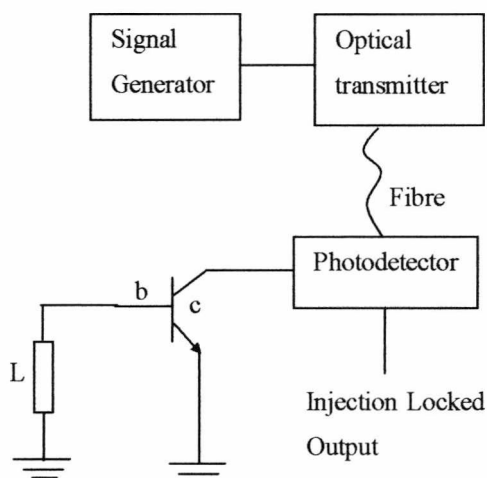


(b) Indirect injection-locked oscillator

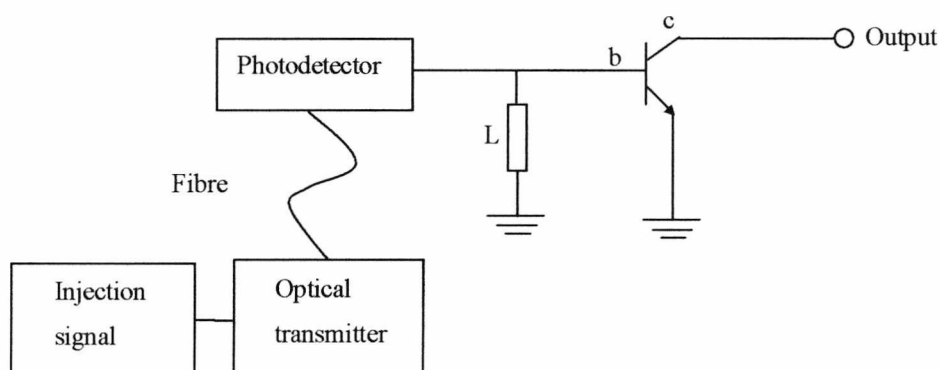
Fig 2.6 Direct and indirect optically injection-locked oscillator

Configurations of reflection and transmission type indirect optically injection-locked oscillators are shown in Fig 2.7. For a reflection type indirect optically injection-locked

oscillator, the injection signal is applied at the oscillator output. Different from the electrical reflection type injection-locked oscillator, no circulator is required for this type of oscillator as the oscillator output is decoupled from injection source by the photodiode (no electrical output signal will be converted to optical signal and interface with the optical injection signal). Different from the electrical transmission type injection-locked oscillator, a photodetector is employed at the input of the transmission type indirect optically injection-locked oscillator to convert the injection-signal from optical domain to electrical domain.



(a) Reflection type indirect optically injection-locked oscillator



(b) Transmission type indirect optically injection-locked oscillator

Fig 2.7 Configurations of indirect optically injection-locked oscillator

2.4.2 Advantages and disadvantages of optically injection-locked oscillators

Optically injection-locked oscillators share the same advantages as those of electrical injection-locked oscillators, such as:

- As injection signal power is lower than the oscillator free-running power, the optically injection-locked oscillator can provide significant gain (typically more than 30 dB) to the injection signal.
- A noisy free-running output signal can be purified by less noisy injection signals.
- Constant output power with variation of injection signal power.

In addition to the above advantages, optically injection-locked oscillators also offer the advantage of high electrical isolation. Optically injection-locked oscillators allow us to synchronise the frequency and phase of free-running oscillators to an optically delivered reference signal. Therefore, high frequency signals modulated on to optical carriers can be distributed for great distances without amplification as a result of the low insertion loss of optical fibres.

Along with the common advantages stated above, different types of optically injection-locked oscillators have their own advantages and disadvantages. Direct optically injection-locked oscillators are the easiest to design and build. However, the responsivity of the active device is normally low, also most of these active devices only work with short wavelength optical signals. These problems can be overcome by using phototransistors which are still not commercially available [14]. Compared with direct optically injection-locked oscillator, indirect optically injection-locked oscillators are more difficult to design and fabricate. However, they do not have the operating wavelength limitation as a separate photodetector is used. Indirect optically injection-locked oscillators can provide a wider locking bandwidth than that of the direct optically injection-locked oscillators (detailed discussion presented in Chapter 4)

2.5 The state of current research into optically injection-locked oscillators

Research on optically injection-locked oscillators has been carried out in both theoretical and experimental arenas.

As the theory of electrical injection-locked oscillators can be applied to optically injection-locked oscillators, most researchers use the theory of electrical injection-locked oscillators to design optically injection-locked oscillators.

2.5.1 Theoretical work on electrical injection-locked oscillators

The pioneering work for the theory of injection-locked oscillators was done by Van De Pol [19]. His theory has been gradually refined, extended, or simplified by other researchers including Adler [20], Kurokawa [21], Tajima [23], and many others [22], [24]-[32]. One of the most important tasks of the theoretical works on electrical injection-locked oscillators was to theoretically calculate the locking bandwidth. The first locking bandwidth equation for reflection type injection-locked oscillators was derived by Adler in 1946 [20]. Using the vector diagram method, Adler showed that the maximum locking bandwidth of an injection-locked oscillator is a function of the oscillator free running frequency, the oscillator free running output power, the injection signal power and the resonator Q . In his paper, Adler also derived theoretical equations to explain the phenomena outside the locking range. Following Adler, several researchers extended his theory for equations of unlocked oscillators [25]-[27]. The most detailed theoretical review of injection-locked oscillators was carried out by Kurokawa in 1973 [21]. In his paper, Kurokawa derived the locking bandwidth equation using the impedance locus method. He also presented a theory of injection locked oscillator noise. Most researchers have assumed that Adler's and Kurokawa's theories are identical, thus no comparison has been performed. Although, both Adler's and Kurokawa's locking bandwidth equations give the factors that affect the locking bandwidth, neither equation can predict the actual locking bandwidth of an injection-locked oscillator with great accuracy. Huang et al

presented a simulation approach for predicting the locking bandwidth and free running frequency of an injection-locked oscillator [22]. Good agreement between the simulation and experimental results has been obtained on oscillator free running frequency and output power [22]. However, the locking bandwidth still cannot be accurately predicted by Huang's approach [22]. Until now, only Adler's and Kurokawa's equations have been available to theoretically calculate the maximum locking bandwidth of an injection-locked oscillator. Theories for subharmonic and superharmonic reflection type injection-locked oscillators were also studied by several researchers [28]-[30]. Moyer and Daryoush presented locking bandwidth equations for subharmonic and superharmonic injection locking [28]. Theories for transmission type electrical injection-locked oscillators were introduced by Tajima et al [23]. He provided a general design guide for transmission type injection-locked oscillators. However, it is very difficult to predict the locking bandwidth of a transmission type injection-locked oscillator using Tajima's equations, as some parameters cannot be calculated theoretically. At present, there are still no equations that can be used to predict the locking bandwidth of a transmission type injection-locked oscillator easily. Adler's, Kurokawa's, and Tajima's theories are reviewed in Chapter 4.

Theoretical work on the application of using injection-locked oscillators as FM receivers has also been carried out. Ruthroff presented good theoretical analysis for such an application [32].

2.5.2 Experimental work on electrical injection-locked oscillators

For the experimental research on electrically injection-locked oscillators, fundamental electrically injection-locked oscillators (with the injection signal frequency equal to the oscillator free-running frequency) have been demonstrated and well explained by numerous researchers between the 1920s-1960s [19]-[21] [23]-[27], while little experimental research has been done since then. The current experimental research interests for electrical injection-locked oscillators are mainly concentrated on the subharmonic injection locking technique [28]-[31], [34]-[35]. Kamogawa et al reported a wide locking range 20-GHz-band subharmonically injection-locked oscillator employing

a novel active shunted-varactor into the oscillator loop [31]. A locking range of 700MHz at each subharmonic factor up to 32 was reported [31]. Kudszus demonstrated subharmonic injection-locking of 94 GHz MMIC oscillators [29]. FM demodulation using injection-locked oscillators has been demonstrated at radio frequencies [33].

2.5.3 Theoretical work on optically injection-locked oscillators

Theories for electrically injection-locked oscillators, such as locking bandwidth equation and noise analysis etc., can be applied to both direct and indirect optically injection-locked oscillators.

For direct optically injection-locked oscillators, the theoretical works for optically injection-locked oscillators have mainly concentrated on the modelling of active devices under optical illumination [2], [4], [36]-[38]. Optical effects in GaAs MESFET were summarised by De Salles in 1983 [4]. As discussed in Section 2.1, semiconductor material can absorb light of photon energy greater than its bandgap energy. This absorption will generate electron-hole pairs, and a current will be generated because the movement of electron-hole pairs. De Salles discussed changes of DC and RF characteristics of MESFETs under illumination. He presented a small signal equivalent circuit for MESFETs under illumination based on his experimental results [4]. A large signal model of HEMTs under illumination was reported by Zhang [38]. Large and small signal models of HEMTs/ MESFETs under illumination are very useful for the simulation of direct optically injection-locked oscillators.

The theoretical work for indirect optically injection-locked oscillators concentrates on wide locking bandwidth design. Sommer presented a design guide for high locking bandwidth indirect optically injection-locked oscillators [17]. Theoretical research on optical phase control for injection-locked oscillators has also been presented by several researchers [39] – [41].

2.5.4 Experimental work on optically injection-locked oscillators

The experimental work on optically injection-locked oscillators started in the late 1970s. Seed et al reported the first observation of injection locking using an IMPATT oscillator [42]. In the 1980s, experimental work on optically injection-locked oscillators concentrated mainly on the direct injection-locking of GaAs MESFET/HEMT oscillators [43]-[45].

Advances in the experimental work on optically injection-locked oscillators occurred in the 1990's [16]-[17], [46]-[54]. Optical injection-locking using different types of oscillators was demonstrated [16], [47], [49]. Bangert et al demonstrated the first direct optical injection-locking of a heterojunction bipolar transistor [16]. Higgins et al reported direct optical injection-locking of a resonant tunnel diode oscillator [48]. Cadiou et al reported direct injection-locking of a 20 GHz superlattice oscillator [49]. Wide-bandwidth injection-locked oscillators using both direct and indirect injection-locking techniques have been reported. Until now, the widest reported absolute locking bandwidth was achieved by Kamitsuna using the direct optical injection-locking technique [50]. A photosensitive HBT was used as the active device. The free-running frequency of the oscillator was 15 GHz, and a maximum locking bandwidth was 567 MHz. The widest relative locking bandwidth was achieved by Sommer et al. using a 2.1 GHz optically indirect injection-locked oscillator. A phototransistor was used as the photodetector. A maximum locking bandwidth of 227 MHz was reported (more than 10% of the free-running frequency) [17]. High frequency optical injection-locked oscillators have also been demonstrated [51]-[52]. The first millimetre-wave optically indirect injection-locked oscillator working with long wavelength optical signal was demonstrated in this work [52]. The first wide locking bandwidth (768 MHz locking range with a free-running frequency of 38 GHz) millimetre-wave direct optically injection-locked oscillator working with long wavelength optical signal was demonstrated by Kamitsuna et al using a millimetre-wave HPT [54]

The future research areas will be improvement of locking bandwidth by using different oscillator structures and investigation of other possible applications.

2.6 Applications of optically injection-locked oscillators

Before the 1990s, the most common application of optically injection-locked oscillators was in beam-steering active phased-array antennas [55]. The application of optically injection-locked oscillators in millimetre-wave radio-over-fibre systems started to attract significant research interest in the 1990s [56]-[58]. The advantages of using millimetre-wave optically injection-locked oscillators in such systems include low-cost, high gain, and low additional phase noise. The major applications of the millimetre-wave radio-over-fibre system are in wireless communication and wireless local area networks.

The target application of the millimetre-wave optically injection-locked oscillator designed and built in this work was in radio-over-fibre systems. Therefore, in the following sections, the architecture of a microwave/millimetre-wave radio-over-fibre system will be introduced. The possible applications of optically injection-locked oscillators in radio-over-fibre systems will be introduced in detail and the advantages of using an optically injection-locked oscillator in such systems discussed. Other applications of optically injection-locked oscillators are introduced in Appendix I.

2.7 Microwave/millimetre-wave fibre radio systems

The demand for high data rate services in mobile communication is increasing and in order to deliver such services over a radio link, a wider radio frequency spectrum is required. As a result, the radio link should use higher frequency carriers because of the spectrum congestion at low frequencies (<20GHz). The use of the 60 GHz band also attracts a lot of interest because of significant atmospheric attenuation (around 17 dB/km), which allows better frequency reuse in cellular systems [59]. This requires low cost base stations installed in large volumes compared to the higher power and more expensive base stations at lower frequencies.

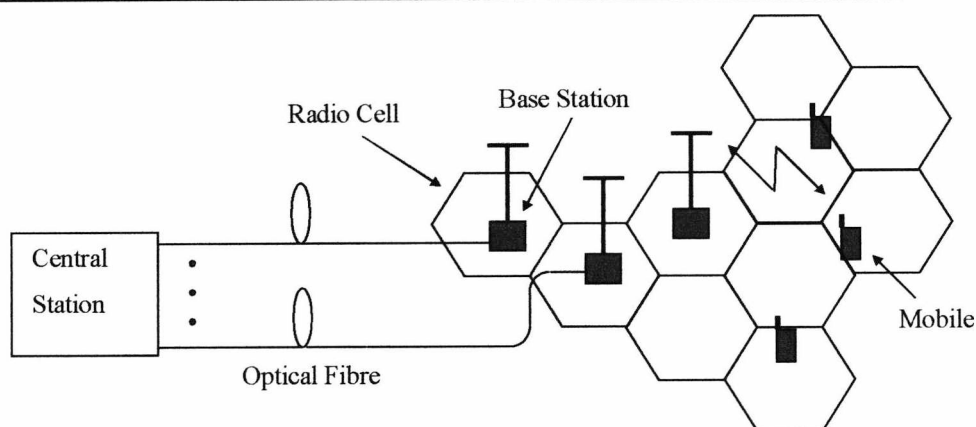


Fig 2.8 Principle of a radio-over-fibre cellular network

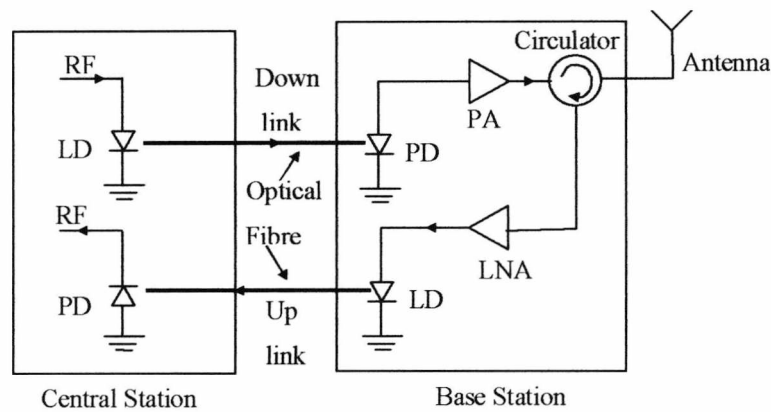
Delivering microwave/millimetre-wave signals between the central station and the base station using coaxial cable would involve high attenuation. For example, a 1 km length of common RG-405 semi-rigid microwave coax cable would have a loss of 2430 dB at 10 GHz [60], while a good quality single mode fibre of the same length has an optical loss of only 0.2 dB at 1550 nm [1] equivalent to an electrical loss of 0.4 dB. Therefore, optical fibre is the only cost effective way to transmit millimetre-wave signals over long distance.

Fibre radio systems are characterised by having both a fibre optic link and a free-space radio path. The use of a free-space radio path as the final drop to the end users enables the possibility of providing services to mobile users. Such systems are important in a number of applications, including indoor mobile communications, wireless local area networks (WLANs), and wireless local loops [61]. Fig 2.8 shows an example of part of a radio-over-fibre system architecture, consisting of one central station and several base stations. The service area is divided into radio cells. The radio link is used between the mobile users and the base stations while the optical link is used between the central station and the base stations. The millimetre-wave local oscillator signal is generated in the central station and transmitted to base stations by the low loss optical fibre. Photosensitive devices in the base stations perform an optical-electrical conversion of the signal in the down-link (central station to base station) and an electrical-optical conversion in the up-link (base station to central station). The millimetre-wave signal is received from and transmitted to the mobile users by the base station antenna units. To reduce cost, no local

millimetre-wave sources are installed in the base station. The operation frequency of the system local oscillator frequency can be easily changed by adjusting the frequency of the millimetre-wave source in the central station.

To summarise the above, we can define microwave/millimetre-wave radio-over-fibre systems as systems that deliver microwave/millimetre-wave signals using optical fibres between the central station and the base stations and have free space radio paths between the base stations and the end-users [56]-[58].

2.8 Radio-over-fibre system architectures employing optically injection-locked oscillators



PD: Photodiode, LD: Laserdiode, PA: Power amplifier, LNA: Low noise amplifier

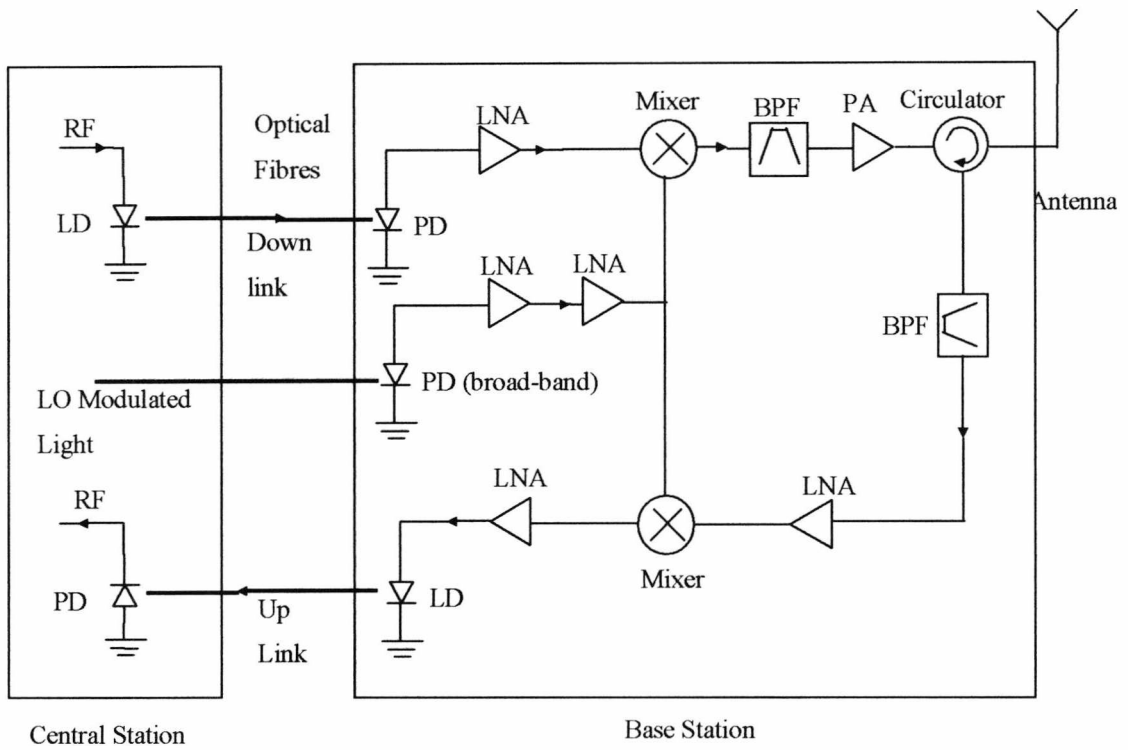
Fig 2.9 Direct modulation direct detection system

To allow duplex operation, both the central station and the base stations should be able to transmit and receive optical signals, and they must be able to perform the conversion of signals between the optical domain and the electrical domain. The most straightforward approach is the direct modulation direct detection (DMDD) scheme depicted in Fig 2.9. In the down-link (central to base station), using an intensity modulation scheme, the optical output signal of the laser diode is modulated by the RF signal which carries the information. The modulated laser diode output signal is delivered to the base station and eventually to the mobile users. At the base station site, a photodiode is used to convert

the RF modulated down-link optical signal into an electrical signal. This signal is finally radiated by the antenna after some amplification. In the up-link (base to central station), the RF signal transmitted from the mobile is first received by the base station antenna. Similar to the down-link, this signal is used to modulate the base station laser diode output directly after some amplification. At the central station, a photodiode is employed to convert the information generated by mobile users from the optical domain to the electrical domain. Circulators are normally employed at base stations to separate the up-link signal from the down-link signal. Such a system is simple and presents low cost solution for radio-over-fibre system. However, the application of this approach is limited by the modulation bandwidth of typical laser diodes to a few GHz. Although semiconductor lasers offering modulation bandwidth of 30 GHz have been realised in research laboratories [61] they are still expensive and difficult to obtain. External modulators can be used to extend the operational frequency of such systems to the millimetre-wave region. A single side band modulation scheme needs to be employed to overcome the dispersion problem in such systems [62].

Fig 2.10 shows a simple millimetre-wave radio-over-fibre system. The millimetre-wave LO and data signals generated at the central station are transmitted to base stations using fibre. At the base station site, a millimetre-wave photodiode is used to convert the LO signal to the electrical domain. The electrical LO signal is amplified and fed into the mixers. In the down-link, the IF signals detected by the down-link photodiode are up-converted to the required millimetre-wave frequency by the down-link mixer. A bandpass filter follows to filter out the unwanted side bands coming from the mixer. This signal is amplified and radiated to the mobile users by the antenna. In the up-link, the base station antenna receives the millimetre-wave signal transmitted by the mobile user. A band-pass filter prevents the following power amplifier from being saturated by signals (such as the down-link signal) at frequencies other than those of interest. The signal from the filter will be amplified first, and then down-converted to IF, amplified again and finally modulated onto an optical carrier. As the LO signal is generated by the central station using an optical single side band modulation scheme, the operating frequency can be easily adjusted by changing the LO frequency generated at the central station, with no

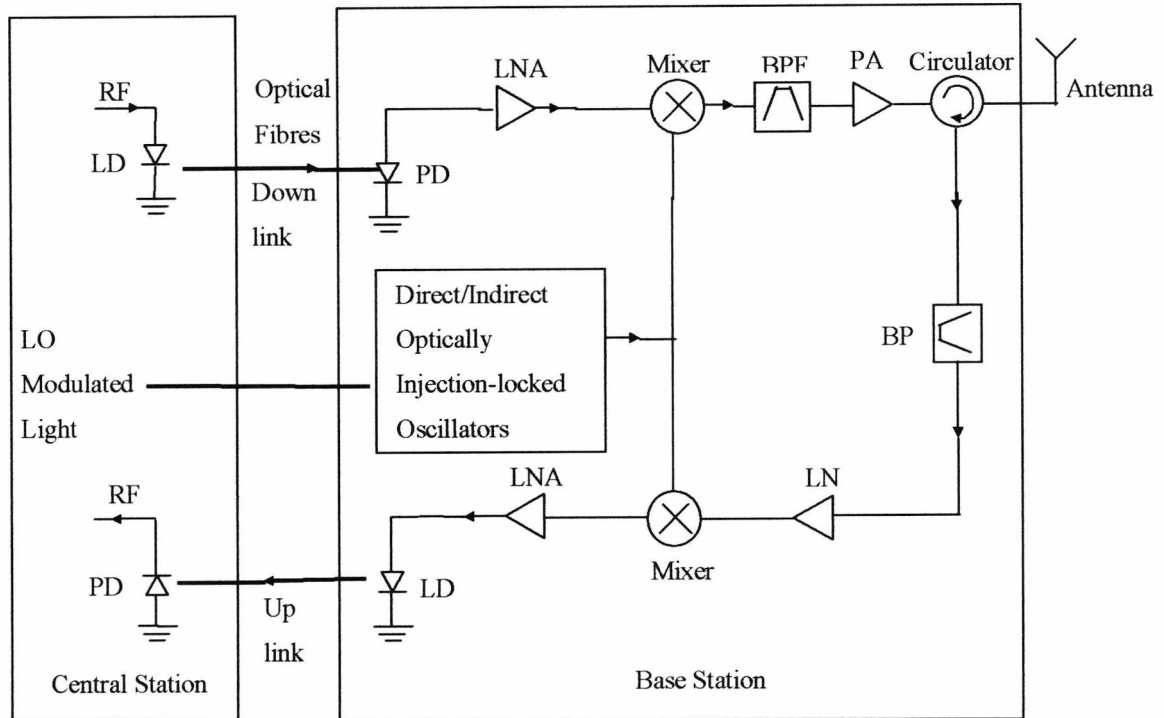
action needed in the base station. From a cost and manufacturing point of view, the base station cost is reduced because of the absence of a local oscillator source and manufacturing is much simpler as no local oscillator tuning is involved.



PD: Photodiode, LD: Laserdiode, PA: Power amplifier, LNA: Low noise amplifier, BPF: Bandpass filter.

Fig 2.10 A millimetre-wave radio-over-fibre system using an optical LO generation scheme.

The millimetre-wave optically injection-locked oscillator is considered as a low cost and high performance replacement for the broadband photodiode and amplifiers that convert the optically modulated LO signal into an electrical signal. Fig 2.11 shows the basic design of base stations for millimetre-wave radio-over fibre systems using an optically injection-locked oscillator. Compared with Fig 2.10, a millimetre-wave optically injection-locked oscillator has replaced the broadband photodiode and the two amplifiers connected with it.



PD: Photodiode, LD: Laser diode, PA: Power Amplifier, LNA: Low Noise Amplifier, BPF: Bandpass Filter. OILO: Optically Injection Locked Oscillator.

Fig 2.11 A Millimetre-wave Radio-over-fibre System Using Optical LO Generation Scheme.

From the cost point of view, the cost of the HEMT used in an optically injection-locked oscillator is less than twenty pounds, and only one of these transistors is needed for each oscillator, while the two amplifiers required for the system shown in Fig 2.10 cost £50.00 each. From a performance point of view, the millimetre-wave optically injection-locked oscillator provides 40 dB electrical gain. The oscillator power is high enough to drive the mixer. However, two amplifiers are required for the photodiode plus amplifier receiver to boost the output signal to the same level. From the manufacturing point of view, the use of a millimetre-wave optically injection-locked oscillator has increased the manufacturing difficulty. However, by implementing the whole oscillator on a monolithic microwave integrated circuit (MMIC), the manufacture of millimetre-wave optically injection-locked oscillators will be much simpler.

Even though millimetre-wave optically injection-locked oscillators have many advantages, such oscillators are extremely difficult to design and fabricate, and no millimetre-wave optically injection-locked oscillators working with 1550 nm optical signals had been reported until the millimetre-wave indirect optically injection-locked oscillators presented in this work.

2.9 A 30 GHz radio-over-fibre system

The general architecture of radio-over-fibre systems has already been introduced. However, the design considerations for radio-over-fibre systems and the central base stations structures have not been discussed and neither has the performance requirement of an optically injection-locked oscillator in such a system. In this section we use a 30 GHz radio-over-fibre system designed at the University of Kent as an example to describe a complete millimetre-wave radio-over-fibre system employing optically injection-locked oscillators.

The millimetre-wave radio-over-fibre system finds its application in indoor picocellular networks. The frequency range from 30-60 GHz is attracting most research interest, because it has relatively high path loss and a high level of frequency-reuse can be achieved. Also, multipath effects caused by reflection from walls, ceiling, and floor on the system performance are significantly reduced. The 60 GHz band has a significant atmospheric attenuation and has been chosen as the target-operating band for radio-over-fibre systems [1], [63], [64]. However, the millimetre-wave components working at this frequency are still quite expensive and difficult to obtain. Bondwires used at lower frequency to connect the MMIC chips and the passive circuits cannot be used at this frequency, because of the high radiation resistance of bondwire above 50 GHz. The alternative Flip-chip interconnection technology for connecting the MMIC devices with the passive circuits requires expensive equipment. Coplanar waveguide (CPW) is normally used for connecting components at 60 GHz, however, the structure of CPW makes design of the active device bias more difficult than when using microstrip. At lower frequency (30GHz), the millimetre-wave components are less expensive and more

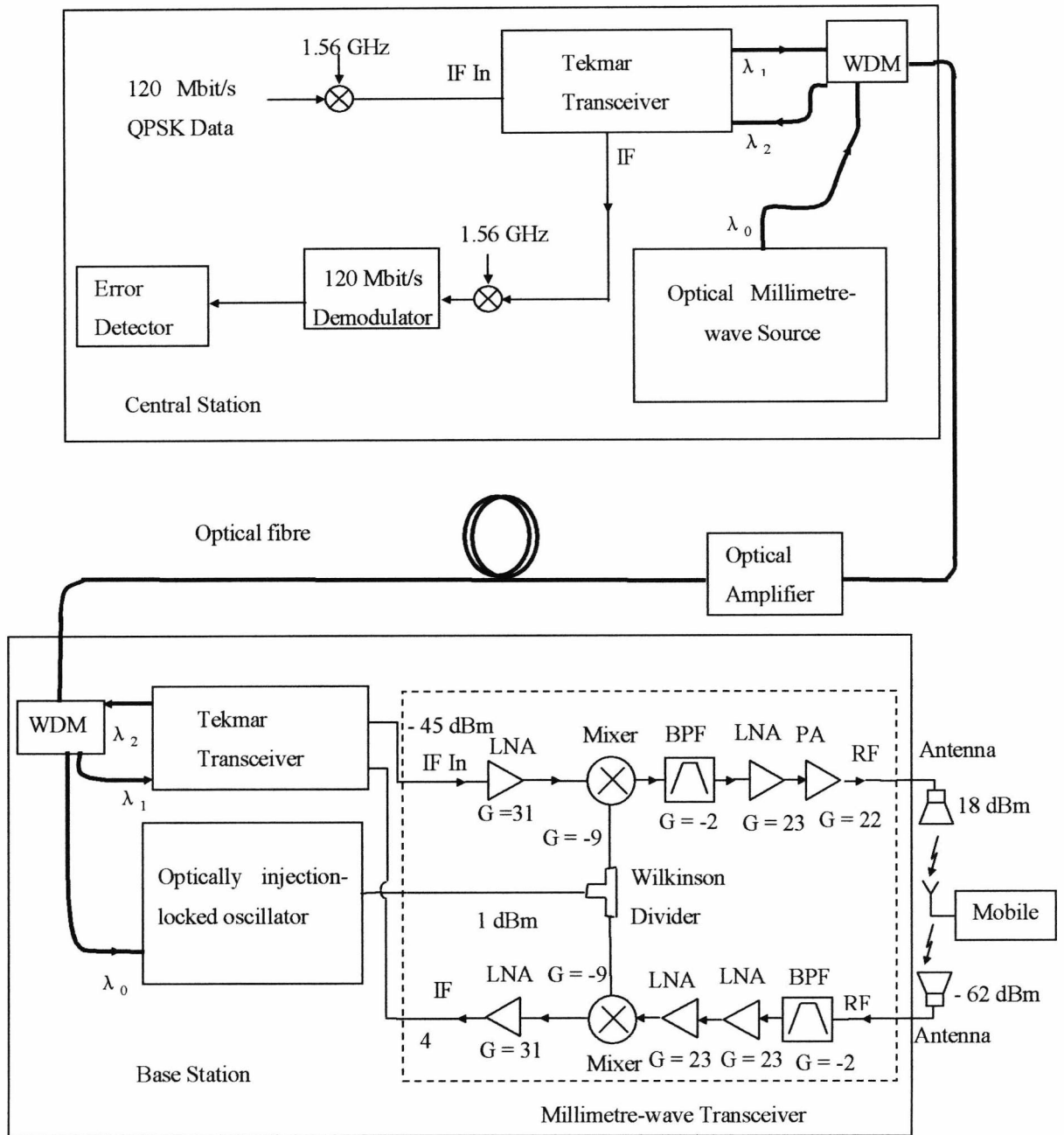
widely available commercially. The passive part of the base station module can be realised in microstrip, and bondwires are used to connect the MMIC chips to the microstrip lines. Also, the 30 GHz radio-over-fibre systems offer the same bandwidth as the 60 GHz systems. Research on 30 GHz radio-over-fibre system architectures can be directly translated to 60 GHz systems once the component costs at 60 GHz falls. For these reasons, the radio frequency of the University of Kent system was chosen to be around 30 GHz. 120 Mbit/s QPSK data is planned to be transmitted by the system.

1. Central Station

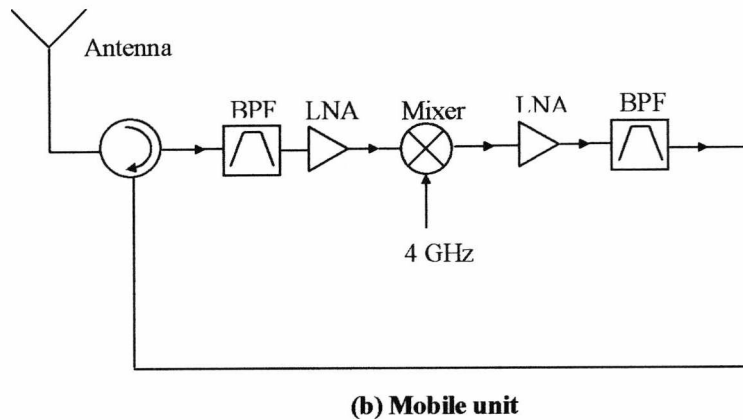
As shown in figure Fig 2.12a, a 120 Mbit/s QPSK generator can be used for the down-link data signal. A commercial Tekmar transceiver is used at the central station (CS) to modulate the data signal onto an optical carrier with a wavelength of λ_1 . The measured RF bandwidth of the Tekmar transceiver is 500MHz centred on 1.75GHz with a gain flatness of 1 dB. The 120 Mbit/s QPSK signal is up-converted on a 1.56 GHz carrier before being fed into the Tekmar transceiver.

The optical signal (λ_1) generated by the Tekmar transceiver is fed to a WDM coupler. The millimetre-wave local oscillator (LO) signal required by the base stations is also generated in the CS. An optical millimetre-wave source that can be implemented by various techniques [2]-[4] is used to generate the millimetre-wave LO signal. The millimetre-wave LO signal carried by the optical signal (λ_0) is fed into the WDM coupler at the CS before being transmitted to the base station by optical fibre.

The up-link signal generated in the base station (BS) with an optical wavelength λ_2 is separated from the other optical signals having different wavelengths (λ_1, λ_0) by the WDM coupler at the CS. Then, this RF-modulated optical signal is fed into the optical input of the Tekmar transceiver and converted into an electrical signal. The up-link signal from the Tekmar transceiver is down-converted by a 1.56 GHz reference signal and fed to a 120 Mbit/s demodulator.



(a) System architecture. (Gain, G, is in dB)



PD: Photodiode, LD: Laserdiode, PA: Power amplifier, LNA: Low noise amplifier, BPF: Bandpass filter. WDM: Wavelength division multiplexing coupler. — RF path. - - - Optical path.

Fig 2.12 30 GHz radio-over-fibre system

2. Link

Standard single model fibre (SSMF) is employed to transport the optical signal between CS and BS. Erbium-doped fibre amplifiers can be used to compensate for the loss from both WDM couplers and the SSMF.

3. Base Station

Down-link signals coming from the CS are first demultiplexed by a WDM coupler at the BS. The demultiplexed down-link signals λ_0 and λ_1 are fed to the optically injection-locked oscillator and Tekmar transceiver, respectively. The LO signal from the optically injection-locked oscillator is split equally by a power divider and fed to the LO input of the up- and down- converter mixers. The down-link signal that was modulated onto the optical carrier λ_1 is converted from the optical domain to the electrical domain at the base station by a Tekmar transceiver; after amplification it is then up-converted to millimetre-wave frequency (32 GHz) by a mixer. The millimetre-wave down-link signal is amplified and radiated to mobile receivers by the BS antenna. The up-link signal (from mobile to BS) received by the BS antenna is filtered and amplified before it is down-converted from millimetre-wave frequency (28 GHz) to microwave frequency (2GHz).

This down-converted signal is then amplified by an IF amplifier and modulated onto an optical carrier (λ_2) by the Tekmar transceiver. The up-link signal (λ_2) is multiplexed by a WDM coupler at the BS and transported to the CS by optical fibre.

4. *Mobile Unit*

The mobile unit antenna is used for both receiving and transmitting millimetre-wave signals (Fig 2.12b). A circulator is used to separate the up- and down-link signals. The down-link signal is received by the antenna then filtered by a millimetre-wave filter. A low noise amplifier is connected to the filter output to boost the down-link signal power. A mixer with a LO signal at 4 GHz is used to convert the millimetre-wave signal on the up-link frequency (32 GHz) to the down-link frequency (28 GHz). A filter follows the mixer to filter out the unwanted upper sideband signal at 36 GHz, and the antenna radiates the amplified output signal from the filter. Thus, the mobile unit here performs a loopback operation for demonstration purposes only.

5. *Performance requirement for millimetre-wave optically injection-locked oscillators*

Millimetre-wave injection-locked oscillators in this system are used to convert the LO signal from the optical domain to the electrical domain in BSs. The free running frequency needs to be the same as the LO frequency (30 GHz). The oscillator output power needs to be higher than 1 dBm to drive the mixers. The locking bandwidth should be wide enough to accommodate the variation of free-running frequency for OILOs in different BSs, and the initial target is set to be 100 MHz. The millimetre-wave optically injection-locked oscillator designed in Chapter 5 is designed using these parameters.

2.10 Other applications of optically injection-locked oscillators

There are other applications of optically injection-locked oscillators, such as the use of optically injection-locked oscillators as FM receivers and the use of optically injection-locked oscillators in phased array antenna systems. However, as the optically injection-

locked oscillator built in this work was designed for application in radio-over-fibre systems, other applications are reviewed briefly in Appendix I.

2.11 Summary

Various types of photosensitive devices for optically injection-locked oscillators have been reviewed. At present, the PIN photodiode is the most suitable for high frequency optically injection-locked oscillators.

Optically injection-locked oscillators can be classified as direct injection-locked oscillators and indirect injection-locked oscillators. The direct optically injection-locked oscillators have advantages of simple design, but, the choice of optical wavelength of the injection signal is limited by the active device. The indirect optically injection-locked oscillators can work with long wavelength signals, but they are more difficult to design. The indirect optically injection-locked oscillators can be classified as reflection and transmission types. The transmission type oscillators are expected to have a wider locking bandwidth than that of the reflection type.

The current state of research into optically injection-locked oscillators has been reviewed. The microwave components and circuits that are used to implement optically injection-locked oscillators have also been reviewed. In earlier work, low frequency optically injection-locked oscillators have been reported on. The highest absolute locking bandwidth was achieved by a direct optically injection-locked oscillator, and the highest relative locking bandwidth was achieved by a transmission type indirect optically injection-locked oscillator.

Millimetre-wave radio-over-fibre is an appealing option for future broadband wireless communication systems. The advantages of using optically injection-locked oscillators in such a system include low cost, low additive noise, and constant output power with variation of injection signal power. These advantages are more valuable at millimetre

frequencies as the output power of a conventional photodiode plus amplifier receiver is very low. However, millimetre-wave optically injection-locked oscillators are extremely difficult to design and fabricate. There is still much research to be done on this important component.

References

- [1] J. M. Senior, *Optical Fibre Communications Second Edition*, Prentice Hall International (UK) Ltd, 1992.
- [2] J. Graffeuil, P. Rossel, and H. Martinot, "Light-induced effects in GaAs FETs," *Electron. Lett.*, Vol. 15, pp. 439-441, 1979.
- [3] C. Baak, B. Elze, and G. Walf, "GaAs MESFET: A high-speed optical detector," *Electron. Lett.*, Vol. 13, pp. 193, 1977
- [4] A. A. A. De Salles, "Optical control of GaAs MESFET's," *IEEE Trans. Microwave Theory and Tech.*, Vol. 31, No. 10, pp 812-820, 1983.
- [5] R. N. Simons, K. B. Bhasin , "Microwave performance of an optically controlled AlGaAs/GaAs high electron mobility transistor and GaAs MESFET," *IEEE MTT-S Int. Microwave Symp. Dig.*, pp. 815-849, 1987.
- [6] M. A. Romero, A. L. A. Cunha, A. A. A. De Salles, "Theory and experiment for the HEMT's under optical illumination," *IEEE MTT-S Int. Microwave Symp. Dig.*, pp. 495-498, 1991.
- [7] M. A. Romero, M. Ludwig, "A direct optical injection locked 8 GHz MMIC oscillator," *IEEE MTT-S Int. Microwave Symp. Dig.*, pp. 499-502, 1991.
- [8] D. H. Newman and R. Sitchie, "Sources and detectors for optical fibre communications applications: the first 20 years," *IEE Proc. Pt. J.*, 133(3), pp. 213-229, 1986.
- [9] K. Kato, "Ultrawide-band/high-frequency photodetectors," *IEEE Trans. Microwave Theory and Tech.*, Vol. 47, No. 7, pp. 1265-1281, 1999.
- [10] M. Yaita, T. Nagatsuma, K. Kato, K. Noguchi, H. Miyazawa, T. Otsuji, "Ultrafast Optical Signal Measurement Using Optoelectronic Techniques," *Opt. Quantum Electron.*, Vol. 30, pp. 1119-1130, 1998.
- [11] D. Wake, T. P. Spooner, S. D. Perrin, L. D. Henning, "50GHz InGaAs edge-coupled pin photodetector," *Electron. Lett.*, Vol. 27, pp. 1073-1075, 1991.

- [12] K. Giboney, R. Nagarajan, T. Reynolds, S. Allen, R. Mirin, M. Rodwell, J. Bowers, "Travelling-wave photodetectors with 172-GHz and 76 GHz bandwidth-efficiency product," *IEEE Photon. Tech.*, Vol.7, pp. 412-414, 1995.
- [13] P. D. Wright, R. J. Nelson and T. Cella, "High gain InGaAsP-InP heterojunction phototransistors," *Appl. Phys. Lett.*, Vol. 37, No.2, pp. 192-194, 1980.
- [14] H. Fukano, Y. Takanashi, M. Fujimoto, "High-speed InP-InGaAs heterojunction phototransistors employing a nonalloyed electrode metal as a reflector," *IEEE Journal of Quantum Electronics*, Vol. 20, No. 12, pp. 2889-2895, 1994.
- [15] H. Kamitsuna, T. Shibata, K. Kurishima, M. Ida, "Direct Optical Injection Locking of InP/InGaAs HPT Oscillato ICs for Microwave Photonics and 40-Gbit/s-Class Optoelectronic Clock Recovery," *IEEE Trans. Microwave Theory and Tech.*, Vol. 50, No. 12, pp. 3002-3008, 2002.
- [16] A. Bangert, T. Lauterbach, "Initial observation of optical injection locking of oscillators using heterojunction bipolar transistors," *Electron. Lett*, Vol. 28, No. 7, pp. 621-623, 1992.
- [17] D. Sommer and N. J. Gomes, "Wide-locking bandwidth optically injection-locked oscillators: S-parameter design and modulation effects," *IEEE Transactions on Microwave Theory and Tech.*, Vol. 43, pp. 1424-1434, 1995.
- [18] T. Edwards, *Foundation for Microstrip Circuit Design Second Edition*, John Wiley & Sons Ltd. (UK), 1992.
- [19] Van De Pol, "Forced oscillation in a circuit with nonlinear resistance," *Phil. Mag.*, Vol. 3, pp. 65-68, 1927.
- [20] R. Adler, "A study of locking phenomena in oscillators," *Proceedings of the I.R.E. and Waves and Electrons*, Vol. 34, pp. 351-357, 1946.
- [21] K. Kurokawa, "Injection locking of microwave solid-state oscillators," *Proceedings of the IEEE*, Vol.61, No.10, pp. 1386-1410, 1973.
- [22] C. Huang, T. Chu, "Analysis of MESFET injection-locked oscillators in fundamental mode of operation," *IEEE Trans. Microwave Theory and Tech.*, Vol. 42, No. 10, pp. 1851-1857, 1994.

- [23] Y. Tajima and K. Mishima, "Transmission-type injection locking of GaAs Schottky-Barrier FET oscillators," *IEEE Trans. on Microwave Theory and Tech.*, Vol. MTT-27, No.5, pp. 386-391, 1979.
- [24] R. D. Huntoon and A. Weiss, "Synchronization of oscillators," *Proc. IRE*, Vol. 35, pp. 1415-1423, 1947.
- [25] T. J. Buckman, "The frequency spectrum of a pulled oscillator," *Proc. IRE*, vol. 40, pp. 958-961, 1952.
- [26] H. L. Stover, "Theoretical explanation for the output spectra of unlocked driven oscillators," *Proc. IEEE (Lett)*, Vol.54, pp. 310-311, 1966.
- [27] M. Armard, "On the output spectrum of unlocked driven oscillators," *Proc. IEEE (Lett)*, Vol. 57, pp. 798-799, 1969.
- [28] H. P. Moyer and A. S. Daryoush, "A unified analytical model and experimental validations of injection-locking processes," *IEEE Trans. on Microwave Theory and Tech.*, Vol.48, No.4, pp. 493-499, 2000.
- [29] S. Kudszus, W.H. Haydl, M. Neumann, A. Bangert, A. Hülsmann, "Subharmonically injection locked 94 GHz MMIC HEMT oscillator using coplanar technology," *IEEE MTT-S Int. Microwave Symp. Dig.*, pp. 1585-1588, 1998.
- [30] J. Y. Lee, U. S. Hong, "Push-push subharmonically injection-locked oscillator," *Electron. Lett.*, Vol. 32, No. 19, pp. 1792-1793, 1996.
- [31] K. Kamogawa, T. Tokumitsu, and I. Toyota, "A 20-GHz-Band subharmonically injection-locked oscillator MMIC with wide locking range," *IEEE Microwave and Guided Wave Letters*, Vol. 7, No.8, pp.233-235, 1997.
- [32] C. L. Ruthroff, "Injection-locked oscillator FM receiver analysis," *Bell Syst. Tech. J.*, Vol. 47, pp. 1653-1661, 1968.
- [33] E. Main, D. Coffing, "FM demodulation using an injection-locked oscillator," *IEEE Radio Frequency Integrated Circuit System Symp. Dig.*, pp. 227 – 230, 2000.
- [34] D. A. Fleri and R. J. Socci, "Amplifying properties of Gunn oscillator in injection locked mode," *Proc. IEEE (lett.)*, Vol. 57, pp. 1205-1206, 1969.

- [35] T. Tokumitsu, K. Kamogawa, I. Toyoda, M. Aikawa, "A novel injection-locked oscillator MMIC with combined ultrawide-band active combiner/divider and amplifiers," *IEEE Trans. Microwave Theory and Tech.*, Vol. 42, No. 12, pp. 2572-2578, 1994.
- [36] D. Warren, J. Golio, "Simulation of optically injection-locked microwave oscillators using a novel spic model," *IEEE Trans. Microwave Theory and Tech.*, Vol. 36, No. 11, pp.1535- 1539, 1998.
- [37] C. Beaulien, M. Chamberland, M. Têtu, and P. Tremblay, "Stability measurement of an optically injection-locked microwave oscillator," *Proceedings of The SPIE*, Vol. 1837, pp.346-357, 1993.
- [38] G. Zhang, R. Pollard, and C. Snowden, "Large-signal optically controlled HEMT model and oscillator design," *IEE Proceeding Microwave Antennas Propag.*, Vol. 143, No. 6, pp.487-490, 1996.
- [49] R. Esman, L. Goldberg, and J. Weller, "Optical phase control of an optically injection-locked FET microwave oscillator," *IEEE Trans Microwave Theory and Tech.*, Vol. 37, No. 10, pp.1512-1518, 1989.
- [40] X. Zhang, A. S. Daryoush, "Full 360 ° phase shifting of injection-locked oscillators," *IEEE Microwave and Guided Wave Letters*, Vol. 3, No.1, pp. 14-16, 1993.
- [41] A. Nagra, O. Jerphagnon, P. Chavarkar, M. VanBlaricum, R. York, "Indirect optical control of microwave circuits using monolithic optically variable capacitors," *IEEE Trans. Microwave Theory and Tech.*, Vol 47, No. 7, pp. 1365-1372, 1999.
- [42] A. J. Seeds and J. R. Forrest, "Initial observations of optical injection locking of a X-band IMPATT oscillator," *Electron. Lett.*, Vol. 14, pp. 829-830, 1978.
- [43] A. Daryoush, , P. Herczfeld, Z. Turski, and P. Wahi, "Comparson of indirect optical injection-locking techniques of multiple X-band oscillators," *IEEE Trans. Microwave Theory and Tech.*, Vol. MTT-34, No. 12, pp. 1363-1369. 1986.
- [44] D. Buck, M. Cross "Optical injection locking of FET oscillator using fibre optics," *IEEE MTT-S Int. Microwave Synp. Dig.*, pp. 611-614, 1986.
- [45] L. Goldberg, "Optical injection locking of X-band FET oscillator using coherent mixing of GaAlAs lasers," *Electron. Lett.*, Vol. 19, No. 2, pp. 69-71, 1983.

- [46] P. Callaghan, S.K. Suresh Babu, N. J., Gomes, and A. K. Jastrzebski, "Optical control of MMIC oscillators," *International Journal of Optoelectronics*, Vol. 19, No. 6, pp. 467-471, 1995.
- [47] T. Higgins, J. Harvey, D. Sturzebecher, A. Paoella, and R. Lux, "Direct optical frequency modulation and injection locking of resonant tunnel diode oscillator," *Electron. Lett.*, Vol. 28, No. 17, pp. 1574-1576, 1992.
- [48] A. Bangert, J. Rosenzweig, A. Hülsmann, G. Kaufel, K. Kohler, and H. Schneider, "Optical control of pseudomorphic HEMT-based MMIC oscillators," *Microwave and Optical Technology Letters*, Vol. 6, No. 1, pp. 36-38, 1993.
- [49] J. Cadiou, J. Guena, E. Penard, P. Legaud, C. Minot, J. Palmier, H. Le Person, and J. Harmand, "Direct optical injection locking of 20 GHz superlattice oscillators," *Electronics Letters*, Vol. 30, No. 20, pp. 1690-1691, 1994.
- [50] H. Kamitsuna, "A 15-GHz direct optical injection-locked MMIC oscillator using photosensitive HBTs," *IEICE Trans. Electron.*, Vol. E79-C, pp. 40-45, 1996.
- [51] R. Saedi, A. S. Daryoush, T. Berceli, "Optically controlled 24 GHz oscillator," *Proc. of The 20th Europ. Microwave Conf.*, pp. 579-583, 1990.
- [52] X. Wang, N. J. Gomes, L. Gomez-Rojas, P. A. Davies, D. Wake, "Indirect optically injection-locked oscillator for millimeter-wave communication system," *IEEE Trans. Microwave Theory Tech.*, Vol 48, No. 12, pp. 2596-2603, 2000.
- [53] A. J. Seeds, "Optical beamforming techniques for phased-array antennas," *Microwave J.*, pp. 74-83, Jul 1992.
- [54] H. Kamitsuna, T. Shibata, K. Kurishima, M. Ida, "Direct optical injection locking of InP/InGaAs HPT oscillator ICs for Microwave Photonics and 40-Gbit/s-class optoelectronic clock recovery," *IEEE Trans. Microwave and Tech.*, Vol. 50, No. 12, pp. 3002-3008, 2002.
- [55] H. Ogawa and D. Polifko, "Fibre Optic Millimetre-wave subcarrier transmission links for personal radio communication systems," *IEEE MTT-S Int. Dig.*, pp. 555-558, 1992.
- [56] H. Ogawa, D. Polifko, S. Banba, "Millimetre-wave fibre optics systems for personal radio communication," *IEEE Trans. Microwave Theory and Tech.*, Vol. 40, No.12, pp. 2285-2293, 1992.

[57] D. Wake , L. D. Westbrook, N. G. Walker and I. C. Smith, "Microwave and millimetre-wave radio fibre," *BT Technical J.*, Vol. 11, No. 2, pp. 76-88, 1993.

[58] Federal communications commission, bulletin number 70: Millimetre wave propagation spectrum management implications, 1997.

[59] RS catalogue.

[60] Special Issue on Wireless Local Loop, *IEE Electronics and Communication Engineering Journal*, Vol. 10, No. 5, 1998.

[61] Y. Matsui, H. Murai, S. Arahira, S. Kutsuzawa and Y. Ogawa, "30 GHz bandwidth 1.55 μ m strain compression InGaAlAs-InGaAsP MQW laser," *IEEE Photonics Technology Letters*, Vol. 9, No.1, pp. 25-27, 1997.

[62] D. S. George, N. J. Gomes, P. A. Davies and D. Wake, "Further observation on the Optical generation of millimeter-wave signals by master/slave laser sideband injection-locking," *International Topical Meeting on Microwave Photonics.*, Digest, Post-deadline papers, pp. 5-7, 1997.

[63] A. S. Daryoush, "Optical synchronization of millimetre-wave oscillators for distributed Architectures," *IEEE Trans. Microwave Theory Tech.*, Vol. 38, No. 5, pp. 467-476, 1990.

[64] A. S. Daryoush, Edward Acherman, Reza Saedi, Richard Kunath, "High-speed fibre-optic links for distribution of satellite traffic," *IEEE Trans. Microwave Theory Tech.*, pp. 510-517, 1990.

Chapter 3

Design of Microwave Oscillators at High Frequencies

3.1 Introduction

The advantages of using millimetre-wave optically injection-locked oscillators in radio-over-fibre systems have been introduced in Chapter 2. The difficulties of designing optically injection-locked oscillators have also been mentioned. Knowledge of how to design and fabricate high frequency oscillators must be gained before designing millimetre-wave optically injection-locked oscillators (the main task of this work). The aim of this chapter is to introduce the steps for the computer aided design of high frequency oscillators.

Oscillators can be designed using various types of active devices. This chapter will only concentrate on oscillators using HEMTs as these have been used to design the optically injection-locked oscillators in this work.

Oscillator design topologies will be introduced at the beginning of this chapter. The negative resistance design method identified for the high frequency oscillator design

will be discussed in detail. Transistor models for HEMTs that will be used during the design will be discussed. The steps for the design of high frequency oscillators using the negative resistance method and HP Microwave/RF Design System (MDS) discussed later in this chapter will be used to design the millimetre-wave optically injection-locked oscillator that will be described in Chapter 5.

3.2 Oscillator design methods

There are two basic methods for designing oscillators [1] – [7]. The first is the closed loop gain design method, while the second is the negative impedance design method. The closed loop gain design method is normally used for designing low frequency oscillators (< 1 GHz) [1], and the negative impedance method is used for designing high frequency oscillators [2]-[7].

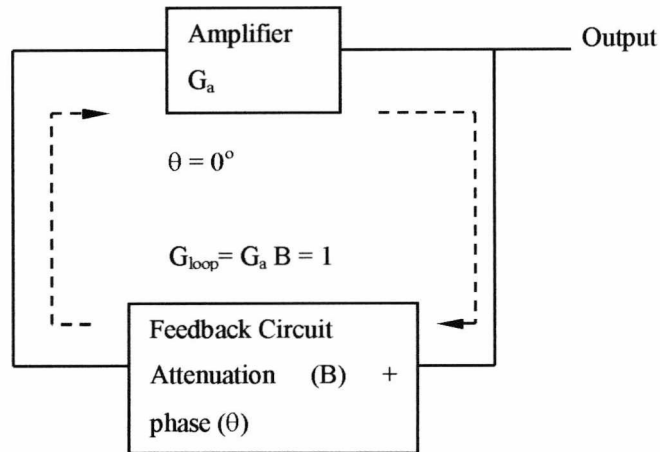
3.2.1 Closed loop gain design method

For the closed loop gain design method (see Fig 3.1), the oscillator usually consists of an amplifier and feedback circuit. Part of the output signal returns to the amplifier input through the feedback. In order to make the oscillator work in a stable state, two conditions must be satisfied:

- a. The phase change around the feedback loop must be zero at the oscillation frequency.
- b. The voltage gain around the closed feedback loop must equal 1.

Both the input and output impedance of the amplifier are assumed to be Z_0 , and practically this is achieved by employing bandpass matching networks operating near the oscillation frequency. The amplifier must also show unconditional stability over a wide range of frequencies. To make sure the oscillation can start, the amplifier gain should be larger than the feedback circuit loss in the start oscillation state.

This design method is widely used for designing low frequency oscillators [8]. At high frequencies where the parasitic capacitance of the active device needs to be considered, the phase change within the feedback loop is difficult to predict. Therefore, this design method is not commonly used for high frequency oscillator design.



The phase shift around the loop is 0° and the closed loop gain is 1.

Fig 3.1 Condition required to obtain stable oscillation in the closed loop design method

3.2.2 Negative resistance design method

The negative resistance method is widely used to design microwave oscillators [3]-[5]. This method models the oscillator active part (normally consisting of a transistor) as a port with negative input resistance. When this part is connected with a resonator, oscillation will build up until limiting reduces the net resistance to zero.

To understand a negative resistor, let us look first at a positive resistor. It is well known that when a voltage is applied to a resistor, a current, $I=V/R$ flows through the resistor R , dissipating power, $P=I^2R$. For a negative resistance, a current $I=-V/R$ will flow out of the resistor, generating a power I^2R . So a negative resistance can be regarded as a voltage or current source.

A diagram for a negative resistance oscillator is shown in Fig 3.2. The whole oscillator is split into an oscillator part (including active device and the load) and a resonator part. The resonator can be a series or parallel resonator. DC power is fed

into the active device via a DC bias circuit. Output matching between the oscillator output and the load improves the output power coupling. The load is included in the oscillator part. The input impedance for the resonator part and oscillator part are Z_R , and Z_{osc} respectively.

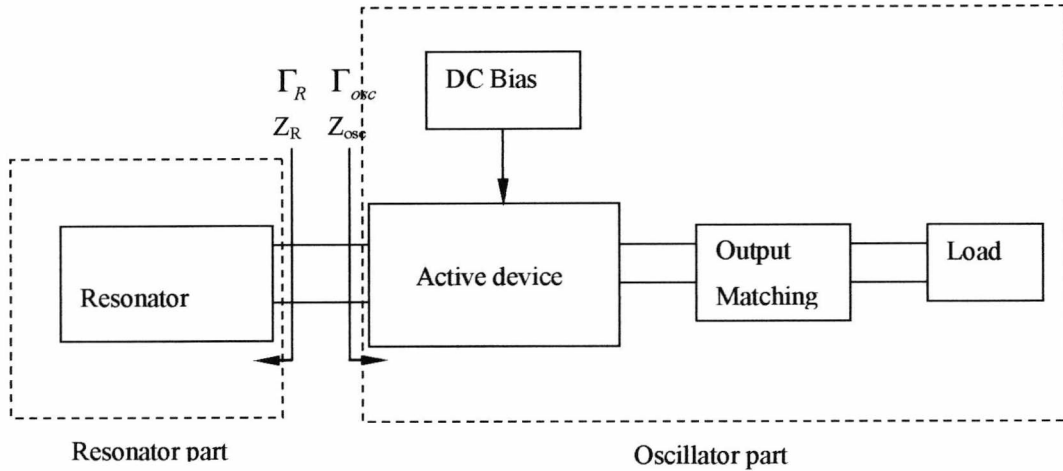


Fig 3.2 Configuration of the microwave transistor oscillator[5].

If the value of $-\text{Re}[Z_{osc}] > \text{Re}[Z_R]$ at the start oscillation state, any noise present in the circuit will be amplified and oscillation will build up within the circuit. The series resonator circuit tends to attenuate any noise except that with a frequency (f_R) at which $\text{Im}[Z_R] = -\text{Im}[Z_{osc}]$. In the stable condition, a sine wave f_R will be generated. Because of the non-linear characteristic of the active device, the magnitude of the negative resistance will decrease. Steady-state oscillation occurs when $Z_R = -Z_{osc}$. A sine wave with a frequency of f_R is generated.

The design equations for a negative resistance microwave transistor oscillator (Fig.3.2) can be given as follows [5]:

a. Start oscillation conditions

$$\text{Re} [Z_R] < |\text{Re} [Z_{osc}]| \tag{3.1}$$

where

$$\operatorname{Re}[Z_{osc}] < 0.0 \quad (3.2)$$

and

$$\operatorname{Im}[Z_R] = -\operatorname{Im}[Z_{osc}] \quad (3.3)$$

b. Steady-state oscillation conditions

$$\operatorname{Re}[Z_R] = |\operatorname{Re}[Z_{osc}(\text{Steady-state})]| \quad (3.4)$$

where

$$\operatorname{Re}[Z_{osc}(\text{Steady-state})] < 0.0 \quad (3.5)$$

and

$$\operatorname{Im}[Z_R] = -\operatorname{Im}[Z_{osc}] \quad (3.6)$$

The oscillation occurs at the frequency where $\operatorname{Im}[Z_R] + \operatorname{Im}[Z_{osc}] = 0$. Reflection coefficients can be also used to define the start and steady oscillation condition. In that case the start oscillation condition is [5]:

$$|\Gamma_R| \cdot |\Gamma_{osc}| > 1 \quad (3.7)$$

$$\arg(\Gamma_R) = \arg(\Gamma_{osc}) \quad (3.8)$$

where Γ_R and Γ_{osc} are the reflection coefficients corresponding to Z_R and Z_{osc} , and the steady-state oscillation condition is [5]:

$$|\Gamma_R| \cdot |\Gamma_{osc}| = 1 \quad (3.9)$$

$$\arg(\Gamma_R) = \arg(\Gamma_{osc}) \quad (3.10)$$

Practically, equation 3.9 is satisfied by carefully choosing the resonator and designing the oscillator part. Equation 3.10 is the main factor in determining the free-running oscillation frequency.

3.3 GaAs HEMT model

GaAs HEMTs are widely used active devices for millimetre-wave applications [9]-[11]. HEMTs were used to design the millimetre-wave optically injection-locked oscillators in this work. HEMT structures and simulation models will be discussed in the following subsections.

3.3.1 HEMT structure

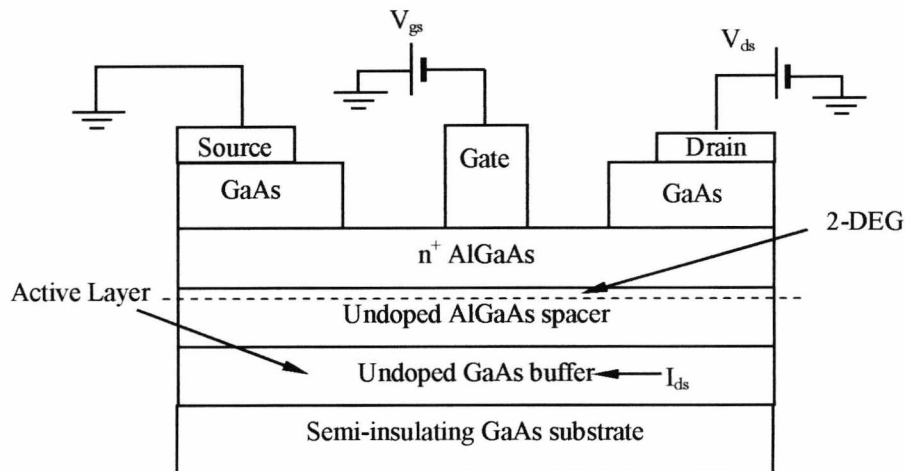


Fig 3.3 Cross section of a typical HEMT[11].

Descriptions of the HEMT can be found in numerous textbooks, for example [9]-[10]. A cross section of the structure of a HEMT is shown in Fig 3.3 [11]. The HEMT is fabricated on a semi-insulating GaAs substrate with the active layer produced by either ion implantation or epitaxial growth. Metal contacts are used to connect the gate, drain, and source to the bias circuit. Due to the higher band gap of AlGaAs compared to the adjacent GaAs region, free electrons diffuse from the AlGaAs into the GaAs and form a two-dimensional electron gas (2-DEG) at the heterointerface [9]. This 2-DEG is used as the channel region for HEMTs. The 2-DEG sheet charge

concentration can be effectively controlled by varying the gate voltage, and the current flowing through the channel is changed consequently [9].

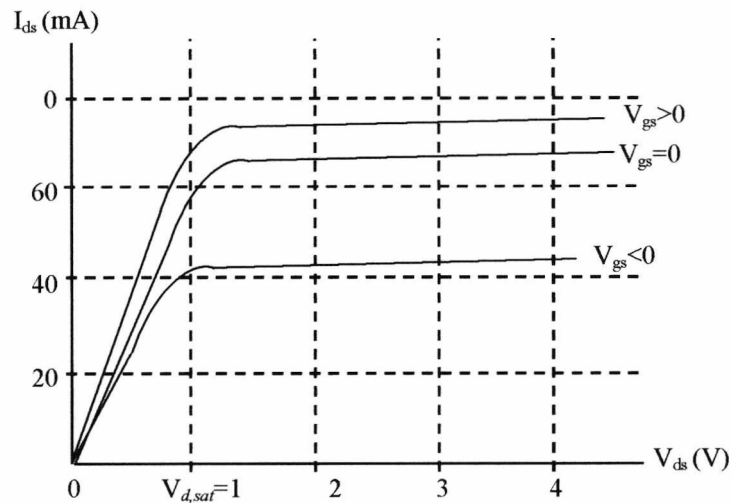


Fig 3.4 DC characteristics of HEMT [9]

A typical HEMT $I_{ds} - V_{ds}$ characteristic is presented in Fig 3.4 [9]. I_{ds} increases with V_{ds} when $V_{ds} < V_{d,sat}$ (saturation voltage); after this point, I_{ds} remains almost constant with increasing V_{ds} in what is termed the saturation region. If the drain voltage continues to increase, it will eventually exceed the gate-drain barrier breakdown voltage, and the HEMT will be damaged. The gate bias voltage is normally negative. I_{ds} is also increased with V_{gs} .

3.3.2 Other types of high frequency transistors

Heterojunction bipolar transistors (HBT) fabricated in gallium arsenide offer advantages of high current gain and cut-off frequency, high voltage handling capability, high transconductance, and high current drive capability per unit chip area [9]. All of these advantages make the HBT a better candidate for high power applications than the HEMT.

InP (indium phosphide) material can be used for fabricating HBTs as well. InP-based HBTs offer numerous advantages over GaAs-based components. These include high thermal conductivity, compatibility with long wavelength optical signals (1.3 and 1.55 μ m), and superior electron transport properties. HPTs have the similar structure as that of HBTs except the structure is optimised for optical performance, and it is the

most suitable components for optically injection-locked oscillators (See 2.2.2). Millimetre-wave HPTs were only demonstrated recently [12], with no such components available during this work.

GaAs based HEMTs were used to design millimetre-wave indirect optically injection-locked oscillators in this work.

3.3.3 Small signal model

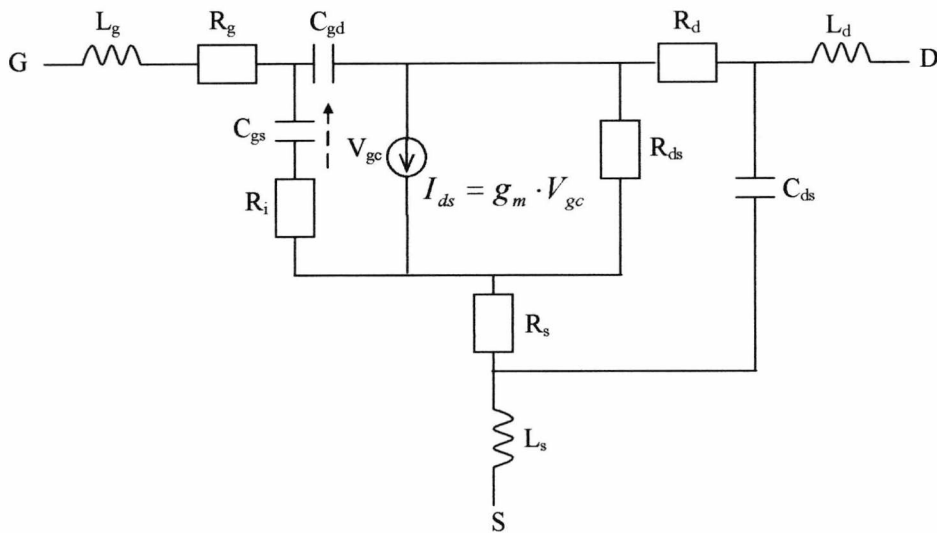


Fig 3.5 HEMT small signal model.

The most important task for modelling a HEMT is to find an appropriate equation to describe the relation between V_{ds} (drain source voltage), V_{gs} (gate source voltage), and I_{ds} (drain source current). A small signal model is commonly used to model a HEMT when the input RF signal is small. A small signal HEMT model makes the assumption that the input and output are linearly related providing the input signal is small. The small signal model is defined under certain bias conditions.

The small-signal equivalent circuit of a microwave HEMT biased in the saturation region is shown in Fig 3.5. Instead of using V_{gs} directly, the channel to gate voltage V_{gc} is used instead to derive the relation between V_{gs} and I_{ds} . The value of V_{gs} is equal to the sum of V_{gc} and the voltage drop on the input resistance R_i . The dependence of output current I_{ds} on the gate voltage is described as the transconductance g_m (the ratio of the small change in drain current produced by a small change in gate to channel voltage V_{gc}):

$$g_m = \left. \frac{\partial I_{ds}}{\partial V_{gs}} \right|_{V_{ds}=\text{Constant}} \quad (3.11)$$

The definitions of the other parameters in Fig 3.5 are:

R_{ds} : RF drain-source resistance

R_i : input resistance

C_{gs} : gate-source capacitance

C_{gd} : gate-drain capacitance

R_g : gate resistance

R_s : source resistance

R_d : drain resistance

C_{ds} : drain-source capacitance

L_s, L_g, L_d : bond wire inductances

Another simple way to model HEMT small signal performance is to use S-parameters. Many companies only provide customers with the S-parameters of the device under different bias conditions. Customers need to import these S-parameters into a “black box” provided by commercial software. The black box will be treated as the transistor small signal model.

3.3.4 Large signal model

With a large RF input signal, the variation of the DC bias voltage and current with the RF input cannot be ignored. In this case, a large signal model is used to model the RF

The Curtice quadratic model was one of the first introduced for the simulation of non-linear microwave FET devices [14], and this model was also widely used for HEMT. In the model, the drain current is described by the equation [13]:

$$I_{ds} = \beta(V_{gs} - V_P)^2(1 + \lambda V_{ds})\tanh(\alpha V_{ds}) \quad (3.12)$$

where α , β , and λ are constants with different values for different HEMT devices. V_P is the pinch-off voltage and varies for different HEMTs. The non-linear capacitance C_{gs} is given by [14]:

$$C_{gs} = C_{gs0} / \sqrt{1 - V_{gs}/V_\phi} \quad \text{for } V_P < V_{gs} \quad (3.13)$$

$$C_{gs} = C_{gs0} / \sqrt{1 + V_P/V_\phi} \quad \text{for } V_P > V_{gs} \quad (3.14)$$

where

C_{gs0} is the capacitance when $V_{gs} = 0$

V_ϕ is the built in potential of the gate-source Schottky barrier diode

The model assumes both C_{gd} and C_{gs} are given by the same equation, but with different constants (C_{gd0} should be used to calculate C_{gd}) and that they are submitted to a different reverse bias (V_ϕ should be the built in potential of the gate-drain Schottky barrier diode in the equation for C_{gd}). The V_{gs} and V_{ds} breakdown voltages are also modelled in the Curtice quadratic model, and the detailed description of this model can be found in [14].

The Curtice cubic model is considered to be an improvement over the quadratic model as a cubic relation is introduced to take account of intermodulation in microwave circuits [15]. The drain current is described by the equation,

$$I_{ds} = (A_0 + A_1V_1 + A_2V_1^2 + A_3V_1^3) \tanh(\alpha V_{ds}) \quad (3.15)$$

$$V_1 = V_{gs} e^{-j\omega\tau} [1 + \beta_c (V_{ds0} - V_{ds})] \quad (3.16)$$

where

V_{ds0} is the drain voltage at which the A_0, A_1, A_2, A_3 coefficients were determined, β_c is the pinch-off voltage coefficient, τ represents the time delay between the gate and the source voltage (transition time).

This model is widely used in the commercial market. The parameters are determined by curve fitting the simulated DC characteristics with measured DC characteristics. The non-linear capacitance and Schottky barrier gate device as depicted in Fig 3.6 are modelled in the same manner as that employed in the quadratic model.

Other larger signal transistor models are also used for modelling the large signal characteristics of HEMTs, such as the Statz-Pucel model [16] and Triquint's own model [17].

Table-based models [19]-[20] are the most accurate models available. Such models are not analytical, as they do not use parameterised equations to represent the drain and gate current as a function of terminal voltages. Instead, a series of DC and S-parameter data acquired by measuring the HEMT over a large combination of gate and drain bias are used to build up a table model. A mathematical treatment on the data generates a model capable of representing DC, small-signal and large-signal operations. The Hewlett-Packard root model [20] fits into this category. In order to build this model, 1000 measurements points need to be taken. Despite the difficulty in

building up this model, the HP root model is the most accurate HEMT model available in simulation software.

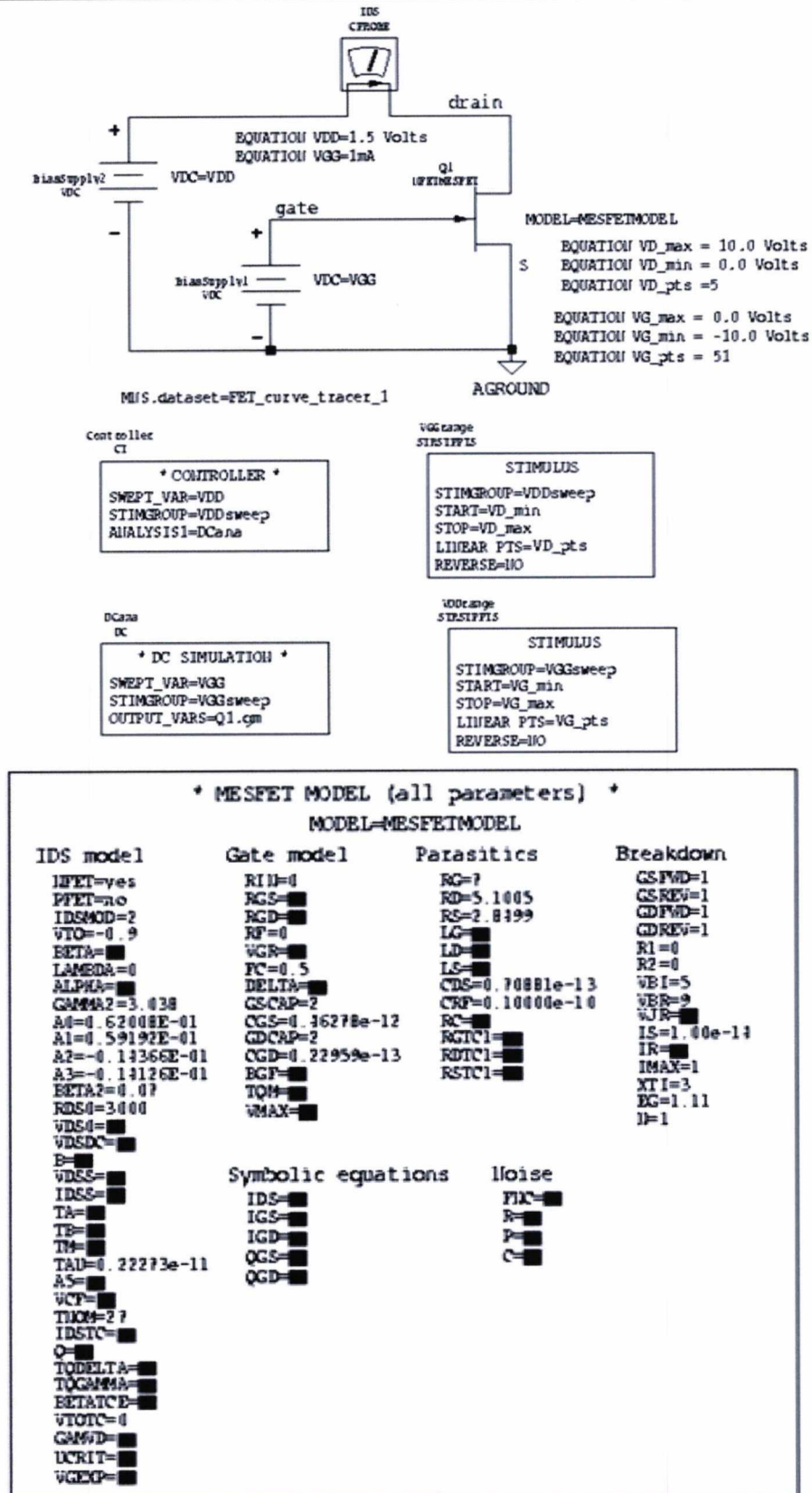
From the discussion above, we can conclude that the more accurate the large signal model, the more effort that needs to be devoted to develop the model. The choice of model is dependent on the requirement of design accuracy. Analytic equation based large signal models are the most popular models for large signal design. The Curtice cubic model of the HEMT was used to design the 15 GHz oscillator described in Appendix II.

3.4 Design of a high frequency oscillator using computer simulation

The introduction of computer simulation has greatly simplified the design of high frequency oscillators. It can give an accurate prediction of oscillation performance and becomes one of the most important steps in the oscillator design process. Special simulation components within the simulation software have been designed for predicting free-running frequency, output power, and output harmonics of high frequency oscillators. In the following subsections, the procedure of designing high frequency oscillators using the HP Microwave Design System (MDS) will be described.

3.4.1 Choice of device and device modelling

The first step for high frequency oscillator design is to find an active device that can fulfil the design targets (gain, bandwidth, and noise requirements). The second step is to match the provided large signal model to the measured DC characteristics. Almost all RF/microwave design software packages provide a special function box to perform this task. Here, the DC characteristic matching and DC simulation using the curve tracer circuit that is present in HP MDS is discussed.



The parameters related to the model in the table need to be filled before simulation

Fig 3.7 MESFET DC characteristic simulation schematic.

Fig 3.7 shows the MDS schematic for DC simulation. The HEMT is represented using a transistor symbol and a parameter form. The HEMT large signal model parameters need to be input into the parameter model form. This form is design to be used for several types of large transistor models. Therefore, parameters that are not related to the current model do not need to be entered. Sweep voltage generators are connected at both gate and drain input. The value of drain source voltage V_{ds} is varied from 0-5 volts with 151 steps, and the gate source voltage V_{gs} is varied from -1-0 volt with 6 steps. The drain current I_{ds} is monitored by a current meter connected in series between the drain and power supply.

Fig 3.8 is a general example provided by MDS showing the typical DC simulation result for a HEMT. We can see that the I_{ds} vs. V_{ds} curve has a similar shape to that of a typical HEMT DC characteristic (Fig 3.4). The model parameters may need to be readjusted to fit to the DC measurement results of the HEMT. MDS provides optimisation tools for matching the DC simulation result to the measured HEMT DC characteristics.

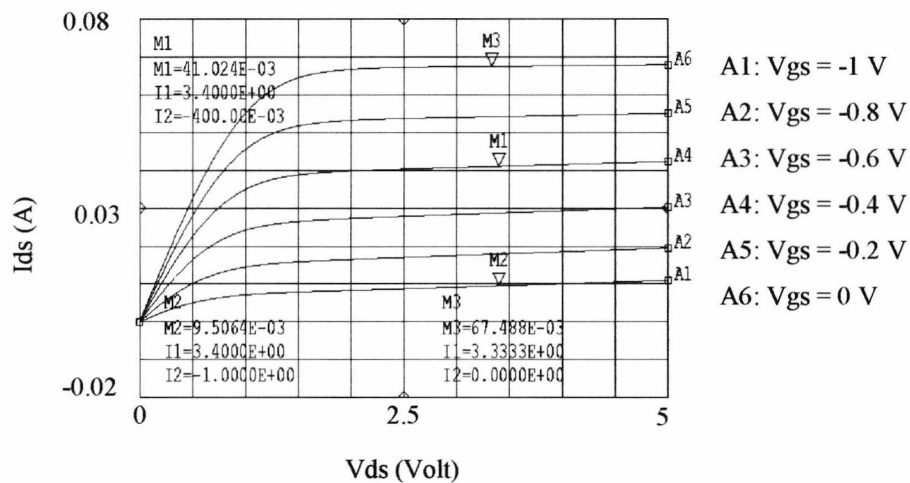


Fig 3.8 HEMT DC simulation result

3.4.2 Choice of bias topology

The second step for high frequency oscillator design is to identify the bias topology for the active devices. Advantages and disadvantages of different HEMT bias topologies will be discussed in this section.

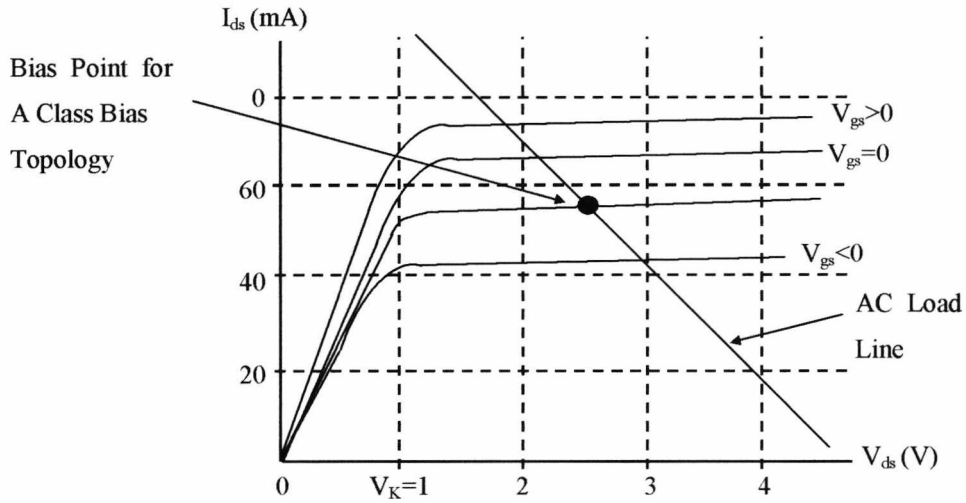
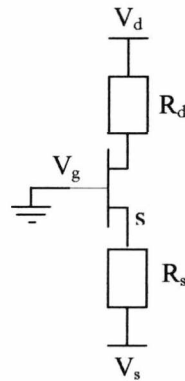
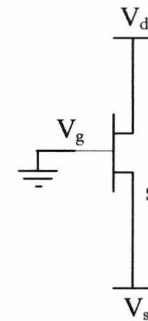


Fig 3.9 Class A Bias topology of HEMT

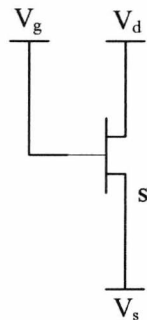
Fig 3.9 shows the AC load line on a HEMT DC characteristic diagram. For the oscillator design, the bias point is normally chosen to be in the middle of the AC load line for high output power [3].



(a) Self-bias topology



(c) Modified self-bias topology



(b) Dual supply bias topology

3.10 HEMT biasing topology

There are three commonly used bias topologies for a HEMT: self-bias topology, modified self-bias topology, and dual supply bias topology (Fig 3.10) [3]. For the self-bias topology (Fig 3.10a) the gate is grounded, DC voltage is applied to the drain through a resistor R_d , and the source is grounded through a resistor R_s . The value of R_d and R_s are determined by [3]:

$$R_s = \frac{V_{gs}}{I_{ds}} \quad (3.17)$$

$$R_d = \frac{V_{dd} - V_{ds} - V_s}{I_{ds}} \quad (3.18)$$

The advantage of the self-bias topology is that only one voltage supply is needed; the drawback is that the bias point is determined by the value of R_d and R_s , and is not easy to adjust. For an oscillator, the bias point needs to be adjusted freely to tune the free-running frequency. So the self-bias topology is not suitable for oscillator design.

Two power supplies are required for the dual supply bias topology (Fig 3.10b) [3]. DC voltages are applied at both the HEMT gate and the HEMT drain, and the HEMT source is grounded. The advantages of the dual power supply bias topology is that no bias resistors are involved and that the bias point can be tuned easily by changing voltages applied at the gate and drain. This bias topology is suitable for oscillators as the bias can be tuned easily.

To give the self-bias topology improved flexibility, the modified self-bias topology has been introduced (Fig 3.10c) [3]. By connecting another power supply to the source the two resistors can be removed, and the HEMT can be biased at any bias point required. This bias topology is also suitable for oscillator design as it also offers bias point tuning.

3.4.3 Choice of oscillator configuration

A transistor can be regarded as a three-terminal network, with the feedback network connected between two of these terminals to obtain a negative resistance at the

transistor input. There are two types of oscillator configuration, the common base configuration and the common source configuration, depending on the manner in which the feedback network is connected (Fig 3.11). In both configurations, the oscillator feedback is obtained by circulating the output RF current back to the resonator through the feedback element. The common source configuration is normally used in FET/HEMT oscillators (Fig 3.11a). For this configuration, the feedback network is realised by a shunt capacitor that is connected between the source and ground, the gate is connected with the resonator, and the drain is connected with the load. The advantage of this configuration is high output power. The common base configuration is normally used in oscillators employing bipolar transistors (Fig 3.11b). For this configuration, a shunt inductor connected between the base and ground is used as the feedback network, the emitter is connected with the resonator, and the collector is connected with the load. A common base oscillator provides lower output signal noise. The common source oscillator configuration was chosen for the design of the optically injection-locked oscillator for higher output power.

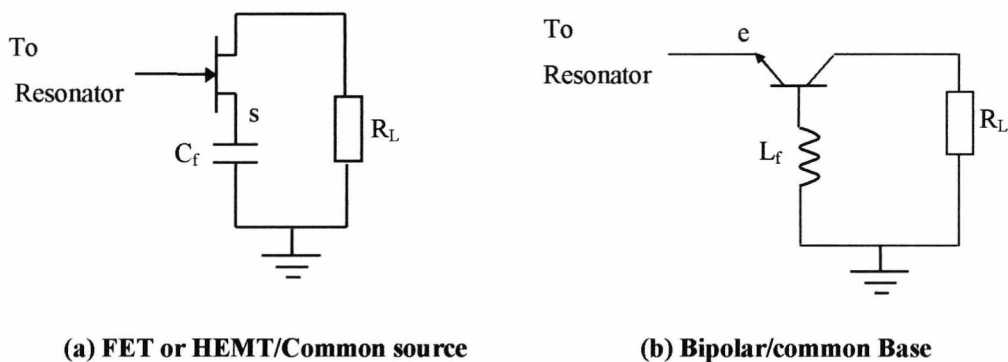


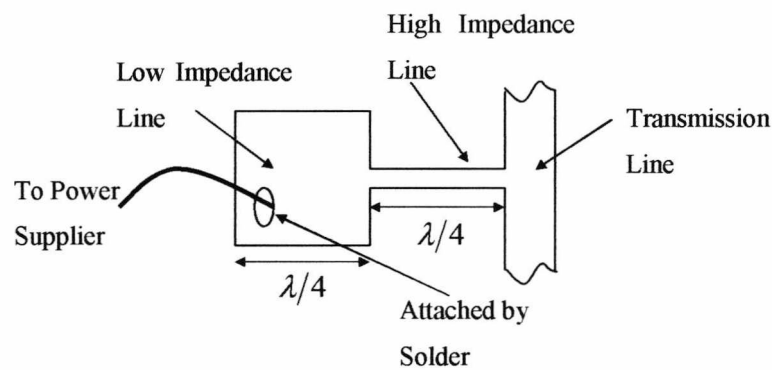
Fig 3.11 Basic microwave transistor oscillator configuration

3.4.4 RF choke design

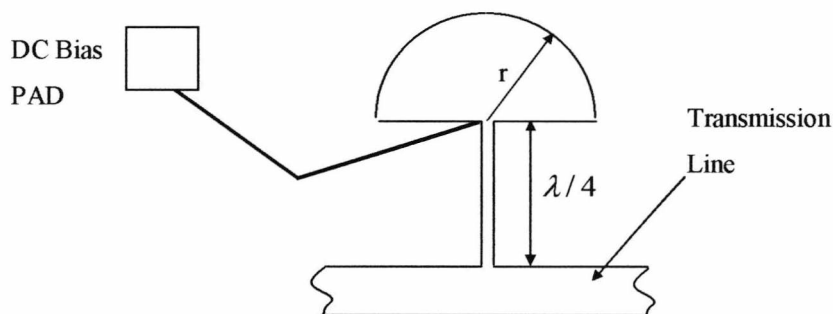
RF chokes are used to connect the bias power supplies to the oscillator to prevent the oscillator RF performance being disturbed by the changes in DC power supply. RF chokes provide a DC path for biasing the HEMT, and prevent the RF signal from the oscillator being shorted by the bias power supplies.

A lumped inductor can be used as an RF choke at low frequencies. As lumped components do not perform efficiently at frequencies higher than 4 GHz because of

parasitic capacitance, microstrip structures are used to implement RF chokes at high frequencies. The microstrip RF choke shown in Fig 3.12a is realised by two microstrip transmission lines with a length of $\lambda/4$ (λ is the microwave signal wavelength in the substrate) [5]. The first transmission line is a narrow, high characteristic impedance line, and the second, a wide, low characteristic impedance transmission line. The DC bias voltage is applied at the low impedance line. Because the dimension of the low impedance line is relatively large, it is equivalent to a shunt capacitor for the RF signal. A transmission line with a length of $\lambda/4$ transforms a short circuit to an open circuit. So the narrow transmission line transforms the RF short circuit provided by the wide transmission line to an open circuit, and the DC bias is almost “invisible” to the RF signal over the designed frequency range. Another explanation for the operation of this circuit is that the low impedance $\lambda/4$ line transforms the open circuit to a short circuit, and the narrow $\lambda/4$ line transforms the short circuit back to an open circuit. This is the reason why the length of the wide line is $\lambda/4$ as well.

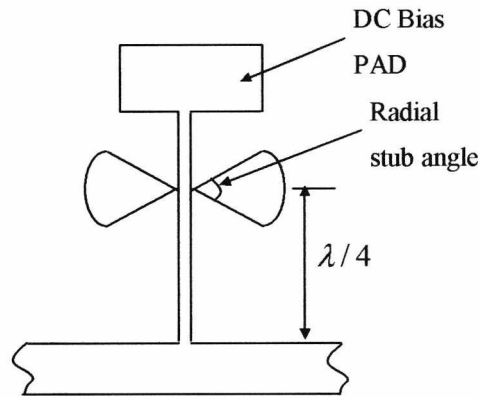


a. Two impedance line choke

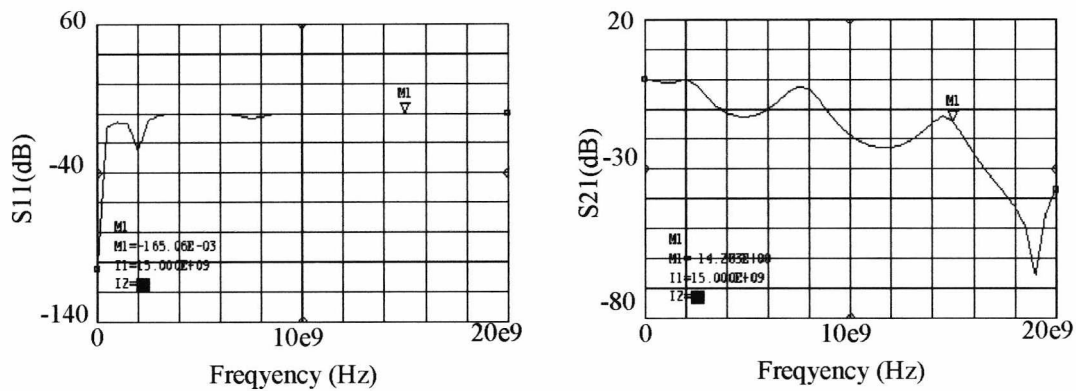


b. Broad-band microstrip DC bias circuit using radial stub [26].

Fig 3.12 Microstrip DC bias circuit



(a) Butterfly shape DC bias circuit



(b) Simulation result

Fig 3.13 Butterfly shape RF choke

Microstrip radial stubs can also be used as RF chokes. A radial stub is an open-circuit stub realised in a radial transmission line. It is a very useful element, primarily for providing a clean (no spurious resonance) broadband short circuit, much broader than that provided by a simple open-circuit stub. Unfortunately, no simple theory describes the radial stub adequately. Atwater approximated it as a cascade of microstrip line sections and gave a simple equation to calculate the dimension of radial stub resonator from 0.3 – 30 GHz [21]. As the radial stub cannot be folded or bent, it occupies a significant substrate area. For this reason, radial stubs are used primarily at high frequency, where they are relatively small. A broad-band microstrip bias circuit using a radial stub was developed by Syrett [22]. In his configuration, the RF choke is realised by a high impedance quarter wavelength microstrip line followed by a radial stub (Fig 3.12b). The DC bias was applied at the junction between the quarter wavelength microstrip line and the radial stub. Similar to the two impedance line bias topology, the radial stub behaves as a short circuit for the RF signal, and the narrow

transmission line transforms the RF short circuit to an open circuit. By changing the radius of the radial stub, we can tune the working frequency of this bias circuit.

To obtain an even wider bandwidth, a butterfly (Fig 3.13a) DC bias structure was chosen for our oscillator DC bias. Instead of having one radial stub, two radial stubs are employed to ensure a broad-band RF grounding. The equivalent circuit of the two radial stubs is two large shunt capacitors. Compared with the topology shown in Fig 3.13b, it has a lower RF grounding reactance. Fig 3.13b shows the simulation results of this bias circuit. The reflection coefficient looking from the oscillator is almost zero, which is equivalent to an open-circuit for the RF circuit. The simulation results indicate the bandwidth of this structure is extremely large (3-20 GHz). A 14 dB insertion loss at 15 GHz shows good RF isolation at the design frequency.

3.4.5 Small signal simulation

Large signal simulation of oscillators is applied at the frequency of oscillation using non-linear simulation, and provides a direct synthesis of the free-running oscillator performance. However, designing a circuit based only on large signal conditions alone does not guarantee the start up of oscillations. Therefore, a check of the small signal oscillation condition [23] is a complementary step to the large signal approach.

As we mentioned earlier, Equations 3.7 – 3.10 need to be satisfied at the resonant frequency for oscillation to start. In practice an oscillator needs to be designed with $|\Gamma_r| \cdot |\Gamma_{osc}| \geq 1.2$ at the free-running frequency to make sure the oscillation will start. For a steady oscillation Equation 3.9 and Equation 3.10 need to be satisfied.

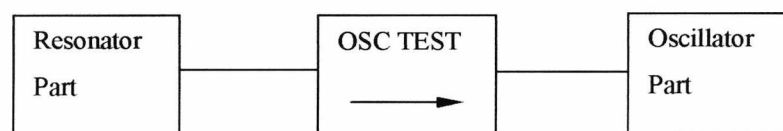


Fig 3.14 Small signal simulation test box in HP MDS

HP MDS provides a test port for oscillator small signal simulations. The port is connected between the resonator part and the oscillator part (Fig 3.14). The arrow in

the test port should be pointed to the oscillator part. The function of the test port is to find out the start oscillation frequency. Fig 3.15 shows the simulation results of a MDS example of a 5 GHz oscillator using the test port. At 5.4 GHz, the loop gain magnitude is higher than 1 dB and the loop gain phase is zero. This result shows that the oscillator would start to oscillate at 5.4 GHz.

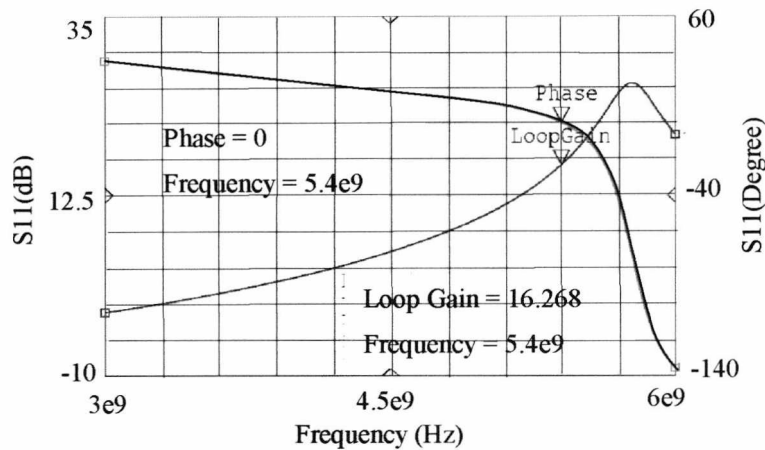


Fig 3.15 Oscillator small signal loop gain simulation

3.4.6 Large signal simulation

In order to simulate oscillator performance in the steady state, such as determination of output signal frequency, power level, harmonics, and time domain waveform, large signal oscillator (non-linear) simulation was introduced.

A HEMT large signal model is required before we can perform oscillator large signal oscillation simulation. Parameters of a large signal model are input into a large signal parameter form within MDS (Fig 3.7). The harmonic balance method is used by MDS for large signal simulation.

Before performing the harmonic balance simulation, the designed oscillation frequency needs to be input into the simulation box. This gives the simulation software a starting point for the simulation, and the software will try to find the free-running frequency of the oscillator that is supposed to be near the designed frequency. Large simulation results for a MDS example of 4 GHz oscillator are shown in Fig 3.16. The simulation results can be presented in both time domain and frequency domain (Fig 3.16). In the frequency domain, the output spectrum is plotted against the frequency (Fig 3.16a). We can see from a typical large signal simulation that the

result shows both the output signal power at the fundamental oscillation frequency and harmonics. In the time domain, the voltage waveform against time is presented (Fig 3.16b). The time domain waveform confirms the frequency domain results that the output signal contains strong harmonics.

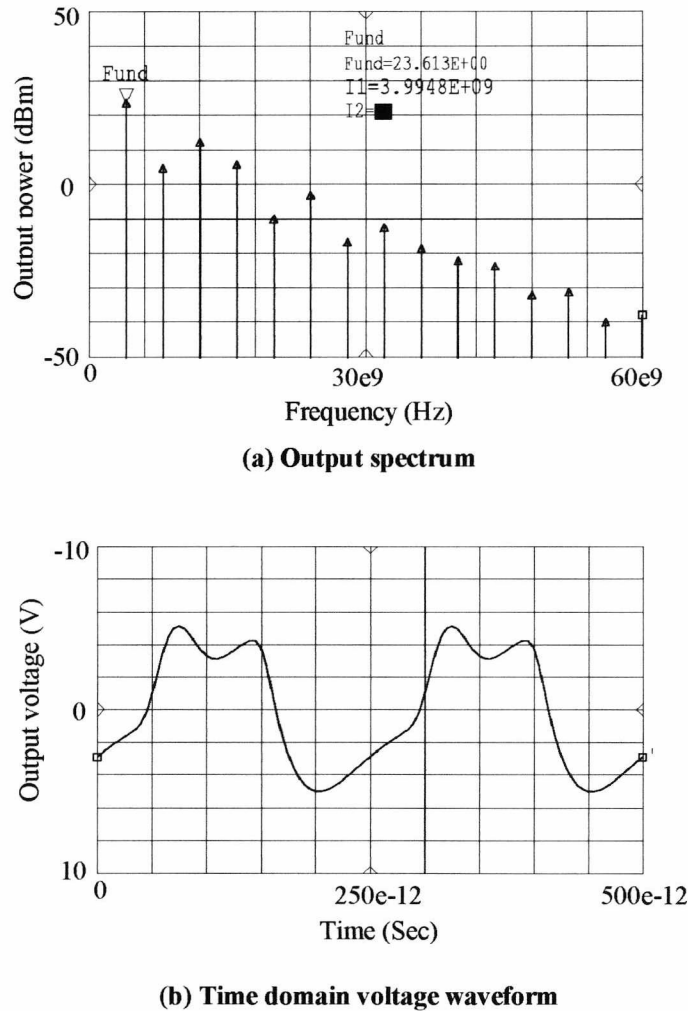


Fig 3.16 Large signal simulation of MESFET oscillator

3.4.7 Design example

The design of a high frequency oscillator using a computer simulation method has been discussed. An oscillator was designed, built, and measured in order to test the accuracy of this design method (Appendix II). Simulation results showed the start oscillation frequency was 15.8 GHz, and the oscillator provided 3 dBm output power at 15.08 GHz. Measurement results of the oscillator showed that the output power at 15 GHz was 5.2 dBm. This example showed that the computer simulation method

discussed in this chapter provides accurate prediction of the oscillator free-running frequency and output power.

3.5 Summary

In this chapter, the design of high frequency oscillators using computer simulation has been discussed. Small signal and large signal models for HEMTs have been described. Small signal models of HEMTs can be used to predict the start oscillation frequency of oscillators. Large signal models can be used to predict the steady state oscillation frequency and output power of the oscillator. Large signal simulation is the most accurate tool for predicting the free-running state of an oscillator. An accurate transistor model is required for such a simulation.

The high frequency oscillator design steps can be concluded as follows:

- a. Choose an active device that can fulfil the design targets. The active device should have sufficient gain and output power at the design frequency.
- b. Optimise the device model using software. The simulated DC and RF performance of the model should be similar to those from the measurement.
- c. Choose an oscillator configuration according to the design targets.
- d. Choose a bias topology. Identify the bias topology that meets the criteria for the best design.
- e. Design the oscillator and resonator part using the small signal simulation technique.
- f. Perform small and large signal simulations to optimise the final oscillator design.

The oscillator design example described in Appendix II shows the computer simulation technique gives a good accuracy in the prediction of the oscillator free-

running frequency. The millimetre-wave optically injection-locked oscillator discussed in Chapter 5 will use the same design steps discussed in this chapter. In Chapter 5, the description will concentrate on the integration of the photodiode.

References

- [1] P. Vizmuller, *RF design guide: Systems, Circuits and Equations*, Artech House, 1995
- [2] H. Abe, "A GaAs MESFET Oscillator Quasi-Linear Design Method," *IEEE Trans. Microwave Theory Tech.*, Vol. MTT-34, pp. 19-25, 1986.
- [3] R. W. Rhea, *Oscillator Design and Computer Simulation*, McGraw-Hill Education, 1996.
- [4] R. J. Gilmore and F. J. Rosenbaum, "An analytic approach to optimum oscillator design using S-parameters," *IEEE Trans. Microwave Theory Tech.*, Vol. MTT-31, pp. 633-639, 1987.
- [5] A. A. Sweet, *MIC and MMIC Amplifier and Oscillator Circuit Design*, Artech House Ltd, 1990.
- [6] R. M. Dougherty, "MMIC oscillator design techniques," *Microwave Journal*, pp. 161-162, Aug 1989.
- [7] E. B. L. Choo, J. A. C. Stewart, and V. F. Fusco, "Computer-aided design of nonlinear optimum output power mesfet oscillator," *Microwave and Optical Technology Letters*, Vol. 1, No.8, pp. 277-281, 1988.
- [8] T. L. Floyd, *Electronics Devices (Fourth Edition)*, Prentice Hall Inc, 1995.
- [9] S. Y. Liao, *HEMT and HBTs: Device, Fabrication, and Circuits*, Artech House Inc., 1991.
- [10] S. Y. Liao, *Microwave Devices and Circuits (Third Edition)*, Pearson Higher Education Inc., 1990.
- [11] H. Smith, and A. W. Swanson, "HEMTs-Low Noise and Power Transistors for 1 to 100 GHz," *Applied Microwave*, pp.63-72, 1989.
- [12] H. Kamitsuna, T. Shibata, K. Kurishima, M. Ida, "Direct optical injection locking of InP/InGaAs HPT oscillator ICs for Microwave Photonics and 40-Gbit/s-class optoelectronic clock recovery," *IEEE Trans. Microwave and Tech.*, Vol. 50, No. 12, pp. 3002-3008, 2002.
- [13] Y. Tajima., B. Wrona, and K. Maishima, "GaAs FET Large-Signal Model and its Application to Circuit Designs," *IEEE Transactions on Electron Devices*, Vol. ED 28, No.2, pp. 171-175, 1981.
- [14] W. Curtice, "A MESFET Model for Use in the Design of GaAs Integrated Circuits," *IEEE Trans. on Microwave Theory and Tech.*, Vol. MTT-28, No.5, pp. 448-456, 1980.

- [15] W. Curtice, and M. Ettenberg, "A Non-linear GaAs FET Model for Use in the Design of Output Circuits for Power Amplifiers," *IEEE Trans. on Microwave Theory and Tech.*, Vol. MTT-33, No.12, pp. 1383-1394, 1985.
- [16] H. Statz, P. Newman, I. M. Smith, R. A. Pucel, and H. A. Haus, "GaAs FET Device and Circuit Simulation in SPICE," *IEEE Transactions on Electron Devices*, Vol. ED 34, pp. 160-169, 1987.
- [17] Triquint Scaleable Non-linear GaAs FET EETPM1, Series IV HP-EESOF, *Microwave & RF Circuit Design Manual: Circuit Catalogue-Non-linear Devices*, Vol. 1, Chapter 12.
- [18] A. Materka, and T. Kacprzak, "Computer Calculation of Large-Signal GaAs FET Amplifier Characteristics," *IEEE Trans. on Microwave Theory and Tech.*, Vol. MTT-33, No.2, pp. 129-135, 1985.
- [19] H. A. Willing, C. Rauscher, and P. de Santis, "A Technique for Predicting Large-Signal Performance of a GaAs MESFET," *IEEE Trans. on Microwave Theory and Tech.*, Vol. MTT-26, No.12, pp. 1017-1023, 1978.
- [20] D. Root, S. Fan, and J. Meyer, "Technology Independent Large Signal Non Quasi-Static FET Models by Direct Construction from Automatically Characterised Device Data," *21st European Microwave Conference Digest*, pp. 927-939, 1991.
- [21] H. A. Atwater, "The Design of the Radial-Line Stub: A Useful Mistrostrip Circuit Element," *Microwave J.*, pp.149-156, Nov 1985.
- [22] B. A. Syrett, "A Novel Broad-Band Element for Device Bias and Microwave Tuning," *IEEE Trans. Microwave Theory and Tech.*, Vol. 28, No.8, pp. 925-926, 1980.
- [23] S. Savaria, and P. Champagna, "Linear Simulation for Use in Oscillator Design," *Microwave Journal*, pp. 98-105, May 1985.

Chapter 4

Theoretical Analysis of Optically Injection-Locked Oscillator

4.1 Introduction

The key concepts of electrical and optically injection-locked oscillators have been introduced in Chapter 2. Classifications of these oscillators have also been discussed. However, the theories for injection-locked oscillators have not yet been discussed and it is very important to understand these theories before designing an optically injection-locked oscillator. Theories for electrical and optically injection-locked oscillators are introduced in this Chapter.

As mentioned in Chapter 1, theories for optically injection-locked oscillators evolved from the theories for electrical injection-locked oscillators. Therefore, the theories of reflection type electrical injection-locked oscillators introduced by Adler and Kurokawa are reviewed first. For the first time, differences between the locking bandwidth equations from Adler and Kurokawa are discussed. The theory of transmission type injection locking is reviewed afterwards. The locking equation for transmission type injection locking derived by Tajima et al will be presented and explained. Finally, concepts of optical injection-locking and optical injection-locking techniques are discussed. Equations for both the transmission type and reflection type optically injection-locked oscillator, derived by the author, will be presented. The theories and equations described in this chapter provide the theoretical basis for the design of the millimetre-wave optically injection-locked oscillators that will be discussed in Chapter 5.

4.2 Reflection type injection locking

Most early injection locked oscillators employed the reflection type injection locking technique [1]-[3]. The following sections will present Adler's and Kurokawa's theories for such oscillators.

4.2.1 Small-signal injection-locking theory

Fig 4.1 shows the representation of a negative impedance injection locked oscillator used by Kurokawa [3]. $Z_c(\omega_i)$ is the resonator input impedance at the injection signal frequency (ω_i), $Z_d(A)$ is the active device input impedance, $E(t)$ is the injection signal voltage present at the injection point and A is the *RF* current flow between the resonator part and the active device. The resonator resistance is normally positive and the active device resistance is normally negative. The amplitude of the free-running current flow between the resonator part and the active device is defined as A_0 .

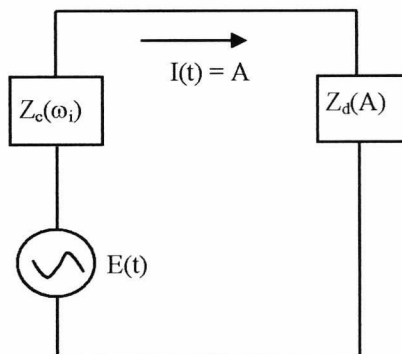


Fig 4.1 Injection -locked oscillator schematic

Under a certain bias current, it is assumed that the active device impedance is only dependent on the RF current (A) and that the resonator impedance is only dependent on the free-running frequency. From circuit theory, it is known that the instantaneous injection voltage is equal to the sum of the voltage drops across the active device and the resonator. The voltage loop equation for a stable injection-locked oscillator shown in Fig 4.1 can be written as [3]:

$$Z_c(\omega_i) \cdot A_0 e^{j\phi} - Z_d(A_0) \cdot A_0 e^{j\phi} = E \quad (4.1)$$

If both sides of the equation are divided by A_0 , this gives:

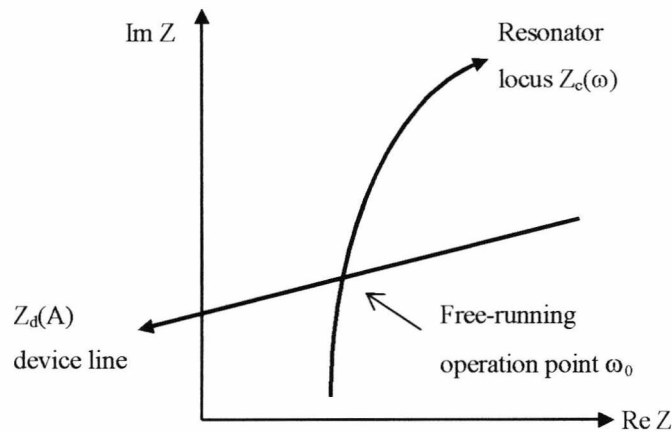
$$Z_c(\omega_i) - Z_d(A_0) = \frac{|E|}{A_0} e^{-j\phi} \quad (4.2)$$

where A_0 is the free-running RF current amplitude, and ϕ is the phase difference between the injection signal voltage amplitude E and the free-running RF current A_0 .

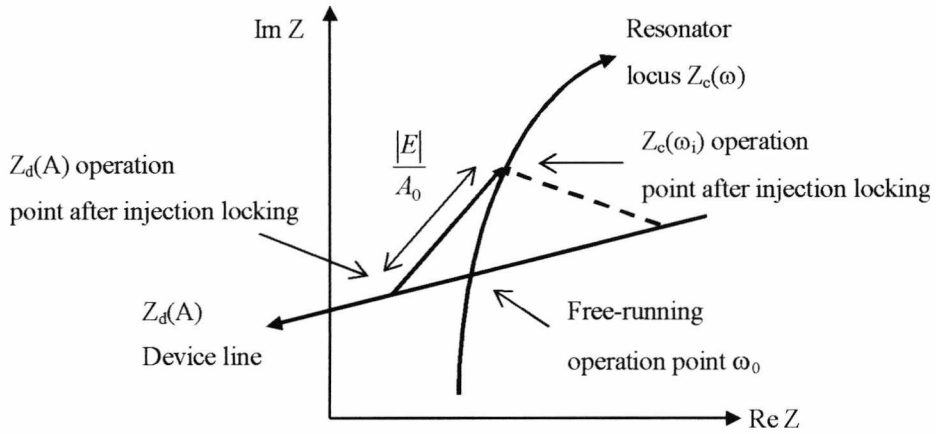
Without the injection signal, $E = 0$, equation 4.2 can be presented as shown in Fig 4.2a. As indicated by the device line and resonator locus respectively, the device resistance decreases with the increment of the RF current, and the resonator reactance increases with frequency (Fig 4.2a). The resistance of the resonator remains almost the same with variation of the frequency, and the reactance of the active device remains almost the same

with variation of the RF current flow between the resonator and active device (Fig 4.2a). The active device characteristic is dependent on the type of device that has been chosen and the design of the resonator is the major challenge when designing an oscillator. The oscillation occurs at the point where the device line and resonator locus intersect. The resonator locus is tuned to ensure the oscillator operates at the design frequency.

Suppose an injection signal is applied to a free-running oscillator. It is well known from experimental results that the oscillation output signal frequency for a locked oscillator will shift to that of the injection signal ω_i (Fig 4.2b). There are in general, two points on the device line that satisfy this condition. The corresponding vector relations are indicated by the solid and dotted arrows in Fig 4.2b. Only the stable locking vector will be discussed in the following sections. Descriptions of the dotted arrow, corresponding to an unstable condition, can be found in Kurokawa's paper [3]. The operation point on the resonator locus will shift to $Z_c(\omega_i)$. The operation point on the device line also needs to be shifted until Equation 4.1 can be satisfied. Fig 4.2b shows a stable condition of an injection-locked oscillator. As shown in Fig 4.2b, an injection signal vector ($|E|/A_0$) is introduced to describe the injection signal, with the "distance" from $Z_d(A)$ and $Z_c(\omega_i)$ equal to the injection signal vector ($|E|/A_0$).



(a) Impedance locus of a free-running oscillator



(b) Impedance locus of an injection-locked oscillator

Figure 4.2 Relationships between the injection vector, device line, and resonator locus. Presented by Kurokawa [3].

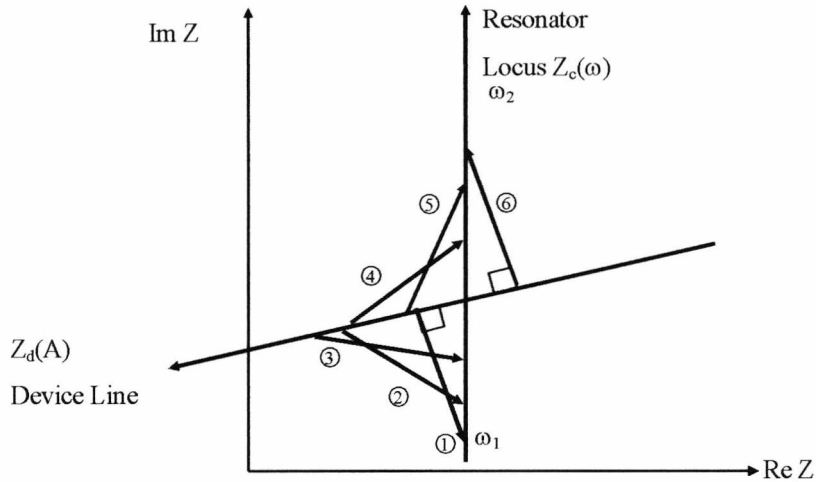


Fig 4.3 Relationship between the injection vector, device line, and circuit locus as the frequency is varied from ω_1 to ω_2 . Presented by Kurokawa [3]. The injection vector is moved from ① - ⑥ as the injection signal frequency changes from ω_1 to ω_2 .

If the injection signal power is kept constant (thus the injection signal vector length, E/A_0 remains constant) and the injection signal frequency ω_i is changed, the injection

vector $|E|/A_0$ will move along the resonator impedance locus and the device line, as shown in Fig 4.3. It can be seen that the minimum and maximum locking frequency, ω_1 and ω_2 , occur when the locking vector becomes perpendicular to the device line. The injection signal power must be increased (injection signal vector length increase) if the oscillator is to be injection-locked at a frequency higher than ω_2 or lower than ω_1 . Normally, we define the locking bandwidth of the injection locked oscillator under a certain injection power as the difference between ω_1 and ω_2 . Also, it can be seen from Fig 4.3 that as the locking frequency is varied from ω_1 to ω_2 , the phase difference between the locking vector and the device line will vary by approximately 180° for small injection signal levels.

4.2.2 Kurokawa locking bandwidth equations

A simple series resonant model of the microwave resonator is introduced by Kurokawa [3] to model the reflection type injection-locked oscillator. This model, shown in Fig 4.4, is based on the assumption of a reflection type injection-locking technique when the injection signal power is small compared with the oscillator free running output power. The oscillator active device is modelled as a negative impedance ($Z_d(A)$). A series LC resonator is used to model the resonator. The resonator resistance is represented as R_a . The injection signal is applied to the oscillator output (a-a') through a circulator. The oscillator output voltage and current at the injection point are V and I respectively. The injection signal voltage is E_i , and the load resistance is R_L . In order to match the output, Kurokawa supposed the injection source resistance was R_L as well. The quality factor of a resonator is very high (>1000) for conventional oscillators, which means the resonator resistance R_a is very small compared to the load resistance. So Kurokawa ignored the injection power loss within the resonator. Based on the assumptions above, Kurokawa calculated the injection signal current to be $E_i/2R_L$ (Fig 4.4). However, this assumption is not exactly correct for injection-locked oscillators where the resonator quality factor is quite low. The inaccuracy of Kurokawa's locking bandwidth equation due to ignoring the

effect of R_a will be discussed in 4.2.4. The resonator circuit impedance as a function of frequency can be written as:

$$Z_c(\omega) = j\left(\omega L - \frac{1}{\omega C}\right) + R_a + R_L \quad (4.3)$$

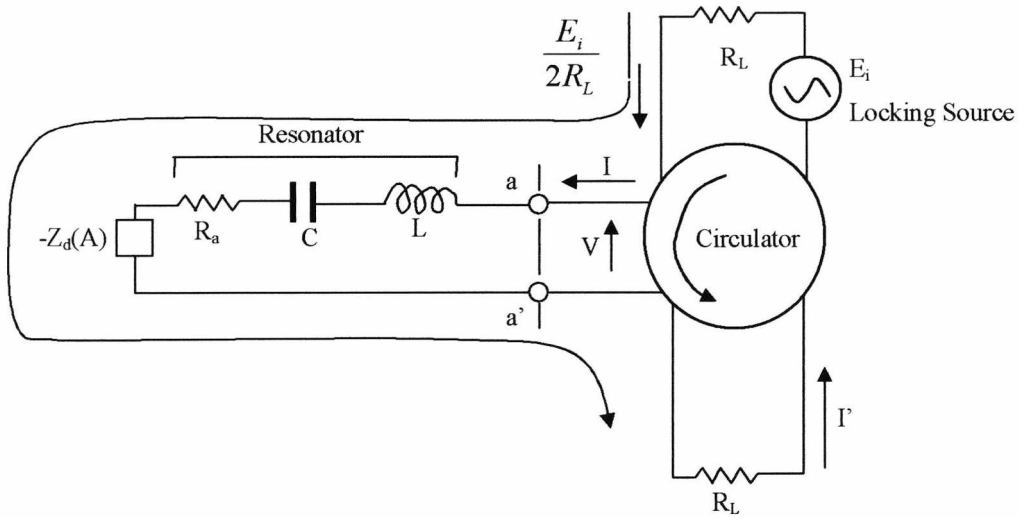


Fig 4.4 The equivalent circuit of an injection-locked oscillator with a single tuned resonator. Presented by Kurokawa [3].

The load impedance is also included as a part of the resonator because the oscillator output power is fed into the load through the circulator. Assuming the free-running frequency is approximately the same as the resonance frequency of the resonator ω_r , a Taylor expansion of equation 4.3 can be performed to give:

$$Z_c(\omega) \approx 2j(\omega - \omega_r)L + R_a + R_L \quad (4.4)$$

where:

$$\omega_r = \frac{1}{\sqrt{LC}}$$

and ω is the instantaneous frequency

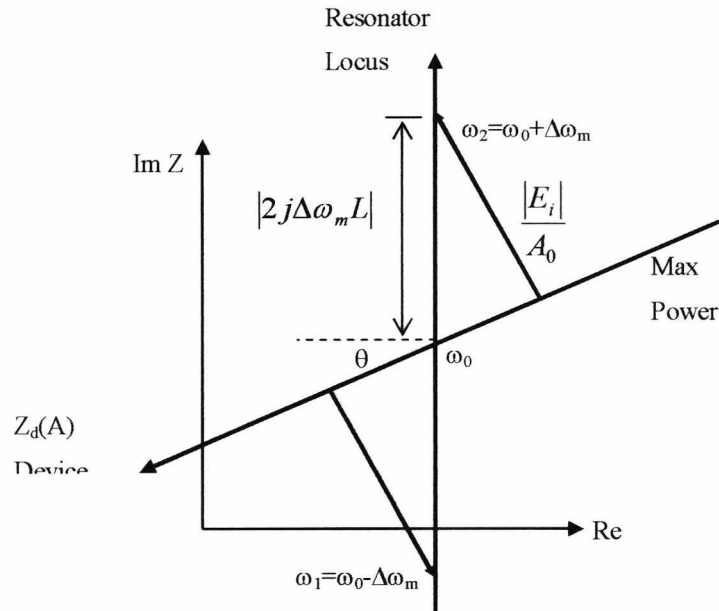


Fig 4.5 Calculation of the locking bandwidth. Presented by Kurokawa [3].

From Kurokawa's experiments, it was found that the locking range is symmetrical about the free-running frequency [3]. As regards the free running frequency ω_0 , we know the maximum and the minimum injection signal frequency to keep the locking stable, $\omega_0 + \Delta\omega_m$ and $\omega_0 - \Delta\omega_m$, occur when the injection vector is perpendicular to the device line (Fig 4.3) The distance between $\omega_0 + \Delta\omega_m$ and $\omega_0 - \Delta\omega_m$ on the resonator locus can be calculated using Equ 4.4,

$$\begin{aligned}
 & |Z_c(\omega_0 + \Delta\omega_m) - Z_c(\omega_0 - \Delta\omega_m)| \\
 &= j \left[(\omega_0 + \Delta\omega_m)L - \frac{1}{(\omega_0 + \Delta\omega_m)C} \right] + R_a + R_L - \left[j \left((\omega_0 - \Delta\omega_m)L - \frac{1}{(\omega_0 - \Delta\omega_m)C} \right) + R_a + R_L \right] \\
 &= 2j\Delta\omega_m L \quad (4.5)
 \end{aligned}$$

The locking bandwidth B is equal to twice the difference between the maximum injection signal frequency that keeps the oscillator in lock, and is equal to $|2j\Delta\omega_m L| = 2\Delta\omega_m L$ (Equation 4.5). The relationship between the resonator impedance locus, the device line,

and the injection signal vector at the maximum and minimum locking frequencies is shown in Fig 4.5. The angle between the resonator impedance locus and the device line is θ . From Fig 4.2, we know that the length of the injection vector is $|E_i|/A_0$, where E_i is the injection signal voltage at the injection point, and A_0 is the oscillator free-running RF current. At the maximum locking frequency, the relation between the injection vector and the locking bandwidth is:

$$|2\Delta\omega_m L \cos\theta| = \frac{|E_i|}{A_0} \quad (4.6)$$

The oscillator free-running output power (the power that a free-running oscillator delivers to the load) can be calculated as:

$$P_0 = \frac{1}{2} R_L A_0^2 \quad (4.7)$$

where R_L is the load resistance, and A_0 is the oscillator free-running RF current. The injection signal power at the point of injection is,

$$P_i = I_i^2 R_L = \left(\frac{E_i}{2\sqrt{2}R_L} \right)^2 \cdot R_L \quad (4.8)$$

The reason we have a $\sqrt{2}$ in the current expression is that E_i refers to the maximum injection signal voltage at the injection point, and we want to know the average injection power at the injection point. The external quality of the resonator Q_{ext} can be calculated by [2],

$$Q_{ext} = \frac{\omega_0 L}{R_L} \approx \frac{\omega_r L}{R_L} \quad (4.9)$$

where ω_0 is the oscillator free-running frequency, and ω_r is the resonance frequency of the resonator. Generally, these two frequencies are similar.

From Equation 4.7 and Equation 4.8 we have:

$$A_0 = \sqrt{\frac{2P_0}{R_L}} \quad (4.10)$$

$$|E_i| = 2\sqrt{2} \cdot \sqrt{P_i} \cdot \sqrt{R_L} \quad (4.11)$$

Substituting Equation 4.10 and 4.11 into Equation 4.6, we obtain the locking bandwidth equation:

$$2\Delta\omega_m = 2 \cdot \frac{1}{\cos\theta} \cdot \frac{R_L}{L} \cdot \sqrt{\frac{P_i}{P_0}} \quad (4.12)$$

Also from Equation 4.9 we have,

$$\frac{R_L}{L} = \frac{\omega_0}{Q_{ext}} \quad (4.13)$$

Substituting Equation 4.13 into Equation 4.12, we have the final locking bandwidth equation given by Kurokawa [3]:

$$B = 2\Delta\omega_m = \frac{2\omega_0}{Q_{ext}} \sqrt{\frac{P_i}{P_0}} \frac{1}{\cos\theta} \quad (4.14)$$

As we can calculate from Equation 4.14, when $\theta = \pi/2$, the resonator locus overlays the device line, and B is infinite. When $\theta = 0$, the resonator locus is perpendicular to the device line, and the locking bandwidth reaches the minimum value:

$$B_{\min} = \frac{2\omega_0}{Q_{ext}} \sqrt{\frac{P_i}{P_0}} \quad (4.15)$$

Normally, we use Equation 4.15 for the theoretical prediction of the oscillator bandwidth because the angle between the resonator locus and the device line is difficult to calculate.

We can see from Equation 4.14, that the resonator loss does not affect the locking bandwidth in Kurokawa's equation. The reason for this is that the resonator loss was ignored in Kurokawa's analysis; he assumed the resonator resistance was very small compared to the load resistance. Q_{ext} in Kurokawa's equation is treated as constant.

4.2.3 Adler's locking bandwidth equation

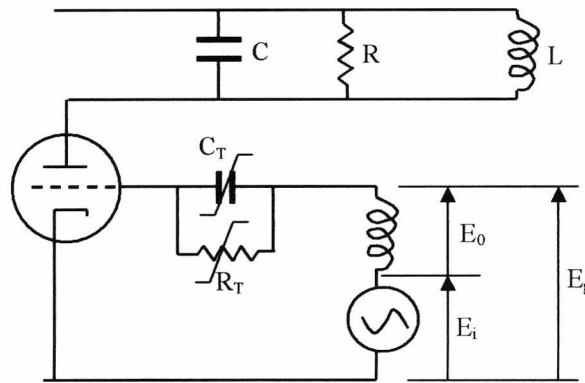


Fig 4.6 Injection-locked oscillator circuit. Presented by Adler [2]

The first locking bandwidth equation for a reflection type injection-locked oscillator was presented by Adler in 1946 [2]. Fig 4.6 shows the circuit model used by Adler. A parallel RLC resonator is used for the resonator model, where R is a resistance, giving the resonator loss. A tube transistor was used as the active device of the oscillator. E_0 is the free-running output voltage amplitude, E_i is the injection signal voltage amplitude, and E_g is the amplitude of the total voltage generated across the load after the application of the external signal.

In Adler's analysis [2], it was assumed that the external signal and the free-running oscillation are of similar frequency. Three conditions were stated as necessary in order to obtain stable injection locking. These conditions are:

The resonator circuit should produce variation of the oscillation frequency without noticeable delay. This means that the pass band of the resonator should be wide compared to the oscillation frequency variation, and the free-running oscillation and injection signal frequencies should be near the centre of this pass band. For a single tuned circuit (Fig 4.6) we can write

$$\frac{\omega_0}{2Q} \gg \Delta\omega_0 \quad (4.16)$$

where Q is the figure of merit of the resonator circuit, and

$\Delta\omega_0 = \omega_0 - \omega_i$ is the difference between the free-running frequency and injection signal frequency.

In the oscillator, some non-linear elements are required to stabilise the amplitude of the self-excited oscillation. The transistor normally introduces these non-linear elements. As the RF current begins to build up within the oscillator, the transistor is driven into the saturation region, and the RF current flowing through the oscillator will stop increasing. C_T and R_T were introduced by Adler to model the non-linear components within an oscillator. It is necessary for the non-linear elements to respond fast enough to maintain stable output signal amplitude. How fast the output signal amplitude varies depends on $\Delta\omega_0$.

Therefore, the time constant of the amplitude control circuit must be shorter than one beat cycle. For Fig 4.6, the device time constant is:

$$T = C_T \cdot R_T \quad (4.17)$$

As $\Delta\omega_0$ corresponds to the shortest beat cycle, we can write:

$$T \ll \frac{1}{\Delta\omega_0} \quad (4.18)$$

If condition (a) and (b) are fulfilled, the output signal amplitude variation is solely determined by the ratio E_i/E . As the oscillator output amplitude is almost the same after applying an external signal, the injection signal amplitude must be very small compared to the free-running oscillator output amplitude,

$$E_i \ll E \quad (4.19)$$

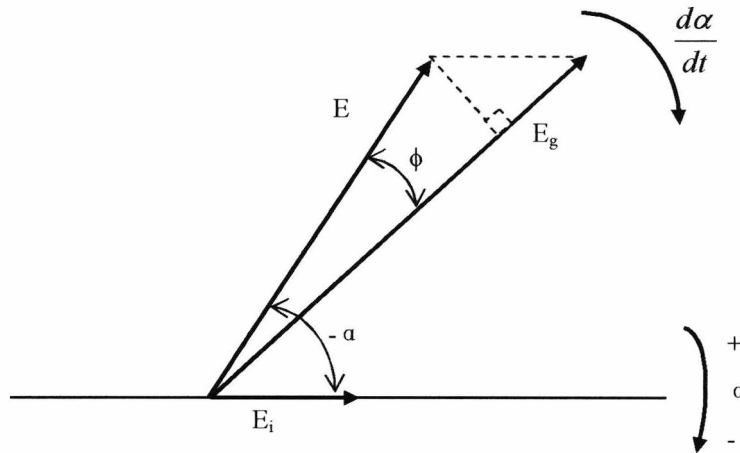


Fig 4.7 Vector diagram of the injection-locked oscillator. Presented by Adler [2].

Under all of the above assumptions, a vector diagram of the signals within an injection-locked oscillator was presented by Adler (Fig 4.7) [2]. E is the instantaneous output vector before the application of the injection signal, E_i is the injection signal vector, and E_g is the instantaneous output vector after the application of the injection signal. Vector E

rotates clockwise with an angular frequency of ω and the injection signal vector rotates clockwise with an angular frequency of ω_i . The instantaneous phase difference between E and E_i is α .

Let vector E_i be the reference plane, the instantaneous frequency can be written as $\omega_i + (d\alpha/dt)$. Or the instantaneous angular beat frequency can be written as:

$$\Delta\omega = \frac{d\alpha}{dt} = \omega - \omega_i \quad (4.20)$$

where ω is the instantaneous output signal frequency of the oscillator.

From Fig 4.7, we can see that without the application of the external signal, E_g and E must coincide. The oscillation phase condition is met at the free-running frequency ω_0 . At any other frequency there will be a phase shift ϕ between E_g and E . Fig 4.8 shows a typical curve of the phase shift versus frequency for a single tuned circuit. For the injection-locked oscillator, the curve can be used to represent the phase between E and E_g as a function of frequency offset from the free running frequency.

Now, if we suppose the external signal E_i is applied, the instantaneous voltage vector diagram for a given beat cycle is shown in Fig 4.7, where E is shown to be lagging behind E_g by a phase angle ϕ .

In order to produce this phase difference, the oscillator output frequency at this instant will exceed ω_0 by an amount that will produce a lag ϕ in the resonator circuit. By assuming $E_i \ll E$, ϕ is calculated using Fig 4.7:

$$\phi = \frac{E_i \sin(-\alpha)}{E} = -\frac{E_i}{E} \sin \alpha \quad (4.21)$$

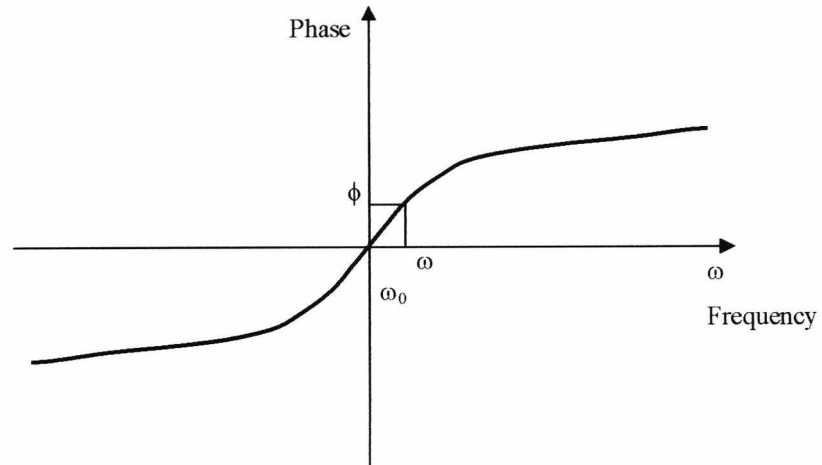


Fig 4.8 Phase versus frequency for a single tuned circuit. Presented by Adler [2].

The output instantaneous phase will follow the curve shown in Fig 4.8. As we assume the external signal frequency is similar to that of the free-running oscillator, only the central linear part of the curve is used. So the slope can be defined as:

$$M = \frac{d\phi}{d\omega} \quad (4.22)$$

Then the phase angle at instantaneous frequency ω is:

$$\phi = M(\omega - \omega_0) \quad (4.23)$$

As mentioned earlier, setting the instantaneous beat frequency as $\Delta\omega = \omega - \omega_i$ and the undisturbed beat frequency as $\Delta\omega_0 = \omega_0 - \omega_i$, we can rewrite Equation 4.23:

$$\phi = M(\omega - \omega_0) = M[(\omega - \omega_i) - (\omega_0 - \omega_i)] = M[\Delta\omega - \Delta\omega_0] \quad (4.24)$$

Substituting Equation 4.20 and Equation 4.21 into Equation 4.24, we get:

$$-\frac{E_i}{E} \sin \alpha = M \left[\frac{d\alpha}{dt} - \Delta\omega_0 \right] \quad (4.25)$$

For the single tuned resonator, the quality factor is [2]:

$$Q = 0.5\omega_0 \frac{d\phi}{d\omega} \quad (4.26)$$

Substituting Equ 4.26 into Equ 4.22, we have:

$$M = \frac{2Q}{\omega_0} \quad (4.27)$$

Substituting into Equ 4.25, we have:

$$-\frac{E_i}{E} \sin \alpha = \frac{2Q}{\omega_0} \left[\frac{d\alpha}{dt} - \Delta\omega_0 \right] \quad (4.28)$$

where $d\alpha/dt$ must be zero when the injection locked oscillator reaches a stable state. So in the steady state Equ 4.24 becomes:

$$\frac{E_i}{E} \sin \alpha = \frac{2Q}{\omega_0} \cdot \Delta\omega_0 \quad (4.29)$$

The maximum undisturbed beat frequency occurs when $\sin \alpha = 1$, so the locking bandwidth derived by Adler is [2]:

$$B = \frac{\omega_0}{Q} \cdot \frac{E_i}{E} = \frac{\omega_0}{Q} \sqrt{\frac{P_i}{P_0}} \quad (4.30)$$

The Q factor in Equ 4.30 equation is a constant.

4.2.4 Differences between Adler's and Kurokawa's locking bandwidth equation

There are three differences between Adler's locking bandwidth Equation 4.30 and Kurokawa's locking bandwidth Equation 4.8.

1. The absence of $1/\cos\theta$ in Adler's equation.

This is a result of neglecting the variation of the active device reactance $X_d(A)$ with the RF current A that flows through the oscillator. The reason is that, in Adler's equation, the device line is supposed to be perpendicular to the circuit impedance locus, thus $\theta = 0$.

2. Larger bandwidth is predicted by Kurokawa's equation

Under the same conditions, the locking bandwidth predicted by Kurokawa is two times larger than Adler's prediction. To find the reason for this difference, we need to investigate the models that Kurokawa and Adler used to derive their locking equation. The circulator is included in Kurokawa's model, the output power is dissipated only at the load, and the external quality factor is given as,

$$Q_{ext} = \frac{\omega_0 L}{R_L} \quad (4.31)$$

However, no such a circulator is assumed in Adler's model (Fig 4.6). The output power will be dissipated at both the injection source resistor and the load in his model.

Imagine the circulator is omitted from Kurokawa's model, the output power will be dissipated at both the load and source resistor, and the injection source resistor should be included for calculation of the oscillator's external quality factor:

$$Q_{ext} = \frac{\omega_0 L}{2R_L} \quad (4.32)$$

and,

$$\frac{R_L}{L} = \frac{\omega_0}{2Q_{ext}} \quad (4.33)$$

If we substitute equation 4.33 into equation 4.12, we have:

$$2\Delta\omega_m = 2 \cdot \frac{1}{\cos\theta} \cdot \frac{R_L}{L} \cdot \sqrt{\frac{P_i}{P_0}}$$

$$B = 2 \cdot \Delta\omega_m = \frac{\omega_0}{Q_{ext}} \cdot \sqrt{\frac{P_i}{P_0}} \frac{1}{\cos\theta} \quad (4.34)$$

$$B_{min} = \frac{\omega_0}{Q_{ext}} \cdot \sqrt{\frac{P_i}{P_0}} \quad (4.35)$$

Comparing this result with Adler's locking equation [2]:

$$B = \frac{\omega_0}{Q} \sqrt{\frac{P_i}{P_0}} \quad (4.36)$$

We can conclude that Equ 4.35 is identical to Adler's locking equation (Equ 4.36) except the difference in Q factor which will be discussed in the following section.

3. The Q factor.

In Adler's equation the Q is the resonator loaded Q instead of the external Q . Looking at Kurokawa's model (Fig 4.4), the injection signal current generated by the injection source is injected into the oscillator output via a circulator. This injection signal flows through the active device and the resonator, and is mixed with the oscillator free-running signal. The injection-locked oscillator free-running output signal containing the injection

signal is applied to the load through the circulator. All resistors within this injection loop will cause a voltage drop and should be include in the calculation. These resistors include the injection source resistance R_L , the load resistance R_L , and the resonator resistance R_a . We can rewrite the equations in terms of the injection power P_i ,

$$P_i = \frac{1}{2} \cdot \left(\frac{E_i}{2R_L + R_a} \right)^2 \cdot R_L, \quad |E_i| = \frac{\sqrt{2} \cdot \sqrt{P_i} \cdot |2R_L + R_a|}{\sqrt{R_L}} \quad (4.37)$$

The loaded Q of the resonator is:

$$Q = \frac{\omega_0 L}{R_L + R_a}, \quad \frac{R_L + R_a}{L} = \frac{\omega_0}{Q} \quad (4.38)$$

Substituting Equation 4.10 and Equation 4.37 into Equation 4.6, we obtain:

$$|2\Delta\omega_m L \cos\theta| = \frac{\sqrt{P_i} \cdot |2R_L + R_a|}{\sqrt{P_0}} \quad (4.39)$$

$$\Delta\omega_m = \frac{1}{2} \cdot \frac{1}{\cos\theta} \cdot \frac{\sqrt{P_i}}{\sqrt{P_0}} \cdot \left(\frac{R_L + R_a}{L} + \frac{R_L}{L} \right) \quad (4.40)$$

Substitute Equ 4.38 and Equ 4.13 into Equ 4.40, we have:

$$\Delta\omega_m = \frac{1}{2} \cdot \frac{1}{\cos\theta} \sqrt{\frac{P_i}{P_0}} \cdot \left(\frac{\omega_0}{Q} + \frac{\omega_0}{Q_{ext}} \right) \quad (4.41)$$

The locking bandwidth B is:

$$B = 2\Delta\omega_m = \frac{1}{\cos\theta} \sqrt{\frac{P_i}{P_0}} \cdot \left(\frac{\omega_0}{Q} + \frac{\omega_0}{Q_{ext}} \right) \quad (4.42)$$

The omission of R_a in Kurokawa's calculation is accurate for conventional oscillators (high Q), as R_a is small compared with R_L . However, for wideband injection locked

oscillators, where R_a is designed to be large and can not be ignored any more, Equ 4.42 should be used to calculate the correct locking bandwidth.

Consider the circulator is omitted, the output signal is dissipated at the injection source as well as the load, and the oscillator loaded Q can be rewritten as:

$$Q = \frac{\omega_0 L}{2R_L + R_a}, \quad \frac{2R_L + R_a}{L} = \frac{\omega_0}{Q} \quad (4.43)$$

Substituting Equ 4.43 in to Equ 4.40, we have

$$\Delta\omega_m = \frac{1}{2} \cdot \frac{1}{\cos\theta} \cdot \frac{\omega_0}{Q} \sqrt{\frac{P_i}{P_0}} \quad (4.44)$$

and the minimum locking bandwidth is:

$$B = 2\Delta\omega_m = \frac{\omega_0}{Q} \cdot \sqrt{\frac{P_i}{P_0}} \quad (4.45)$$

The equation is identical to Adler's locking bandwidth equation 4.30. Adler's equation is correct for reflection type injection-locked oscillators without a circulator.

4. Conclusion

Kurokawa's equation is only applicable to high Q reflection type electrical injection-locked oscillators that employ circulators, and the correct locking bandwidth equation for such oscillators is Equ 4.43. Even though Adler's locking equation is developed for reflection type electrical injection-locked oscillators, his equation is not suitable for such oscillators, as the circulator required for these type of oscillator to isolate the injection and oscillator free-running signal is not included in his model. However, his equation is a good theoretical basis for developing the locking bandwidth equation for reflection type injection-locked oscillators which do not require circulators, i.e. reflection type optically injection-locked oscillators.

4.2.5 Noise of an injection-locked oscillator

In the following, the noise for an injection-locked oscillator is analysed. Only noise generated within the oscillator is considered. The injection signal is assumed to be noise free.

1. Noise of the free running oscillator

Before investigating the noise of an injection-locked oscillator, it is useful to look at a noisy free-running oscillator first.

The noise analysis of a free-running oscillator can be represented graphically. Fig 4.9 shows the model of a noisy injection-locked oscillator. As the free-running oscillator noise originates in the active device, we can graphically model it by device line transverse and longitudinal vibration. The resonator locus does not vibrate because the resonator is a passive device, and assumed to be noise free. The device line vibrates both transversely and longitudinally. A noise vector is introduced to model the oscillator noise.

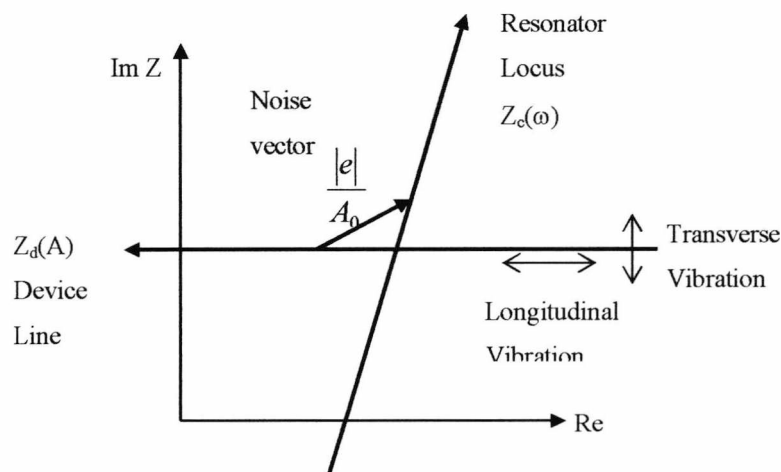


Fig 4.9 Noise vector diagram of a noisy oscillator. Presented by Kurokawa [3].

The equation used by Kurokawa to describe a noisy free-running oscillator is [3]:

$$[Z(\omega) - Z(A)]I = e \quad (4.46)$$

where e is the noise voltage amplitude, and I is the noise current that flows through the oscillator. For a useful oscillator, the noise must be small. So we can approximate I by a free-running current of amplitude A_0 multiplied by a phase factor, $e^{j\phi}$. Equation 4.47 can be rewritten as:

$$Z(\omega) = Z(A) + \frac{|e|}{A_0} e^{-j\phi} \quad (4.47)$$

The longitudinal vibration for the device line will cause the free-running current amplitude A_0 to change, as does the output signal power. In other words, the longitudinal vibration of the device line will generate AM noise. Transverse vibration of the device line will cause the free-running point to move along the resonator locus, and generates FM noise. Compared with a low Q resonator, the same amount of transverse displacement of the device line on the high Q resonator locus corresponds to a smaller frequency deviation. Therefore, FM noise will decrease with the increment of the resonator Q. On the other hand, AM noise does not change with the increment of the resonator quality factor. This is because the AM noise is primarily determined by the movement on the device line which is independent of the resonator Q. Both FM and AM noise increase if the intersecting angle between the resonator locus and device locus becomes smaller. This is because for a given amplitude of the vibration of the device line, the motion of the intersection is larger and therefore the AM and FM noise greater.

2. Noise for locked oscillator

Consider Fig 4.10: here a noise-free injection signal is applied to the injection-locked oscillator. Again, the resonator locus remains stable, and the device line vibrates both transversely and longitudinally. The intersection between the injection-locking signal

vector and the resonator locus is fixed at ω_i on the resonator locus and the vector length is kept constant.

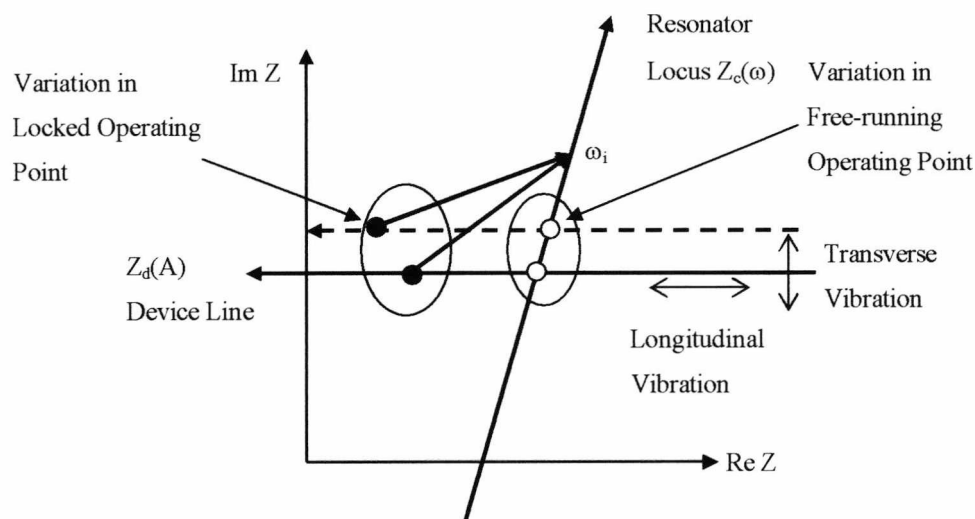


Fig 4.10 Noise vector diagram of the locked-oscillator. Presented by Kurokawa [3].

Under longitudinal vibration, the tail of the locking vector moves along the device line causing a change in the oscillation amplitude. However, the intersection between the injection signal and the resonator locus remains fixed on the resonator locus, so the oscillation frequency does not change. Thus, the longitudinal vibration primarily causes AM noise.

Transverse vibration of the device line causes mainly FM noise due to movement of the oscillator point along the resonator locus. This noise is reduced when the oscillator is locked because the injection signal remains fixed at ω_i . However, FM noise is not completely eliminated because the locking vector direction changes with the transverse vibration of the device line. This corresponds to a phase change in RF current, and the rate of phase change is frequency.

If we increase the injection signal power, the signal vector length will be increased, and the output signal phase change is reduced with the same amount of transverse displacement of the device line. Therefore, the oscillator output signal phase noise is reduced.

To summarise the analysis above, we can conclude that the injection-locked oscillator output noise can be purified by the injection of a less noisy signal, and the noise can be reduced further by increasing the injection power.

4.2.6 The locking transient

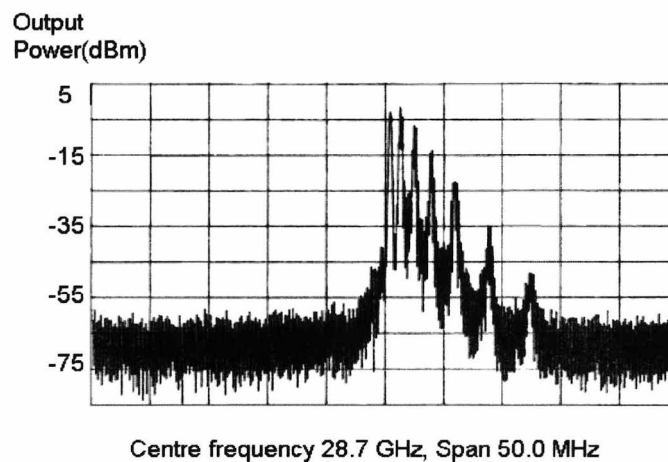


Fig 4.11 Oscillator output signal spectrum before locked or just unlocked.

Just before an oscillator locks or just after it unlocks, the output spectrum contains strong sidebands (Fig 4.11). The theoretical explanation of this phenomenon has been given by several researchers [2], [4]-[6].

4.3 Transmission type injection-locked oscillator

A new configuration of electrical injection-locked oscillator, transmission type injection-locking, was introduced by Tajima [7], [8] in the 1970's. The transmission type injection-

locked oscillator does not require a circulator to apply the injection signal to the oscillator. As the injection signal will be applied at the point where the free-running signal power is smallest, it provides potentially wider locking bandwidth than that of the reflection type. Also, the circuit complexity is reduced significantly. Tajima [8] also developed a circuit model of the transmission type oscillator (Fig 4.12). In his model, the injection-locked oscillator is considered as a two-port oscillation circuit. The two-port circuit Y shown in Fig 4.12 includes an active device, feedback circuit, resonant circuit and all surrounding parasitics. The loads Y_S and Y_L are connected with port 1 and port 2 respectively. Y_S and Y_L are considered to be real, while the circuit admittance parameters Y (Y_{11} , Y_{12} , Y_{21} , Y_{22}) are functions of frequency and voltage amplitudes at ports 1 and 2. The output voltage amplitude at port 1 and port 2 are $V_1=A$ and $V_2=B$ respectively. The injection-current source will be applied at port 1 and port 2 respectively. When the injection source is connected to port 2, the circuit is a reflection type locked oscillator, and when connected to port 1, it is a transmission type locked oscillator

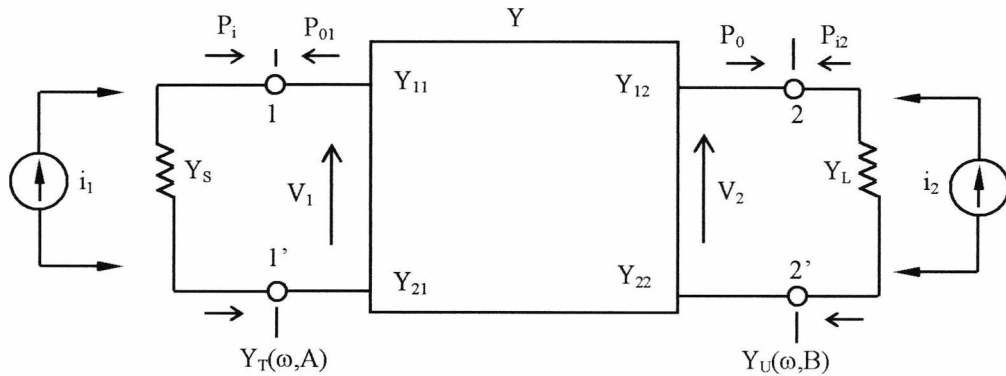


Fig 4.12 Transmission type injection-locked oscillator. Presented by Tajima [8].

Tajima also derived the locking bandwidth equation for transmission type injection-locking [8]:

$$B = \frac{2\omega_0}{Q_{ext}} \frac{G_s}{G_p} \sqrt{\frac{P_i}{P_0}} \frac{1}{\cos \theta} \quad (4.48)$$

where G_s is the maximum stable gain of the circuit Y , θ is the angle between the device locus and the circuit locus, P_i is the injection signal power, P_o is the output signal power, and G_p is the square root of the ratio of the free-running output power at port 2, P_{o2} , to that at port 1, P_{o1} . As discussed in Section 4.2.2 the external Q in Equation 4.49 should be replaced with loaded Q for the general case.

Suppose we have two electrical injection-locked oscillators, one of which is reflection type and the other is transmission type. These two oscillators have the same Q , free-running output power, and injection signal power. The bandwidth ratio of these two oscillators is,

$$\frac{B_{tran}}{B_{ref}} = \frac{2 \cdot \frac{\omega_0}{Q} \frac{G_s}{G_p} \sqrt{\frac{P_i}{P_o}} \frac{1}{\cos \theta}}{2 \cdot \frac{\omega_0}{Q} \sqrt{\frac{P_i}{P_o}} \frac{1}{\cos \theta}} = \frac{G_s}{G_p} \quad (4.49)$$

The G_s/G_p factor for a transmission type injection-locked oscillator should therefore be designed higher than one. Therefore, compared with the reflection type injection-locked oscillator, transmission type injection-locked oscillators normally provide a higher locking bandwidth. The G_s/G_p factor must be maximised for a wideband transmission type injection-locked oscillator design.

As most of the parameters defined in Fig 4.12 are obtained during the free-running state, and existing simulation software cannot simulate and obtain these parameters directly, theoretical predictions regarding locking bandwidth using the software are not possible. Therefore, there is still no easy way to calculate the locking bandwidth of a transmission type injection-locked oscillator. Tajima's experimental results showed that the locking bandwidth of a transmission type injection-locked oscillator was 1.8 times higher than that of a reflection type injection-locked oscillator. This number is used to theoretically

predict the locking bandwidth of the millimetre-wave transmission type optically injection-locked oscillator in Chapter 5.

4.4 Optically injection-locked oscillators

4.4.1 Introduction

Advantages of optically injection-locked oscillators have been addressed in Chapter 1 as well as by a number of other researchers [10]-[17]. However, as mentioned in Chapter 1, other researchers have used the locking bandwidth equation for electrical injection-locked oscillator to design optically injection-locked oscillators. No locking bandwidth equation for indirect optically injection-locked oscillators using PIN photodiodes has been derived in previous publications. In the following sections, the locking bandwidth equations for optically injection-locked oscillators are derived. The noise performance of such oscillators is also analysed.

For a general optically injection-locked oscillator, the electrical locking signal is first modulated onto an optical carrier, and this microwave/millimetre-wave modulated optical signal is delivered to the oscillator. At the oscillator an electrical injection signal is obtained by converting the microwave modulated optical signal into an electrical signal using a photosensitive device. As introduced in Chapter 2, the photosensitive device can be a PIN photodiode, an avalanche photodiode, a phototransistor, or the oscillator active device itself. PIN photodiodes were used in this work to design optically injection-locked oscillators. Therefore, the equations and theories in the following sections will concentrate on oscillators using a PIN photodiode.

4.4.2 Locking bandwidth of optically injection-locked oscillators

The equations for locking bandwidth of the electrical injection-locked oscillators can be applied to optically injection-locked oscillators with some modifications. As the electrical

injection signal is applied to the oscillator after photodetection, it is necessary to know what the electrical injection power is for a given optical injection signal power before calculating the locking bandwidth.

1. Output power from a photodiode

The optical-electrical conversion efficiency of a photodetector is described by its responsivity, R (A/W). The average output electrical current from a photodetector is:

$$I_p = P_{optical} \cdot R \quad (4.50)$$

where $P_{optical}$ is the average incident optical power. For a load resistance of R_L ohm, the photodetector electrical output signal power in terms of the load can be calculated as:

$$P_{out} = I_p^2 \cdot R_L = (P_{optical} \cdot R)^2 \cdot R_L \quad (4.51)$$

2. Locking bandwidth of a reflection-type indirect optically injection-locked oscillator

The locking bandwidth of a reflection-type indirect optically injection-locked oscillator can be obtained by substituting Equation 4.51 into Adler's equation (Equ 4.45):

$$B_{min} = 2\Delta\omega_m = \frac{\omega_o}{Q} \sqrt{\frac{P_i}{P_o}} \frac{1}{\cos\theta} = \frac{\omega_o \cdot P_{optical} \cdot R}{Q} \sqrt{\frac{R_L}{P_o}} \frac{1}{\cos\theta} \quad (4.52)$$

where ω_o is the free-running frequency of the oscillator, P_o is the oscillator free-running output power, $P_{optical}$ is the incident optical power, R_L is the oscillator input resistance looking from the injection port, and Q is the resonator loaded Q .

3. Locking bandwidth of a transmission-type indirect optically injection-locked oscillator

The locking bandwidth of a transmission-type indirect optically injection-locked oscillator is obtained by substituting Equ 4.52 into Tajima's locking equation [7]:

$$B = \frac{2P_{optical} \cdot R \cdot \omega_0}{Q} \frac{G_s}{G_p} \sqrt{\frac{R_L}{P_{02}}} \frac{1}{\cos \theta} \quad (4.53)$$

where:

$$\frac{G_s}{G_p} = \frac{Q_{ext2}}{Q_{ext1}} \quad (4.54)$$

and G_s is the maximum stable gain of the circuit Y (Fig 4.13) and G_p is the square root of the ratio of the free-running output power at port 2, P_{02} , to that at port 1, P_{01} . R_L is the oscillator input resistance looking from the injection port. However, as we discussed earlier, there is still no general equation for calculating G_p .

4.4.3 Noise of an indirect optically injection-locked oscillator

The noise level of an indirect optically injection-locked oscillator is expected to be worse than that of the electrically injection-locked oscillator, as a result of the photodetector noise.

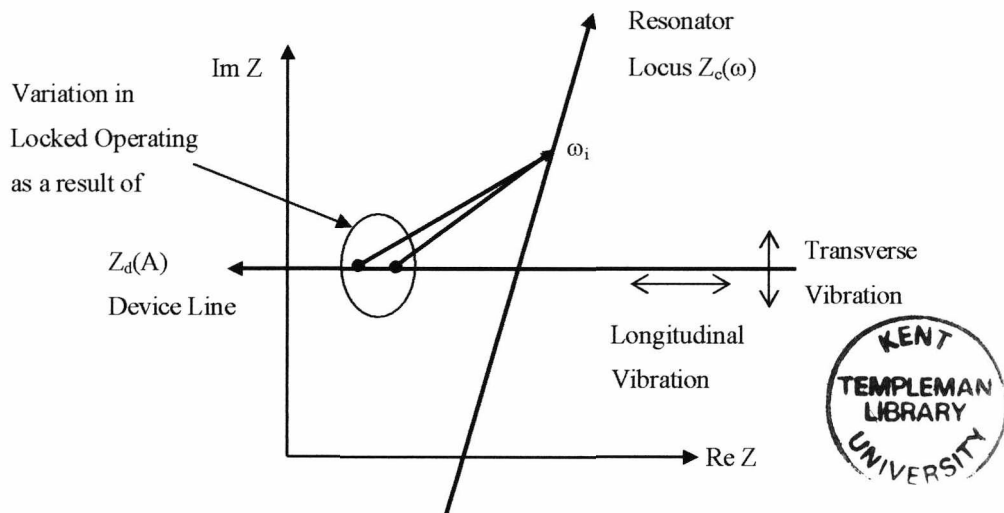


Fig 4.13 Noise vector diagram for an indirect optically injection-locked oscillator

It is well known that the noise of a PIN photodiode includes dark noise and quantum noise [18]. The photodiode generates additional AM noise. As shown in Fig 4.13, the injection vector length is changed as a result of the injection signal AM noise. The intersection point between the injection signal vector and the resonator locus is unchanged because the position of this point is decided by the injection signal frequency that is unchanged. However, the intersection point between the injection signal vector and the device line is changed because of the changes in injection signal vector length. This generates more AM and FM noise in addition to the output noise generated by the oscillator itself (Section 4.2.5). Therefore, the output noise performance for optically injection-locked oscillators is worse compared with that of electrically injection-locked oscillators.

4.5 Summary

Both Kurokawa's and Adler's theories of the reflection type injection-locking of microwave oscillators have been discussed in detail. For the first time, the differences between Adler's and Kurokawa's locking equation have been clarified. Based on the comparison and analysis, it was found Adler's equation is suitable for reflection type injection-locked oscillators that do not employ circulators. Kurokawa's equation is only accurate for high Q electrical reflection type injection-locked oscillators. For low Q electrical reflection type injection-locked oscillators Equ 4.43 should be used to calculate the bandwidth.

The Q factor in Adler's and Kurokawa's equation is constant. However, later experimental results in Chapter 5 show that it varies with injection signal power. Therefore, this equation cannot accurately predict the locking bandwidth. More detailed discussions are presented in Chapter 5.

Next, Tajima's theory of transmission type injection-locking was introduced and his results showed that transmission type injection-locked oscillators gave a wider locking bandwidth than that of the reflection type injection-locking.

Finally, the locking bandwidth equation for indirect optically injection-locked oscillators was derived. The locking bandwidth for a reflection type indirect optically injection-locked oscillator is:

$$B = \frac{\omega_0 \cdot P_{optical} \cdot R}{Q} \sqrt{\frac{R_L}{P_0}} \frac{1}{\cos \theta} \quad (4.56)$$

The locking bandwidth equation for a transmission type optically injection-locked oscillator is:

$$B = \frac{2P_{optical} \cdot R \cdot \omega_0}{Q} \frac{G_s}{G_p} \sqrt{\frac{R_L}{P_{02}}} \frac{1}{\cos \theta} \quad (4.57)$$

As the factor G_s/G_p is difficult to obtain theoretically, the locking bandwidth of a transmission type indirect optically injection-locked oscillator cannot be easily obtained using Equ 4.57.

The noise for optically injection-locked oscillators has been discussed. Photodiode shot noise generates AM noise for the injection signal. The noise for optically injection-locked oscillators is worse than that of the electrical injection-locked oscillators because of photodiode shot noise.

Theories and bandwidth equations for optically injection-locked oscillators discussed in this chapter will be used for directing the design of transmission type indirect optically injection-locked oscillators that will be described in Chapter 5.

References

- [1] Van. Der. Pol, "Forced oscillator in a circuit with nonlinear resistance," *Phil. Mag.*, pp. 65-80, Vol. 3, 1927.
- [2] R. Adler, "A study of locking phenomena in oscillators," *Proceedings of the I.R.E. and Waves and Electrons*, pp. 351-357, 1946.
- [3] K. Kurokawa, "Injection locking of microwave solid-state oscillators," *Proceedings of the IEEE*, Vol.61, No.10, pp. 1386-1410, 1973.
- [4] T. J. Buckman, "The frequency spectrum of a pulled oscillator," *Proc. IRE*, Vol. 40, pp. 958-961, 1952.
- [5] H. L. Stover, "Theoretical explanation for the output spectra of unlocked driven oscillators," *Proc. IEEE (Lett)*, Vol.54, pp. 310-311, 1966.
- [6] M. Armard, "On the output spectrum of unlocked driven oscillators," *Proc. IEEE (Lett)*, Vol. 57, pp. 798-799, 1969.
- [7] Y. Tajima, "GaAs FET applications for injection-locked oscillators and self-oscillating mixers," *IEEE MTT-S Int. Microwave Symp. Dig.*, pp. 303-305, 1978.
- [8] Y. Tajima and K. Mishima, "Transmission-type injection locking of GaAs schottky-barrier FET oscillators," *IEEE Trans. on Microwave Theory and Tech.*, Vol. MTT-27, No.5, pp. 386-391, 1979.
- [9] W. A. Edson, "Noise in oscillators," *Proc. IRE*, vol. 48, pp. 1454-1466, 1960.
- [10] R. A. Kiehl, "Behaviour and dynamics of optically controlled TRAPATT oscillators," *IEEE Trans. Electron. Devices*, Vol. ED-25, pp.703-710, 1978.
- [11] H. W. Yen and M. Barnoski, "Optical injection locking and switching of transistor oscillators," *Appl. Phys. Lett.*, Vol. 32, pp. 182, 1978.

- [12] A. J. Seeds and J. R. Forrest, "Initial observations of optical injection-locking of an X-band IMPATT oscillator," *Electron. Lett.*, Vol. 14, pp. 829-830, 1978.
- [13] A. A. Salles, "Optical control of MESFET's," *IEEE Trans. Microwave Theory Tech.*, Vol. MTT-31, pp. 812-820, 1983.
- [14] H. Fetterman and D. Ni, "Control of millimeter-wave devices by optical mixing," *Microwave Opt. Technol. Lett.*, Vol. MOTL-1, pp. 34-39, 1988.
- [15] A. S. Daryoush and P. R. Herzfeld, "Indirect optical injection-locking of oscillators," *Electron. Lett.*, Vol. 22, No. 3, pp. 133-134, 1986.
- [16] D. Sommer and N. J. Gomes, "Wide-locking bandwidth optically injection-locked oscillators: S-parameter design and modulation effects," *IEEE Transactions on Microwave Theory and Techniques.*, Vol. 43, pp. 1424-1434, 1995.
- [17] X. Wang, N. J. Gomes, L. G. Rojas, P. A. Davies, D. Wake.: 'Indirect optically injection-locked oscillator for millimetre-wave communication system', *IEEE Trans. Microwave Theory Tech.*, Vol 48, No. 12, pp. 2596-2603, 2000.
- [18] J. M. Senior, *Optical Fibre Communications 2nd ed.*, Prentice Hall International (UK) Ltd, 1992.

Chapter 5

Millimetre-wave Indirect Optically Injection-locked Oscillator Design and Measurement Results

5.1 Introduction

This chapter will describe the main achievement of this work: the design and fabrication of a millimetre-wave indirect optically injection-locked oscillator. The possible applications of optically injection-locked oscillators, such as in radio-over-fibre systems have been discussed in Chapter 2. Advantages of using optically injection-locked oscillators as receivers over the more standard photodiode plus amplifier approach were also included in Chapter 2.

The current research stage of optically injection-locked oscillators was reviewed in Chapter 2. At lower frequencies (below millimetre-wave frequency), optically injection-locked oscillators have been demonstrated by a number of researchers [6-11]. However,

at millimetre-wave frequency, despite all the advantages that the millimetre-wave optically injection-locked oscillator offers, the design and fabrication of optically injection-locked oscillators remain challenging. Only a few millimetre-wave optically injection-locked oscillators were demonstrated recently [12]-[13]. The first millimetre-wave indirect optically injection-locked oscillator working with long wavelength optical signal was demonstrated in this work [12]. The design and measurement result for this oscillator is discussed in this chapter.

The design targets and the implementation techniques for indirect optically injection-locked oscillators are introduced first in this chapter. The design techniques and theories for injection-locked oscillators described in Chapter 3 and Chapter 4 are used. The measurement results of the oscillators are then presented in the following section. A comparison in terms of output power and noise performance between an optically injection-locked oscillator and a conventional photodiode plus amplifier receiver is presented at the end of this chapter.

5.2 Design targets and procedures

5.2.1 Design targets

The free-running frequency of the oscillator is targeted to be 30 GHz. The targeted output power of the optically injection-locked oscillator at 30 GHz is 1dBm. The initial locking bandwidth is targeted to be around 100 MHz.

5.2.2 Design procedures

The negative resistance design method and computer simulation technique discussed in Chapter 5 are used to design the oscillator. As discussed in Chapter 4, in contrast to typical oscillator design, for an injection-locked oscillator it is necessary to design an oscillator with a low loaded Q. Minimizing the Q will generally lead to higher locking bandwidth.

The locking bandwidth of a reflection-type indirect optically injection-locked oscillator based on Adler's equation [14] is given in Chapter 4:

$$B_{\min} = \frac{\omega_0 \cdot P_{\text{optical}} \cdot R}{Q} \sqrt{\frac{R_L}{P_0}} \frac{1}{\cos \theta} \quad (5.1)$$

where ω_0 is the free-running frequency of the oscillator, P_0 is the oscillator free-running output power, P_{optical} is the incident optical power, R is the responsivity, R_L is the oscillator input resistance looking from the injection port, and Q is the resonator loaded Q.

The locking bandwidth for transmission type injection-locked oscillators is also given in Chapter 4:

$$\Delta\omega_m = \frac{P_{\text{optical}} \cdot R \cdot \omega_0}{Q} \frac{G_s}{G_p} \sqrt{\frac{R_L}{P_0}} \frac{1}{\cos \theta} \quad (5.2)$$

where P_0 is the free-running output power. G_s is the maximum stable gain of the circuit Y (Fig 4.12) and G_p is the square root of the ratio of the free-running output power at output port, P_o , to that at input port, P_{oI} .

The transmission type injection-locked oscillator structure was chosen for this work because of the higher locking bandwidth compared with that of the reflection type [16].

The theoretical loaded Q factor can be calculated by [15]:

$$Q = \frac{f_o}{2} \frac{d\varphi}{df} \quad (5.3)$$

where φ is the input reflection coefficient phase slope of the oscillator and f is frequency. From Equation 5.2 and Equation 5.3, it can be seen that in order to increase the locking bandwidth, we need to have a resonator with a flat input reflection phase slope.

As the resonator Q decreases, the effect of the oscillator part on the resonator Q can no longer be ignored, and the phase slope of the input reflection coefficient for the oscillator part should also be minimized [11].

Incident optical power, $P_{optical}$, and free-running output power P_o also need to be optimised in order to maximise the locking bandwidth. As P_o is normally fixed by the system requirement, Optimum insertion point and matching circuit for the photodiode need to be designed to maximised the amount of injection signal power that is deliver from the photodiode to the oscillator.

For the transmission type indirect optically injection-locked oscillator designed in this work, the photodiode will be integrated within the resonator circuit, and the resonator Q will be affected. A photodiode insertion circuit needs to be designed with high injection power and low Q .

The design procedure for a wide locking bandwidth millimetre-wave optically injection-locked oscillator can be summarised as:

- a.* Design a transistor feedback circuit and output matching circuit to obtain a high gain, low input phase slope and negative input resistance.
- b.* Design a resonator circuit with photodiode incorporated that satisfies the design frequency requirement while trying to obtain a reactance (phase) slope which is as flat as possible and while maximising the injected power into the oscillator.
- c.* Use the negative resistance design method and computer simulation technique to optimise and finalise the oscillator design.

5.3 Implementation techniques

The implementation choices for a millimetre-wave injection-locked oscillator include the choice of substrate, active device and photosensitive device, and these will be discussed separately in this section.

5.3.1 Substrate

Generally, alumina substrate and thin-film technology is employed to fabricate millimetre-wave circuits. The advantages of alumina substrate include low loss and small circuit dimension. The drawbacks of this substrate are high fabrication cost and difficulty in handling. The millimetre-wave injection-locked oscillators must be low-cost, so they can be installed in large numbers within millimetre-wave radio-over-fibre systems. Therefore, alumina substrate is not suitable for these millimetre optically injection-locked oscillators. 5580 RT/Duroid of 0.127 μm thickness was chosen as the substrate because of easy handling and low loss (loss tangent of 1.5×10^{-3} at 30GHz). The duroid substrate will be mounted on a brass plate for extra support.

5.3.2 Active device

As mentioned earlier, the active device that is used by the millimetre-wave injection-locked oscillator has to provide enough gain at the design frequency, and its input reflection coefficient phase slope should be as flat as possible. The active device, a transistor, needs to be easily incorporated into the microstrip circuit.

Two HEMT chips were found that can operate at 30 GHz. One was the JS9P11-AS (discontinued now) from Toshiba, the other was the EC2612 from United Monolithic Semiconductors (UMS) [17]. The JS9P11-AS is a power HEMT that provides a output power of 23 dBm at 30 GHz, while the EC2612 is a low-noise PHEMT providing an associated gain of 9.5 dB at 40 GHz. Both of these transistors have sufficient gain to power the oscillator at 30 GHz. However, the JS9P11-AS provides more output power, while the EC2612 has a higher cut off frequency. The input reflection coefficient phase

slopes of both transistors have been plotted for further comparison (Fig 5.1). Over the frequency band from 28 GHz to 32 GHz, the input reflection coefficient phase slope of the EC2612 is much flatter than that of the JS9P11-AS. For this reason, the EC2612 was chosen as the active device for our oscillator.

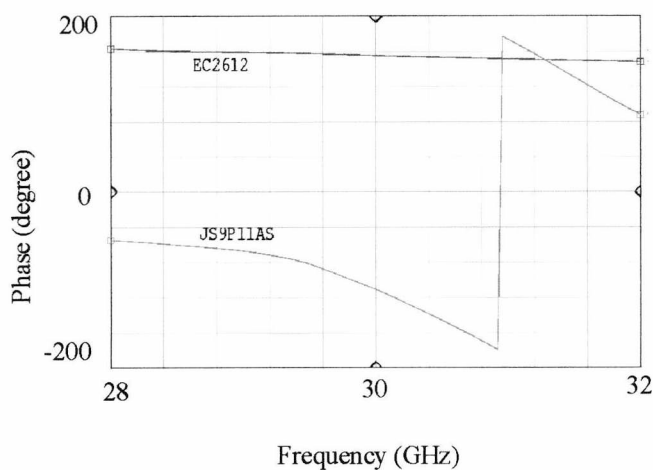


Fig 5.1 Input reflection coefficient phase slope for EC2612 and JS9P11-AS

Both the small signal model and S-parameter data of the EC2612 are provided by UMS (Appendix IV). The manufacturer recommends the use of a small signal model for simulation. No large signal model is available from the manufacturer; therefore, the simulation of the millimetre-wave optically injection-locked oscillator is limited to the less accurate small signal simulation. The small signal model of the EC2612 is shown in Fig 5.2. The meaning of the small signal model parameters and their values are given in Table 5.1. The bondwire inductance for both the gate and the drain are included in the model, and the inductance value is based on the type and length of bondwire that was used by the manufacture during the modelling. However, different type and length of bondwire is used during this work, and the performance of the oscillator will change accordingly. So it is necessary to remodel the bondwires using the type and length of bondwire that we used for the millimetre-wave optically injection-locked oscillator.

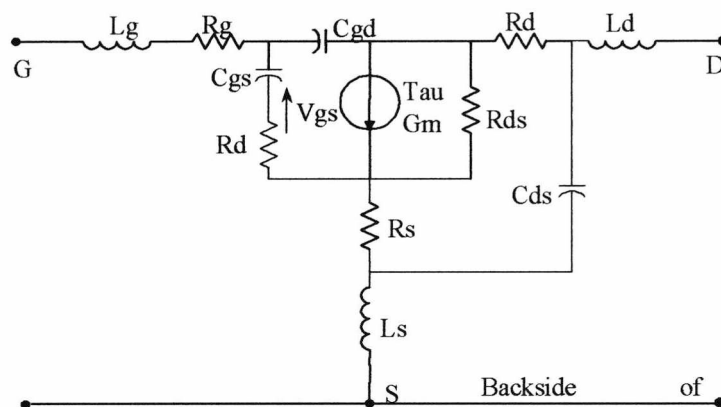
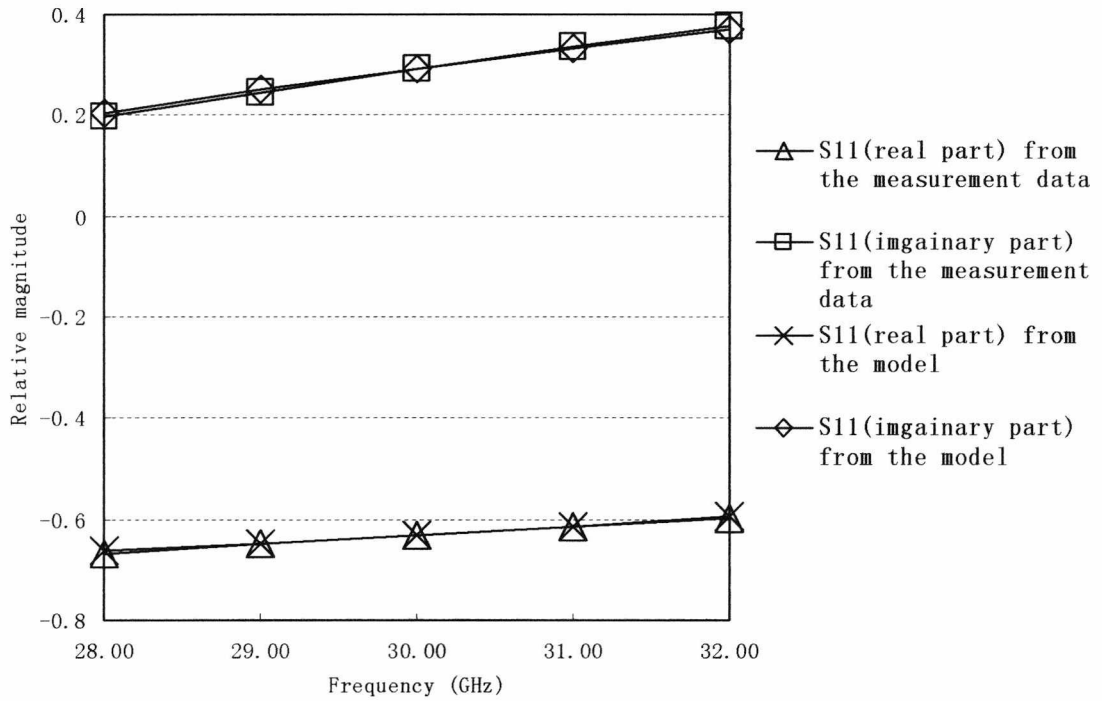


Fig 5.2 Small-signal model of the HEMT – parameter values given in Table I.

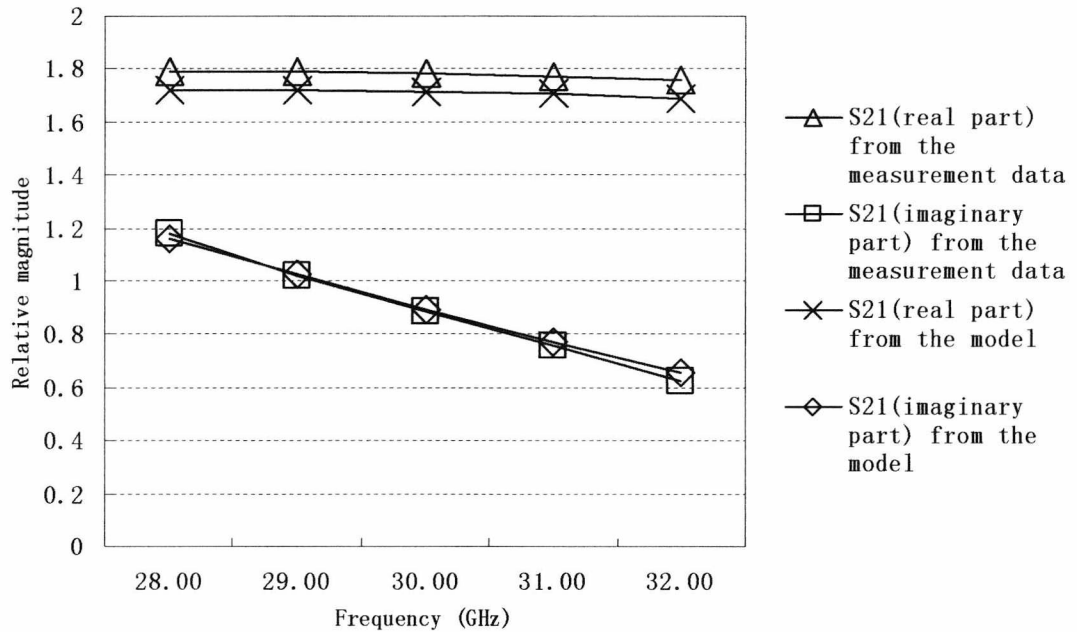
Parameter	Description	Unit	Value
Lg	Gate bondwire inductance	PH	152.54
Rg	Gate resistance	Ohms	0.13
Cgs	Gate-source capacitance	FF	142.6
Ri	Intrinsic resistance	Ohms	3.2
Cgd	Gate-drain capacitance	FF	39.57
Rs	Source resistance	Ohms	2.83
Ls	Source inductance	pH	0.11
Gm	Transconductance	mS	98.14
Tau	Gate-drain time delay	ps	2.8
Cds	Drain-source capacitance	fF	46.84
Rds	RF drain-source resistance	Ohms	116.8
Rd	Drain resistance	Ohms	2.83
Ld	Drain inductance	pH	117.01

Table 5.1 Parameter values for small-signal HEMT model [19].

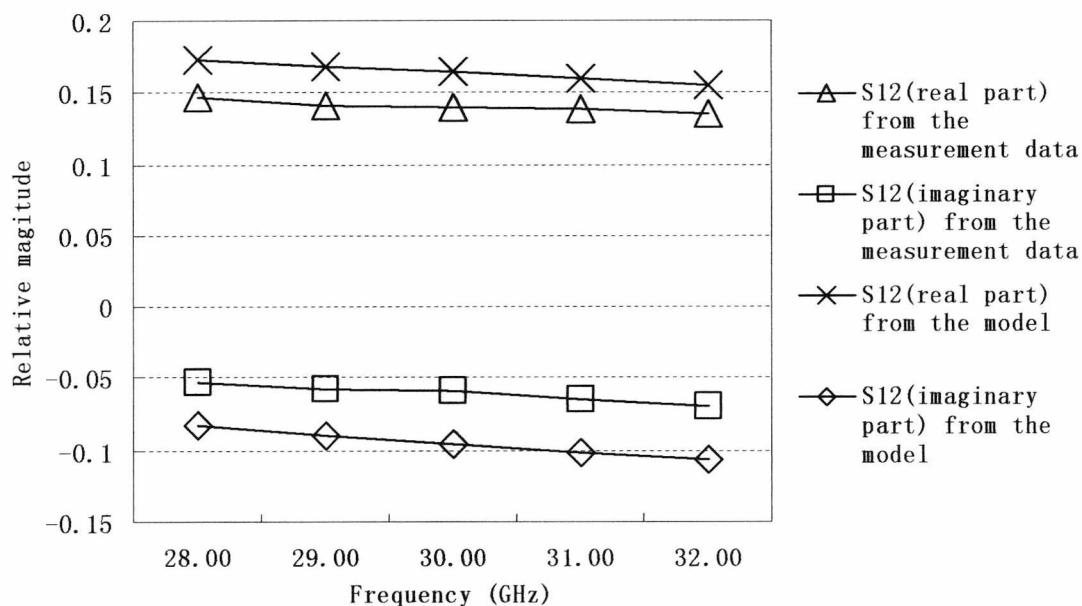
The small signal model is input into HP MDS for small signal simulation. The simulation results are compared with the measured small signal S-parameter data provided by UMS (Fig 5.3). A good match between the simulation and measurement results have been obtained.



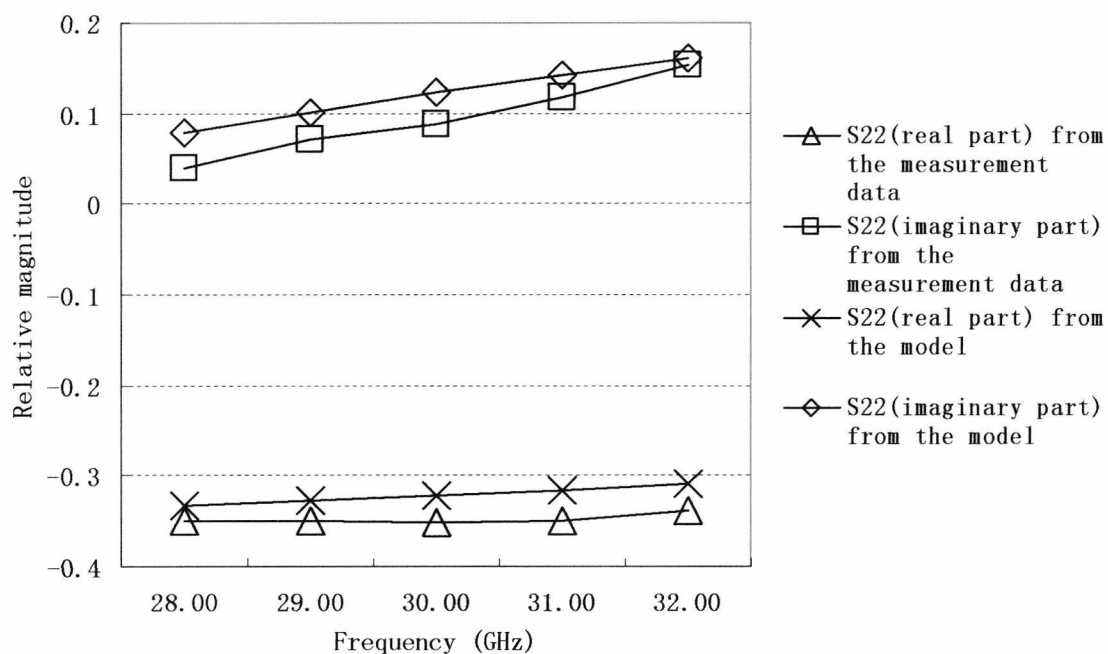
(a) Comparison of the simulated and measured S11



(b) Comparison of the simulated and measured S21



(c) Comparison of the simulated and measured S12



(d) Comparison of the simulated and measured S22

Fig 5.3 Comparison of small signal simulation and measurement results.

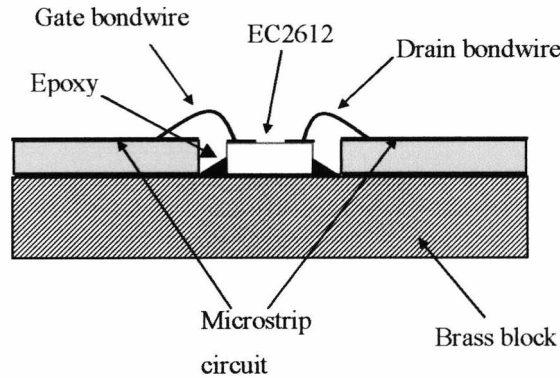


Fig 5.4 Mounting of EC2612

Fig 5.4 shows the mounting method of the EC2612. Bondwires are required to connect the transistor gate and drain. The source is grounded via the backside of the transistor chip. The EC2612 chip is glued on a brass block by conductive epoxy. This provides grounding for the source. Duroid is sited on the brass block as well. Bondwires are used to connect the gate and drain to microstrip circuits.

5.3.3 Photodiode

A BT edge-coupled PIN photodiode is used in the design of the millimetre-wave optically injection-locked oscillator [18]. The photodiode has an InGaAs absorber layer, for use up to wavelengths of 1.67 μm .

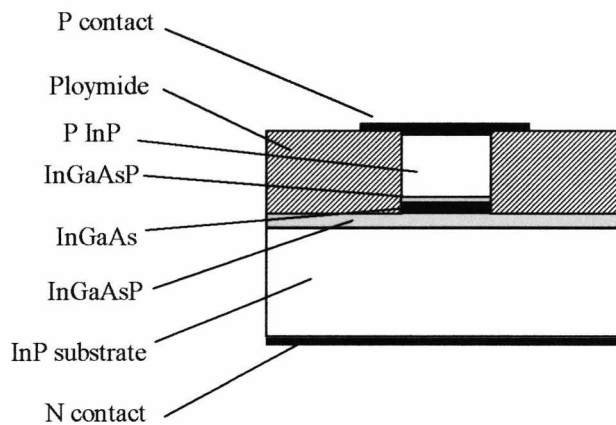


Fig 5.5 Cross section of BT edge-coupled photodiode [18].

Fig 5.5 shows the cross section of the edge-coupled photodiode. To obtain maximum bandwidth, the PN junction capacitance of the photodiode is minimised by having a small junction area. As a result, the junction is only $10 \mu\text{m}$ long by $5 \mu\text{m}$ wide. The total chip capacitance is less than 0.1 pF , to be compatible with the design target of bandwidth greater than 40 GHz . A responsivity of 0.4 A/W has been reported [18].

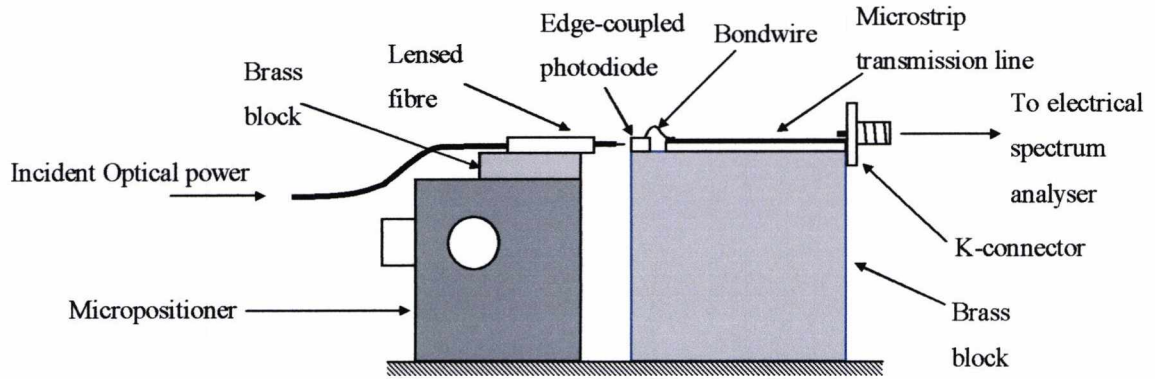


Fig 5.6 Mounting setup for the BT edge-coupled photodiode.

Fig 5.6 shows a typical mounting setup for a BT edge coupled photodiode. The photodiode is glued onto a brass block using epoxy, and the brass block is ground for both DC and RF. A bondwire is used to connect the P contact to a 50 ohm microstrip line, and the output RF signal is observed by an electrical spectrum analyser. A bias-T is required at the output for applying a negative bias voltage on the P contact. Due to the small junction area, lensed fibre is used to maximise the optical coupling efficiency into the edge-coupled photodiode. The fibre was positioned by a micropositioner.

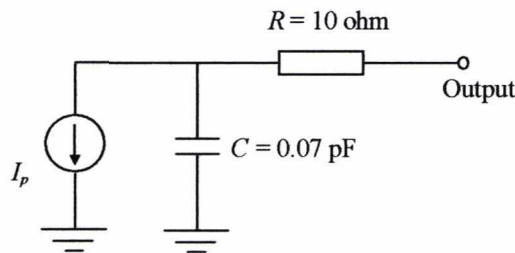


Fig 5.7 BT photodiode model.

The BT photodiode model that is used for simulation is shown in Fig 5.7. The capacitance, C , for the BT photodiode is 0.07 pF , and the series resistance, R , is 10 ohm .

A current source is used to model the photo current, I_p , and this current source is treated as open-circuit when we perform small signal S-parameter simulation.

5.3.4 Bondwire

For the proposed millimetre-wave optically injection-locked oscillators, bondwires are required for interconnecting both the transistor and photodiode with microstrip lines, and it is necessary to understand and model the behaviour of bondwires at millimetre-wave frequencies.

At millimetre-wave frequencies, both bondwire inductance and resistance are affected by the bondwire length and shape. A simple equation for calculating the bondwire inductance is given by [19]:

$$L = 2 \times 10^{-4} \cdot l \cdot \left[\ln\left(\frac{4l}{d}\right) - 1 + \mu\epsilon \right] \quad (5.4)$$

Where

L = inductance (μH)

l = length of the wire (μm)

d = wire diameter (μm)

μ = relative permeability (assumed to be 1)

ϵ = skin effect correction factor (a function of wire diameter and frequency)

This equation shows that the bondwire inductance increases with increasing bondwire length. The frequency dependence of the bondwire inductance is described by the skin effect correction factor ϵ .

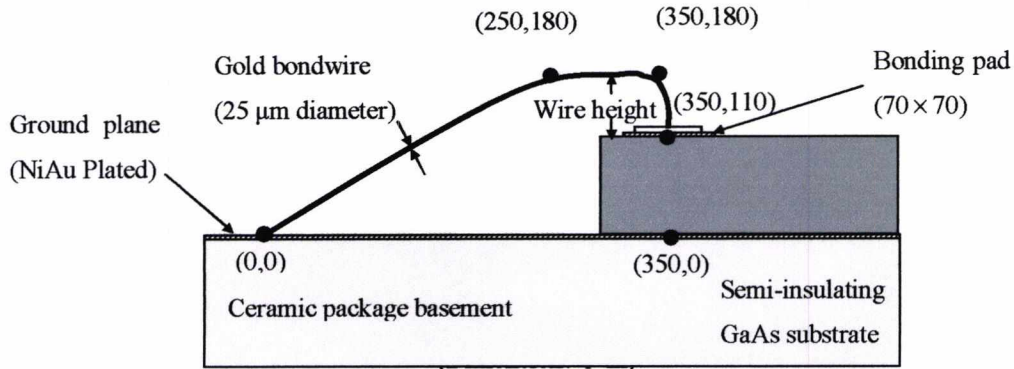


Fig 5.8 Typical geometry of a grounded ball-bondwire on a 100 μ m GaAs substrate with a minimum 480 μ m total length statistically obtained by bonding experiments [19].

An accurate analysis of bondwire impedance from 0-100 GHz has been given by Lee [19]. The typical shape of a grounded bondwire is shown in Fig 5.8. In his analysis, Lee showed that the bondwire impedance includes skin-effect resistance and radiation resistance. At low frequencies (<17 GHz), the radiation resistance is hardly observed, the bondwire inductance increases with frequency linearly at lower frequency and increases greatly for frequencies above 30 GHz, however, when the frequency is higher than 40 GHz, the radiation resistance becomes significant and cannot be ignored. For frequencies higher than 70 GHz, the radiation resistance becomes higher than the skin-effect resistance, and dominates the bondwire resistance. Lee suggested lowering the bondwire resistance by using thicker bonding wires and multiple wire bondings.

The resonant frequency of a bondwire is determined by the parallel-LC resonant frequency between bondwire inductance and capacitance of the bonding pad. A resonant frequency of 97 GHz was obtained based on the setup shown in Fig 5.8. Lee [19] also pointed out that the resonant frequency is inversely proportional to the bondwire height,

and that the bondwire height should be accurately controlled and minimised in order to reduce radiation and maintain a low insertion loss.

To summarise the above, in order to obtain a low insertion loss and high bandwidth, the bondwire interconnection should meet several criteria:

- a. The bondwire should be as short as possible.
- b. The bondwire width should be as wide as possible.
- c. Multiple bondwires should be used if it is possible.
- d. The height of the bondwire should be minimised.

The free-running frequency of the millimetre-wave optically injection-locked oscillator is 30 GHz, where the radiation loss is not significant compared with the skin-effect loss. So at this frequency, commercial CAD software that only models the skin-effect loss is reasonably accurate for bondwire modelling. The bondwire inductance given in the supplied EC2612 model is based on a 18 μm diameter pure gold wire (Fig 5.2), and the bondwire resistance is ignored. However, for the millimetre-wave optically injection-locked oscillator designed here, 25 μm diameter pure gold wire is used for bonding. Therefore, the bondwire impedance needed to be remodelled. The bond pad for the gate and drain are $60 \times 60 \mu\text{m}$ respectively. The chip height of the EC2612 is 100 μm , and the chip is fabricated on a GaAs substrate. The bonding pad capacitance is calculated as 0.0042 pF, and the 480 μm long bondwire inductance is 0.29 nH obtained by Lee's result [19]. The bandwidth is given by,

$$B = \frac{1}{2\pi\sqrt{LC}} \quad (5.5)$$

where L is bondwire inductance and C is bonding pad capacitance. A bandwidth of 142 GHz is obtained, and this is well above the oscillator free-running frequency. The bondwire insertion loss is 1 dB at 30 GHz (obtained from simulation), and this is acceptable for the oscillator design.

5.3.5 Circuit fabrication

The wavelength of a 30 GHz electromagnetic wave in vacuum is only 10 mm, and the dimension of the proposed millimetre-wave optically injection-locked oscillator is 20mm(L)×35mm(W). The width of a 50 ohm transmission line on the duroid we are using is 0.372 mm. Therefore, the circuit physical size is quite large in terms of the operating wavelength, and the effects of fabrication error on the oscillator performance are more significant than those that would occur at lower frequencies. The impact of fabrication error on the microstrip line characteristic impedance was investigated.

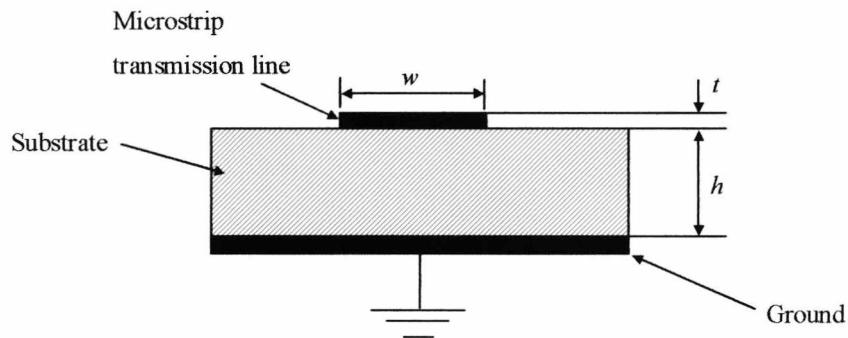


Fig 5.9 Transverse cross-section of microstrip transmission line.

Fig 5.9 shows the cross-section of a microstrip line. The factors that decide the characteristic impedance are line width (w), microstrip thickness (t), substrate height (h), and substrate effective permittivity (ϵ_{eff}) which is decided by substrate permittivity (ϵ_r) and the ratio of microstrip line width and substrate height [20].

Rogers RT/duroid is used as substrate for the millimetre-wave optically injection locked oscillator, and the specifications are:

Substrate height (h): 0.125 mm

Cladding thickness (t): 17 μ m

Substrate permittivity (ϵ_r): 2.2

Using the line calculator provided by MDS, we ascertained that the width of a 50 ohm is 372 μ m. In order to find the impact of fabrication error on microstrip transmission line characteristic impedance, the microstrip transmission line characteristic impedance with different line width is calculated (Table 5.2).

Microstrip line width (μ m)	Difference in width from 50 ohm line (μ m)	Characteristic impedance (ohm)	Impedance error from 50 ohm line (%)
372	0	50	0
389	17	48.609	-2.78
406	34	47.278	-5.4
355	-17	51.522	3
338	-34	53.122	6.2

Table 5.2 Variation of microstrip line characteristic impedance with line width.

The width of 50 ohm line width is varied by up to 34 μ m with a step of 17 μ m. Results show a maximum impedance change of 6.2%, and the impedance change is less when the line width increases, rather than decreases. The line width of a microstrip line is often measured by a microscope, and the shape of a microstrip line transverse cross-section is trapezoid instead of oblong (Fig 5.10). The line width at the top (W_{top}) is shorter than that of the bottom by $2t$ (t is the metal thickness as defined in Fig 5.10), the characteristic impedance is determined by W_{bottom} . The microscope only measures W_{top} , therefore it is

necessary to add $2t$ to the measurement result from the microscope to obtain the correct line width.

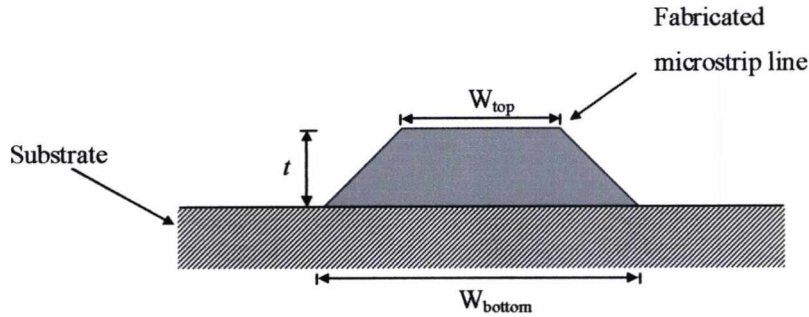


Fig 5.10 Transverse cross-section of fabricated microstrip transmission line.

It is shown in Table 5.2 that the variation in width has a bigger impact on the high impedance line than the low impedance line. So high impedance lines (>50 ohm) should be avoided in the oscillator RF path. The characteristic impedance of low impedance lines (<50 ohm) is less affected by the variation in line width.

5.4 Design of millimetre-wave indirect optically injection-locked oscillators

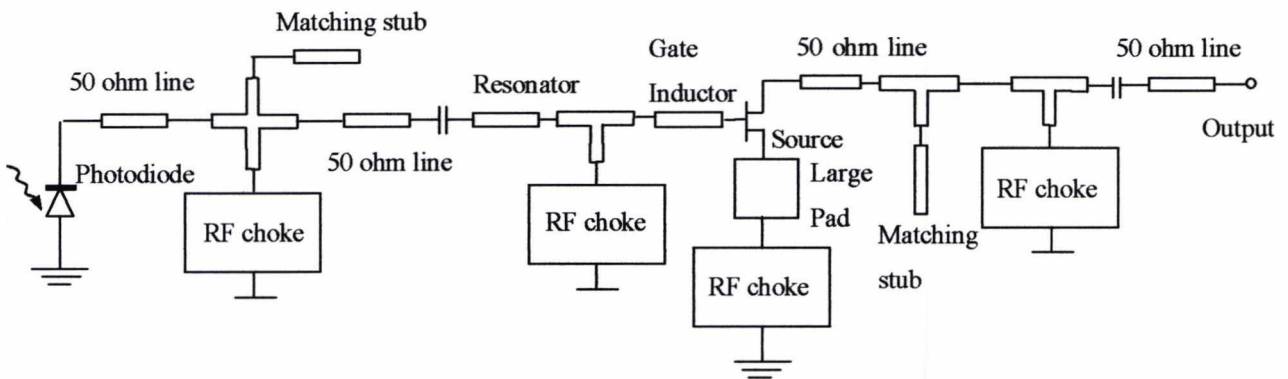


Fig 5.11 Circuit schematic of the millimetre-wave optically injection-locked oscillator.

The design procedures for a millimetre-wave indirect optically injection-locked oscillator are similar to the oscillator design procedures described in Chapter 3. Fig 5.11 shows the circuit schematic of the millimetre-wave indirect optically injection-locked oscillator.

The 5580 RT/Duroid of 0.127 μm thickness described earlier was chosen as the substrate because of easy handling and low loss (loss tangent of 1.5×10^{-3} at 30GHz).

5.4.1 Design of the oscillation part

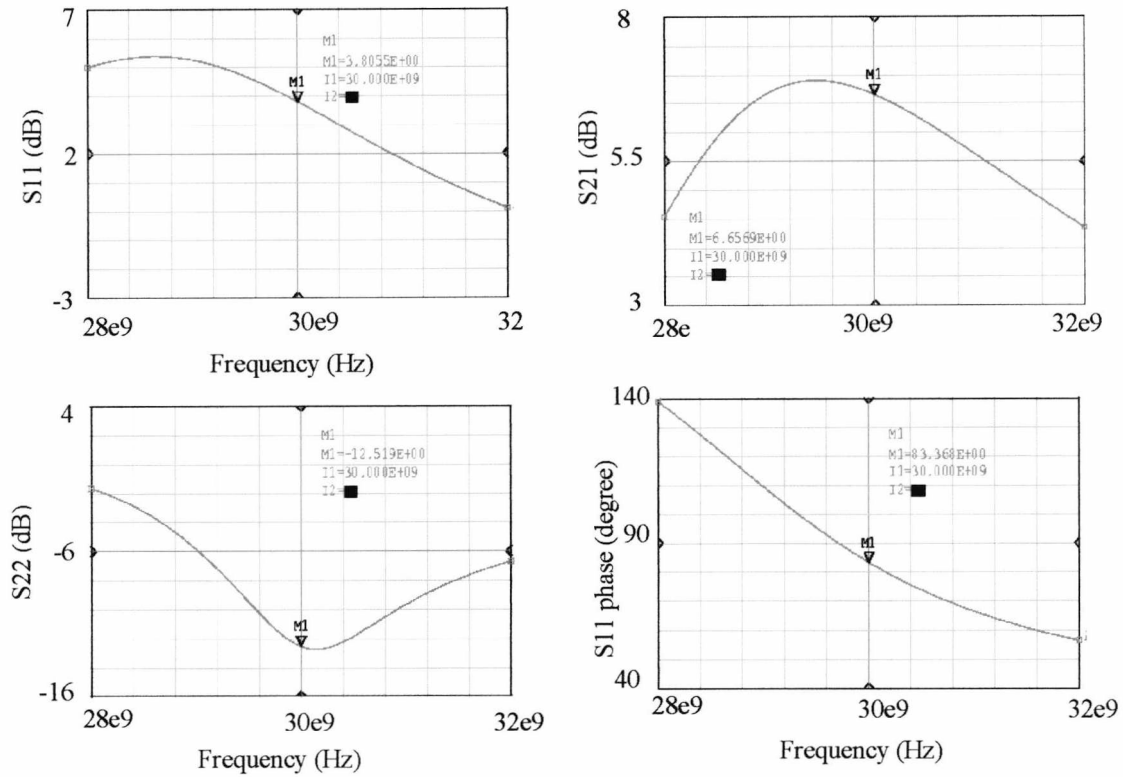


Fig 5.12 Small signal S-parameter simulation results for the millimetre-wave optically injection-locked oscillator active part.

A dual power supply bias topology is used to bias the HEMT. The active part of the oscillator is designed first. A commercial HEMT (UMS EC2612) has been chosen for use in the oscillator. A small-signal model made available by the suppliers (see Appendix I) was implemented in MDS to perform circuit simulations. The common source configuration was chosen for the oscillator to allow sufficient output power for the application being considered. The source feedback capacitor, necessary to ensure a negative resistance at the gate input, was realised by a large pad connected at the source. An inductor, realised by a thin microstrip line, was connected to the gate to improve the

input matching [21]. The drain was connected to a 50Ω line and an open circuit stub was chosen for output matching. Then the whole oscillator part was put into MDS for optimisation. First, the optimisation goal was set to achieve $|S_{11}| \geq 1.5$ while maximising $|S_{21}|$. Although the phase slope of $|S_{11}|$ was optimised for different output matching circuits, it was found to be more dependent on the HEMT characteristics than the output matching circuit. Thus, a simple 50Ω open-circuited line was used for output matching as it is easily fabricated and has a good tolerance to fabrication error.

Fig 5.12 shows the small signal simulation results of the oscillator active part. At the design frequency the HEMT provides a gain of 6.65 dB and the output reflection coefficient is less than -10 dB. The input reflection coefficient phase changes by 82 degrees as the frequency changes from 28 GHz to 32 GHz. Compared with the device S-parameter data (Fig 5.1 and Fig 5.3), an additional 66 degrees phase change has been introduced by insertion of the passive circuits, increasing the circuit Q.

5.4.2. Design of the resonator part

The next step was to design the resonator part and integrate the photodiode within the resonator. The factors that were considered during the design of the resonator were:

- 1) Q factor of the resonator should be as low as possible.
- 2) The resonator should be simple and easy to fabricate.
- 3) The RF signal from the photodiode should be coupled into the oscillator with maximum efficiency.
- 4) The DC bias of the photodiode needs to be integrated within the resonator part without interfering with the HEMT biasing point.

A microstrip transmission line was chosen as the resonator because of low possible Q and ease of fabrication. Both short-circuited and open-circuited transmission line can be used as resonators. A large microstrip pad is required by the short-circuit resonator to act as

the RF short, while no additional microstrip passive circuits are required by the open-circuit resonator. For the first millimetre-wave optically injection-locked oscillator design, the open-circuited resonator was employed because the photodiode output signal can be easily injected at the end of the resonator.

The microstrip resonator Q factor in terms of microstrip line characteristic impedance and length was investigated. The resonator loaded Q is defined by [15]:

$$Q = \frac{f_o}{2} \frac{d\varphi}{df} \quad (5.6)$$

where φ is the input reflection coefficient phase slope of the resonator in radians and f_o is the resonant frequency. Therefore, the flatter the input reflection coefficient phase slope, the lower the resonator loaded Q.

For a microstrip transmission line, the input reflection coefficient phase changes linearly with frequency, therefore, the flatness of the phase slope can be related to the total phase change between two frequency points.

Table 5.3a shows the variation of the microstrip line resonator input reflection coefficient phase slope with changes of line width, and Table 5.3b shows changes with respect to transmission line length. As the transmission line electrical length changes from 45 degrees to 360 degrees, the resonator input reflection coefficient phase changes from 3.85 to 24 degree, and the resonator loaded Q changes. Comparing the transmission electrical length, the transmission line width has less impact on the input reflection coefficient phase slope (less than 15% when the transmission line characteristic impedance changes from 30-90 ohm). The dimensions of most millimetre-wave components, e.g. capacitors, are often designed to match the width of 50 ohm transmission lines for minimum insertion loss. Therefore, a 50 ohm microstrip transmission line was chosen as the resonator of the millimetre-wave optically-injection locked oscillator.

Line width (mm)	Line length (mm)	Characteristic impedance (ohm)	Phase change from 29-31 GHz (degree)
0.772	5	30	15.21
0.52	5	40	16.29
0.372	5	50	17.22
0.276	5	60	16.04
0.209	5	70	15.57
0.16	5	80	15.27
0.123	5	90	14.626

(a) Changes of microstrip line resonator input reflection coefficient phase with respect of line width.

Line width (mm)	Electrical length (degree)	Characteristic impedance (ohm)	Phase change from 29-31 GHz (degree)
0.372	45	50	3.85
0.372	90	50	6.87
0.372	135	50	9.84
0.372	180	50	12.83
0.372	225	50	15.81
0.372	270	50	18.83
0.372	315	50	21.72
0.372	360	50	24

(b) Changes of microstrip line resonator input reflection coefficient phase with respect of line length.

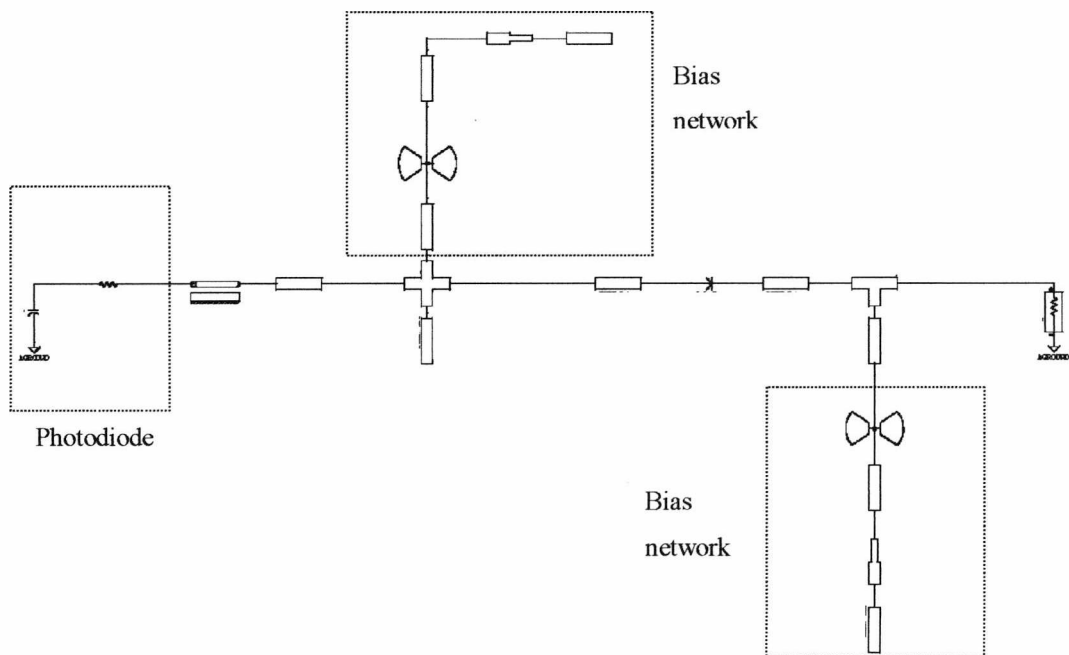
Table 5.3 Changes of microstrip line resonator Input reflection coefficient phase with respect of line width and length.

As no large signal model of the EC2612 was available, only small signal S-parameter simulations could be performed for prediction of the oscillator free-running frequency. Therefore, it was deemed necessary to design a 30 GHz oscillator to test the simulation accuracy first, before the optically injection-locked oscillator was designed. Measurement values from the 30 GHz oscillator showed a reasonable agreement with the simulation result except that the oscillation frequency was shifted 1 GHz higher than the design frequency.

5.4.3. Design of the photodiode insertion circuit

The end of the open circuit resonator was regarded as the best injection point (the point to be connected with the photodiode output) as the level of the free running signal of the oscillator was supposed to be lowest at this point. This maximises the locking bandwidth, which is inversely proportional to the square root of the oscillator's free running output power at the injection point as expressed in Equ 5.2. A commercial chip capacitor was connected in series with the resonator to block the photodiode DC bias. The capacitor has an insertion loss of 2 dB at 30 GHz.

An edge-coupled pin photodiode, supplied by BT [18], was sited on a brass base to ensure RF grounding. The P connection was connected to a 50Ω microstrip line by a bondwire (same bonding method as shown in Fig 5.6). An open circuit stub was used to match the photodiode. Perfect matching to 50Ω is not needed as it will stop the oscillation. The matching circuit should allow most of the 30 GHz signal from the photodiode to pass through to the resonator. Also, the matching circuit needs to maintain the low Q property of the microstrip resonator.



(a) Circuit schematic for RF simulation

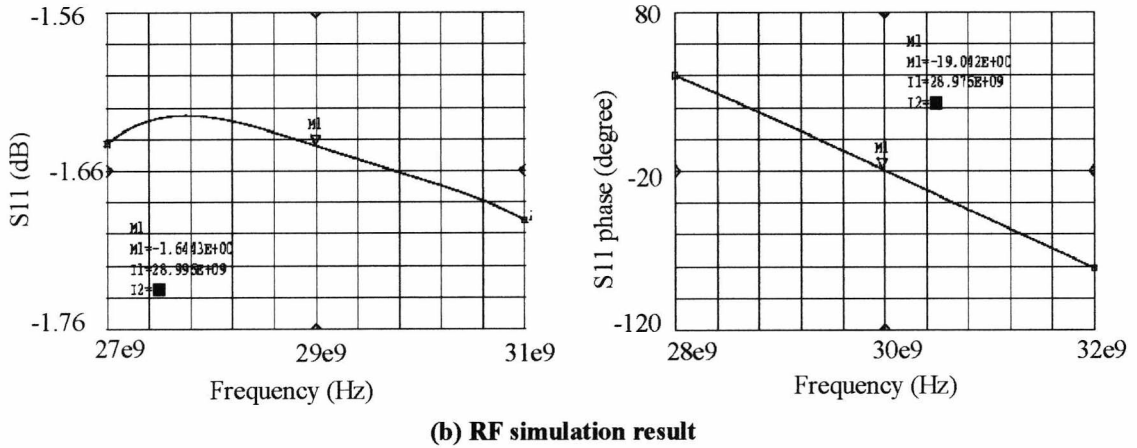
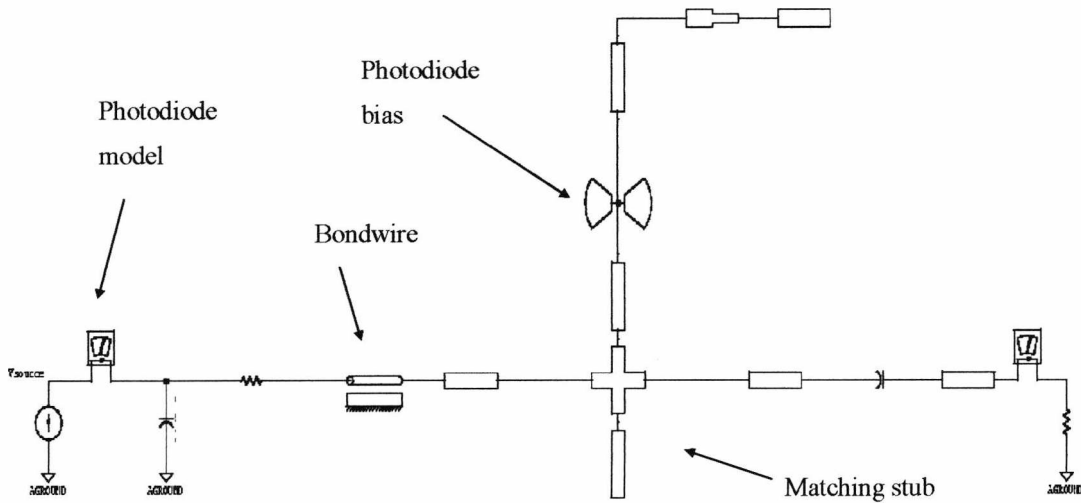


Fig 5.13 RF simulation of the photodiode circuit

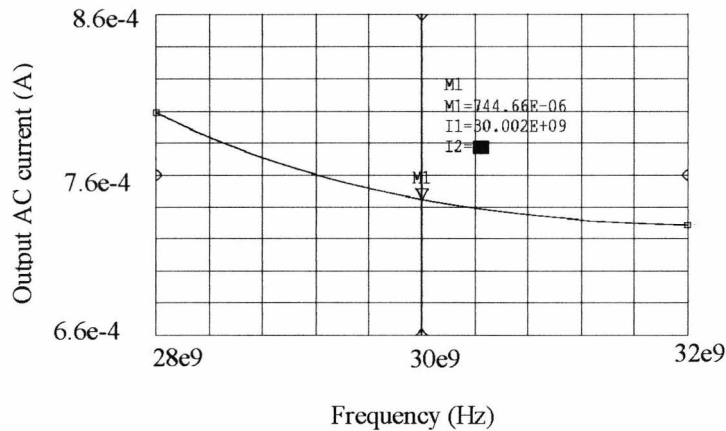
The impact of photodiode insertion on resonator RF performance was investigated first. Fig 5.13a shows the photodiode circuit schematic for RF simulation. Because of the insertion of the photodiode at the resonator end, the resonator cannot be treated as an open-circuited resonator any more. The photodiode needs to be treated as a part of the resonator. The DC bias circuit for the photodiode and the photodiode itself was included in the simulation. One side of the DC decoupling capacitor is connected to the end of the resonator, the other side is connected with the photodiode output by a 50 ohm transmission line. The length of the 50 ohm transmission line connected with the capacitor is optimised to make sure the oscillator free-running frequency is the designed frequency. The insertion of the photodiode increases the resonator Q (the length of the resonator is increased). However, this is inevitable in the case of the optically injection-locked oscillator, as the photodiode has to be inserted. The deviation of phase in relation to the frequency ($d\phi/df$) can be calculated using Fig 5.13b, and the loaded Q of the resonator is calculated to be 8 using Equ 5.13. The oscillation phase condition is satisfied by varying the length of the 50Ω microstrip resonator.

Fig 5.14 shows the AC simulation of the photodiode circuit. An AC current source was used to model the photocurrent and a resistor with a value equivalent to the input resistance of the oscillator part was used to model the load. The output current was

monitored by a current meter connected in series with the load (Fig 5.13a). With an input RF photocurrent of 0.8 mA, an output current of 0.74 mA was obtained from the simulation (92% of the input current).



(a) Circuit schematic for AC simulation.



(b) AC simulation result

Fig 5.14 AC simulation of the photodiode circuit

5.4.4 Completed optically injection-locked oscillator

Finally the oscillator part and resonator part were connected together to form the complete oscillator. A start oscillation frequency test port provided by MDS (described specifically in Chapter 3) is used for testing the start oscillation frequency. Fig 5.15

shows the simulation results of the complete optically injection-locked oscillator. Fig 5.15a shows the oscillator feedback loop gain. The oscillator loop gain is 3.9 dB at 29 GHz. Fig 5.15b shows the loop gain phase. The loop gain phase is 0 at 29 GHz, which means that the oscillator starts to oscillate at 29 GHz. The oscillator loaded Q is calculated using Equ 5.13 and Fig 5.15b:

$$\begin{aligned}
 Q &= \frac{f_o}{2} \frac{d\varphi}{df} \\
 &= \frac{29 \times 10^9}{2} \frac{d(18.1 - 0)}{d(29.4 \times 10^9 - 28.6 \times 10^9)} \\
 &= 40
 \end{aligned} \tag{5.7}$$

The increases in loaded Q compared with the resonator alone is caused by the reactive components in the oscillator active part.

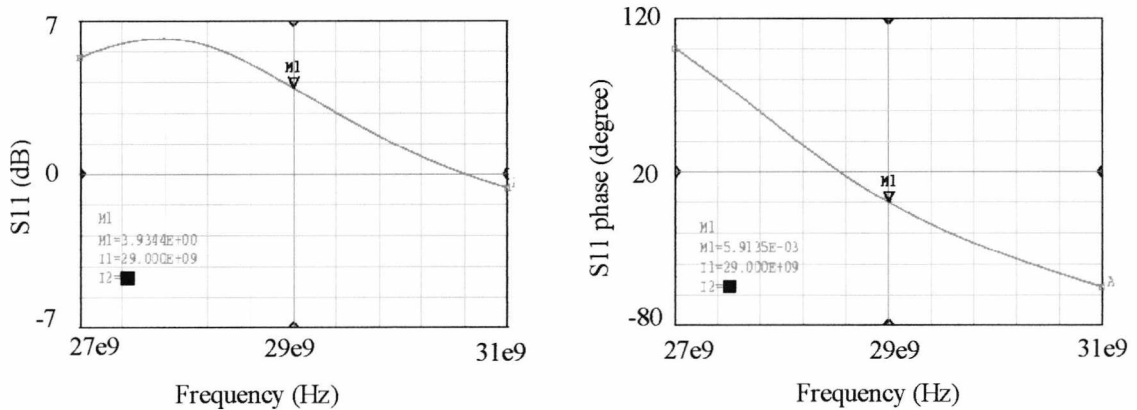


Fig 5.15 Simulation result of the completed optically injection-locked oscillator

5.5 Experimental results

5.5.1 Set-up

The fabricated optically injection-locked oscillator circuit was sited on a brass block with the photodiode connected to it via a bondwire (Fig 5.16). Lensed fiber was used to maximise the optical coupling efficiency into the edge-coupled photodiode. The fiber was positioned by a 3-axis, 20 nm resolution translation stage. The RF output was

measured using a HP8563 spectrum analyzer with an external waveguide mixer (HP11704C).

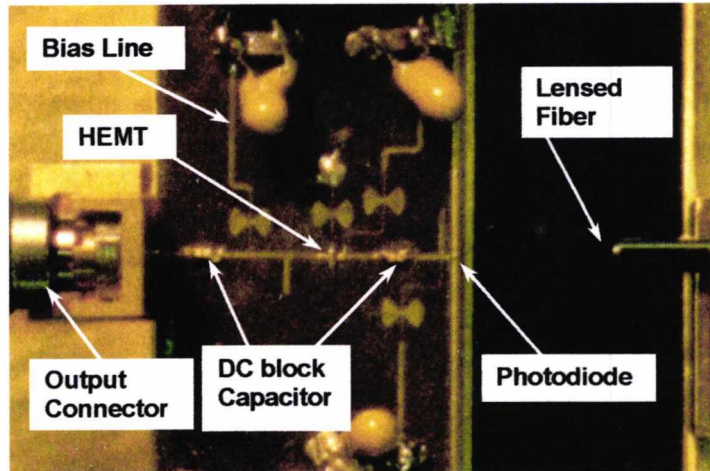


Fig 5.16 Optically injection-locked oscillator

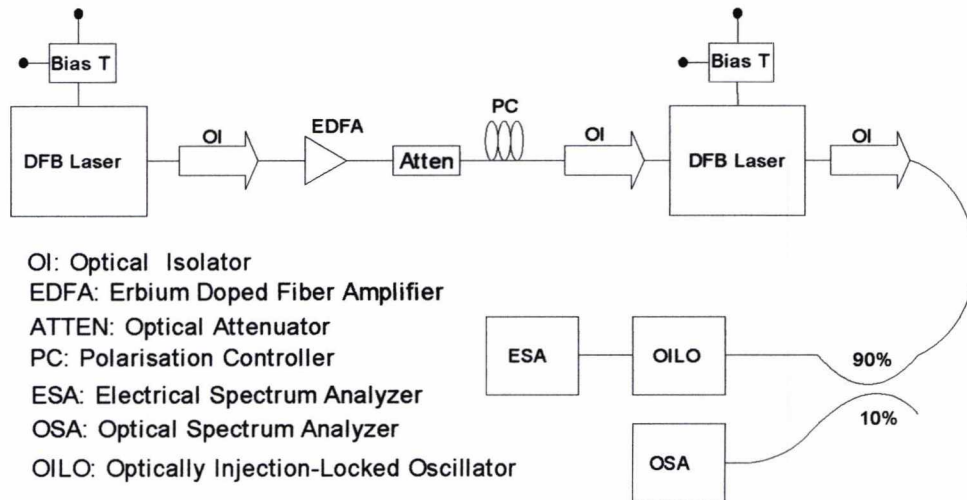


Fig 5.17 Measurement setup for the optically injection-locked oscillator using the master/slave sideband injection-locking millimetre-wave source.

A master/slave laser sideband injection-locking scheme [22] was used for the 30 GHz locking signal generation (Fig 5.17). The modulation index of the master/slave millimetre-wave signal generation system was first measured using a commercial New Focus photodiode. The maximum measured RF power from the photodiode was -35

dBm. However, 5 dB cable loss was measured for the system and half of the generated photocurrent is consumed by the matching resistor in the New Focus photodiode module. The peak RF current generated by the photodiode was then calculated to be 0.4 mA. As the measured DC current was 0.478 mA, the maximum modulation depth obtained from the set-up was 83.7%.

5.5.2 Measurements of 30 GHz optically injection-locked oscillators

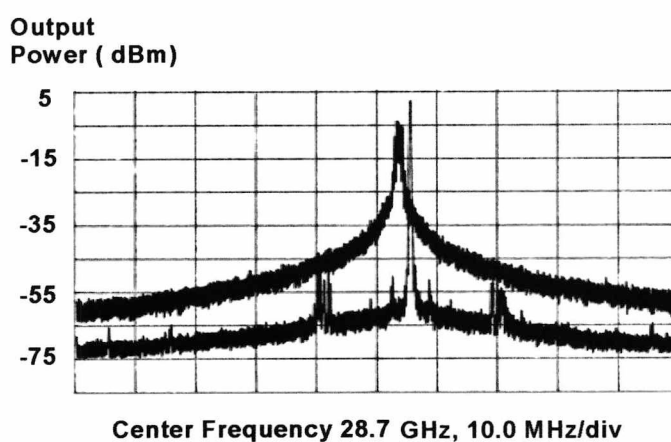


Fig 5.18 Comparison of the oscillator output before and after locking. Bias point: $V_{gs} = 0$ V, $V_{ds} = 3$ V, $I_{ds} = 20$ mA.

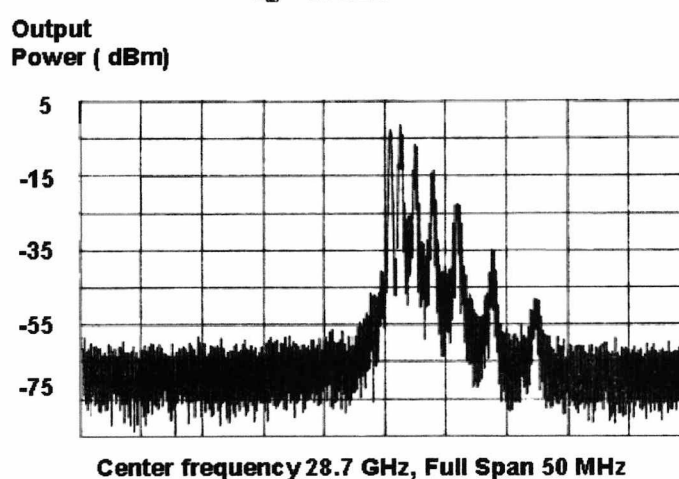


Fig 5.19 Output spectrum of the optically injection-locked oscillator just beyond the edge of the locking bandwidth.

Several optically injection-locked oscillators have been fabricated. Their free-running frequencies were in the range of just over 28 GHz to just under 32 GHz, with microstrip

circuit fabrication variations, device variations (transistor, photodiode and chip capacitor) and bondwire length variations all potential causes of the different free-running frequencies.

The maximum output power without locking was 5.3dBm which is similar to that obtained from an oscillator without photodiode integration (6 dBm). The output power level of the oscillator can be adjusted by varying the bias conditions. Fig 5.18 shows the comparison of the locked and unlocked output signals. The sidebands which are 650 kHz away from the oscillation signal are due to bias circuit oscillations; these have been reduced to a level 55 dB lower than the output using decoupling capacitors, but not completely removed. The locking bandwidth was measured by varying the millimetre-wave frequency of the injected signal. Just beyond the edges of the locking bandwidth, the output signal can clearly be seen to “collapse” in a familiar way [14] into spurious products (Fig 5.19).

The maximum locking bandwidth is achieved with lower oscillation power, obtained by reducing the transistor bias voltage. A 2.6 MHz locking bandwidth was observed with an oscillator output power of -12dBm ($V_{gs} = 0V$, $V_{ds} = 1V$) and a measured DC photocurrent of 0.27 mA. Fig 5.20 shows the variation of locking bandwidth with the injected optical power. A best fit for the expected dependence of locking bandwidth on optical power from an application of Adler’s equation is also shown. For wider measured locking bandwidths, the theoretical fit holds well, but measurement inaccuracies become more significant for the lower locking bandwidth results. The optical coupling efficiency in the measurement set-up is typically 60% of that achievable with an optimum arrangement, thus some improvement in locking signal and locking bandwidth can be expected.

The locking bandwidth that theoretically can be expected from the oscillator can be calculated from Equation 5.2. The maximum stable gain, G_s , has been obtained from simulation to be 7dB. The value of G_p is more difficult to ascertain as it depends on power dissipation in the photodiode; it can be presumed that G_p will be greater than 1

(more power is dissipated on the load than the resonator), but less than G_s . The injected RF power was calculated from the DC photocurrent, modulation depth and the 5dB roll-off in photodiode response at 30 GHz when unbiased (as it was in this case) giving an equivalent injected power (into 50 Ω) of -31 dBm. Using the previously calculated external Q of 40, this suggests a locking bandwidth of between 11 MHz (oscillator power = 5.3 dBm, $G_p = G_s$) and 410 MHz (oscillator power = -12 dBm, $G_p = 1$) should be achievable. Two possible reasons can be considered for the much lower measured locking bandwidth, one is the injection signal loss in the photodiode mismatch circuit and the microstrip line resonator, and the other is the inaccuracy of the locking bandwidth equation.

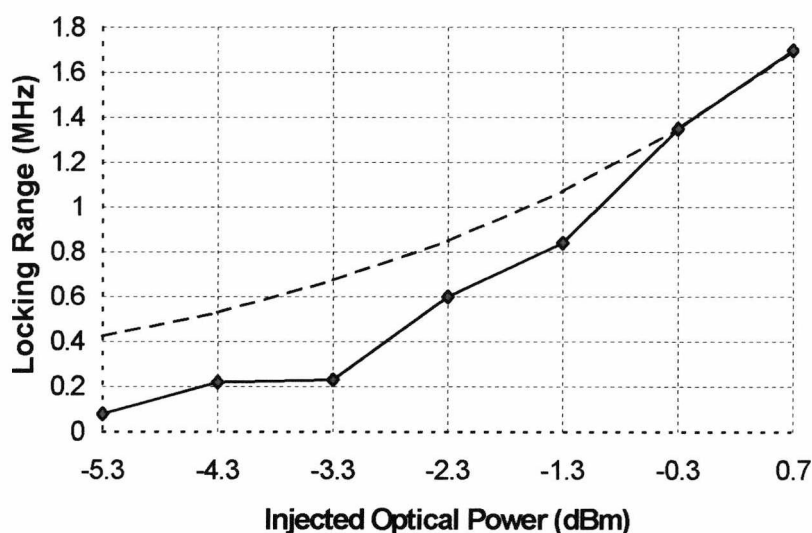


Fig 5.20 Dependence of locking bandwidth according on the average optical power. Bias point: $V_{gs} = 0$ V, $V_{ds} = 3$ V, $I_{ds} = 19$ mA, modulation index of the master/slave millimetre-wave source: 34.9%.

----- Calculated locking bandwidth
 ————— Measured locking bandwidth

The loaded Q of the optically injection-locked oscillator is measured using a 25.6 - 40 GHz circulator from Midisco (Isolation: 14 dB, Insertion loss: 0.8 dB). The oscillator output was connected with one of the circulator ports, and the injection signal from an HP 83640L 10MHz - 40 GHz signal source was injected into the oscillator through the circulator (Fig 5.21). The locking bandwidth was measured by an electrical spectrum

analyser (HP8563E). The oscillator loaded Q was calculated from measurement results using Equation 5.1. Table 5.4a shows the calculated loaded Q of a 31 GHz optically injection-locked oscillator. The loaded Q of the oscillator varies from 240 to 550 depending on the injection signal power. The 31 GHz optically injection-locked oscillator Q is 10-22 times that of the 31 GHz oscillator using microstrip resonator. The measured Q for a 31 GHz oscillator is 3 times the calculated value, while the measured Q for optically injection-locked oscillator is 6-13 times the calculated value.

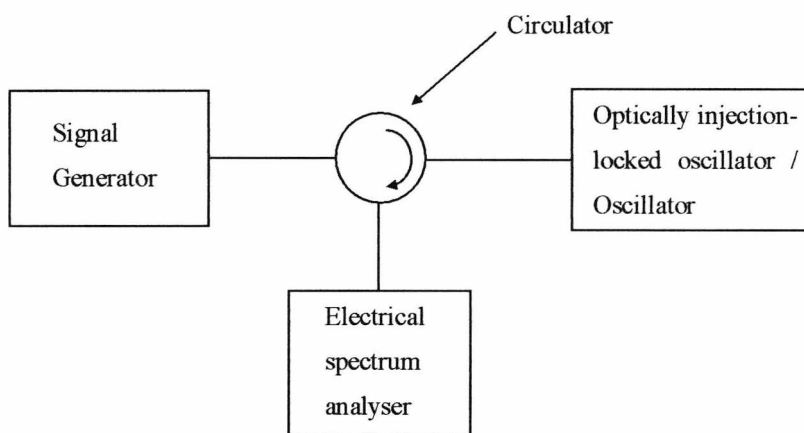


Fig 5.21 Measurement setup for optically injection-locked oscillator Q measurement.

Free running frequency (Hz)	Locking bandwidth (Hz)	Injection signal power (dBm)	Free running signal power (dBm)	Loaded Q
3.13E+10	3.80E+06	-26.5	-3	550.1525721
3.13E+10	2.76E+07	-16.5	-3	239.6819092
3.13E+10	7.57E+07	-6.5	-3	276.3429937

(a) Loaded Q of optically injection-locked oscillator

Free running frequency (Hz)	Locking bandwidth (Hz)	Injection signal power (dBm)	Free running signal power (dBm)	Loaded Q
2.76E+10	4.9E+07	-16.5	10.3	25.78350523
2.76E+10	1.42E+08	-6.5	10.3	28.09446315

(b) Loaded Q of a typical 30 GHz oscillator using microstrip transmission line resonator

Table 5.4 Loaded Q of a optically injection-locked oscillator and a 30 GHz microstrip oscillator.

Summarising all of the above, we can conclude that the oscillator loaded Q is normally higher than the value calculated from the small signal simulation results, and the loaded Q can be decreased by increasing the injection signal power. The reason for this is that the active device (HEMT) and photodiode characteristics that affect the loaded Q more significantly comparing with the conventional oscillators are highly dependent on the signal power for the injection-locked oscillator. For the injection-locked oscillator, the oscillator loaded Q is increased due to the insertion of the photodiode (proved by both simulation and experiment results). A low Q resonator incorporating a photodiode is crucial for improving the locking bandwidth. Locking bandwidth equation for transmission-type injection-locked oscillator presented in Chapter 4, which treat the Q as constant, are not accurate.

5.6 Noise performance comparison with a photodiode plus amplifier module

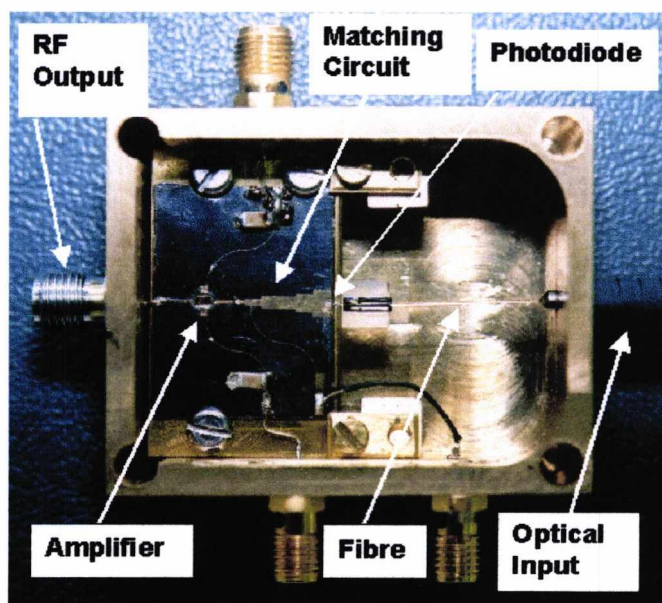


Fig 5.22 Photodiode plus amplifier module.

In order to verify the advantages of optically injection-locked oscillators, a comparison with a photodiode plus amplifier receiver (PD+AMP) was performed [23]. In the PD+AMP receiver, shown in Fig 5.22, a lensed fibre is used to inject the optical signal into the photodiode. A matching circuit is inserted between the photodiode and amplifier, offering a 9 dB improvement over a photodiode with a broadband 50 Ω matching resistor followed by an amplifier with the same gain. Under the same optical input signal conditions as discussed in the previous section, this receiver will produce an output power of -12 dBm. The receiver bandwidth is 2 GHz around 29GHz.

Clearly, by employing the PD+AMP receiver, the optical reference signal frequency can be changed over bandwidths of about 2 GHz without significant loss. The current injection-locked oscillator has a very narrow locking bandwidth; re-design may lead to locking bandwidths of several hundred MHz, but a trade-off with output power can be expected.

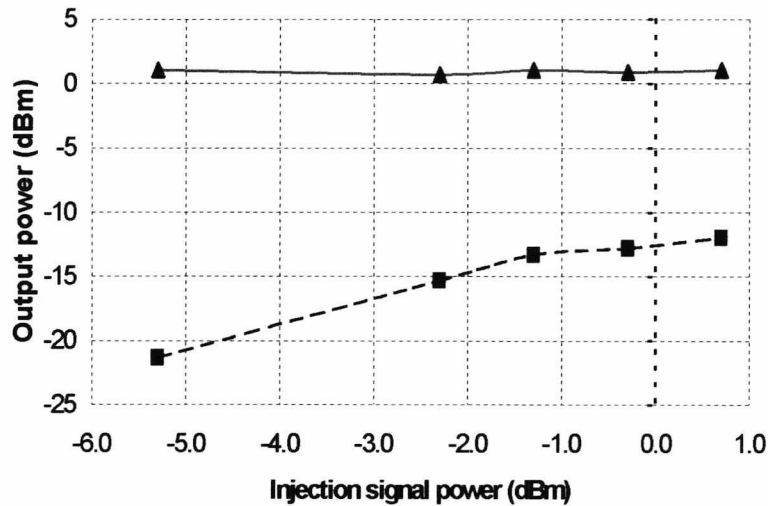


Fig 5.23 Comparison of RF output power dependence on incident average optical power for the optically injection-locked oscillator and impedance-matched photodiode plus amplifier circuit.

- RF output power from the optically injection-locked oscillator
 - - - - - RF output power from the photodiode plus amplifier circuit

Although the photodiode plus amplifier module does have wide bandwidth, the output signal power is limited (to -2 dBm, with optimum coupling conditions and 100% modulation). The output signal power of the optically injection-locked oscillator is mainly dependent on the bias condition. Of course, in both cases additional amplification can be added, but this will add to the antenna unit subsystem complexity. The optically injection-locked oscillator can meet the 1 dBm output power requirement, albeit with limited locking bandwidth. As can be seen from Fig 5.23, the optically injection-locked oscillator output power does not change with an injected optical power variation of at least 6dB. The reason for this is that the oscillator operates in a self-limiting mode. The transistor bias condition defines the oscillator output power. The photodiode plus amplifier receiver output power changes with optical signal power giving it less tolerance to system variations.

5.7 Performance comparison with commercial packaged PD+AMP receivers

The power advantages of optically injection-locked oscillators have been addressed in Section 5.6. As discussed in chapter 4, the phase noise of a free-running optically injection-locked oscillator can be purified by injecting a less noisy signal. This can give a phase noise advantage for an optically injection-locked oscillator. A comparison of phase noise performance between the optically injection-locked oscillator (OILO) and a commercial packaged PD+AMP receiver was carried out using an optical injection phase-lock loop source (OIPLL) [24] and 25 km standard single mode fibre.

5.7.1 Experimental setup

Fig 5.24 shows the measurement set up for the OILO and PD+AMP. An optical reference signal was generated by the OIPLL, at a wavelength of 1550 nm. The maximum modulation index of the OIPLL is 70%, and the maximum output optical power 3 dBm. The optical signal was transmitted to the OILO/PD+AMP either directly (back-to-back)

or through 25km single mode fibre. The signals generated from the OILO and the PD+AMP were observed using an electrical spectrum analyser.

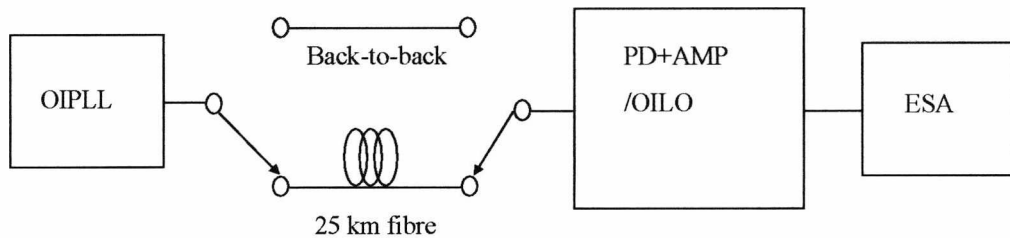


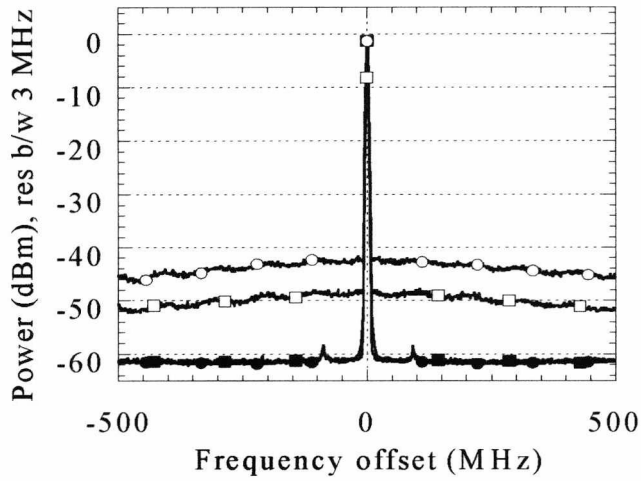
Fig 5.24 Experiment setup for PD-AMP and OILO output spectrum/phase noise measurement. ESA : Electrical spectrum analyser.

5.7.2 Experiment results

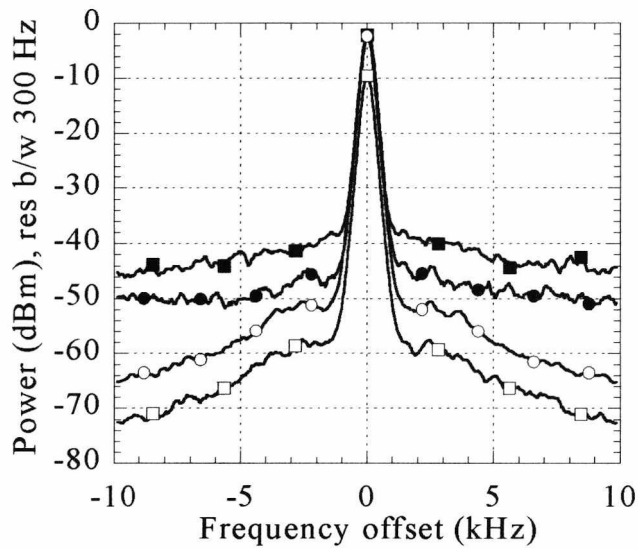
The free-running frequency of the OILO is 32 GHz, the output power at this frequency is -1.15 dBm. With a DC photocurrent in the photodiode of 0.26 mA which corresponds to a -35.8 dBm electrical injection (in terms of a 50 ohm system), the maximum locking bandwidth is 300 kHz. The equivalent OILO electrical gain is 34.85 dB (2 dB higher than the amplifier used by the PD+AMP). In the PD+AMP, a commercial packaged photodiode from Discovery Semiconductor Inc. was employed. The photodiode has a responsivity of 0.47 A/W @ 32 GHz, and the operation wavelength is up to 1550 nm. A millimetre-wave packaged amplifier from Spacetek Labs inc. (Gain: 35.2 dB @ 32 GHz, Noise figure: 3.4 dB @ 32 GHz) is used to boost the photodiode output. The PD+AMP receiver provides an output power of -1.3 dBm @ 31.8869 GHz (amplifier gain: 32.7 dB @ 32 GHz). Fig. 25 shows the PD+AMP and the locked OILO output RF spectra for back-to-back and after 25 km single mode fibre transmission.

Fig 5.25a shows the output spectra for the PD+AMP and the OILO over a span of 1 GHz. For the PD+AMP, both the output power and noise floor are reduced by 7 dB after the reference signal is transmitted by 25 km fibre because of transmission loss, therefore the signal to noise ratio remains the same. For the OILO, the output power remains the same even though the input optical power is reduced by 25 km fibre transmission. The OILO noise floor is identical for both 0 km and 25 km fibre length (Fig 5.25a). For the fibre

length of 25 km, at 50 MHz frequency offset, the OILO output noise floor is 12 dB lower than that of the PD+AMP receiver.



(a) Output spectrum with a span of 1GHz.



(b) Output spectrum with a span of 20 kHz

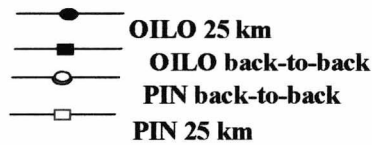


Fig 5.25 Comparison of OILO and PIN+AMP output spectrum.

Fig 5.25b shows the output spectra with a narrower span (20 KHz). The OILO output signal power remains the same after 25 km fibre transmission, but the noise floor is increased by 6 dB near the centre frequency. Both the output power and noise floor of the PD+AMP receiver are reduced by 7 dB after 25 km fibre transmission.

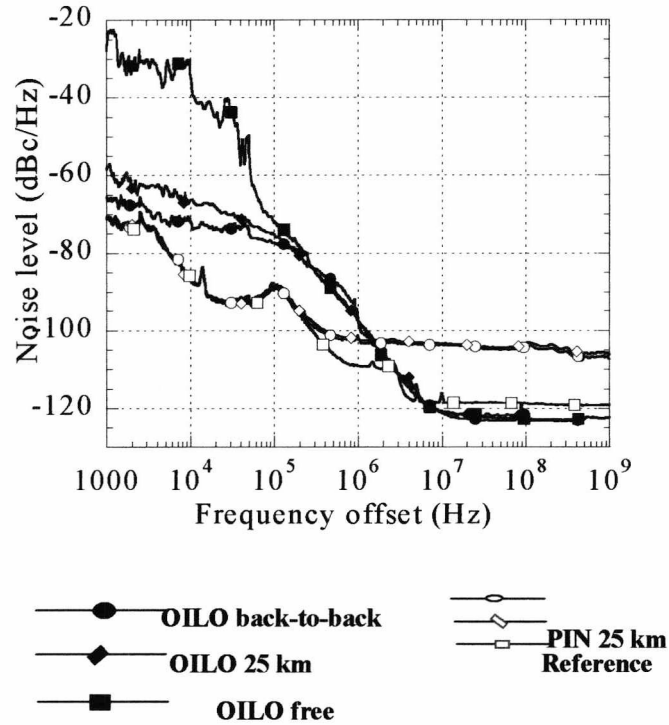


Fig 5.26 Phase noise for OILO, PIN+AMP, and the reference.

The phase noise plots of the reference signal detected by a photodiode, the PD+AMP output and the OILO output are shown in Fig 5.26. At low frequency offsets ($<10^7$ Hz), the OILO free-running output phase noise is higher than that of the reference, while it is lower at high frequency offsets ($>10^7$ Hz). The phase noise for PIN+AMP is identical for both 0 km and 25 km fibre length, and follows the reference phase noise curve up to the offset frequency of 0.28 MHz; above this point, the phase noise is higher than that of the reference as a result of amplifier noise. The locked OILO phase noise is better than that of the free-running output at low frequency offsets ($<0.19 \times 10^6$ Hz), and follows the free-running output phase noise for high frequency offsets. The phase noise of the OILO

output (locked and free-running) is lower than that of the PD+AMP receiver from frequency offsets of 1.9 MHz upwards.

5.7.3 Analysis

The improvement of the output phase noise at low offsets after injection-locking is a result of locking to a less noisy reference signal (Fig. 5.26) [25], and further improvements of low offset noise are expected with stronger locking (wider locking bandwidth). With a wider locking bandwidth, the locked OILO low offset output phase noise would be similar to that of the reference signal [25]. The locked OILO output phase noise is higher after the reference signal is transmitted through 25 km fibre, as this provides a lower injection signal; this results in a decrease in the OILO locking bandwidth.

Observing the phase noise curves of *OILO free* and *OILO 0 km* (Fig. 5.26), we notice that the *OILO 0 km* curve follows the *OILO free* curve after the frequency offset 150 kHz. Noting that the OILO locking bandwidth is 300 KHz, we can conclude that the locked OILO output phase noise is the same as that of the OILO free-running output outside the locking band.

From a frequency offset of 1.9 MHz upwards (Fig. 5.26), the output phase noise of OILO is lower than that of the PD+AMP, and from a frequency offset of 7.3 MHz upwards the OILO output phase noise is lower than that of the reference. The reason is that, outside the locking bandwidth, the OILO output phase noise is dependent on the property of the active device (transistor) and the resonator quality factor [21], and the photodiode shot noise affects the OILO output phase noise only within the locking band. However, for PD+AMP, the output phase noise is affected by the photodiode shot noise within the whole band. By designing the locking bandwidth of an OILO, the narrow-band OILO output phase noise can be similar to that of the reference at lower frequency offsets, and lower than that of the reference at high frequency offsets.

The use of a narrow-band OILO for carrier detection is extremely appealing for broadband communications (~100 MHz) employing a digital modulation scheme, where the system bit-error-rate is affected by the mean noise power within the channel. The use of OILOs in such systems provides lower mean noise power than that of conventional systems employing PD+AMPs.

5.7.4 Summary

A comparison of narrow-band OILO and PD+AMP performance at millimetre-wave frequencies has been presented. The OILO power bonus and low phase noise property have been demonstrated. Narrow-band millimetre-wave OILOs are good replacements for PD+AMP receivers to convert the clock signal from optical domain to electrical domain in broadband radio-over-fibre systems.

5.8 Summary

The design of the first millimetre-wave indirect optically injection-locked oscillator working with a long wavelength signal (1300nm – 1600 nm) has been discussed. The negative impedance design method and computer simulation technique described in Chapter 3 were used for the design. Design challenges such as bondwire modelling and fabrication error simulation have been described.

Optically injection-locked oscillator advantages such as constant output power with variations of injection signal power and improved output phase noise of locked signals have been demonstrated through experiments.

The locking bandwidths of the fabricated oscillators are low. The reasons behind this are low injection signal power coupling efficiency and high oscillator loaded Q as a result of photodiode insertion. These two factors need to be considered further for increasing the oscillator locking bandwidth.

The phase noise comparison of a narrow-band OILO and a PD+AMP performance before and after 25 km transmission has been demonstrated for the first time. The phase noise of the OILO at high frequency offsets is better than that of the reference signal (signal coming out of the photodiode). A narrow-band millimetre-wave OILO is a good replacement for a PD+AMP receiver in broadband radio-over-fibre system.

References

- [1] D. Wake, L. D. Westbrook, N. G. Walker, I. C. Smith, "Microwave and millimetre-wave radio fibre," *BT Technol. J.*, vol.11, pp. 76-88, 1993.
- [2] N. Imai, H. Kawamura, K. Inagaki, Y. Karasawa, "Wide-band Millimetre-wave/optical-network applications in Japan," *IEEE Trans. Microwave Theory Tech.*, vol. 45, pp. 2197-2207, 1997.
- [3] M. Sauer, K. Kojucharow, H. Kaluzni, W. Nowak, "RF-front end and optical feeding system for a millimetre-wave broadband communication system at 60 GHz," *1997 SBMO/IEEE MTT-S Int. Microwave and Optoelectronics Conference 'Link to the Next Generation' Proceedings*, vol. 1, pp. 227-232, Natal, Brazil, 1997.
- [4] K. Kojucharow, H. Kaluzni, M. Sauer, W. Nowak, "A Wireless LAN at 60 GHz - Novel system design and transmission experiments," *1998 IEEE MTT-S Int. Microwave Symp. Dig.*, vol. 3, pp. 1513-1516, Baltimore, 1998.
- [5] J. Y. Liang, C. S. Aitchison, "An optical photo-detector using a distributed amplifier and P-I-N photodiode combination," *1994 IEEE MTT-S Int. Microwave Symp. Dig.*, vol.2, pp. 1101-1104, San Diego, USA, 1994.
- [6] A. J. Seeds and A. A. de Salles, "Optical control of microwave semiconductor devices," *IEEE Trans. Microwave Theory Tech.*, Vol. 38, pp. 577-585, 1990.
- [7] H. Kamitsuna, "A 15-GHz direct optically injection-locked MMIC oscillator using photosensitive HBTs," *IEICE Trans. Electron.*, Vol. E79-C, pp. 40-45, 1996.
- [8] P. Callaghan, S. K. Suresh Babu, N. J. Gomes and A. K. Jastrzebski, "Optical control of MMIC oscillators," *Int. J. Optoelectronics*, Vol. 10, pp. 467-471, 1995.
- [9] M. Karaküçük, W. Q. Li, P. N. Freeman, J. R. East, G. I. Haddad, and P. K. Bhattacharya, "A direct optically injection-locked 2.6 GHz HBT oscillator," *Microwave Opt. Technol. Lett.*, Vol. 6, pp. 609-611, 1993.
- [10] M. Fendler, P. Descamps, J. P. Gouy, J. P. Vilcot, and D. Decoster, "Fibre radio link based on microwave oscillator optical control," *Microwave Opt. Technol. Lett.*, Vol. 18, pp. 193-196, 1998.

- [11] D. Sommer and N. J. Gomes, "Wide-locking bandwidth optically injection-locked oscillators: S-parameter design and modulation effects," *IEEE Trans. Microwave Theory Tech.*, Vol. 43, pp. 1424-1434, 1995.
- [12] X. Wang, N. J. Gomes, L. Gomez-Rojas, P. A. Davies, D. Wake, "Indirect optically injection-locked oscillator for millimeter-wave communication system," *IEEE Trans. Microwave Theory Tech.*, Vol 48, No. 12, pp. 2596-2603, 2000.
- [13] H. Kamitsuna, T. Shibata, K. Kurishima, M. Ida, "Direct optical injection locking of InP/InGaAs HPT oscillator ICs for Microwave Photonics and 40-Gbit/s-class optoelectronic clock recovery," *IEEE Trans. Microwave and Tech.*, Vol. 50, No. 12, pp. 3002-3008, 2002.
- [14] R. Adler, "A study of locking phenomena in oscillators," *Proceedings of the I.R.E. Waves and Electrons*, Vol. 34, pp. 351-357, 1946.
- [15] F. Diamand, and M. Armand, "External Q factor measurement of an oscillator by the injection-locking ellipse," *Electron. Lett.*, Vol. 8, pp. 406-407, 1972.
- [16] Y. Tajima and K. Mishima, "Transmission-type injection-locking of GaAs schottky-barrier FET oscillators," *IEEE Trans. Microwave Theory Tech.*, Vol. MTT-27, pp. 386-391, 1979.
- [17] UMS EC2612 HEMT data available at: <http://www.ums-gaas.com/>
- [18] D. Wake, T. P. Spooner, S. D. Perrin, L. D. Henning, "50GHz InGaAs edge-coupled PIN photodetector," *Electron. Lett.*, Vol. 27, pp. 1073-1075, 1991.
- [19] H. Y. Lee, "Wideband characterization of a typical bonding wire for microwave and millimeter-wave integrated circuits," *IEEE Trans. Microwave Theory Tech*, Vol. 43, No. 1, pp. 63-68, January 1995.
- [20] T. Edwards, *Foundations for Microstrip Circuit Design Second Edition*, John Wiley & Sons, 1992.
- [21] R. W. Rhea, *Oscillator Design & Computer Simulation, Second Edition*, McGraw-Hill, New York, 1997.
- [22] D. S. George, N. J. Gomes, P. A. Davies and D. Wake, "Further observation on the Optical generation of millimeter-wave signals by master/slave laser sideband injection-locking," *International Topical Meeting on Microwave Photonics.*, Digest, Post-deadline papers, pp. 5-7, Duisburg/Essen, Germany, 1997.

[23] L. G. Rojas, N. J. Gomes, X. Wang, P. A. Davies and D. Wake, "High performance optical receiver using a PIN photodiode and amplifier for operation in the millimetre-wave region," *30th European Microwave Conference*, Paris, France, 2000.

[24] L. A. Johansson and A. J. Seeds, "Fibre-integrated heterodyne optical injection phase-lock loop for optical generation of millimetre-wave carriers," *IEEE MTT-S International Microwave Symposium*, Vol. 3, pp. 1737-1740, 2000.

[25] K. Kurokawa, "Injection-locking of microwave solid-state oscillators," *Proceedings of the IEEE*, Vol. 61, pp1386-1410, 1973.

Chapter 6

Improvement of the Locking Bandwidth of the Millimetre-Wave Optically Injection-Locked Oscillator

6.1 Introduction

The locking bandwidth of the millimetre-wave indirect optically injection-locked oscillators designed in Chapter 5 was narrow. Measurement results presented in Chapter 5 showed that the loaded Q of the oscillator increased significantly after integration of the photodiode, and the resonator circuit introduced attenuation of the injection signal power. For increased locking bandwidth, a new resonator configuration needs to be implemented.

In this chapter, a wide-band optically injection-locked structure is proposed. The idea presented in this Chapter will provide a sound foundation for future work.

First, the matching circuit of the photodiode for maximum injected RF signal power and low- Q is investigated first. Then, the insertion point of the photodiode in the

resonator is investigated. A short-circuited resonator incorporating the photodiode and having low-Q and high injection signal power properties is presented. The design of the oscillator active part remains the same as the first oscillator except for the bias topology. The measurement results and problems with this structure are given at the end of this chapter.

6.2 Resonator design

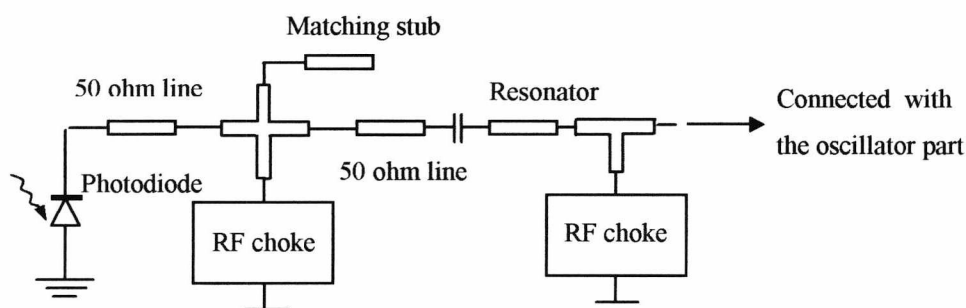


Fig 6.1 Resonator design for the first millimetre-wave optically injection-locked oscillator.

The open circuit resonator design used by the first millimetre-wave optically injection-locked oscillator was quite complex (Figure 6.1). An open-circuit stub was used to match the imaginary part of the photodiode impedance. An additional transmission line is used between the photodiode output and the open-circuit stub to match the real part of the photodiode impedance. This resonator design increases the oscillator loaded Q as several transmission lines are required (longer transmission lines have a higher Q [1]).

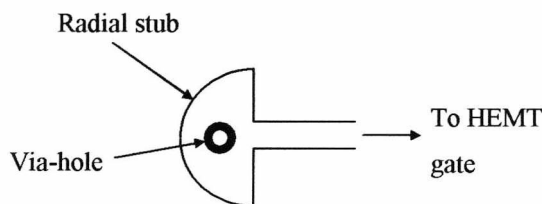


Fig 6.2 RF and DC ground.

In the new low Q resonator design a much simpler short circuit resonator is used (Figure 6.2). The modified self-bias topology described in Chapter 3 is required for short circuit resonator design, and the resonator need to provide ground for both RF (30 GHz) and DC. The resonator ground design is shown in Fig 6.2. The radial stub is

used as the RF short, it is equivalent to a shunt capacitor at 30 GHz. The DC short is realised by a via-hole from the stub to the ground. This DC short is used for both the photodiode and the HEMT gate.

The next task is to design the photodiode integration circuit. The issues related to the photodiode integration circuit design, photodiode matching and choosing of photodiode insertion point, are discussed in the following two subsections.

6.2.1 Photodiode matching

In the new resonator configuration, the bondwire that connects the photodiode anode and microstrip is used to match the photodiode. The photodiode with a bondwire connection is shown in Fig 6.3. The junction capacitance, $C_{junction}$, is 0.7 pF, and the junction resistance, $R_{junction}$, is 10 ohm. A current source is used to model the photocurrent, i_p , and the bondwire is modelled by an inductor (bondwire resistance is ignored).

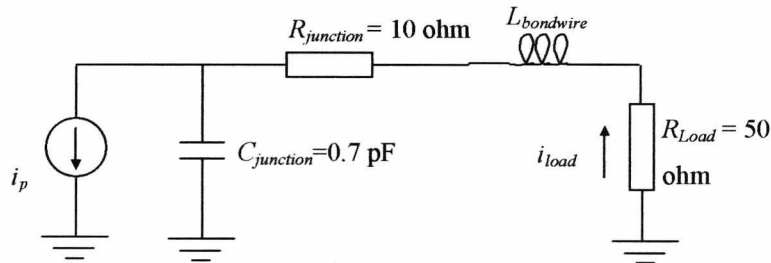


Fig 6.3 Photodiode with a bondwire output matching.

The output current at the load i_{load} is given by:

$$i_{load} = \frac{\frac{i_p}{j\omega C_{junction}}}{R_{junction} + \frac{1}{j\omega C_{junction}} + j\omega L_{bondwire} + R_{Load}} \quad (6.1)$$

Consider the case where the junction capacitance is completely matched by the bondwire inductance. Then:

$$\frac{1}{j\omega C_{junction}} + j\omega L_{bondwire} = 0 \quad (6.2)$$

and we have:

$$i_{load} = \frac{\frac{i_p}{j\omega C_{junction}}}{R_{junction} + R_{Load}} \quad (6.3)$$

For the BT photodiode, $C_{junction} = 0.07$ pF, and the junction resistance, $R_{junction} = 10$ ohm. Suppose the input current is 0.8 mA RF current, the output current of the BT photodiode is 1.01 mA with a load resistance of 50 ohm.

The bondwire length can be calculated by substituting Equ 5.7 into Equ 6.2,

$$\frac{1}{j\omega C_{junction}} + j\omega \cdot 2 \times 10^{-4} \cdot l \cdot \left[\ln\left(\frac{4l}{d}\right) - 1 + \mu\varepsilon \right] \cdot 1 \times 10^{-6} = 0 \quad (6.4)$$

where

l = length of the wire (um)

d = wire diameter (um)

μ = relative permeability (assume to be 1)

ε = skin effect correction factor (a function of wire diameter and frequency)

The final length of the matching bondwire can be optimised by microwave simulation software, such as MDS.

Real part matching of the photodiode is not considered for optically injection-locked oscillators, as additional matching will increase the oscillator Q. Real part matching circuits also increase the complexity of the oscillator resonator.

For the new OILO, the photodiode is matched only by a bondwire.

6.2.2 Photodiode insertion point

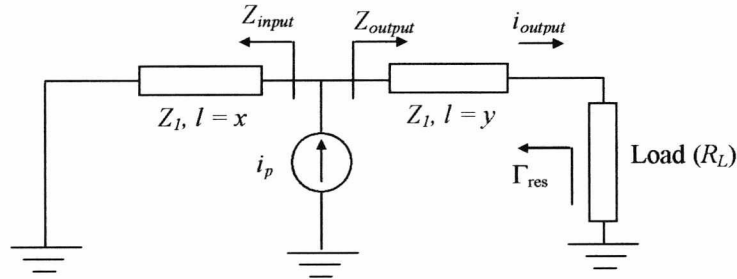


Fig 6.4 Circuit model for a short-circuited resonator with photodiode.

The point on the short circuit where the photodiode is inserted also needs to be investigated to maximise the injection signal power. An equivalent circuit model for a short-circuited resonator with photodiode is shown in Fig 6.4. The characteristic impedance of the resonator is Z_1 . The photodiode is modelled by a current source, i_p . Photodiode capacitance and resistance are ignored for simplicity. The photodiode is inserted at a distance x from the RF short. Z_{input} is the impedance looking from the insertion point to the RF short, and Z_{output} is the input impedance looking from the insertion point to the load. The output current i_{output} , is:

$$i_{output} = i_p \cdot \frac{Z_{input}}{Z_{output} + Z_{input}} \quad (6.5)$$

$$Z_{input} = jZ_1 \tan(\beta x) \quad (6.6)$$

$$Z_{output} = Z_1 \frac{R_L + jZ_1 \tan(\beta y)}{Z_1 + j \cdot R_L \cdot \tan(\beta y)} \quad (6.7)$$

where

$$\beta = \frac{2\pi}{\lambda_g} \quad (6.8)$$

and λ_g is the wavelength in the substrate at the design frequency. Consider both Z_{input} and Z_{output} are positive; then it is not difficult to conclude from Equation 6.6, that we should keep Z_{output} as small as possible to maximise i_{output} . Minimum Z_{output} , R_L , is obtained when $y = 0$ in Equ 6.7, then Equation 6.5 becomes,

$$i_{output} = i_p \cdot \frac{Z_{input}}{R_L + Z_{input}} \quad (6.9)$$

If we fix the length x to a quarter-wavelength ($\beta x = \pi/4$), Z_{input} will be infinity, and R_L in the denominator of (6.9) can be ignored, and the maximum output current, $i_{output} = i_p$ is obtained. Therefore, to maximise the output current, the resonator length should be a quarter-wavelength and the photodiode should be inserted at the load end of the resonator.

Another explanation of this quarter wavelength configuration resonator is that the quarter-wavelength resonator transforms the RF short circuit to open circuit. The photocurrent from the photodiode that is inserted at the end of the resonator will flow to the load instead of to the high-impedance RF open circuit.

Finally, the characteristic impedance of the resonator (Z_I) is chosen to be high (>70 Ohm) for low Q (Table 5.3).

6.2.3 Summary

To summarise the description in the previous two sections, for a wideband optically injection-locked oscillator the resonator configuration should be a short-circuited resonator (both DC and RF) with a length of one quarter wavelength. The photodiode should be matched by a bondwire, and should be inserted at the load end (transistor side) of the resonator.

6.3 Design of new optically injection-locked oscillator

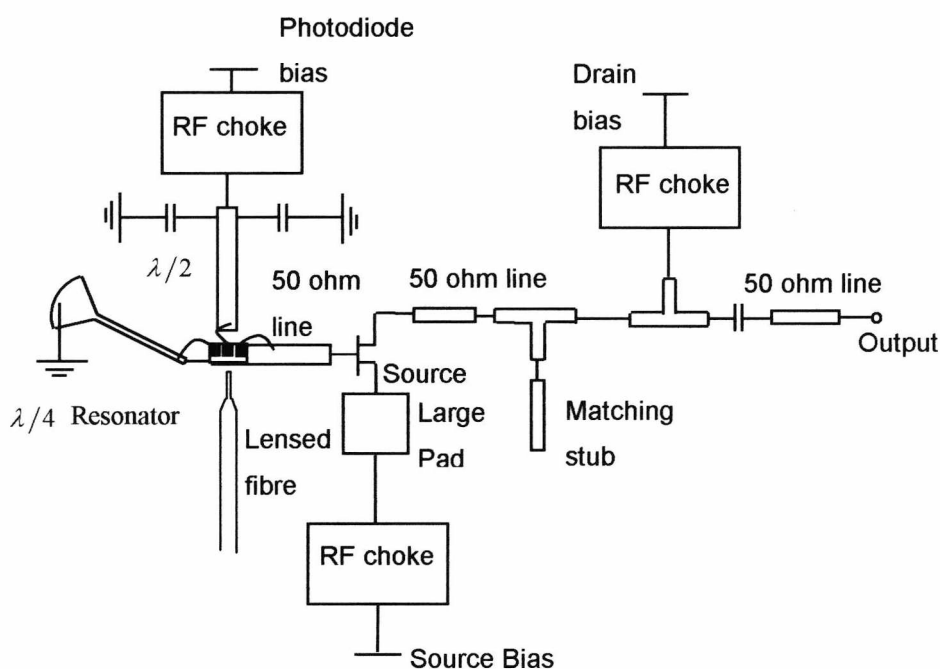


Fig 6.5 Optically injection-locked oscillator with a short-circuited resonator.

Fig 6.5 shows the circuit schematic of the optically injection-locked oscillator with a short circuit resonator. The oscillator design was simulated and optimised using MDS.

The design procedure and targets of the oscillator part were the same as the optically injection-locked oscillator discussed in Chapter 5.

For the resonator part, a 77 Ohm quarter wavelength transmission line was used as the resonator. As described in Section 6.2.2, the cathode of the photodiode will be connected with the end of this resonator for maximum injection power. A radial stub described in Section 6.2 was used as the RF and DC ground. Instead of a BT photodiode, a millimetre-wave photodiode provided by the University of Lille was used as the photodetector in the OILO. The photodiode capacitance is 0.04 pF, and series resistance is 1.2 ohm. Comparing with the BT photodiode, the Lille photodiode has a higher output RF current. However, the quality factor (Q) of the photodiode is lower because of lower junction resistance. There are three bond pads on the photodiode, the centre pad was connected with the photodiode cathode, and the other two pads on the side were connected with the photodiode anode. The photodiode was

sited on the end of a 50 Ohm phase matching transmission line. The length of this transmission line was optimised to meet the oscillation phase condition. The DC bias voltage was applied to the central pad through a bondwire; the bondwire length was optimised using MDS to achieve maximum injection power (Section 6.2.1). The other end of bondwire was connected with a 50 Ohm half wavelength long microstrip line. The gap between this microstrip line and the photodiode is chosen to achieve the required bondwire length. The other end of the microstrip line was RF shorted using two capacitors. The other two pads of the photodiode were connected with the resonator and phase matching transmission line respectively. The bondwires length for these two connections needs to be as short as possible to minimise the inductance.

The final design was optimised using MDS. The design procedure was the same as that described in Chapter 5. The small signal simulation results show the start oscillation frequency is 30 GHz.

6.4 Measurement results and problems

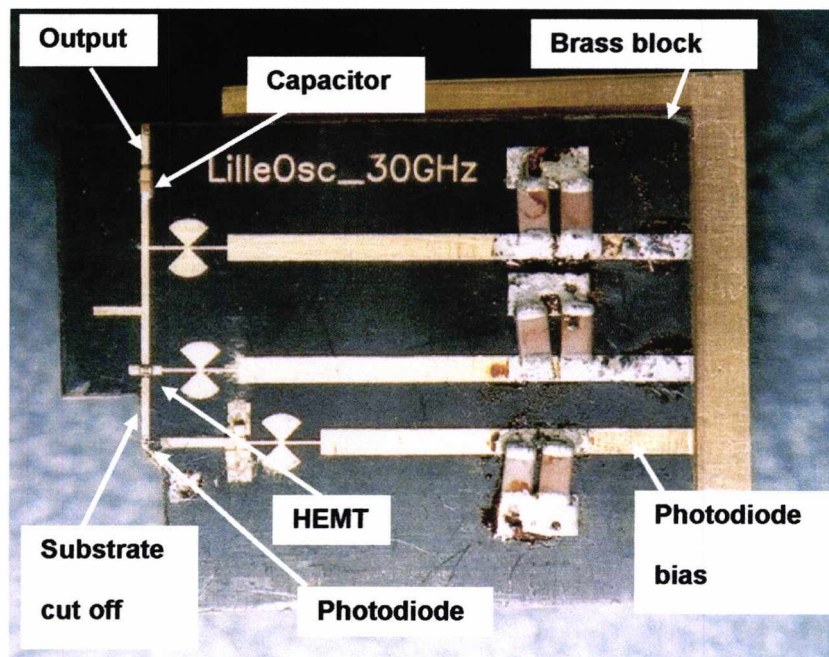


Fig 6.6 Optically injection-locked oscillator with short-circuited resonator.

Figure 6.6 shows the fabricated oscillator. The oscillator was fabricated on RT duriod. The circuit was gold plated for wire bond. The whole circuit was sited on a brass

block test jig. The oscillator was tested using the same setup as described in Chapter 5. With a bias condition of, $V_{gs} = 0$ V, $V_{ds} = 3$ V, and $I_{ds} = 34$ mA, the OILO oscillated at 6.57 GHz with an output power of 1.67 dBm. At the 5th harmonic of 33.88 GHz, the oscillator provides an output power -11.63 dBm.

Both the output power and free running frequency were far away from the design specification. The reason was the removal of the duroid substrate (Substrate cut off shown in Figure 6.6). In order to align the lensed fibre to the photodiode, the substrate was cut along the resonator and the 50-ohm line connected between the photodiode and the HEMT. The electromagnetic fields along the microstrip line, therefore, are significantly changed. The lines can not be treated as microstrip lines anymore.

In future designs, removal of the substrate near microstrip lines needs to be minimised and the effect of doing so must be taken into account.

6.5 Summary

A millimetre-wave indirect injection-locked oscillator using a short-circuit resonator has been presented in this chapter. This design gives a start point for future wideband millimetre-wave indirect optically injection-locked oscillators. According to the simulation result, this configuration offers advantages including low-Q, and high injection signal power. However, experimental results of fabricated oscillators have shown a significant difference from the simulation result. The reason is that the removal of the substrate near microstrip lines has not been considered during simulation.

References

- [1] Terry Edwards, *Foundations for Microstrip Circuit Design, Second Edition*, John Wiley & Sons, 1992.

Chapter 7

Conclusions and Future Work

7.1 Summary of the thesis

This thesis has presented a theoretical analysis and experimental results on millimetre-wave indirect optically injection-locked oscillators. The first millimetre-wave indirect optically injection-locked oscillator working with a long wavelength optical signal has been fabricated during the work reported in this thesis. For the first time, differences between Kurokawa's locking equation and Adler's locking equation have been highlighted. Finally, advantages of using optically injection-locked oscillators in millimetre-wave radio-over-fibre systems such as constant output power and low phase noise have been demonstrated for the first time.

7.1.1 Summary of theoretical work

Photosensitive devices for optically injection-locked oscillators were reviewed in this thesis. Due to the inavailability of high frequency HPTs, the PIN photodiode was

identified as the most suitable optical detector for high frequency optically injection-locked oscillators for this work.

Optically injection-locked oscillators were classified as direct optically injection-locked oscillators and indirect optically injection-locked oscillators. Direct optically injection-locked oscillators have the advantage of simple design, however, the wavelength of the injection signal is generally limited to short wavelength. Indirect optically injection-locked oscillators can work with long wavelength signals, but they are more difficult to design.

The application of optically injection-locked oscillators in millimetre-wave radio-over-fibre communication systems has been discussed in this thesis. The advantages of using optically injection-locked oscillators in these systems include low cost, constant output power, and low noise.

The negative resistance method was identified for designing optically injection-locked oscillators and has been reviewed. Computer simulation techniques can be used for the design. Large signal simulation provides more accurate results for oscillation frequency and output power than small signal simulation, but large signal models for devices may not always be available.

Both Kurokawa's and Adler's theories for reflection type injection-locking were reviewed in detail. Differences between Adler's and Kurokawa's locking equations were identified by the author for the first time.

Theories of transmission type injection-locking developed by Tajima were reviewed. Tajima's test results showed transmission type injection-locked oscillators have a wider locking bandwidth than that of reflection type injection-locking oscillators.

Theories for optically injection-locked oscillators were introduced. Locking bandwidth equations for reflection type and transmission type optically injection-locked oscillators were derived.

7.1.2 Summary of design and measurement work

The design of the first millimetre-wave indirect optically injection-locked oscillator was presented in this thesis. Design considerations such as bondwire modelling and fabrication error simulation were described. A novel microstrip resonator incorporating a PIN photodiode has been designed. Measurement results showed that the maximum oscillator free-running output power was 5.3dBm. The oscillator output phase noise has been reduced significantly by locking to a cleaner signal. The advantages of optically injection-locked oscillator such as constant output power and low output phase noise have been demonstrated by experiment results.

7.2 Achievements of the work

The main achievements of the work presented in this thesis are:

1. The Differences between Adler's and Kurokawa's locking bandwidth equations have been identified.
2. Locking bandwidth equations for optically injection-locked oscillators have been developed.
3. The first millimetre-wave indirect optically injection-locked oscillator working with a long wavelength optical signal has been developed.
4. The advantages of using optically injection locked oscillators in millimetre-wave radio-over fibre systems have been demonstrated through experimental results.

7.2.1 Difference between Adler's and Kurokawa's locking bandwidth equation

The differences between these equations that have been identified are:

1. The absence of $1/\cos\theta$ in Adler's equation.
2. The difference in Q factor between Adler's equation and Kurokawa's equation.
3. Larger locking bandwidth predicted by Kurokawa's equation.

Adler's equation is suitable for reflection type injection-locked oscillators that do not employ circulators. Kurokawa's equation is only accurate for high Q electrical reflection type injection-locked oscillators employing circulators.

7.2.2 Locking bandwidth equation for optically injection-locked oscillators

The locking bandwidth equation for optically injection-locked oscillator based on Adler's and Tajima's equations for electrical injection-locked oscillators have been derived during this work. The locking bandwidth equation for a reflection-type indirect optically injection-locked oscillator is:

$$B_{\min} = \frac{\omega_0 \cdot P_{\text{optical}} \cdot R}{Q} \sqrt{\frac{R_L}{P_0}} \frac{1}{\cos\theta} \quad (7.1)$$

The locking bandwidth of a transmission-type indirect optically injection-locked oscillator is:

$$B = \frac{P_{\text{optical}} \cdot R \cdot \omega_0}{Q} \frac{G_s}{G_p} \sqrt{\frac{R_L}{P_{02}}} \frac{1}{\cos\theta} \quad (7.3)$$

where:

$$\frac{G_s}{G_p} = \frac{Q_{ext2}}{Q_{ext1}} \quad (7.4)$$

7.2.3 First millimetre-wave indirect optically injection-locked oscillator working with long wavelength signals

The first millimetre-wave indirect optically injection-locked oscillator working with long wavelength optical signals has been successfully built in this work [1].

The oscillator was designed using computer simulation techniques that can accurately predict the oscillator free-running frequency. A maximum output power of 5.3 dBm and a maximum locking bandwidth of 2.6 MHz were measured from the fabricated oscillator. Results from several fabricated oscillators showed that the free-running frequencies were in the range of just over 28 GHz to 32 GHz. This result shows a good agreement with the small signal simulation result that predicted a free running frequency of 29 GHz. The variation of the locking bandwidth with the injected optical power has a good fit with Adler's equation. However, the calculated locking bandwidth was much higher than the measurement result. The reason for this is that the loaded Q cannot be predicted accurately by small signal simulation. Large signal simulation is necessary for the correct theoretical prediction of the oscillator loaded Q.

7.2.4 Experimental demonstration of advantages of optically injection-locked oscillator

The advantages of replacing PD+AMP receivers with optically injection-locked oscillators have also been demonstrated in this work. Measurement results showed the optically injection locked oscillators provided an extra gain of over 10 dB compared with the PD+AMP receiver that was used in this work. Also, the output power of a locked oscillator remained the same with reduced injection signal power, while the output power of PD+AMP receivers changes linearly with the input signal power. The noise performance comparison between optically injection-locked oscillators and PD+AMP

receivers has been carried out for the first time. Within the locking bandwidth, the output phase noise of a locked oscillator was similar to that of the reference signal (injection signal). Outside the locking bandwidth, the output phase noise of a locked oscillator is determined by the oscillator characteristic, and can be lower than that of the reference signal.

7.3 Suggestions for future work

7.3.1 Extensions to theoretical work

Neither Adler's nor Kurokawa's locking bandwidth equations can accurately predict the actual locking bandwidth of a reflection type injection-locked oscillator. The loaded Q is treated as a constant in these equations while measurement results from this work have shown that the loaded Q changes with the injection power. A new locking bandwidth equation including the effect of changing Q with injection power needs to be developed for predicting the locking bandwidth accurately. Significant theoretical and practical work is required to characterise the relationship between the oscillator Q and the injection signal power.

Until now, only Tajima developed a locking bandwidth equation for transmission type injection-locked oscillators. However, as some of the parameters in his equation cannot be obtained theoretically, this equation cannot be used practically. No locking bandwidth equations are available that can be used practically to direct the design of transmission type injection-locked oscillators. Significant characterisation work needs to be done on transmission type injection-locked oscillators to develop a locking bandwidth equation with parameters can be obtained theoretically for transmission-type injection-locked oscillators. Such an equation is crucial for the design of future wideband optically injection-locked oscillators.

Simulation methods/tools also need to be investigated/developed for predicting the performance of optically injection-locked oscillators correctly. During this work, only

small signal simulation was performed, and only the free-running frequency was predicted. In the future, large signal simulations need to be performed to predict the free-running frequency and output power. The simulation also needs to take into account the change of the loaded Q with injection signal power. The possibility of performing such a simulation using a commercial software package needs to be investigated first. A customised software tool needs to be developed if the commercial software cannot perform the required simulation. The powerful simulation method/tool can be used in commercial/research environments to design transmission type optically injection-locked oscillators. This will speed up the pace of the commercial application of optically injection-locked oscillators.

7.3.2 Future experimental work

The first millimetre-wave indirect optically injection-locked oscillator built in this work has met the output power requirement for a proposed radio-over-fibre system. However, the locking bandwidth was still too narrow for the proposed system. Optically injection-locked oscillators can not be used in radio-over-fibre systems without sufficient bandwidth.

Low loaded Q and high injection signal power must be achieved for a high locking bandwidth. Different oscillator structures can be investigated in the future to achieve this target. A wide bandwidth design presented in Chapter 6 is a good start for the wideband oscillator design.

Millimetre-wave phototransistors were available and used to build direct optically injection-locked oscillators recently [2]. The locking bandwidth has been increased significantly because of high injection signal power when using such devices. It would be very interesting to build an indirect optically injection-locked oscillator using such devices and compare the performance of direct and indirect optically injection-locked oscillators using phototransistors. This comparison can help to identify which type of

optically injection-locked oscillator is most suitable for millimetre-wave radio-over fibre systems.

Another possibility of reducing the loaded Q of an injection-locked oscillator is to reduce the loaded Q of the active device (transistors). The active devices that were used in this work were designed for other applications, and the devices' Q is not optimised to a minimum. The possibility of designing and using customised active devices that have low Q is another area for future work.

As discussed in Chapter 5, the noise of an optically injection-locked oscillator can be optimised by designing the locking bandwidth carefully. Another exciting research area to work on is to develop optically injection-locked oscillators with optimised noise performance. Such oscillators are particularly useful for broadband radio-over-fibre communication systems that require a low jitter clock source.

The use of optically injection-locked oscillators as FM receivers has been demonstrated at low frequency [3]. Due to the limited locking bandwidth of the current oscillator, the same experiments could not be repeated at millimetre-wave frequencies. However, it would be useful to do this experiment using wideband millimetre-wave optically injection-locked oscillators. This experiment will demonstrate the possibility of using millimetre-wave optically injection-locked oscillators as millimetre-wave FM receivers which is another interesting application for optically injection-locked oscillators.

Another useful application for optically injection-locked oscillators is to use them as a clock recovery unit. As the data rates of optical communication systems reach tens of gigabits per second, timing extraction is becoming more difficult and requires complex schemes to provide bit rate flexibility and low jitter clock synchronization. Optically injection-locked oscillators can be simple and cost effective solutions for clock recovery units for such systems. Clock recovery at millimetre frequencies using direct injection locking has been demonstrated [2] [4]. Similar experiments can be done in the future

using millimetre-wave wideband indirect injection-locked oscillators. A performance comparison of using direct and indirect optically injection-locked oscillators can identify the most suitable injection-locked oscillator structure for this useful application. The impact of locking bandwidth on clock recovery performance also needs to be investigated. If the locking bandwidth is too wide, the oscillator may wander away from the locked frequency too easily when there is insufficient clock content. Significant experimental and theoretical work will be required to find the optimum locking bandwidth for this application.

With the realisation of the future developments stated above, optically injection-locked oscillators can be a crucial component for future high performance and low cost optical communication systems.

References

- [1] Xu Wang, Nathan J. Gomes, Luis Gomez-Rojas, Phillip A. Davies, Dave Wake.: 'Indirect optically injection-locked oscillator for millimeter-wave communication system', *IEEE Trans. Microwave Theory Tech.*, Vol. 48, No. 12, pp. 2596-2603, 2000.
- [2] H. Kamitsuna, T. Shibata, K. Kurishima, M. Ida, "Direct optical injection locking of InP/InGaAs HPT oscillator ICs for Microwave Photonics and 40-Gbit/s-class optoelectronic clock recovery," *IEEE Trans. Microwave and Tech.*, Vol. 50, No. 12, pp. 3002-3008, 2002.
- [3] D. Sommer and N. J. Gomes, "Wide-locking bandwidth optically injection-locked oscillators: S-parameter design and modulation effects," *IEEE Transactions on Microwave Theory and Tech.*, Vol. 43, pp 1424-1434, 1995.
- [4] J. Lasri, D. A. Bilenca, G. Eisenstein, D. Ritter, "Clock Recovery at Multiple Bit Rates Using Direct Optical Injection Locking of a Self-Oscillating InGaAs-InP," *IEE Photnics Tech. Lett.*, Vol. 13, No. 12, pp. 1355 – 1357, 2001.

Appendix I

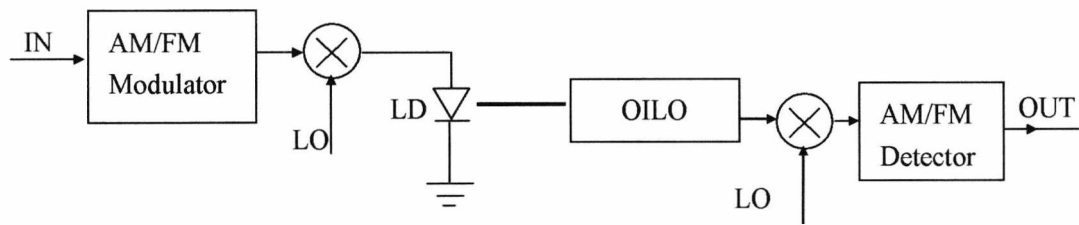
Other Applications of Optically Injection-locked Oscillators

In addition to the radio-over-fibre systems, optically injection-locked oscillators can also be used in other applications.

1. Use of optically Injection-locked oscillator as FM receiver

If an injection-locked oscillator remains in lock over a wide bandwidth, it should be possible to vary the instantaneous frequency of the locking signal (within the locking bandwidth) and obtain a frequency-modulated output while retaining the performance advantage of locked operation. Based on this concept, FM transmission using a wide bandwidth optically injection-locked oscillator has been reported by Sommer et al [1]. Fig 1 shows the system set-up for the FM transmission test. The FM modulated information is first up-converted by a mixer. The LO signal frequency is at the free-running frequency of the optically injection-locked oscillator without injection of the locking signal. The mixer output signal is then used to modulate the laser diode output. The microwave modulated optical signal from the laser diode is transmitted through optical fibre and detected by the optically injection-locked oscillator at the

receiver. The signal from the optically injection-locked oscillator is then down-converted and detected by a FM detector.



LO: Local oscillator, LD: Laserdiode, OILO: Optically injection-locked oscillator,

Fig 1 Transmission set-up for optically injection-locked oscillator used as AM/FM receiver

Sommer reported that a FM signal with a bandwidth of 14.4 MHz ($f_m = 1\text{MHz}$, $\beta = 4$) was successfully modulated onto a 2.1 GHz carrier and detected by an optically injection-locked oscillator (Free running frequency: 2.1 GHz, Locking bandwidth: 200 MHz) [1]. The same experiment could be performed at millimetre-wave frequencies if a suitable locking bandwidth was achieved within the millimetre-wave optically injection-locked oscillators.

2. Application of optically injection-locked oscillators in active phased-array antennas

Active phased-array antennas play an increasingly important role in both civilian and military communication systems [2]-[3]. The advantages of such systems include offering the flexibility necessary for airborne and space-based platforms to handle the demand for rapid beam-hopped, variable area coverage communication links. Conventionally, a mechanical or electrical system would be employed to steer the antenna radiation pattern to the desired direction. These systems suffer the disadvantages of bulky feed structures and electromagnetic disturbance caused by unwanted signals, e.g cross talk between waveguides. The optical beam steering systems are good alternatives to overcome the above disadvantages. There is no

electromagnetic interference for optical fibres, and optical components are much smaller than those used in the conventional electrical or mechanical systems. In the following subsections we will discuss the theory of optical beam steering and the application of optically injection-locked oscillators in such systems.

2.1 Beam steering theory

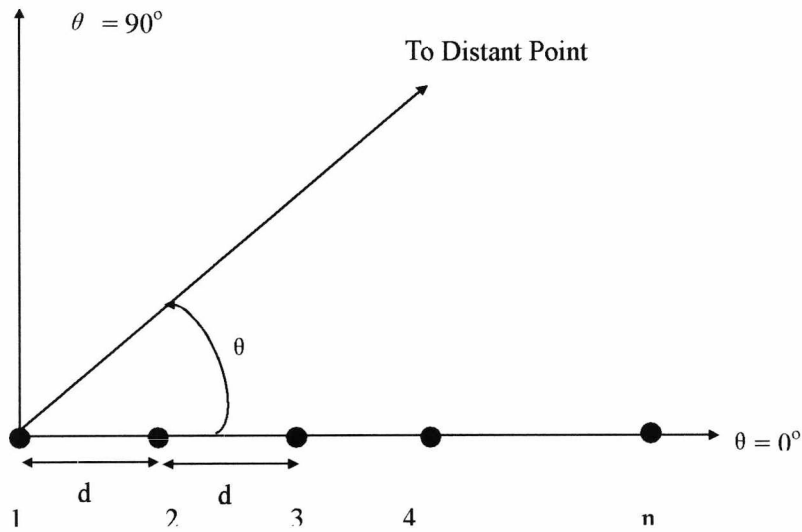


Fig 2 Linear array of n isotropic point sources

Consider a linear array of n isotropic point sources of unit amplitude fed voltage and spacing, d (Fig 2); then the total field E at a large distance in the direction θ is given by [5]:

$$E = 1 + e^{j\psi} + e^{j2\psi} + e^{j3\psi} + \dots + e^{j(n-1)\psi} \quad (1)$$

where ψ is the total phase difference of the fields from the adjacent sources given by:

$$\psi = \frac{2\pi d}{\lambda} \cos\theta + \delta \quad (2)$$

where d is the spacing between sources and δ is the phase difference of the emitted radiation between adjacent sources. Equation 3 can be rewritten as [5]:

$$E = e^{j\xi} \frac{\sin(n\psi/2)}{\sin(\psi/2)} \quad (3)$$

$$\xi = \frac{n-1}{2}\psi \quad (4)$$

The maximum value of $E = n$ is approached when $\psi = 0$. If we set the phase difference between adjacent source δ to 0, we can rewrite Equ 2 as,

$$\psi = \frac{2\pi d}{\lambda} \cos\theta \quad (5)$$

To make $\psi = 0$ requires that $\theta = (2k+1) \cdot \frac{\pi}{2}$, where $k = 0, 1, 2, 3, \dots$. then magnitude of the far field is a maximum.

For this particular type of array, the maximum field is in a direction normal to the array. Hence, this condition, which is characterised by in-phase sources ($\delta = 0$), results in a “broad-side” type array. The beam steering for phased array antennas has been achieved by changing the phase difference δ between each source. For example, we have an n elements array with $d = \lambda/2$, and we want to steer the beam 45 degrees clockwise from the “broad-side” position ($\theta = \pi/2$). The maximum field direction should be steered to have an angle of $3\pi/4$ from the array ($\theta = 3\pi/4$). Equation 2.2 is then used to calculate the required phase difference between each source δ :

$$0 = \frac{2\pi \cdot \lambda/2}{\lambda} \cdot \cos\frac{3\pi}{4} + \delta \quad (6)$$

A δ of 127 degree is calculated from the equation above, to obtain the required beam steering angle. In order to steer the beam ± 90 degrees, a phase change δ of ± 180 degrees is required.

From all of the above, we can summarise that the beam of an antenna array can be steered by changing the phase difference of the signals fed to different elements.

2..2 Use of the optically injection-locked oscillators in active phased-array antennas

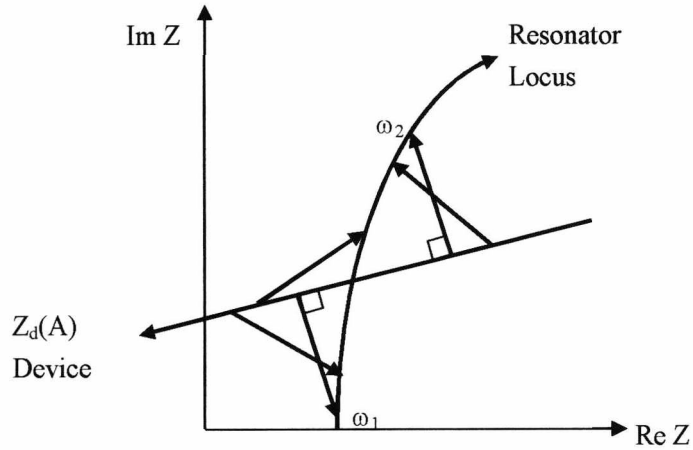


Fig 3 Relationship between the injection vector, device line, and circuit locus as the frequency is varied from ω_1 to ω_2 . Presented by Kurokawa [4].

The oscillator output signal phase is shifted when the injection signal frequency changes within the locking bandwidth. If we keep the injection signal amplitude constant (E_i constant) then changing the injection signal frequency ω_i will cause the injection vector to move along the resonator impedance locus and the device line (Fig 3) [4]. The maximum and minimum injection frequency, ω_1 and ω_2 , occur when the locking vector becomes perpendicular to the device line. As the locking frequency is varied from ω_1 to ω_2 , the phase difference ϕ between the output current and output voltage of the locked oscillator will vary by approximately 180° for small injection signal levels.

The output signal phase change ϕ of an injection locked oscillator is given by [4]:

$$\phi = \arcsin \left[\frac{2(f_i - f_0)}{B} \right] \quad (7)$$

where f_i and f_o are the injection signal frequency and oscillator free running frequency respectively, and B is the locking bandwidth.

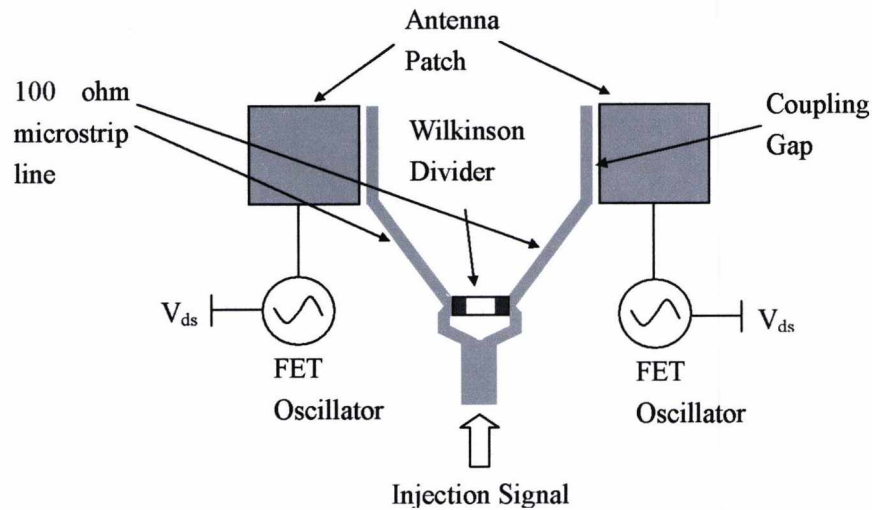


Fig 4 Electrically injection-locked array of two oscillating antennas. Presented by G. Forma [6]

G. Forma has demonstrated an active phased-array microstrip antenna using the injection-locking technique [6]. In his design, each microstrip patch antenna was fed by a FET oscillator, the injection signal was applied to the microstrip antenna patches through a feed network, and coupled to the antenna patch by a 100 ohm microstrip line (see Fig 4). The gap between the 100 ohm microstrip line and patch antenna was carefully designed to ensure efficient coupling of the injection signal to the patch antenna. The beam steering experiment was carried out by tuning the FET drain-source voltage (V_{ds}) of each oscillator while synchronising the array using an injection signal. Generally, both the oscillator output frequency and phase will vary with the change of V_{ds} . However, for the active phase array design shown in Fig 4, the oscillator output frequency was fixed because of injection-locking, and only the oscillator output signal phase changed as a result of V_{ds} tuning. A beam steering potential of ± 30 degrees was reported [6] by tuning V_{ds} .

There are a few disadvantages for this type of injection-locked phased-array antenna. First, there is the complexity of the injection signal feeding network; for large arrays, large numbers of Wilkinson power dividers need to be designed. Also, the port

isolation resistor required by the wilkinson divider is difficult to implement at millimetre-wave frequency. Second, unwanted radiation from the feed network will deteriorate the far-field radiation pattern of the array. The use of optical injection-locking techniques can overcome these problems. Fig. 5 shows the improved phased-array structure employing optical injection-locking. First, an electrical injection signal is modulated onto an optical carrier by direct modulation technique. This signal is then carried by optical fibre to the antenna site and used to optically injection-lock the FET oscillators. Both direct and indirect optical injection-locking techniques can be employed here to lock the FET oscillator. The beam steering is performed by tuning V_{ds} . The use of optical fibre eliminates the interference of the feed network on the antenna radiation pattern. Also the feed network is much simpler than in the beam steering of the antenna array using an electrical injection-locking technique. Extremely high frequency signals can be generated by using optical heterodyne techniques [8].

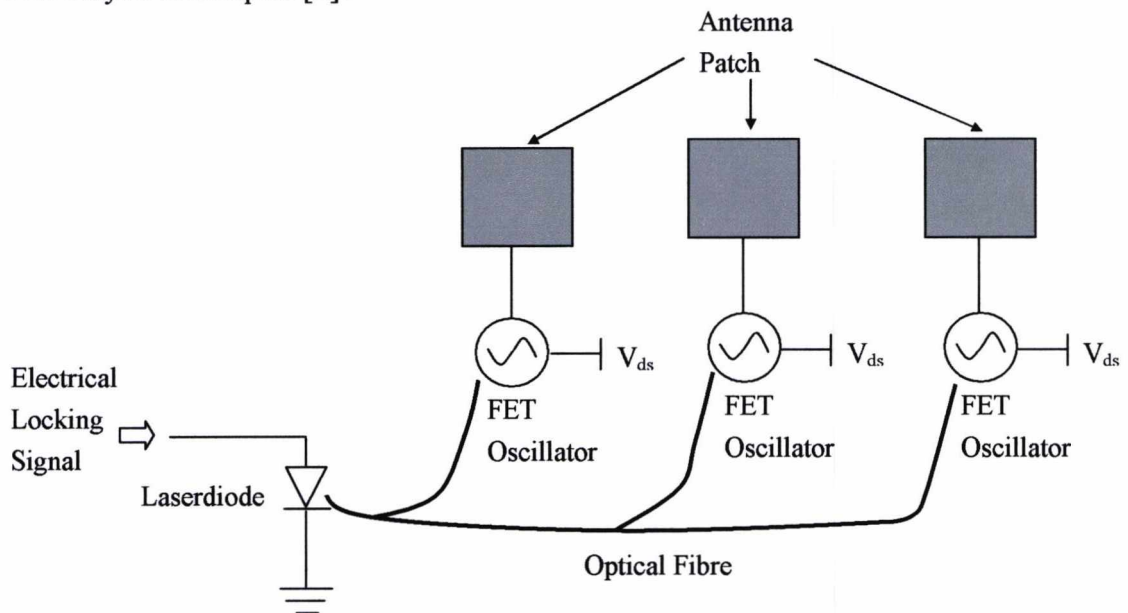
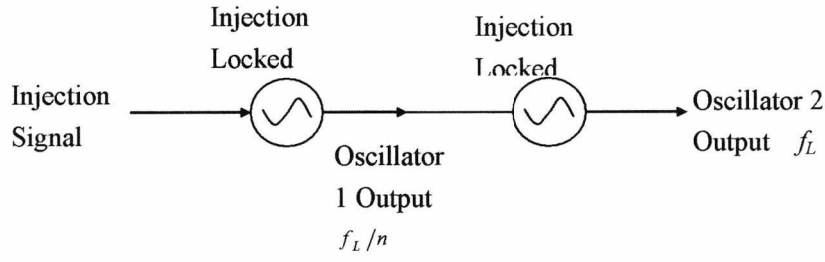


Fig 5 Optically injection-locked array of three oscillating antennas

One of the problems of phased-arrays employing optical injection-locking techniques is that only a 180 degree phase change at the oscillator output can be achieved when the injection signal frequency varies within the locking bandwidth. Only 90 degree beam steering of the phased-array antenna can be performed with a 180 degree phase



f_L is the output signal frequency from oscillator 2, f_1 and f_2 are the free-running frequencies of oscillator 1 and oscillator 2 respectively, f_L/n and f_L are locked frequencies for them where $f_1 \approx$

$$f_2/n$$

Fig 6 Injection-locked oscillators with 360 degree phase shifted. Presented by Zhang et al [19]

change between the input signals at the adjacent antenna patches. A full 360 degree phase shifting between each radiation patch is required for 180 degree beam steering. Zhang et al [8] demonstrated full 360 degree phase shifting of injection-locked oscillators using the sub-harmonic injection-locking technique (Fig 6). The circuit utilised two cascaded sub-oscillators. The first sub-oscillator oscillates at the n th subharmonic of the oscillation frequency of the second sub-oscillator. The reference signal will injection-lock the first sub-oscillator either fundamentally or subharmonically, then the locked output from the first sub-oscillator will injection-lock the second sub-oscillator at a subharmonic factor of n to generate a stable output signal. For an injection signal with fixed frequency and phase, the total phase change ϕ_{total} between the second oscillator output and the injection signal is given by [8]:

$$\begin{aligned} \phi_{total} &= n\phi_1 + \phi_2 \\ &= n \arcsin \left[\frac{2\Delta f_1}{B_1} \right] + \arcsin \left(\frac{2\Delta f_2}{B_2} \right) \end{aligned} \quad (8)$$

Where n is the subharmonic factor for the second injection-locked oscillator, ϕ_1 and ϕ_2 are the phase changes caused by the first and second oscillator respectively, Δf_i

and Δf_2 are the frequency differences between the injection signal and the free-running signal frequency of the first and second oscillators respectively, and B_1 and B_2 are the locking bandwidths of the first and second oscillators respectively.

Clearly, Equation 8 shows that the available variation range of the first term is $n \times 180^\circ$ and the second term varies over a range of 180° . Even without subharmonica injection-locking for the second oscillator ($n = 1$), a phase shift over 360° can be obtained. Zhang [8] observed a 360° phase shift from such a cascaded injection-locked oscillator.

Optical injection locking of an oscillator with phase control by changing the average injection signal optical power was demonstrated by Esman et al [9]. The phase control was realised by varying the bias current to the laser to change the average optical power without significantly changing the microwave optical modulation depth or the effective injected signal power level. Experimental results showed a 180 degree phase shift with an optical power variation from $\sim 20 \mu\text{W}$ to 1.2 mW. The oscillator output power variation is less than 1 dB. This result demonstrates an even simpler way of beam steering, as the electrical tuning of FET oscillators can be removed from Fig 6. The frequency synchronisation of the FET oscillators is realised by injection-locking as before and the phase control is simply done by changing the optical power applied at each oscillator.

References

- [1] D. Sommer and N. J. Gomes, "Wide-locking bandwidth optically injection-locked oscillators: S-parameter design and modulation effects," *IEEE Trans. Microwave Theory Tech.*, Vol. 43, pp. 1424-1434, 1995.
- [2] A. S. Daryoush, "Optical Synchronization of Millimetre-wave Oscillators for Distributed Architectures," *IEEE Trans. Microwave Theory Tech.*, Vol. 38, No. 5, pp467-476, 1990.
- [3] A. S. Daryoush, Edward Acherman, Reza Saedi, Richard Kunath, "High-speed Fibro-optic Links for Distribution of Satellite Traffic," *IEEE Trans. Microwave Theory Tech.*, pp510-517, 1990.
- [4] K. Kurokawa, "Injection-locking of microwave solid-state oscillators," *Proceedings of the IEEE*, vol.61, No.10, pp1386-1410, 1973.
- [5] J. D. Kraus, *Electromagnetics 4th ed.*
- [6] G. Forma and J. M. Laheurte, "Design for Injection-locked Oscillator Arrays," *Electronics Letters*, Vol. 34, No. 7, 1998.
- [7] D. S. George, N. J. Gomes, P. A. Davies and D. Wake, "Further observation on the Optical generation of Millimetre-wave signals by Master/Slave laser sideband injection-locking," *International Topical Meeting on Microwave Photonics.*, Digest, Post-deadline papers, pp5-7, Duisburg/Essen, Germany, 1997.
- [8] X. Zhang, A. S. Daryoush, "Full 360° phase shifting of injection-locked oscillators," *IEEE Microwave and Guide Wave Letters.*, Vol. 3, No. 1, pp14-16, 1993.
- [9] R. D. Esman, L. Goldberg, J. F. Weller, "Optical phase control of an optically Injection-Locked FET microwave oscillator," *IEEE Trans. Microwave Theory and Tech.*, Vol. 37, No. 10, pp1512-1518, 1989.

Appendix II

Design of Oscillator at 15 GHz

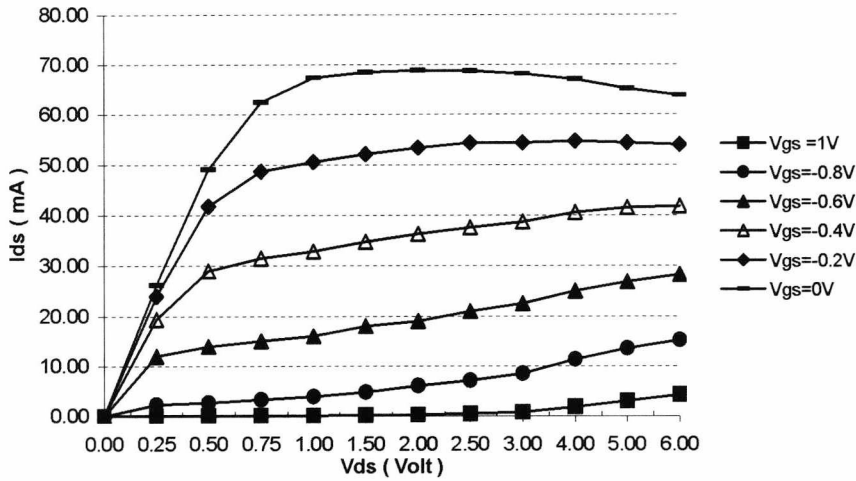
Predicting the performance of an oscillator is very difficult even using the best method. Design of high frequency oscillators has been discussed in Chapter 3. In the following section, the design procedure and measurement results of a 15 GHz oscillator are given. This example gives a practical guidance of high frequency design using computer simulation technique.

1. Choice of device

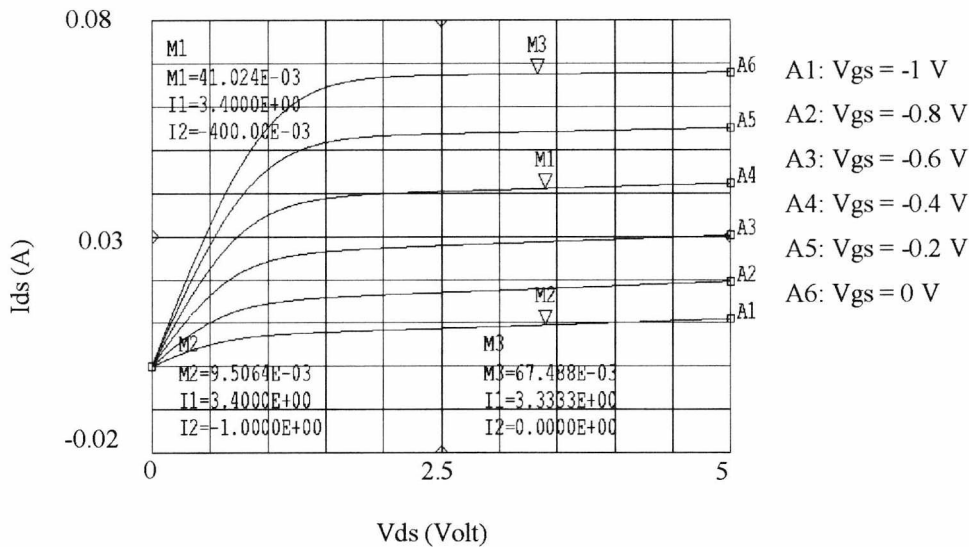
RT Duroid 5880 was chosen as the substrate for the oscillator for ease of fabrication. The height of the substrate is $h = 0.508\text{mm}$, and $\epsilon_r = 2.2$. Microstrip is used to realise the passive components of the oscillator because low-cost and ease of fabrication. A PHEMT from Filtronic (appendix III) was chosen as the active component for high gain. It provides 9.5 dB gain at 18 GHz, and the typical output power at this frequency is around +20 dBm.

A large signal model (Curtice cubic model) of the HEMT was provided by the manufacturer. The first step of the design is to optimise the large signal model to fit to the measurement results. The optimisation includes both RF and DC characteristics. Fig 1a

shows the measured DC characteristic of the LPD200-P70. The simulated DC characteristic was optimised by changing A_0, A_1, A_2 (see Equation 1 in Chapter 3 for the definition of these parameters) using MDS. Fig 1b is the simulated DC characteristics for the optimised model. A good match is obtained between Fig 1a and Fig 1b.



(a) Measured LPD200P70 DC characteristics.



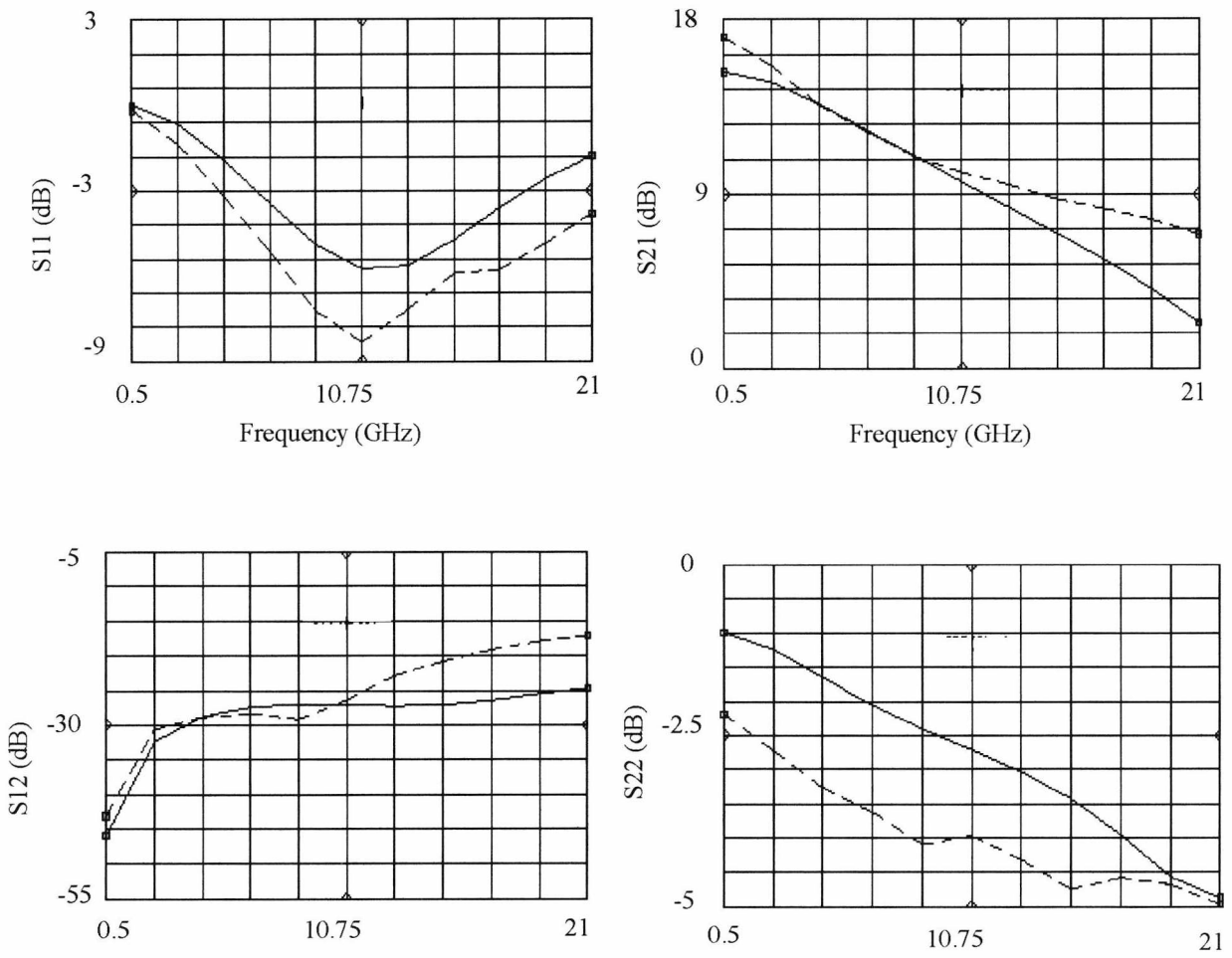
(b) Simulated LPD200P70 DC characteristics

Fig 1 LPD200P70 DC characteristics optimisation

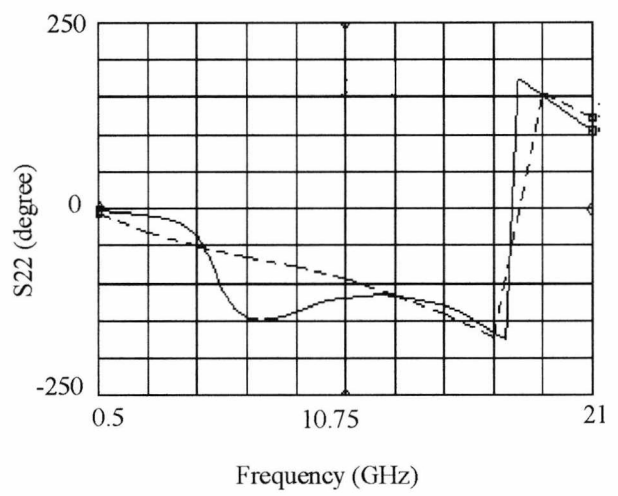
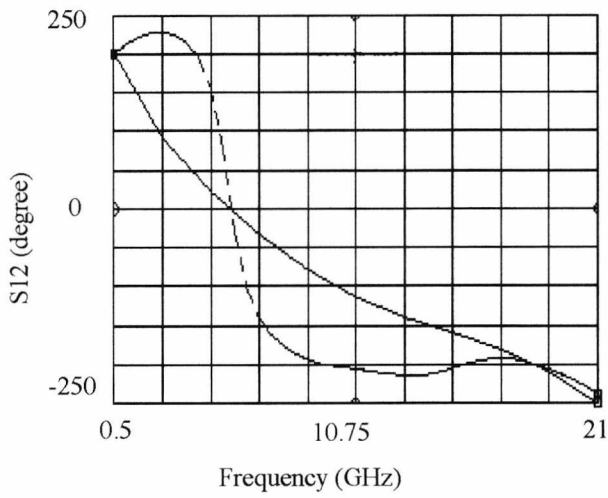
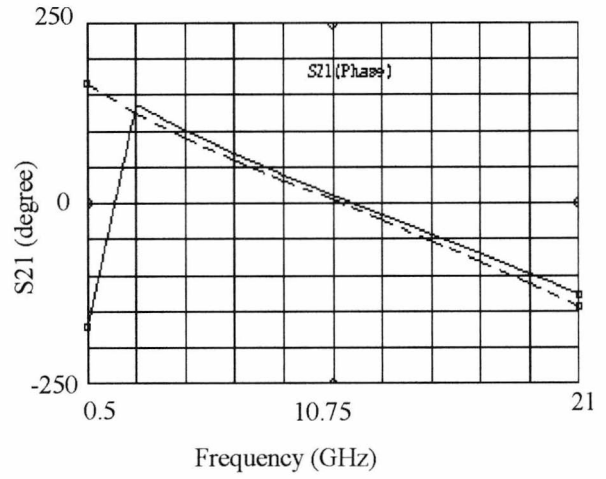
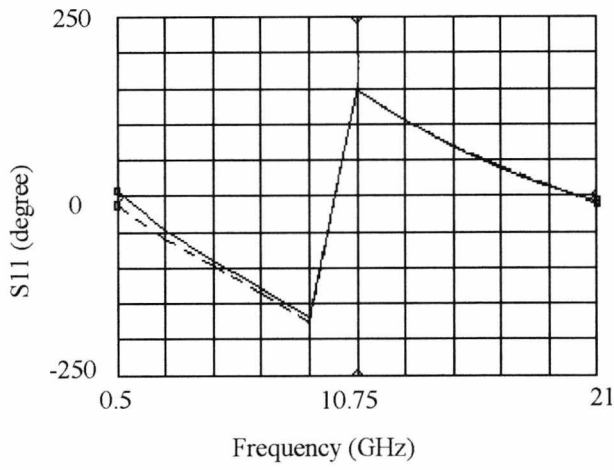
The simulated RF performance was also optimised after the optimisation of DC characteristic. The optimisation is done by comparing the simulated S-parameters results to the measurement results. The parameters in the large signal model are changed to

match the measured S parameter data. The optimisation target is to have a good match for S21, and a reasonable match for the other parameters.

The optimised result is shown in Fig 2. At the design frequency (15 GHz), there are less than 2dB differences between the simulated and measured results for S11, S21, and S22. For the least important parameter, S12, there is 5 dB differences. The maximum phase difference is 20 degree. This result is good enough for the oscillator design.



(a) S-parameter magnitude



----- Measurement results

_____ Simulated Results

$V_{gs}: -0.5V, V_{ds}: 5V, I_{ds}: 34\text{ mA}$

(b) S-parameter phase

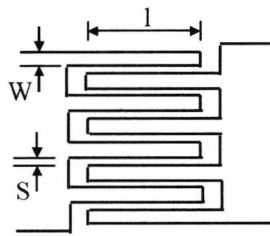
Fig 2 LPD200P70 RF Performance Optimisation

2 Bias topology and oscillator configuration

The A class biasing and dual supply bias topology described in Chapter 3 was chosen to bias the HEMT. Common source oscillator configuration was chosen to achieve high output power

3 Interdigital capacitor

A DC blocking capacitor is normally required between the oscillator output and the load. The function of this DC blocking capacitor is to eliminate the effect of the load on the HEMT DC bias point. The DC blocking capacitor needs to provide a low insertion loss for the oscillator output RF signal. At low frequencies, surface mount capacitors are commercially available to be used as a DC blocking capacitor, however, the cut-off frequency of such capacitors is typically only a few GHz. A microstrip DC blocking capacitor was designed for the 15 GHz oscillator.



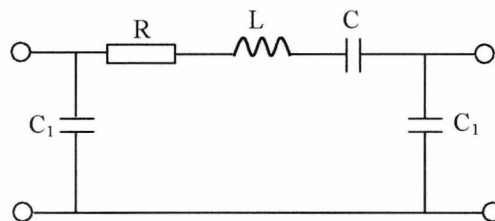
l : Figure length.

W : Figure width.

S : Gap between figures.

(a) Interdigital capacitor

(b) Equivalent Model of



Interdigital capacitor

Fig 3 Interdigital capacitor

A microstrip interdigital capacitor (Fig 3) is considered as the DC blocking capacitor. An interdigital capacitor consists of a group of fingers (Fig 3a). The capacitance is a strong

function of the number of fingers and the gap between the fingers and increases with the length of the fingers.

Fig 3b shows the equivalent circuit of an interdigital capacitor. The capacitor is modelled by a resistor R , an inductor L , and capacitor C connected in series. The equivalent capacitance value is mainly determined by C . C_1 models the shunt capacitance between the fingers to the ground. The analysis of interdigital capacitors has been reported by several researchers [1]-[3]. An approximate close-form expression for the series capacitance is given as [2]:

$$C(pF) = \frac{\epsilon_{re} 10^{-3}}{18\pi} \frac{K(k)}{K'(k)} (n-1)l \quad (1)$$

where $k = \tan^2\left(\frac{a\pi}{4b}\right)$, $a = \frac{W}{2}$, $b = \frac{W+S}{2}$ (2)

and $\frac{K(k)}{K'(k)} = \frac{\pi}{\ln[2(1+\sqrt{k'})/(1-\sqrt{k'})]}$ for $0 \leq k \leq 0.707$ (3)

$$\frac{K(k)}{K'(k)} = \frac{1}{\pi} \ln[2(1+\sqrt{k})/(1-\sqrt{k})] \quad \text{for } 0.707 \leq k \leq 1 \quad (4)$$

and $k' = \sqrt{1-k^2}$ (5)

In the above equations n is the number of fingers, ϵ_{re} is the effective dielectric constant of the microstrip line of width W , and S is the gap between fingers. Both dimensions are in microns.

The parameters of the 1 pF interdigital capacitor were calculated using equation 1-5 first and then the calculated parameters were optimised using HP MDS with goals of $S_{11} < -10\text{dB}$, and $S_{21} < 1\text{dB}$. The number of fingers n was set to six, and the gap between fingers was set to 0.15mm which is the smallest gap that could be fabricated using the facility available.

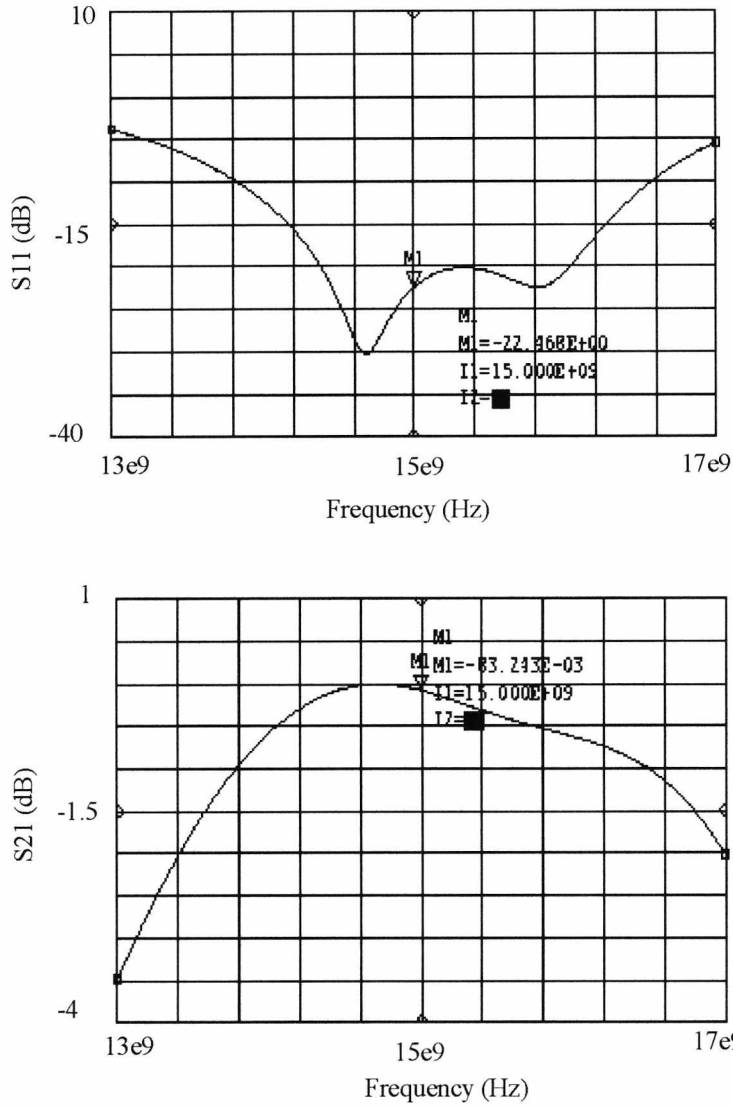


Fig 4 Optimisation result of the interdigital capacitor

The optimisation results (Fig 4) show that the insertion loss (S21) of the interdigital capacitor at 15 GHz is 0.83 dB, and the input reflection coefficient (S11) at this frequency is -22 dB.

4 Oscillator part design

For the design of a common source oscillator, the first step is to select the value of feedback shunt capacitor C_f (Fig. 5) The initial value of C_f was given arbitrarily by the designer and the final value was optimised by HP MDS for a goal of maximum negative

resistance at the input terminal over the band of interest. The initial simulations with lumped capacitors leads to an optimised shunt capacitor value of 0.15pF.

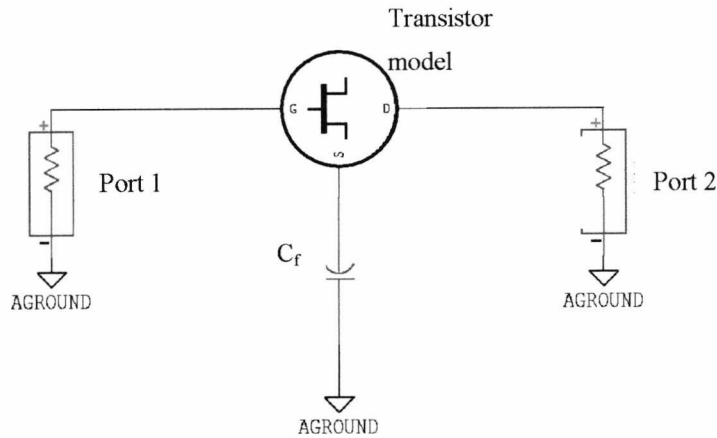


Fig 5 Simulation of the feedback capacitor.

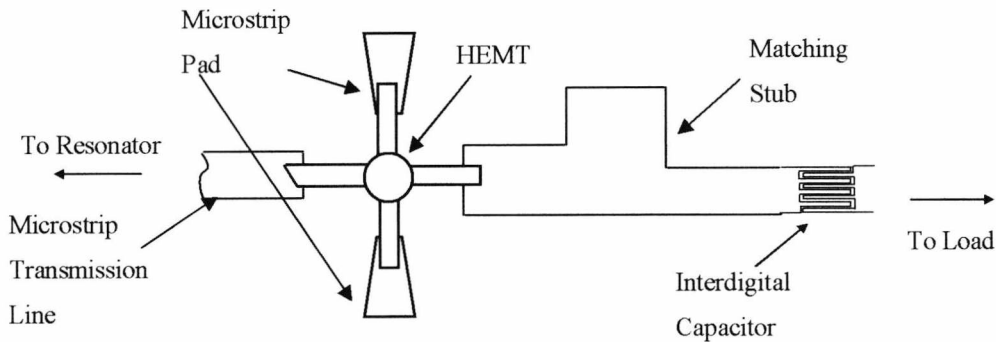


Fig 6 Microstrip pad connected with the HEMT source pad

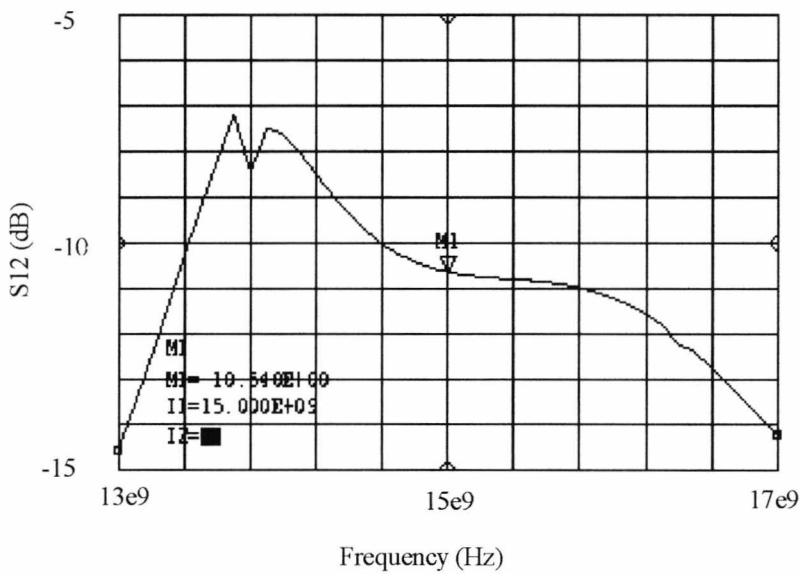
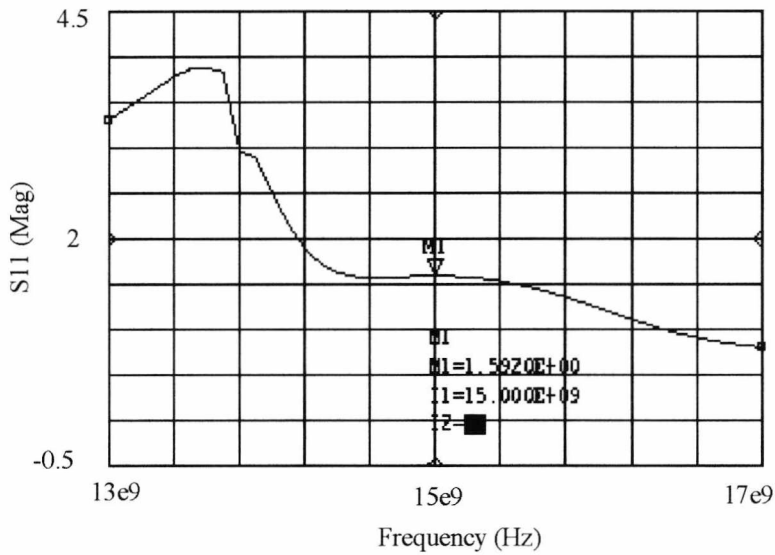
As it is difficult to implement lumped capacitor working at 15 GHz, a large microstrip pad is normally used in place of the lumped shunt capacitor. The size of the microstrip pad is estimated by:

$$C = \frac{\epsilon_0 \epsilon_r A}{h} \quad (6)$$

Where $\epsilon_0 = 8.8419 \times 10^{-12}$, $h = 0.508\text{mm}$ is the height of the substrate, and $\epsilon_r = 2.2$ is the relative permittivity of the substrate. Using equation 6 we approximate the size of the pad for 0.15pF capacitance as 7.8 mm^2 . Later, this value is optimised to 6.2 mm^2 using MDS. The microstrip pad was implemented as a taper shape to reduce the unwanted

coupling to the gate and drain (Fig 6). An open-circuit stub is used to improve the output matching, and a microstrip line connected with the gate improves the gate-drain isolation while maintain the input negative resistance.

The final optimisation results shown in Fig 7. S21 (Gain) is equal to 7.8 dB, S11 was equal to 1.59, S12 (Isolation) was equal -10.54 dB, and S22 (Output matching) was equal to -8.27 dB. These results were acceptable for oscillator part design.



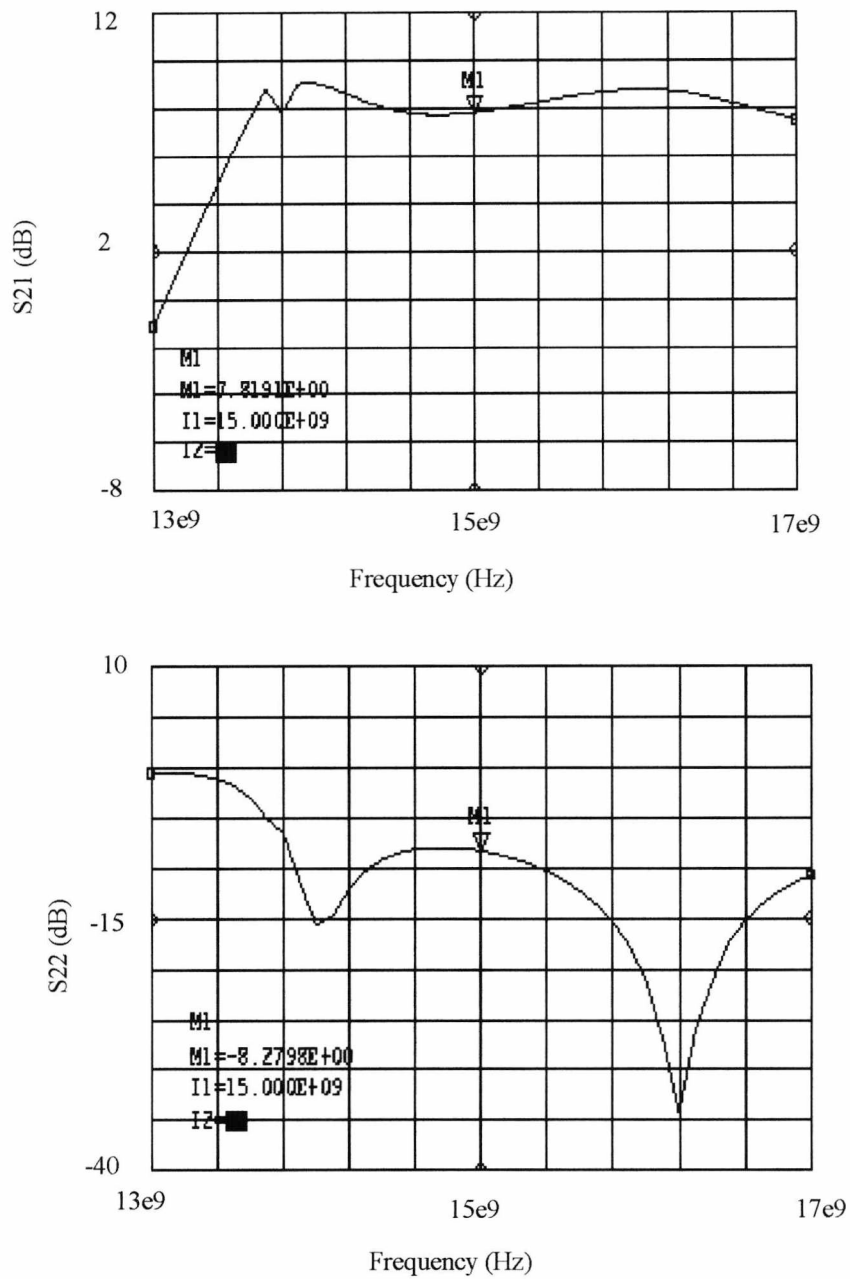


Fig 7 Small signal simulation results of the oscillator part

The bias circuits for the HEMT are not shown in the completed design of the oscillator part in Fig 7, as it is assumed the bias circuits are invisible to the RF path of the oscillator. The resonator will be connected to the gate and the load will be connected to the interdigital capacitor.

5 Resonator

The most commonly used resonator for microwave oscillators are dielectric and microstrip resonators [28]. The dielectric resonator is widely used because of its high Q property (>1000). Dielectric resonator oscillators offer advantages of low phase noise and low output phase noise. The microstrip resonator is realised by a microstrip transmission line. The quality factor of such resonators is lower than that of the dielectric resonator. Therefore, the output phase noise for oscillators using microstrip resonators is not as good as those using dielectric resonators. The advantages of microstrip resonator oscillators are low-cost, ease of fabrication, and no requirement for mechanical tuning. The low- Q property of the microstrip resonator also makes it a good candidate for high locking bandwidth injection-locked oscillators. Microstrip resonators were chosen for the 15 GHz oscillators based on the advantages stated above.

After choosing the resonator, it is necessary to make sure that the real part of the resonator input impedance is lower than the absolute value of the oscillator part input impedance. The phase condition which determines the free-running frequency of the oscillator, was obtained by connecting the resonator part and the oscillator part using a microstrip transmission line.

6 Final layout and simulation result

The final layout of the 15 GHz oscillator is shown in Fig 8. Butterfly shape RF chokes described in Chapter 3 were used to connect bias power supplies to the active device. Two bias lines are connected with the gate and drain respectively. The HEMT source is DC grounded by a via-hole at the end of the source bias line.

Simulation results (Fig 9) of the completed design show that the start oscillation frequency of the 15 GHz oscillator is 15.8 GHz (Fig 9a). The stable state for oscillation is predicted by large signal simulation (Fig 9b). Large signal simulation results show the fundamental oscillation frequency is 5GHz. At 15.08 GHz, the oscillator provides 3 dBm output power. The target of this example is to test the accuracy of the free-running frequency predicted by ADS. Therefore, the oscillator was still built even though the large signal simulation predicted a fundamental free-running frequency of 5 GHz.

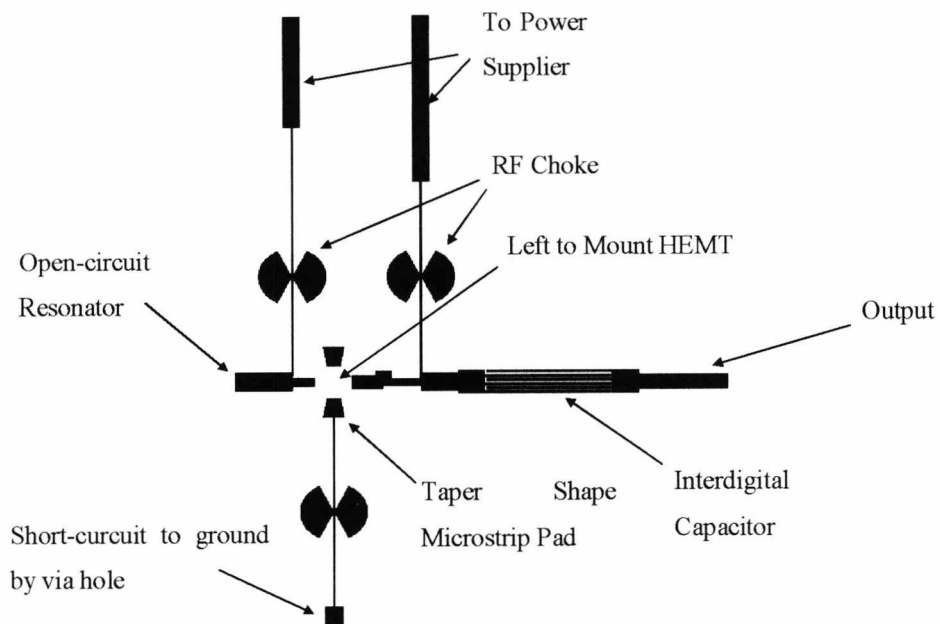
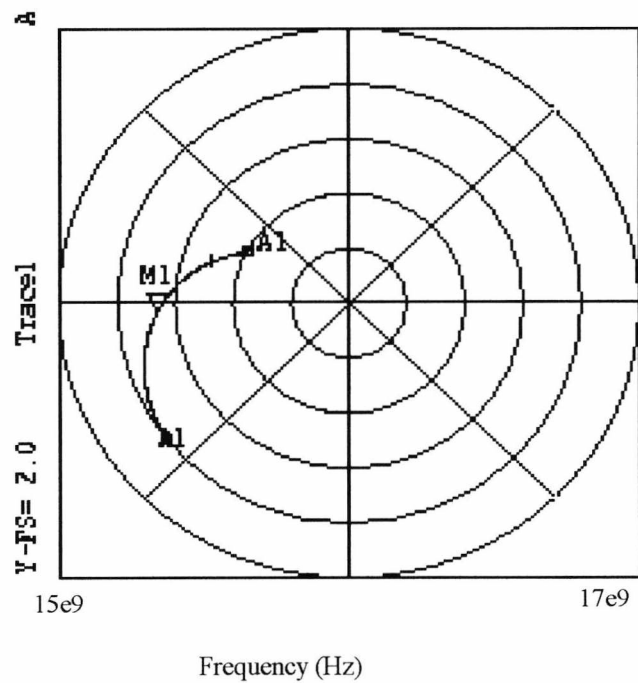
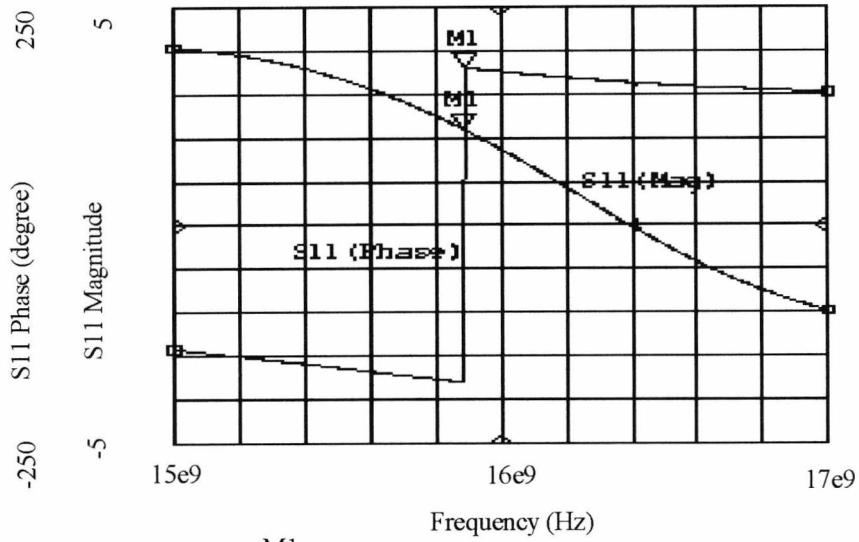


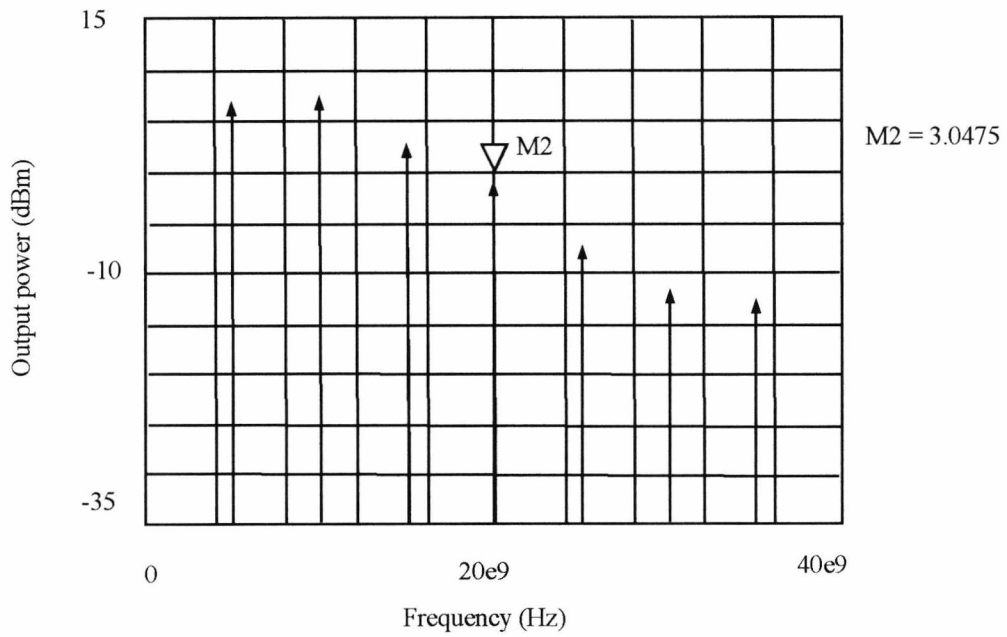
Fig 8 GHz oscillator layout



M1:
 Magnitude = 1.32
 Frequency = 1.582e9



(a) Start oscillation test



(b) Large signal simulation (output spectrum)

Fig 9 Simulation result of the 15 GHz oscillator

7 Measurement result

Two power supplies are used to bias the oscillator; one is connected with the HEMT gate, the other is connected with the drain. An electrical spectral analyser is used to observe the 15GHz oscillator output. The fundamental oscillation frequency is 5 GHz ($V_{gs} : -0.6$ V, $V_{ds} : 5$ V, $I_{ds} : 47.8$ mA), and the output power at this frequency is 17 dBm. Similarly to the simulation results, we see the second harmonic at 15 GHz. The maximum output power is 5.2 dBm ($V_{gs} : -1.2$ V, $V_{ds} : 5$ V, $I_{ds} : 30.7$ mA). The output frequency can be tuned from 14.6 to 15.3 GHz by varying V_{gs} from -1.2 V to 0 V (Fig 3.27). The output frequency changed significantly when V_{gs} varied from 0 V to -0.38 V, beyond -0.38 V the output frequency has less dependence on V_{gs} .

Measurement results of the 15 GHz oscillator proved that the simulation results give a good prediction of the actual oscillation frequency. The next step for the 15 GHz oscillator design will be to try to move the oscillator fundamental oscillation frequency to 15 GHz. This will be achieved by adding shunt stubs to suppress oscillations at 5 and 10 GHz. No further work has been done to improve the 15 GHz oscillator because the objective was to use to test the software accuracy and a example for high frequency oscillator design using computer simulation.

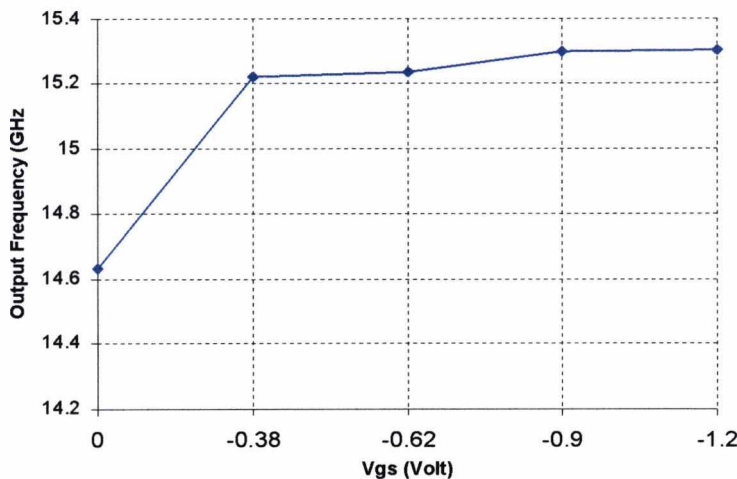


Fig 10 Tuning of the 15 GHz oscillator output frequency with V_{gs}

8 Summary

A microwave oscillator design example using computer simulation technique was described. This example shows the computer simulation technique gives a very good accuracy for predicting the free running oscillation frequency of high frequency oscillators.

References

- [1] G. D. Alley, "Interdigital Capacitors and Their Application to Lumped-Element Microwave Integrated Circuits," *IEEE Trans. Microwave Theory and Tech.*, Vol. MTT-18, No. 12, pp 1028-1033, 1970.

- [2] K. C. Gupta, R. Garg, I. Bahl, P. Bhartia, *Microstrip Lines and Slotlines*, ISBN: 0-89006-766-X, Artech House Inc.

- [3] V. K. Sathir, I. J. Bahl, and D. A Willems, "CAD Compatible Accurate Models of Microwave Passive Lumped Elements for MMIC Applications," *Int. J. Microwave and Millimetre-Wave Computer-Aided Engineering*, Vol. 4, pp148-162, 1994.

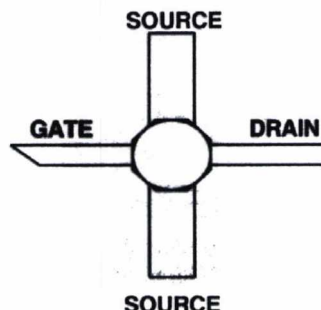
- [4] K. Ogawa, H. Ikeda, T. Ishizaki, K. Hashimoto, Y. Ota, "25 GHz Dielectric Resonator Oscillator using an ALGaAs/GaAs HBT," *Electronics Letters*, Vol. 26, No. 18, pp1514-1516, 1990.

Appendix III

LPD200-P70 Specifications

FEATURES

- +20 dBm Typical Power at 18 GHz
- 9.5 dB Typical Power Gain at 18 GHz
- 16 dB Typical SSG at 2 GHz
- 0.8 dB Typical Noise Figure at 2 GHz
- Low Intermodulation Distortion
- Color-Coded by I_{DSS} range



DESCRIPTION AND APPLICATIONS

The LPD200-P70 is a packaged Aluminum Gallium Arsenide / Indium Gallium Arsenide (AlGaAs/InGaAs) Pseudomorphic High Electron Mobility Transistor (PHEMT), utilizing an Electron-Beam direct-write 0.25 μm by 200 μm Schottky barrier gate. The recessed "mushroom" Ti/Pt/Au gate structure minimizes parasitic gate-source and gate resistances. The epitaxial structure and processing have been optimized for high dynamic range. The LPD200's active areas are passivated with Si_3N_4 , and the P70 ceramic package is ideal for low-cost, high-performance applications that require a surface-mount package. Packages are color-coded by I_{DSS} range.

Typical applications include high dynamic range receiver preamplifiers for commercial applications including Cellular/PCS systems, broad bandwidth commercial instrumentation and military EW amplifiers, and commercial Space applications.

The LPD200 die-level screening is patterned after MIL-STD-19500, JANC grade.

PERFORMANCE SPECIFICATIONS ($T_A = 25^\circ\text{C}$)

SYMBOLS	PARAMETERS	MIN	TYP	MAX	UNITS	
I_{DSS}	Saturated Drain-Source Current $V_{DS} = 2V$ $V_{GS} = 0V$	LPD200-P70-1 GREEN 40 LPD200-P70-2 RED 66		65 85	mA mA	
P_{1dB}	Output Power at 1dB Gain Compression at $f = 18$ GHz $V_{DS} = 5.0V$, $I_{DS} = 50\% I_{DSS}$	19.0	20.0		dBm	
G_{1dB}	Power Gain at 1dB Gain Compression at $f = 18$ GHz $V_{DS} = 5.0V$, $I_{DS} = 50\% I_{DSS}$	8.0	9.5		dB	
NF_{MIN}	Minimum Noise Figure at $f = 2$ GHz $V_{DS} = 3.3V$, $I_{DS} = 25\% I_{DSS}$		0.8		dB	
η_{ADD}	Power-Added Efficiency		50		%	
I_{MAX}	Maximum Drain-Source Current	$V_{DS} = 2V$ $V_{GS} = +1V$	125		mA	
G_M	Transconductance	$V_{DS} = 2V$ $V_{GS} = 0V$	60	80	mS	
V_P	Pinch-Off Voltage	$V_{DS} = 2V$ $I_{DS} = 1mA$	-0.25	-0.8	-1.5	V
I_{GSO}	Gate-Source Leakage Current	$V_{GS} = -5V$		1	15	μA
BV_{GS}	Gate-Source Breakdown Voltage	$I_{GS} = 1mA$	-6	-7		V
BV_{GD}	Gate-Drain Breakdown Voltage	$I_{GD} = 1mA$	-8	-9		V

Get Package Model

DSS-022 WE

Phone: (408) 988-1845

Internet: <http://www.filtronicssolidstate.com>

Fax: (408) 970-9950

ABSOLUTE MAXIMUM RATINGS (25°C)		
SYMBOL	PARAMETER	RATING ¹
V _{DS}	Drain-Source Voltage	8V
V _{GS}	Gate-Source Voltage	-3V
I _{DS}	Drain-Source Current	I _{DSS}
I _G	Gate Current	5 mA
P _{IN}	RF Input Power	60 mW
T _{CH}	Channel Temperature	175°C
T _{STG}	Storage Temperature	-65/175°C
P _T	Power Dissipation	400mW ^{3,4}

RECOMMENDED CONTINUOUS OPERATING LIMITS		
SYMBOL	PARAMETER	RATING ²
V _{DS}	Drain-Source Voltage	5V
V _{GS}	Gate-Source Voltage	-0.8V
I _{DS}	Drain-Source Current	0.50 x I _{DSS}
I _G	Gate Current	2 mA
P _{IN}	RF Input Power	30 mW
T _{CH}	Channel Temperature	150°C
T _{STG}	Storage Temperature	-20/50°C
P _T	Power Dissipation	350 mW ^{3,4}
G _{XdB}	Gain Compression	6 dB

NOTES:

1. Operating conditions that exceed the Absolute Maximum Ratings could result in permanent damage to the device.
2. Recommended Continuous Operating Limits should be observed for reliable device operation.
3. Power Dissipation defined as: $P_T = (P_{DC} + P_{IN}) - P_{OUT}$, where: P_{DC} = DC bias power, P_{OUT} = RF output power, and P_{IN} = RF input power.
4. Power Dissipation to be de-rated as follows above 25°C:
 Absolute Maximum: $P_T = 400mW - (3.1mW/°C) \times T_{HS}$
 Recommended Continuous Operating: $P_T = 350mW - (3.1mW/°C) \times T_{HS}$
 where T_{HS} = heatsink or ambient temperature.

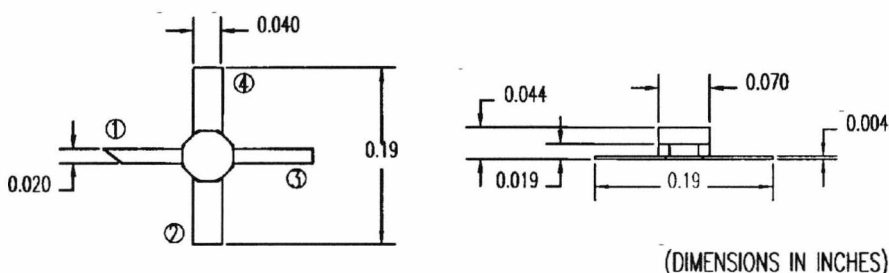
HANDLING PRECAUTIONS:

Proper Electrostatic Discharge (ESD) precautions should be observed at all stages of storage, handling, assembly, and testing. These devices should be treated as Class 1A (0-500V), and further information on ESD control measures can be found in MIL-STD-1686 and MIL-HDBK-263.

PACKAGE CHARACTERISTICS:

The P70 package is available with a standard gold over nickel finish. The package lids are epoxy sealed and are capable of passing MIL-STD hermeticity (Gross Leak).

PACKAGE OUTLINE:



Get Package Model

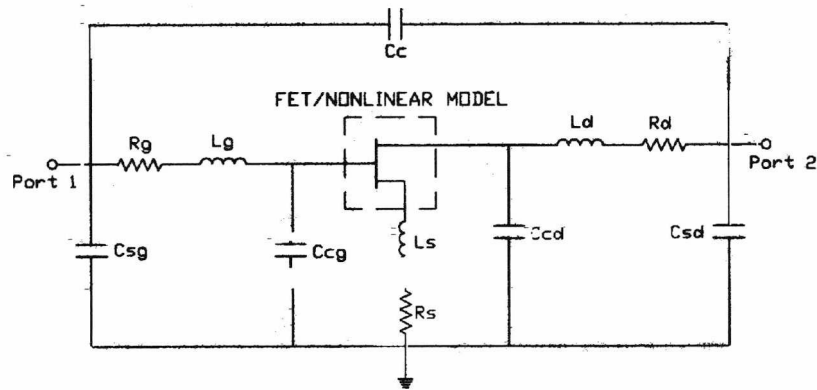
DSS-022 WE

Phone: (408) 988-1845

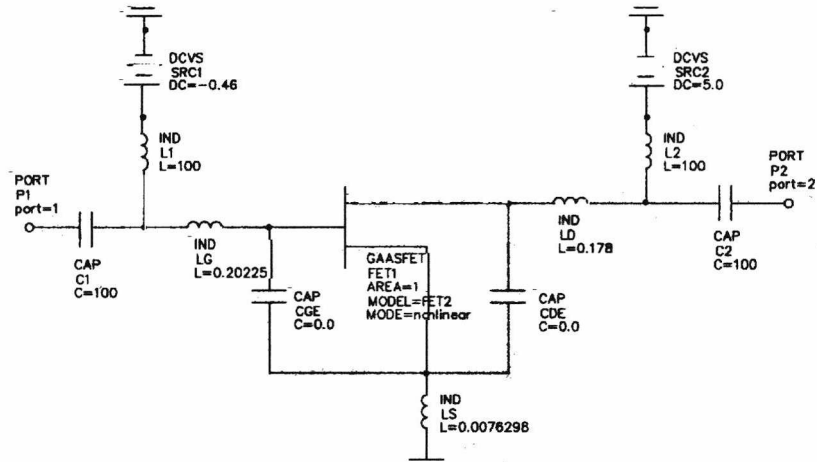
Internet: <http://www.filtronicssolidstate.com>

Fax: (408) 970-9950

PACKAGE MODEL



	Package Number						
	Plastic			P70		P100	
	SOT-89	SOT-23	SOT-223	1-12 GHz	12-26 GHz	1-12 GHz	12-26 GHz
Rg (Ohm)	0.250	0.250	0.250	0.250	0.250	0.250	0.250
Rs (Ohm)	0.100	0.015	0.800	0.100	0.050	0.010	0.100
	0.250	0.250	0.250	0.250	0.250	0.250	0.250
	1.100	0.450	0.400	0.350	0.280	0.280	0.230
	0.040	0.080	0.090	0.080	0.070	0.050	0.100
	0.900	0.450	0.400	0.350	0.480	0.320	0.330
	0.340	0.200	0.420	0.150	0.090	0.200	0.080
	0.000	0.030	0.450	0.010	0.120	0.100	0.110
	0.030	0.040	0.100	0.010	0.010	0.010	0.010
	0.000	0.030	0.450	0.010	0.120	0.100	0.110
	0.330	0.200	0.420	0.150	0.090	0.200	0.080



LIBRA Model:

CURTICE3					
FET2					
BETA= 0.10257	A3= -.14126E-01	IS= 1.00E-14	RIN= 0	KF= 0	FFE1= 1
GAMMA= 3.038	TAU= .22273E-11	N= 1	CGS0= .46278E-12	AF= 1	
VOUO= 9.969	R1= 0	RDS= 3000	CGD0= .22959E-13	TNOM= 27	
VTO= -0.9	R2= 0	CRF= .10000E-10	FC= 0.50	XTI= 3	
A0= .62008E-01	VB0= 9	RD= 5.1005	CDS= .70881E-13	EG= 1.11	
A1= .59192E-01	VBI= 5	RG= 7	CGS= 0	VTOTC= 0	
A2= -.14366E-01	RF= 0	RS= 2.8499	CGD= 0	VTOTC= 0	

Appendix IV

EC2612 Specifications



40GHz Super Low Noise PHEMT

Pseudomorphic High Electron Mobility Transistor

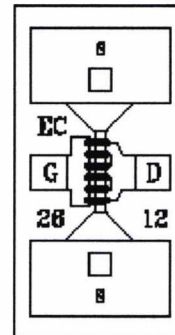
Description

Chip size : 0.63 x 0.37 x 0.1 mm

The EC2612 is based on a 0.15 μ m gate pseudomorphic high electron mobility transistor (0.15 μ m PHEMT) technology. Gate width is 120 μ m and the 0.15 μ m T-shaped aluminium gate features low resistance and excellent reliability.

The device shows a very high transconductance which leads to very high frequency and low noise performances.

It is available in chip form with sources via holes connection. Only gate and drain wires bounding are required.



D: Drain
G: Gate
S: Source

Main Features

- | 0.8dB minimum noise figure @ 18GHz
- | 1.5dB minimum noise figure @ 40GHz
- | 12dB associated gain @ 18GHz
- | 9.5dB associated gain @ 40GHz

Main Characteristics

Tamb = +25°C

Symbol	Parameter	Min	Typ	Max	Unit
I _{dss}	Saturated drain current	10	40	60	mA
NF _{min}	Minimum noise figure (F=40GHz)		1.5	1.9	dB
G _a	Associated gain (F=40GHz)	8	9.5		dB

ESD Protections: Electrostatic discharge sensitive device observe handling precautions!

Electrical Characteristics

Tamb = +25°C

Ref. : DSEC26120077 -17-Mars-00

1/8

Specifications subject to change without notice

United Monolithic Semiconductors S.A.S.
Route Départementale 128 - B.P.46 - 91401 Orsay Cedex France
Tel. : +33 (0)1 69 33 03 08 - Fax : +33 (0)1 69 33 03 09

Symbol	Parameter	Test Conditions	Min	Typ	Max	Unit
I _{ds}	Saturated drain current	V _{ds} = 2V V _{gs} = 0V	10	35	60	mA
V _p	Pinch off voltage	V _{ds} = 2V I _{ds} = 0.1mA	-1.0	-0.7	-0.3	V
G _m	Transconductance	V _{ds} = 2V I _{ds} = 25mA	50	70		mS
I _{gsd}	Gate to source/drain leakage current	V _{gsd} = -2V			5	μA

Dynamic characteristics

T_{amb}=25°C

Symbol	Parameter	Test Conditions	Min	Typ.	Max	Unit	
NF	Minimum noise figure	V _{ds} =2V I _{ds} =I _{ds} /3	F= 12GHz		0.5	0.7	dB
			F= 30GHz		1.3	1.7	
			F= 40GHz		1.5	1.9	dB
Ga	Associated Gain	V _{ds} =2V I _{ds} =I _{ds} /3	F= 12GHz	13	14		dB
			F= 30GHz	9	10		
			F= 40GHz	8	9.5		dB

Absolute Maximum Ratings (1)

T_{amb} = +25°C

Symbol	Parameter	Values	Units
V _{ds}	Drain to source voltage	3.5	V
V _{gs}	Gate to source voltage	-2.5	V
P _t	Total power dissipation	280	mW
T _{ch}	Operating channel temperature	+175	°C
T _{stg}	Storage temperature range	-55 to +175	°C

(1) Operation of this device above any one of these parameters may cause permanent damage

Typical Scattering Parameters

Tamb = +25°C

S Parameters, including Lg=Ld~0.15nH

Vds = 3V, Ids = 30mA

Freq. GHz	S11 dB	S11 °	S12 dB	S12 °	S21 dB	S21 °	S22 dB	S22 °
1	-0.14	-11.0	-34.26	81.5	15.88	169.7	-4.78	-8.8
2	-0.19	-21.6	-28.41	76.1	15.69	162.2	-4.89	-18.3
3	-0.35	-32.3	-25.12	70.0	15.48	154.5	-5.11	-27.2
4	-0.62	-42.5	-22.92	64.0	15.20	146.7	-5.39	-36.0
5	-0.89	-52.5	-21.36	58.1	14.87	139.3	-5.80	-44.4
6	-1.12	-62.2	-20.14	52.2	14.53	132.3	-6.19	-53.5
7	-1.39	-71.9	-19.30	46.4	14.16	125.7	-6.67	-61.5
8	-1.70	-80.5	-18.69	42.0	13.74	119.5	-7.07	-68.5
9	-1.96	-88.2	-18.10	38.0	13.34	113.9	-7.38	-75.6
10	-2.15	-95.9	-17.61	33.5	12.96	108.3	-7.69	-83.2
11	-2.34	-104.1	-17.23	29.4	12.57	103.0	-8.04	-90.1
12	-2.47	-111.8	-16.88	25.8	12.23	97.6	-8.30	-96.9
13	-2.62	-118.7	-16.56	22.1	11.83	92.4	-8.55	-104.7
14	-2.78	-125.5	-16.35	18.7	11.40	87.4	-8.85	-111.9
15	-2.91	-132.8	-16.23	15.4	11.02	82.5	-9.03	-118.3
16	-3.00	-138.8	-16.11	12.9	10.60	78.1	-9.20	-123.8
17	-3.05	-144.2	-15.89	10.0	10.24	73.7	-9.29	-130.8
18	-3.08	-150.1	-15.79	6.7	9.86	69.5	-9.28	-137.3
19	-3.13	-156.5	-15.82	4.1	9.49	65.2	-9.34	-143.2
20	-3.17	-161.6	-15.77	1.5	9.14	61.2	-9.38	-148.9
21	-3.24	-166.5	-15.80	-2.0	8.75	57.2	-9.45	-155.9
22	-3.26	-171.9	-15.90	-4.8	8.40	53.3	-9.47	-160.6
23	-3.30	-176.7	-16.00	-6.9	8.02	50.0	-9.50	-164.8
24	-3.27	179.3	-15.96	-9.8	7.68	46.8	-9.43	-169.2
25	-3.26	175.8	-16.06	-12.6	7.39	43.6	-9.31	-174.6
26	-3.20	172.0	-16.12	-14.9	7.12	40.4	-9.20	-177.9
27	-3.17	167.4	-16.14	-17.2	6.86	37.1	-9.13	-177.8
28	-3.15	163.5	-16.16	-20.0	6.62	33.4	-9.06	-173.5
29	-3.19	159.2	-16.36	-22.2	6.28	29.7	-8.95	-168.4
30	-3.15	155.1	-16.39	-23.1	5.98	26.5	-8.81	-166.0
31	-3.10	151.2	-16.29	-24.9	5.70	23.1	-8.67	-161.3
32	-3.03	147.7	-16.37	-27.5	5.40	19.5	-8.59	-155.5
33	-2.99	144.1	-16.54	-28.8	5.12	16.7	-8.45	-152.7
34	-2.98	139.8	-16.62	-30.6	4.89	13.4	-8.38	-150.0
35	-2.97	136.5	-16.74	-32.6	4.68	10.1	-8.34	-145.6
36	-2.89	132.3	-16.88	-34.5	4.51	6.4	-8.26	-141.4
37	-2.85	128.2	-16.84	-36.4	4.24	3.0	-8.10	-138.3
38	-2.83	124.9	-16.86	-39.7	4.04	-0.7	-7.89	-133.7
39	-2.82	121.6	-17.04	-43.4	3.84	-4.4	-7.77	-129.7
40	-2.83	116.9	-17.11	-46.0	3.47	-8.6	-7.71	-127.3

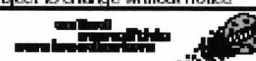
Tamb = +25°C

Ref. : DSEC26120077 -17-Mars-00

3/8

Specifications subject to change without notice

Route Départementale 128 - B.P.46 - 91401 ORSAY Cedex - FRANCE
 Tel. : +33 (0)1 69 33 03 08 - Fax : +33 (0)1 69 33 03 09



EC2612

40GHz Super Low Noise PHEMT

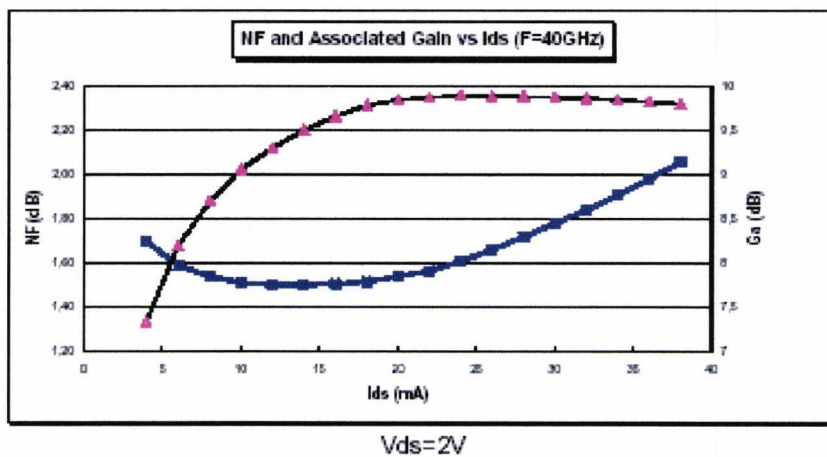
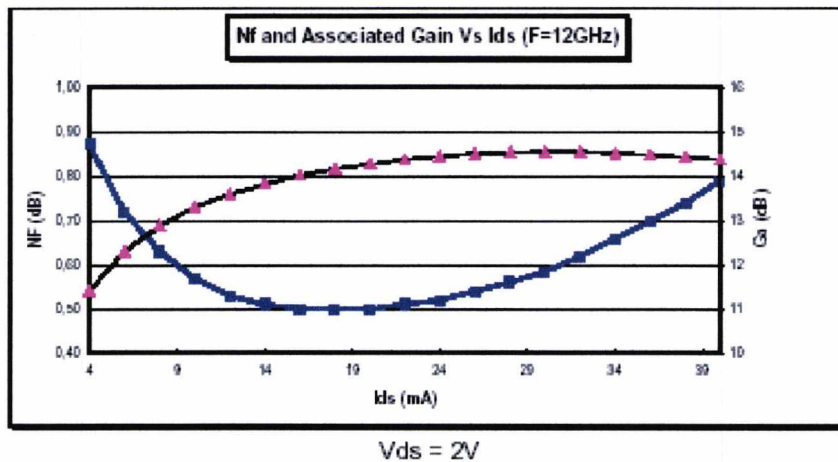
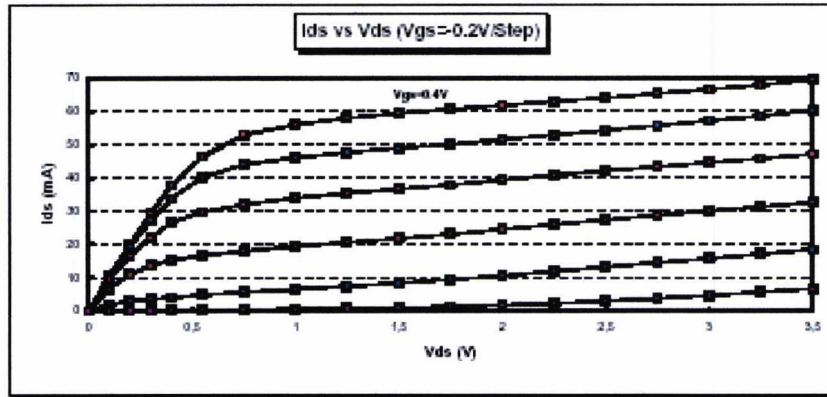
"S" Parameters, including Lg=Ld~0.15nH
Vds = 2V, Ids = 10mA

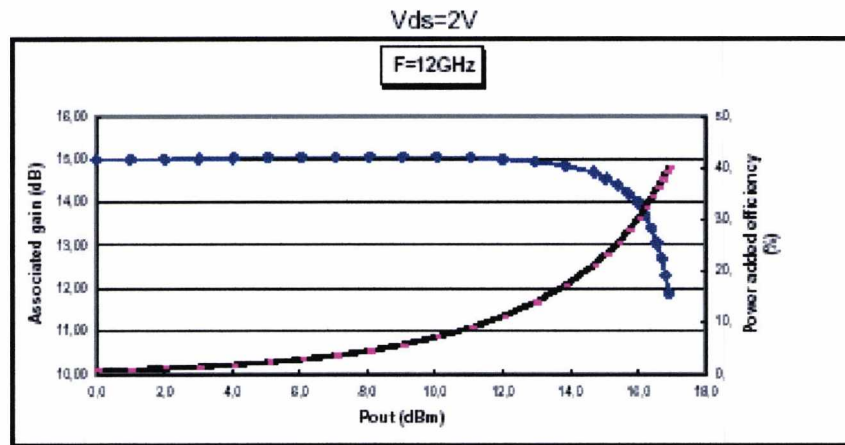
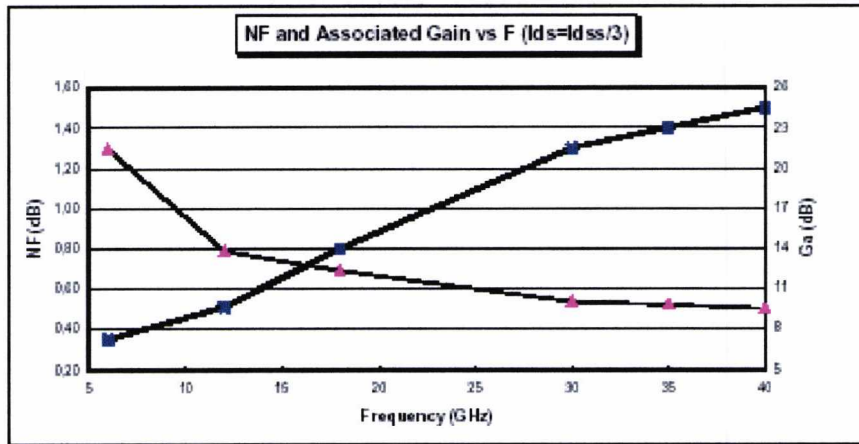
Freq. GHz	S11 dB	S11 °	S12 dB	S12 °	S21 dB	S21 °	S22 dB	S22 °
1	-0.11	-10.5	-33.67	82.3	13.52	170.6	-4.76	-7.4
2	-0.26	-20.7	-27.77	77.0	13.38	163.7	-4.81	-16.4
3	-0.45	-29.8	-24.45	71.2	13.22	156.4	-4.99	-24.5
4	-0.66	-38.4	-22.20	65.4	13.01	149.0	-5.21	-32.6
5	-0.85	-47.7	-20.57	59.6	12.74	141.8	-5.56	-40.5
6	-1.03	-56.5	-19.27	53.7	12.48	135.0	-5.88	-49.0
7	-1.20	-65.7	-18.36	47.9	12.19	128.5	-6.29	-56.6
8	-1.41	-73.9	-17.68	43.3	11.85	122.4	-6.65	-63.3
9	-1.64	-81.2	-17.04	39.2	11.51	116.7	-6.91	-70.0
10	-1.85	-88.7	-16.49	34.5	11.19	111.0	-7.19	-77.4
11	-2.04	-96.7	-16.08	30.1	10.85	105.6	-7.53	-84.0
12	-2.19	-104.2	-15.69	26.3	10.56	100.1	-7.78	-90.6
13	-2.35	-111.0	-15.33	22.3	10.22	94.7	-8.03	-98.0
14	-2.51	-117.8	-15.09	18.5	9.82	89.6	-8.34	-105.2
15	-2.66	-125.3	-14.94	14.9	9.49	84.5	-8.49	-111.6
16	-2.78	-131.4	-14.82	12.0	9.12	79.9	-8.67	-117.1
17	-2.86	-136.9	-14.57	8.9	8.78	75.2	-8.82	-124.0
18	-2.92	-142.9	-14.47	5.3	8.43	70.9	-8.91	-130.5
19	-3.00	-149.4	-14.48	2.3	8.08	66.4	-9.02	-136.3
20	-3.08	-154.6	-14.41	-0.5	7.76	62.2	-9.07	-141.9
21	-3.15	-159.8	-14.41	-4.3	7.40	58.0	-9.18	-149.1
22	-3.20	-165.3	-14.50	-7.5	7.07	54.0	-9.27	-154.0
23	-3.23	-170.4	-14.60	-9.8	6.72	50.4	-9.29	-158.4
24	-3.25	-174.7	-14.56	-12.9	6.38	47.1	-9.27	-162.8
25	-3.26	-178.3	-14.65	-16.0	6.10	43.6	-9.22	-168.4
26	-3.27	177.7	-14.71	-18.5	5.83	40.3	-9.16	-171.9
27	-3.27	173.0	-14.72	-21.1	5.57	36.8	-9.08	-176.3
28	-3.26	169.0	-14.74	-24.0	5.34	33.1	-9.05	179.2
29	-3.25	164.6	-14.93	-26.6	5.03	29.3	-8.91	174.0
30	-3.21	160.2	-15.00	-27.9	4.73	26.0	-8.80	171.5
31	-3.18	156.1	-14.93	-30.1	4.47	22.4	-8.67	166.5
32	-3.13	152.5	-15.01	-33.0	4.18	18.6	-8.58	160.6
33	-3.09	148.6	-15.21	-34.6	3.91	15.8	-8.49	157.5
34	-3.07	144.3	-15.27	-36.7	3.69	12.3	-8.39	154.9
35	-3.03	140.9	-15.31	-39.8	3.49	9.0	-8.30	151.3
36	-3.00	136.6	-15.48	-42.0	3.33	5.2	-8.20	146.8
37	-2.98	132.1	-15.49	-44.1	3.07	1.7	-8.08	143.3
38	-2.97	128.6	-15.53	-47.7	2.89	-2.2	-7.95	138.6
39	-2.94	125.3	-15.77	-50.7	2.67	-6.0	-7.86	133.6
40	-2.93	120.6	-15.86	-53.4	2.33	-10.2	-7.78	131.3



Typical results

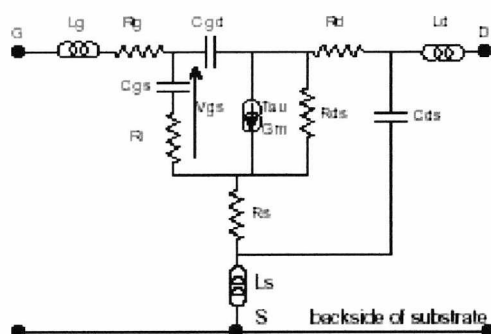
Tamb = +25°C





V_{ds} = 3V, I_{ds} = 31mA

(CHIP) Equivalent Circuit model (Drain and Gate bond wires included)

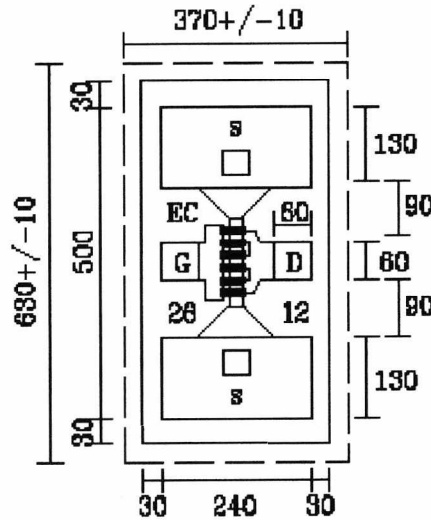


Parameter	Unit	Value
Lg	pH	152.54
Rg	Ohms	0.13
Cgs	fF	142.6
Ri	Ohms	3.2
Cgd	fF	39.57
Rs	Ohms	2.83
Ls	pH	0.11
Gm	mS	98.14
Tau	ps	2.8
Cds	fF	46.84
Rds	Ohms	116.8
Rd	Ohms	2.83
Ld	pH	117.01

Typical Noise Parameters at $V_{ds}=2V$, $I_{ds}=14mA$
(Drain and Gate bond wires included)

FREQUENCY MHz	NF min dB	Γ_{opt}		Rn
		MOD.	Ang.(°)	
5000	0.26	0.811	19.888	14.089
8000	0.356	0.746	32.28	13.33
12000	0.492	0.658	49.899	11.87
15000	0.595	0.598	64.263	10.51
20000	0.762	0.514	91.037	7.965
24000	0.892	0.473	114.916	5.923
28000	1.01	0.460	139.673	4.16
30000	1.07	0.465	151.723	3.473
32000	1.137	0.475	163.219	2.966
35000	1.223	0.5	179.087	2.63
38000	1.307	0.533	-166.857	2.923
40000	1.362	0.556	-158.467	3.538
42000	1.415	0.581	-150.795	4.536
45000	1.493	0.618	-140.488	6.843

Chip Mechanical Data



dimensions in μm

Drain area = $60 \times 60 \mu\text{m}$
 Gate area = $60 \times 60 \mu\text{m}$

Thickness = $100 \mu\text{m}$

Recommended die attach :

Stage temperature = 300°C
 (minimize temp. and time whenever possible)
 Preforms = Au/Sn (80/20)
 Atmosphere : dry nitrogen or forming gas flow

Recommended bonding :

$\varnothing 18 \mu\text{m}$ very pure gold wire
 (thermal compression)
 The bonder should be properly grounded

Source pads are directly connected to back face metallization through the via holes



Ordering Information

Chip form : EC2612-99F/00

Information furnished is believed to be accurate and reliable. However United Monolithic Semiconductors S.A.S. assumes no responsibility for the consequences of use of such information nor for any infringement of patents or other rights of third parties which may result from its use. No license is granted by implication or otherwise under any patent or patent rights of United Monolithic Semiconductors S.A.S.. Specifications mentioned in this publication are subject to change without notice. This publication supersedes and replaces all information previously supplied. United Monolithic Semiconductors S.A.S. products are not authorised for use as critical components in life support devices or systems without express written approval from United Monolithic Semiconductors S.A.S.

